PHASE INVERSION IN NONIONIC SURFACTANT-OIL-WATER SYSTEMS

by

Howard N. Richmond

Doctoral Thesis

Submitted in partial fulfilment of the requirements for the award of

Doctor of Philosophy of the Loughborough University of Technology

March 1992

Dedication

To Christine for everything.

Acknowledgements

I would like to acknowledge the following for their help and assistance during this study:

(i) Special thanks to Professor B.W. Brooks for his invaluable time, guidance and enthusiasm, (ii) the technical and laboratory staff of the Chemical Engineering Department, (iii) the Science and Education Research Council (SERC) for their financial support.

SUMMARY

This study has been concerned with the inversion of water in oil (W/O) emulsions, to oil in water (O/W) emulsions and vice-versa. It has been shown that there are two types of emulsion phase inversion that can occur in nonionic Surfactant-Oil-Water (nSOW) systems: (i) A "transitional" inversion, which is brought about by changing the nSOW phase behaviour, by altering the surfactant's affinity for the oil and water phases and, (ii) a "catastrophic" inversion, induced by increasing the dispersed phase fraction and occurs at closest packing of unstable dispersed phase drops. The inversion mechanism of the two inversion types has been characterised. The two inversion types can be represented as boundaries on a "map" relating nSOW phase behaviour with water to oil volume ratio. The form of the map depends on the nature of the oil. At the transitional point, the nSOW system can be 3 phase - an oil phase, a water phase and a surfactant phase microemulsion. Ultra-low interfacial tension exists between the phases - this property is of interest for producing extremely fine emulsions with low energy input. Transitional inversions are sometimes reversible. In nSOW systems, true catastrophic inversions can be induced by moving the water to oil ratio in one direction only. Double emulsion drops (W/O/W or O/W/O) are sometimes produced before inversion and inversion points are dependent on dynamic conditions. A thermodynamic relationship between nSOW phase behaviour, oil type, surfactant type, surfactant concentration and temperature has been derived, based on the partitioning of surfactant between oil, water and a surfactant micelle phase. It has been shown how this can be used to classify nonionic surfactants. The effect of agitation conditions, water addition rate and oil phase viscosity, on the drop types and drop sizes of emulsions present before and after inversion (for each inversion type) has been studied extensively. Surfactant type and concentration also affect drop behaviour and drop sizes. Various drop types have been identified and qualitative and quantitative analysis of the factors controlling the drop sizes of emulsions at each stage of a phase inversion has been developed.

TABLE OF CONTENTS

INTRODUCTION TO THESIS

Procedures for the direct emulsification of organic liquids in aqueous media are well established. These are important in the manufacture of creams, emulsified food stuffs, water based surface coatings and adhesives. The procedures for the preparation of emulsions by phase inversion are not well developed and hence, it is not widely used. However, in certain emulsification processes, phase inversion cannot be avoided and also, it has been shown that phase inversion can be used to produce very fine emulsions with low energy input (Shinoda 1986). Therefore, there are good reasons for developing the understanding of phase inversion processes.

Relatively few published studies deal with the dynamics of phase inversion. The role of agitation (or turbulence) has not been established and the conditions necessary for the induction of phase inversion are difficult to define. Often the nature of the final emulsion cannot be predicted. Hence, a number of important points must be clarified if the production of emulsions by phase inversion on a large scale, is to be a reliable and reproducible process.

Objectives

When this research was initially proposed, it was to be concerned primarily with the dynamics of phase inversion in nonionic surfactant - oil - water systems (nSOW). The relationship between chemical composition of the nSOW system and phase inversion was to receive less attention. The chemical composition of the nSOW system (at constant temperature) determines the number of phases that are present at equilibrium and the location of the surfactant micelles ie. the system's chemical composition determines its phase behaviour. However, in the course of this study, it was quickly recognized that phase inversion in nSOW systems is closely related to their phase behaviour. Hence, the development of an understanding of nSOW phase behaviour is essential to the understanding of phase inversion in nSOW systems. Very few studies in the literature have examined the relationship between phase inversion and phase behaviour, hence, in the initial part of this study, an understanding of this relationship is developed.

The aim of this research is to provide some answers to important questions concerning the formation of oil-in-water emulsions by phase inversion:

(a) Which factors affect nSOW phase behaviour and how may nonionic surfactants be classified?

(b) How does phase inversion relate to nSOW phase behaviour and what are the mechanisms of inversion?

(c) Does the drop size immediately before inversion affect the drop sizes after inversion?

(d) How are drop sizes affected by the type of agitation and the level of turbulence? (Do established correlations for coarser liquid-liquid dispersions apply?).

(e) Are hysterisis effects (observed in some systems - Dickinson 1981) to be expected generally? ie. When can the inversion be regarded as reversible?

(f) How do drop sizes after phase inversion compare with sizes obtained by direct emulsification?

(g) How does the rate of water addition affect the inversion process? (A definite period of time may be required to establish a steady-state drop size distribution before phase inversion).

(h) How does the course of the phase inversion depend on the viscosity of the organic liquid?

Detailed quantitative theory for phase inversion cannot be developed until the essential features of the process have been established (re the above questions). Emphasis is placed on improving understanding of those aspects of phase inversion which are important for the choice, design and operation of phase inversion processes. Particular attention is given to systems in which the viscosity of the oil phase is appreciably higher than that of the aqueous phase because a number of important cases are of this type, eg. when the final emulsion is to be used to create a surface coating.

The need to establish the relationship between phase inversion and nSOW phase behaviour, before beginning drop size studies, has influenced the structure of this thesis:

Thesis Structure

This study has two interconnected parts:

The first part (chapters 1, 2 and 3), lays down the ground work essential for the understanding of phase inversions. In chapter 1, nSOW phase behaviour and phase inversion literature is reviewed. In chapter 2, a mapping procedure for relating dynamic inversion points with nSOW phase behaviour is developed. The map is used as an experimental framework for investigating dynamic phase inversion phenomena. It is shown which factors affect inversion boundaries on the map. Drop types present at each stage of a dynamic inversion are described and inversion mechanisms are characterised. Chapter 3 is concerned with nSOW phase behaviour. A thermodynamic relationship between nSOW phase behaviour and surfactant partitioning between oil, water and a interfacial surfactant phase is developed. It is shown how this can be used to classify nonionic surfactants.

Having developed an experimental framework and characterised inversion mechanisms in chapters 1, 2 and 3, the second part (chapters 4, 5 and 6) concerns the drop size studies. The drop size distribution of an emulsion is the key factor (over which some control is possible during processing) affecting the emulsion's rheology and stability. Hence, to compare the effectiveness of different emulsion processes, is to compare the drop size distribution produced by each process. Chapter 4, is a review of drop breakage and drop coalescence literature. In chapter 2, it is shown that there are two types of phase inversion that can occur in nSOW systems: (i) A "transitional" inversion induced by altering the nSOW phase behaviour and, (ii) a "catastrophic" inversion induced by changes in the emulsion's water to oil ratio. The changes in the drop types and drop sizes occurring during transitional inversions, is the subject of chapter 5. The changes in the drop types and drop sizes occurring in catastrophic inversion, is the subject of chapter 6. The affects of changing oil phase viscosity is examined and a comparison with direct emulsification is made, for each inversion type.

In the final chapter (chapter 7), the separate (but interconnected) studies of chapters 2, 3, 5 and 6 are drawn together in a concluding discussion.

CHAPTER 1

Nonionic Surfactant-Oil-Water Systems (nSOW) Phase Behaviour and Phase Inversion Literature Review

1.1 INTRODUCTION

By way of an introduction, this chapter reviews the relevant literature concerning nonionic surfactant-oil-water (nSOW) phase behaviour and emulsion phase inversion. The IUPAC definition of an emulsion is:

"An emulsion is a dispersion of droplets of one liquid in an another with which it is incompletely miscible. Emulsions of droplets of an organic liquid (an "oil") in an aqueous solution are indicated by the symbol O/W and emulsions of aqueous droplets in an organic liquid as W/O. In emulsions the droplets often exceed the usual limits for colloids in size."

At this stage, the above definition is adequate, however, it will be seen in the course of this study that a description of an emulsion must indicate the nature of the surfactant.

In emulsion phase inversion the continuous phase becomes the dispersed phase and vice-versa.

A third component is usually required for the emulsification process, which has the property of accumulating at the oil-water interface ie. a surface active material or "surfactant". In simple terms the role of the surfactant is to aid drop break up (by reducing the system's interfacial tension and causing interfacial tension gradients) and to provide a mechanism for stabilising the emulsion drops against coalescence. Surfactants are available in many forms, usually either, ionic type, nonionic polymer or polyelectrolyte, finely divided solids or any combination of two or more of these materials. In this study we will be concerned with nonionic type surfactants. Nonionic surfactant molecules contain a polar hydrophilic chain group (usually a polyoxyethylene group) and a nonpolar (lipophilic) head; this character is called amphipathy or amphilicity and results in a double affinity which can only be satisfied at a polar-nonpolar interface. Commercial nonionic surfactants are polydisperse, having a distribution of hydrophilic chain lengths, they are sold as having an average chain length.

nSOW systems are usually pseudo ternary ie. the surfactant may be a mixture of surfactants, the aqueous phase may be a salt solution and the oil phase may be a mixture of oils or contain dissolved polymers.

See appendix 6 for a list of reference acronyms

Emulsions are a meta-stable state ie. they are not thermodynamically stable and even emulsions stabilised by a surfactant will phase separate over a period of time. A thermodynamically stable nSOW phase is termed a microemulsion; this can be an aqueous solution of solubilised oil in surfactant micelles, an oleic solution of solubilised water in surfactant micelles, or a surfactant solution containing cosolubilised oil and water. The relevance of these terms will become apparent when discussing nSOW phase behaviour.

1.2 DISSOLUTION STATE OF NONIONIC SURFACTANTS

For a comprehensive review of interfacial phenomena, see Tadros (1983). When a nonionic surfactant is added to a two phase system of oil and water, it preferentially adsorbs at the interface forming an adsorbed monolayer. At low surfactant concentrations an equilibrium exists between surfactant monomers dissolved in the oil phase, surfactant monomers dissolved in the water phase and the interfacial surfactant. In the case of a phase separated system (constant interfacial area), as the concentration of surfactant in the system increases, the amount of surfactant at the interface reaches a maximum possible concentration and, on further increase in surfactant concentration, excess surfactant will now form micelles in the oil or water phases, or form a surfactant phase depending on its affinity for the oil and water phases (see part 1.3 of this chapter). The break point is termed the critical-micelle-concentration (CMC).

A surfactant micelle is generally pictured as a sphere of surfactant molecules (although the actual shape may be unclear) with a liquid phase core, eg. an aqueous micellar solution has a water continuous structure containing micelles with an oil phase core. This phase is thermodynamically stable and the oil within the micelle is termed solubilised.

For conditions below the CMC, the effect of the adsorbed interfacial surfactant on the nSOW system's interfacial tension is governed by the Gibbs adsorption equation:

$$\Gamma = \frac{-1.}{RT}\frac{d\sigma}{d\ln C} \qquad [1.1]$$

where, Γ = surface excess surfactant ($mol.m^{-2}$),
R = Gas constant,
T = temperature,
σ = interfacial tension,
C = surfactant concentration.

Equation [1.1] is useful for calculating the amount of surfactant adsorbed or the surfactant molecule area of coverage at the interface, from the variation of σ with lnC (see chapter 5).

To stabilise an emulsion, the surfactant must be present at a concentration >CMC, hence, we shall be mainly concerned with systems of this sort. The phase that the surfactant forms micelles in (ie. the nSOW phase behaviour) is dependent on the surfactant's affinity for oil and water (hereafter termed "surfactant affinity"). The surfactant's affinity is controlled by a number of factors, these will be reviewed in part 1.4 of this chapter. Winsor (1948) and (1954), first addressed the problem of describing surfactant affinity:

Winsor Interaction Energies

Winsor introduced the concept of interaction energies between surfactant molecules adsorbed at the interface and the oil and water phases. Figure 1.1 (Salager 1988) summarises the interactions. The ratio of the total interaction energies (per unit area of interface) of the surfactant for the oil and water phases is known as Winsor R.

$$R = \frac{A_{co}}{A_{cw}} = \frac{A_{lco} + A_{hco} - A_{oo} - A_{ll}}{A_{lcw} + A_{hcw} - A_{ww} - A_{hh}} \qquad [1.2]$$

The three cases of R, R<1, R=1 and R>1, correspond to Type 1, Type 3 and Type 2 nSOW phase behaviour respectively. Although Winsor's approach is purely quantitative, researchers have shown that it allows interpretation of all known effects, eg. For a case R<1, with a rise in temperature the hydration forces between the water phase and the hydrophilic group of the surfactant (A_{hcw}) decreases and therefore, R increases; a progressive change from Type 1 to Type 3 to Type 2 phase behaviour is seen with rise in temperature (see Shinoda 1986).

The 3 phase behaviour types are outlined below (refer to figure 1.2). Figure 1.2 shows schematically the change in nSOW phase diagrams with changing surfactant affinity. The settled phase volumes for a point in the multiphase region are also shown. M represents surfactant phase microemulsion, W water phase and HC hydrocarbon oil phase. Note, other types of phases can form in nSOW systems (eg. Liquid crystal phases), however, for simplicity these are not shown.

TYPE 1 (R<1)

In this case the affinity of the surfactant for the water phase exceeds its affinity for the oil phase. In Type 1 systems the interface will be convex towards water. From the Type

1 triangular phase diagram of figure 1.2, it can be seen that a Type 1 nSOW system can be 1 or 2 phase. A system in the two phase region will split into an oil phase containing dissolved surfactant monomers at CMC_o (critical micelle concentration in the oil phase) and an aqueous microemulsion - a water phase containing solubilised oil in surfactant micelles.

TYPE 2 (R>1)

In Type 2 systems, the affinity of the surfactant for the oil phase exceeds its affinity for the water phase and the interface will be convex towards oil. Again 1 or 2 phase nSOW systems are possible. A system in the two phase region will split into a water phase containing surfactant monomers at CMC_w (critical micelle concentration in the water phase) and an oleic microemulsion - an oil phase containing solubilised water in surfactant micelles.

TYPE 3 (R=1)

Here the surfactant's affinity for the oil and water phases is balanced. The interface will be flat. A Type 3 nSOW system can have 1, 2 or 3 phases depending on its composition. In the multiphase region the system can be:

(a) 2 phase - a water phase and an oleic microemulsion,
(b) 2 phase - an oil phase and an aqueous microemulsion,
(c) 3 phase - a system whose composition is in the tie triangle splits into a water phase containing surfactant monomers at CMC_w, an oil phase containing surfactant at CMC_o and a "surfactant phase". The surfactant phase has a bicontinuous structure, being composed of cosolubilised oil and water separated from each other by an interfacial layer of surfactant. A schematic illustration of the structure of a surfactant phase is shown in figure 1.3 (Shinoda 1986). The surfactant phase is sometimes called the middle phase because its intermediate density means it appears between the oil and water phases in a phase separated Type 3 nSOW system.

The tie line on the W-O side of the triangular diagram connects the CMC_o and CMC_w compositions. The tie line slopes down from the oil side to the water side because generally, $CMC_o >> CMC_w$.

Note for certain Type 3 nSOW system compositions that are two phase, an aqueous microemulsion can contain more oil than water despite it being the "water" phase, similarly, an oleic microemulsion can contain more water than oil despite it being the "oil" phase.

1.3 CHANGE OF EMULSION TYPE WITH CHANGE IN nSOW PHASE BEHAVIOUR

Bancroft's rule, first forwarded in 1913, can be used as a guide to which emulsion type will be formed on agitation of nSOW systems of each phase behaviour type:

"A hydrophile colloid will tend to make water the dispersing phase, while a hydrophobe colloid will tend to make water the disperse phase."

The limitations of this rule will be fully discussed in chapter 2. From Bancroft's rule, Type 1 systems may be expected to form O/W emulsions on agitation and Type 2 systems, W/O emulsions on agitation. Type 3 systems are more complex, however, it has been suggested that the surfactant phase becomes continuous in 3-phase systems (Shinoda 1986).

The change in nSOW phase behaviour with surfactant affinity is shown on figure 1.2 (the change in the phase diagram with temperature for a cyclohexane-water-polyoxyethylenenonylphenylether (NPE) system has been shown by Smith (1985), derived from data by Shinoda (1986)). Hence, from Bancroft's rule, it may be expected that by changing the surfactant's affinity, a phase inversion can be brought about.

Change of Phase Behaviour with Temperature

Increasing temperature is one way in which the surfactant's affinity can be altered. Shinoda (1986) produced equilibrium phase diagrams showing the change in phase behaviour with temperature at a constant surfactant concentration (see figure 1.4(a), Shinoda 1986). As the temperature rises, the surfactant's affinity for oil increases ie. it becomes more lipophilic, hence, the system moves from Type 1 to Type 3 to Type 2 phase behaviour with increase in temperature. In figure 1.4(b), the emulsion types at each point on the diagram are shown; it is clear that the oil phase is continuous at high temperature, the surfactant phase is continuous at medium temperature and the water phase is continuous at low temperature.

The changes in the phase volumes with rise in temperature was shown by Shinoda (1986) (see figure 1.5). The solubilisation of oil into an aqueous micellar solution phase increases rapidly as the Type 3 phase region is approached. In the Type 3 region, as the temperature rises, the system moves from 2 phases (O and D, where D = surfactant phase), to 3 phases (O, W and D) and then back to two phases (W and D). With further rise in temperature, water solubilised in the oleic micellar phase is released to the water phase.

Figure 1.5 also shows the variation of the interfacial tension across the transition from Type 1 to Type 2 phase behaviour. In the 3 phase region the interfacial tension is "ultra-low"; this has important consequences for the drop sizes and stability of emulsions of Type 3 systems (this will be discussed in detail in chapter 5).

1.4 FACTORS AFFECTING THE PHASE INVESION

It is apparent from the literature that the following factors can influence phase inversion in nSOW systems:

(i) Type of oil,
(ii) Type of surfactant,
(iii) Surfactant concentration,
(iv) Temperature,
(v) Water to oil ratio,
(vi) Additives in the oil and water phases,
(vii) The presence of alcohols,
(viii) Mixing conditions,
(ix) Rate and order of component additions.

Factors (i) to (vii) affect the surfactant's affinity and factors (viii) and (ix) are dynamic variables. Dynamic variables will be studied in detail in chapters 4, 5 and 6. Various techniques and concepts have been used to correlate surfactant affinity variables and hence, the emulsion type, these are described in chronological order below:

1.4.1 Hydrophile-Lipophile Balance (HLB)

Full descriptions of the HLB concept are given by Becher (1966) and Becher and Schick (1987). Griffin (1949) first defined the affinity of a nonionic surfactant in terms of an empirical quantity - the hydrophile-lipophile-balance (HLB). Surfactants are assigned a HLB number at 25°C on a scale of 1 to 20, where, low HLB numbers represent lipophilic surfactants and high HLB numbers hydrophilic surfactants. Generally, the application of a surfactant can be derived from its HLB number in accordance with table 1.1.

TABLE 1.1 - Application of surfactants based on HLB number.

HLB number range	Application
3 - 6	W/O emulsifier
7 - 9	Wetting agent
8 - 18	O/W emulsifier
13 - 15	Detergent
15 - 18	Solubiliser

HLB numbers are calculated for a surfactant from simple formulae based either on analytical or composition data.

Examples:

For poloxyethylenenonylphenylethers (NPE) HLB=E/5
where, E = the wt% of polyoxyethylene in the surfactant
NPE12 (12 oxyethylene groups in the hydrophilic chain) HLB=14.2.

For a polyhydric fatty acid ester, HLB=20(1-S/A)
where, S = Saponification number of the ester, A = acid number of the fatty acid
Polyoxyethylene(20)sodiummonolaurate (Tween 20), S=45.5, A=276, HLB=16.7

Attempts have been made to assign HLB numbers to various oils for which surfactants will produce the most stable emulsion; these are called the required HLB of the oil (see Table 1.2).

TABLE 1.2 - Required HLB numbers of various oils.

OIL	W/O emulsion	O/W emulsion
Paraffin oil	4	10
cyclohexane		15
Toluene		15

However, it is well recognized that the HLB concept is limited; many researchers have found no correlation between emulsion type and HLB number, also, changes in emulsion type have been found with water to oil ratio, surfactant concentration and temperature. The HLB concepts main failing stems from the fact that it does not allow surfactants to have different affinities for different oils. In a move to incorporating oil type, Graciaa (1989) showed that it was the HLB of the interfacial surfactant, rather than the overall

system HLB, that is the important affinity variable. This observation was made from the results of a model that describes the partitioning of surfactant between oil, water and an interfacial surfactant phase (this will be discussed in detail in chapter 3).

1.4.2 Phase Inversion Temperature (PIT) or HLB Temperature

(i) Effect of Oil Type

Nonionic surfactants (unlike ionic) become increasingly more lipophilic at elevated temperatures. The change in nSOW phase behaviour with temperature can bring about a phase inversion. The phase inversion takes place when the system is three phase (surfactant affinity balanced) and the temperature at inversion is known as the phase inversion temperature (Shinoda 1986).

Shinoda (1986) has shown that HLB is a function of temperature using a number of different oils (see figure 1.6). HLB numbers have been assigned to surfactants by measuring the PIT of an emulsion containing the surfactant and checking this against a PIT vs HLB calibration curve. Generally, HLB numbers derived from PIT measurements differ from formulae values by <2 HLB numbers.

From figure 1.6 it can be seen a general rule applies, that for any oil, the higher the HLB of a surfactant the higher the PIT will be. Shinoda (1986) also found that the solubility of a nonionic surfactant in a particular oil was inversely proportional to the PIT.

(ii) Phase Volume Ratio

The effect of the phase volume ratio of emulsions on the PIT depends on the kind of oil, the concentration of surfactant (Shinoda 1986) and the distribution of the polyoxyethylene chain lengths of the surfactant (Mitsui 1970).

In the case of nonpolar and saturated oils with surfactant concentrations >5%, the PIT has been shown to be reasonably constant for a wide range of phase volume ratios (see figure 1.7). However, Shinoda (1986) describes the behaviour of aromatic hydrocarbons and polar oils as "abnormal" and shows that phase volume ratio has a marked affect on the PIT (see figure 1.8). The PIT was also affected by the "way of shaking" in these cases.

Shinoda (1986) showed that the PIT does not vary significantly with phase ratio, in nonpolar oil systems, with surfactant concentration >5wt%, but does change in dilute solution (below 3wt%), see figure 1.9. Shinoda explains the variation of PIT with surfactant concentration as follows: "The saturation concentrations of nonionic homologues in water are all very small, but those in hydrocarbon are much larger and

depend largely on the ethyleneoxide chain length. Lipophilic homologues (shorter chain length) dissolve better than hydrophilic homologues in the oil phase. Hence, there will be a selection of more hydrophilic surfactant to be adsorbed at the oil/water interface. This effect is amplified in dilute solutions and when the volume fraction of oil is large". The nature of surfactant partitioning will be discussed in detail in chapter 3.

(iii) Surfactant Mixtures

In the HLB system it has been generally assumed that the HLB of a mixture of surfactants is the algebraic sum of the HLB of the individual surfactants. There is evidence that more stable emulsions are produced when a blend of surfactants is used (Shinoda 1986). PIT data indicate that when the difference of HLB of the surfactants in a blend is small, the surfactant mixture HLB is approximately that of the weight average HLB, however, this was not the case for blends of surfactants with large differences in HLB (see figure 1.10).

(iv) The Effect of Additives in the Water and Oil Phases

Water Phase

The PIT has been shown to vary with the amount and chemical type of additives in the water phase (see figure 1.11).

Oil Phase Mixtures

The PIT of emulsions in which the oil phase is a mixture of oils was found to be expressed by the volume average of the PITs of the respective oils (see Figure 1.12).

$$PIT_{mix} = \Sigma v_i PIT_i$$

where, v_i = volume fraction of oil i in the mixture,

PIT_i = PIT of oil i (°C).

Additives - Fatty Acids and Alcohols

The effect of added fatty acids and alcohols on 1:1 volume ratio paraffin/water systems is shown in figure 1.13. The effect on PIT was found to be similar regardless of the chain length of the acid or alcohol.

(v) Other Studies

Shinoda et al's studies refer almost exclusively to oil/water systems containing polyoxyethylenenonylphenylether (NPE) surfactants. However, other researchers have used different surfactant types and some have found different trends from those shown

by Shinoda eg. Parkinson and Sherman (1972) who used Tween-Span blends and found that a maximum PIT occurred at a HLB corresponding to maximum stability (see figure 1.14).

1.4.3 Emulsion Inversion Point (EIP)

Much of Emulsion Inversion Point (EIP) work is due to Marszall; the concept and results are reviewed in Marszall (1987). The EIP is related to the inversion of W/O emulsions to O/W emulsions at constant temperature. The experimental method is described below:

50 ml of oil is placed in a 250 ml beaker and surfactant dissolved/dispersed in it (2 wt%). The aqueous phase is then added in 1 ml aliquots. The system is agitated by a 6000 rpm turbine blender for 15 s on each addition and the emulsion type determined. A plot of EIP vs HLB is made where:

$$\text{EIP} = \frac{\text{volume of aqueous phase at inversion}}{\text{volume of oil phase}}$$

The EIP tends to decrease with increasing HLB of the surfactant until a minimum is observed, the value of the HLB at the minimum is the required HLB of the oil to produce an emulsion with maximum stability (Chand 1980). Figure 1.15 is a typical EIP diagram. However, Marszall has noted that the exact position of the EIP minimum can be affected by the agitation conditions.

Marszall (1987) discusses the events occurring in an EIP experiment in terms of the changes in the interface. It is argued that initially the interface is concave relative to water (W/O emulsion), hence, Winsor R>1. At the EIP it is proposed that the hydrophile-lipophile nature of the surfactant is balanced (R=1) and once the EIP has been passed R<1, giving a concave interface relative to oil (O/W emulsion).

The findings of EIP experiments are summarised below:

(i) At the EIP minimum the inversion W/O to O/W occurs and produces emulsions with very small drops.
(ii) The EIP increases with increasing concentration of lipophilic surfactant, whereas, the EIP decreases with increasing concentration of the hydrophilic surfactant.
(iii) In a series of alkanes the higher the EIP the lower the required HLB.
(iv) Highest viscosity and minimum surface tension occur at the EIP.
(v) For aromatic hydrocarbons with increasing methyl group substitutions, the EIP and

required HLB value decrease (PIT increases) (Marszall 1985).
(vi) EIP has been demonstrated to show accurately changes in the required HLB of an oil brought about by the addition of additives eg. polyethylene glycol (Marszall 1977a) and alcohols (Marszall 1977b).

1.4.4 Equilibrium Water-Oil-Ratio (WOR) Maps

Salager in a series of papers (1982), (1983a), (1983b), (1991), Anton(1986), Minana-Perez(1986), develops the work of Shinoda further. He reviews his work in Salager (1988).

Formulation Variables

Salager points to the following formulation variables which are capable of changing the surfactant's affinity for oil and water:

(i) The salinity of the aqueous phase (expressed as wt% salt in aqueous solution). With increasing salt concentration the nSOW phase behaviour moves from Type 1 to Type 3 to Type 2.

(ii) The surfactant HLB, where increasing HLB results in the phase transitions Type 2 to Type 3 to Type 1.

(iii) Temperature, where increasing temperature results in the phase transitions Type 1 to Type 3 to Type 2 (note, Shinoda et al's PIT work).

(iv) The addition of alcohols, which cause the transition Type 1 to Type 3 to Type 2 with increasing concentration.

(v) The nature of the oil. This was expressed as, ACN - alkane carbon number for alkanes and EACN - equivalent alkane carbon number for non-alkanes. The system was derived as follows:

Many researchers have shown there to be a direct relationship for increasing carbon number in a homologous series of hydrocarbons with PIT (see figure 1.16). By measuring the interfacial tension between an aqueous phase and alkanes, Cash et al (1977), developed a calibration curve (interfacial tension vs alkane carbon number), then by mixing various hydrocarbons with alkanes and measuring the interfacial tension, an EACN could be given to the mixture and hence, to the hydrocarbon. They showed that by using molar mixing rules a range of EACN numbers could be produced. It was also shown that parts of molecules had specific EACN:

eg. phenyl group, EACN=0 (each CH_3 addition=1)
cyclohexyl group, EACN=4.

An increase in EACN results in the phase behaviour transition Type 2 to Type 3 to Type 1.

Bi-Dimensional Scanning Procedure

To scan the effect of each of the above variables an equilibrium technique was used by Salager et al (1983b):

nSOW samples with a set water volume fraction (f_w) and surfactant concentration, were made up progressively changing one of the formulation variables. The samples were allowed to come to equilibrium over a 48 hour period without emulsifying. The phase behaviour was then noted (2-phase, 3-phase). The sample was emulsified with a turbine blender (set time and speed) and the emulsion type determined. Figure 1.17 shows the result of a bidimensional scan using salinity as the formulation variable. The diagram is a map of emulsion type, nSOW phase behaviour and an inversion locus.

Optimum Formulation

It has been found that ultra-low interfacial tension is associated with three phase behaviour. This condition enables the production of very fine emulsions with low energy input (as will be shown in chapter 5). It is also of interest for enhanced oil recovery processes because ultra-low interfacial tension offsets the capillary forces which maintain the residual oil trapped in the porous matrix of a reservoir (Salager 1988). Maximum oil recovery is obtained in the 3-phase region, hence, 3-phase systems have been termed "optimum formulations".

Attempts have been made to correlate formulation variables with the optimum formulation eg. Bourrel and Salager (1980) for ethoxylated nonionic surfactants:

$$\alpha - EON - kEACN + mA_i + bS + C_t(T-28) = 0 \qquad [1.2]$$

where, α depends on the lipophilic group of the surfactant,

EON = average number of ethyleneoxide groups per surfactant molecule,

A_i = alcohol concentration,

S = salinity of the aqueous phase,

T = temperature.

m and b are parameters depending on the type of alcohol and electrolyte and k and C_t are constants.

Therefore, the optimum formulation may be written as a linear relationship between formulation variables:

$$SAD = \Sigma D_i E_i \quad \text{[1.3]}$$

where, D_i = *formulation coefficient*

E_i = formulation variable,

SAD = surfactant affinity difference, which relates to the nSOW phase behaviour:

SAD<0 Type 1 phase behaviour (termed SAD-),

SAD>0 Type 2 phase behaviour (termed SAD+),

SAD=0 Type 3 phase behaviour.

SAD represents the same concept as the Winsor R, but it is expressed in terms which are experimentally obtainable and is therefore, more useful for practical applications. Salager uses SAD plus optimum formulation in a schematic diagram which describes all equilibrium emulsion types.

Schematic WOR Map (see figure 1.18)

The bidimensional map is divided into 6 regions by the optimum formulation (SAD=0) line and the inversion locus:

(1) For positive SAD, phase behaviour at equilibrium is Type 2 and according to Bancroft's rule a W/O emulsion is expected. This is true in regions B^+ and A^+, however, in region C^+ an "abnormal" O/W emulsion is produced because the volume of oil is too small to make it the continuous phase. The abnormal C^+ emulsions are often W/O/W type, which is a way in which Bancroft's rule is partially satisfied.

(2) For negative SAD the nSOW phase behaviour is Type 1. A^- and C^- are O/W emulsion regions and B^- is an "abnormal" W/O emulsion region.

(3) Emulsion stability is closely related to the region boundaries; normal A^+, B^+ (W/O emulsion) and A^-, C^- (O/W emulsion) regions are found to be relatively stable, with increasing stability (at a constant SAD) approaching the A^+/C^+ or A^-/B^- limit ie. with increasing disperse phase fraction. Stability decreases from both sides as the A^+/A^- boundary is approached ie. near the 3-phase region. It is found that abnormal (B^-, C^+) emulsions break readily.

(4) The viscosity of emulsions in the A^+, A^- regions far from SAD=0 are high with respect to their external phase, however, close to SAD=0 in the MOW region, the emulsion viscosity is extremely low, probably because of the low interfacial tension, which allows easy deformation of droplets along the stream lines. Abnormal emulsions have low internal phase ratio and exhibit viscosities similar to their external phase.

However, real systems can show large deviations from the schematic WOR map:

Factors Affecting the Inversion Locus

The central A^+/A^- boundary depends on the position of the optimum formulation transition, however, it does not always correspond to a straight line crossing the 3-phase region. In systems which exhibit wide 3-phase regions (vertically) and a narrow A region (horizontally) there is no neat plateau.

The position of the lateral branches of the inversion locus may depend on surfactant type and alcohol formulation. The oil viscosity may also alter and shift the locus (see figure 1.19),

Salager also notes that increase in mechanical energy input during emulsification can widen the A region. This indicates the importance of using a set procedure when determining WOR maps, even when using pre-equilibrated samples.

However, Salager states that most industrial applications involve non-equilibrium systems (steady addition of dispersed phase until inversion), Salager (1988) discusses the problem of relating dynamic inversion with equilibrium systems using WOR maps and introduces the concept of apparent equilibrium time.

Apparent Equilibrium Time and Dynamic Inversion

In Salager (1988), two experiments are discussed which concern dynamic inversions:

(1) The first considered the minimum contact time between phases before emulsification so that the resulting emulsion was indiscernable from an equilibrium system. He terms this contact time, "apparent equilibrium time" and concluded that the equilibrium time decreases as SAD$\rightarrow$0 and that it is essentially zero for some near optimum formulations.

(2) The second study tried to mimic actual processes by starting with an emulsion produced from a pre-equilibrated mixture and shifting its position on the WOR map eg. By changing temperature, or by changing its WOR at constant SAD. A shift across the inversion locus is a dynamic inversion. The results are schematically shown on figure 1.20.

The arrows on figure 1.20 show the direction of change of WOR or SAD for each inversion. The dynamic inversion due to SAD change through the A^+/A^- boundary occurs at the same point regardless of the direction of change ie. this inversion is reversible. On the other hand, the dynamic inversions due to change in WOR induced by addition of dispersed phase under agitation, show hysterisis effects ie. inversion O/W to W/O occurs at a different WOR to inversion from W/O to O/W. Therefore, the emulsion type in the shaded zone is dependent on its history. Note the hysterisis zone widens as SAD moves further from SAD=0. Hysterisis effects have also been noted by Becher (1966) for nSOW systems.

This leads to the observation that there are two inversion types:

I TRANSITIONAL

The inversion across SAD=0 is continuous from W/O to MOW to O/W and is induced by altering the surfactant's affinity, which alters the nSOW system phase behaviour.

II CATASTROPHIC

Inversion across A^+/C^+ and A^-/B^- boundaries, is a catastrophic change from W/O to O/W and O/W to W/O respectively. Inversions of this type are induced by altering the system's WOR.

This completes the review of nSOW phase behaviour and phase inversion literature. Chapter 2, will describe the development of dynamic inversion maps derived in this study as an experimental framework.

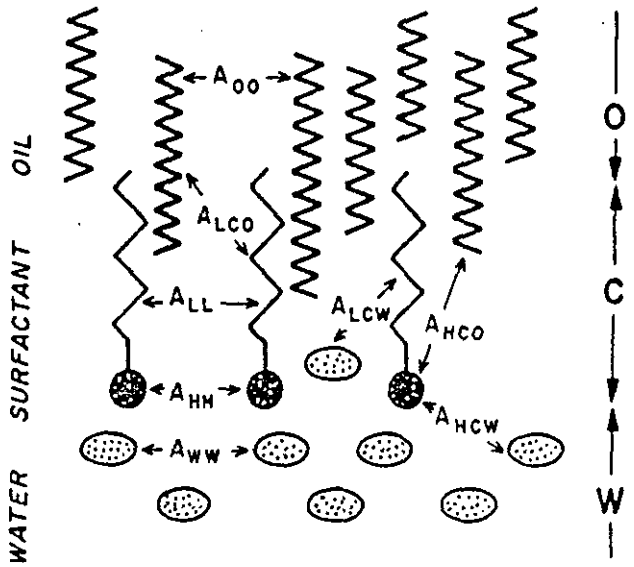

FIGURE 1.1 - Interactions according to the Winsor model (Salager 1988)

Notation

C adsorbed surfactant layer

O oil phase

W water phase

H surfactant hydrophilic group

L surfactant lipophilic group

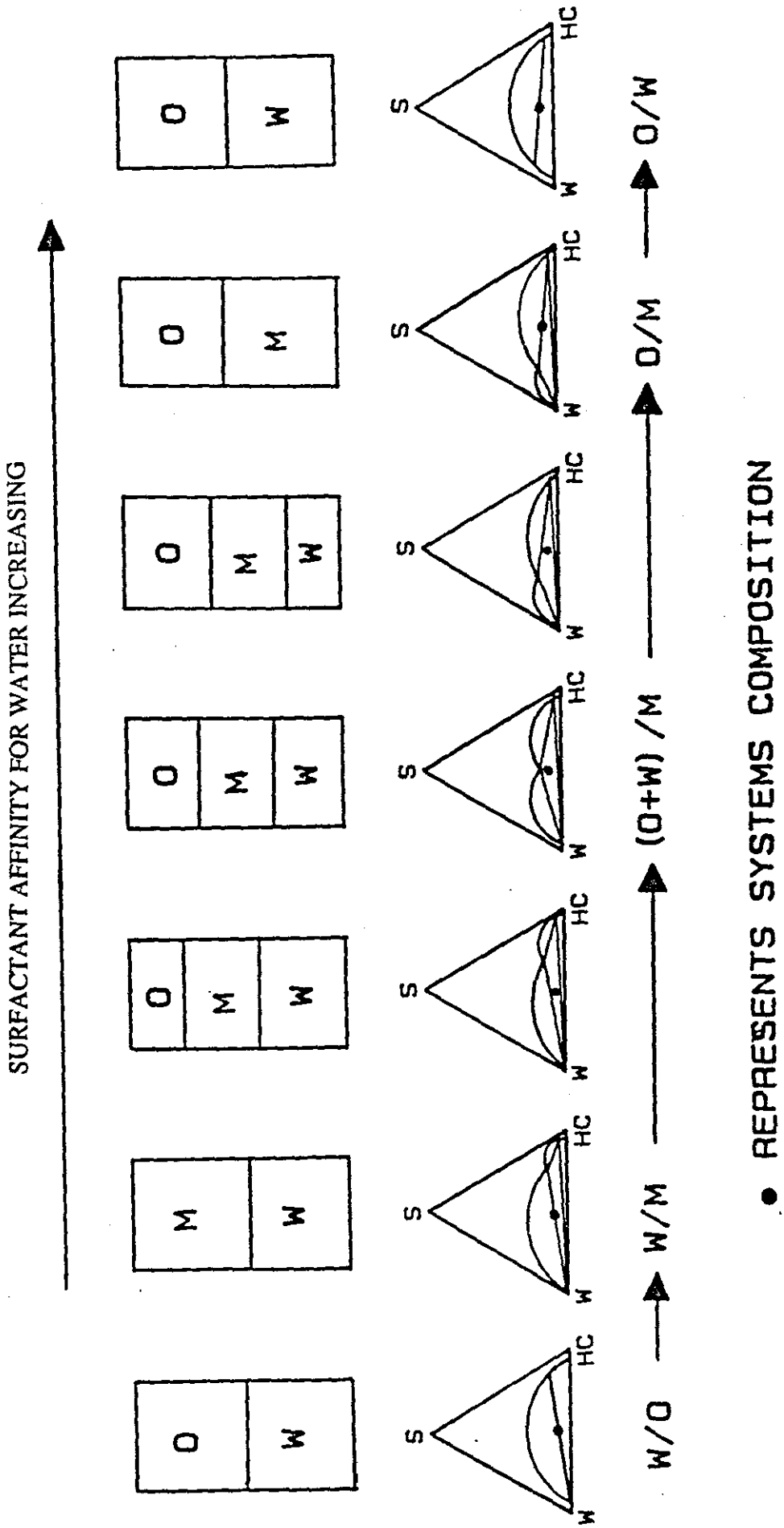

FIGURE 1.2 - Schematic representation of the change in nSOW phase behaviour with surfactant affinity

FIGURE 1.3 - Schematic illustration of the structure of a surfactant phase. Black and white stripes represent water and oil layers bound between surfactant monomers (Shinoda 1986).

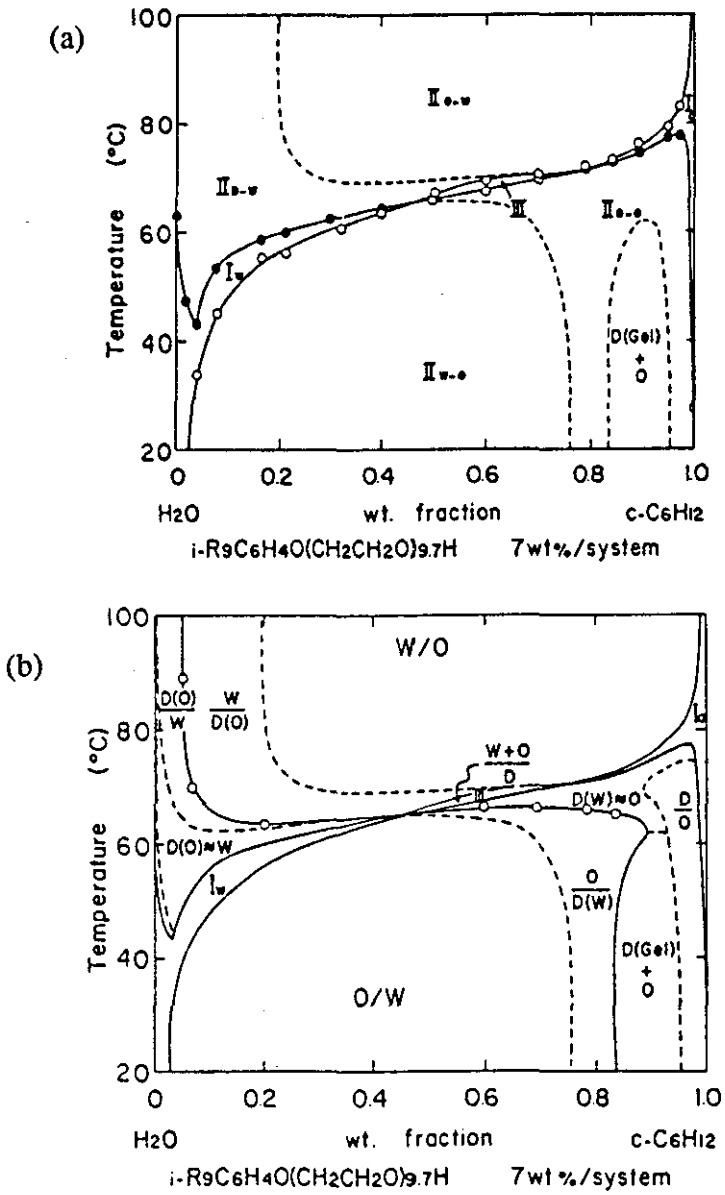

FIGURE 1.4 - Change in phase behaviour (a) and emulsion type (b), with temperature - water - cyclohexane - polyoxyethylenenonylphenylether (NPE) system (Shinoda 1986).

Notation

I_w aqueous micellar solution with solubilised oil

I_o oleic micellar solution with solubilised water

III 3 phase region

II_{D-o} two phase region of surfactant phase and oil

II_{D-w} two phase region of surfactant phase and water

II_{o-w} surfactant rich water phase plus oil

II_{w-o} surfactant rich oil phase plus water

D(gel)+O a liquid crystal phase

(a) (b)

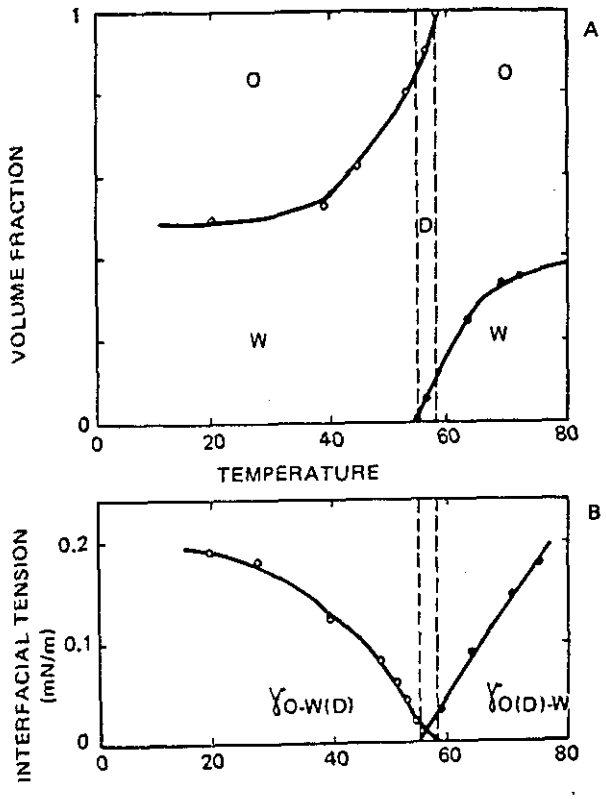

FIGURE 1.5 - Effect of temperature on the volume fractions of water and oil and surfactant phases and, the interfacial tension between these phases. The system is composed of 5wt%NPE(8.6) - (chain length=8.6 oxyethylene units), 47.5wt% water and 47.5wt% cyclohexane (Saito 1970).

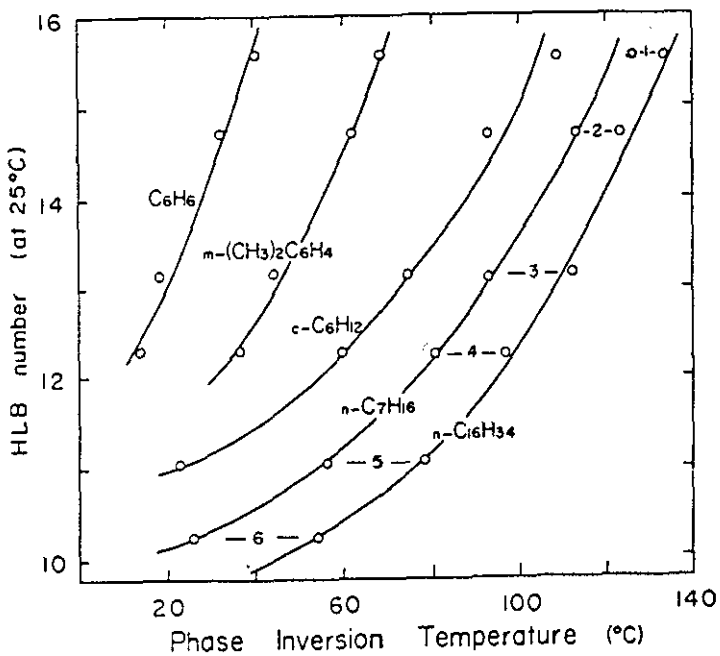

FIGURE 1.6 - The correlation between HLB numbers and the PITs in various oil/water (1:1) emulsions stabilised with nonionic surfactants (1.5wt%) (Shinoda 1986).

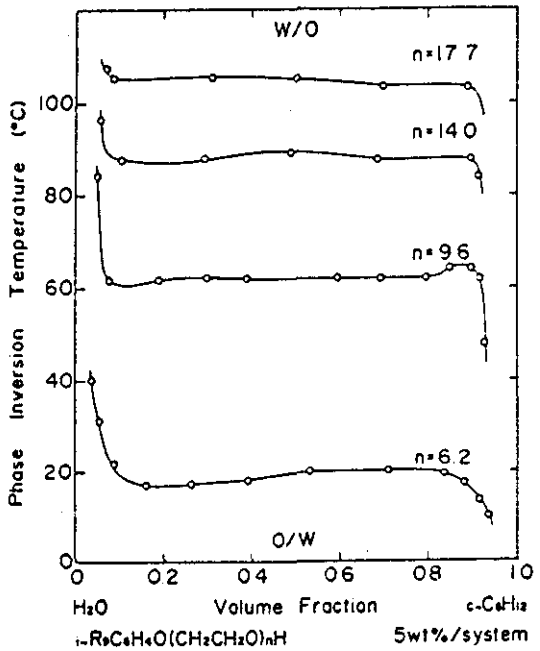

FIGURE 1.7 - The effects of the hydrophilic chain length of nonionic surfactants on the PIT versus phase volume curves of cyclohexane/water emulsions (Shinoda 1986).

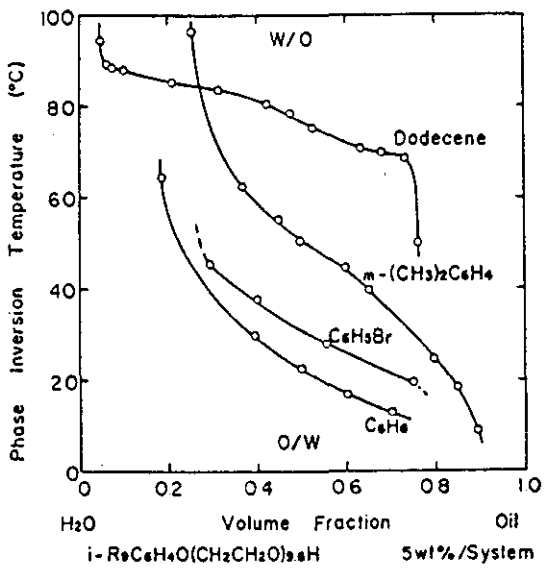

FIGURE 1.8 - The effect of phase volume on the PIT of emulsions stabilised with NPE(9.6) 5wt% (Shinoda 1986).

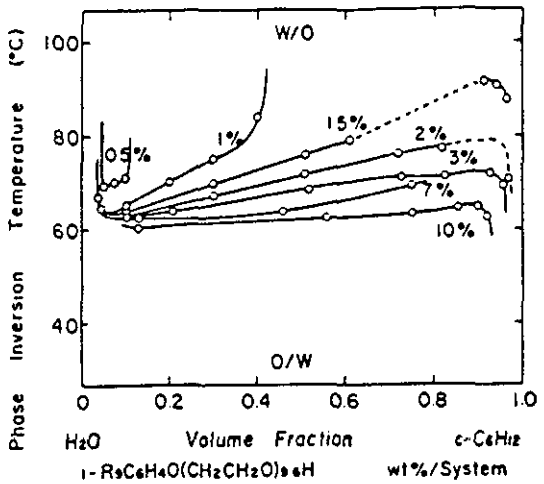

FIGURE 1.9 - The effect of surfactant concentration on the PIT versus phase volume curve (Shinoda 1986).

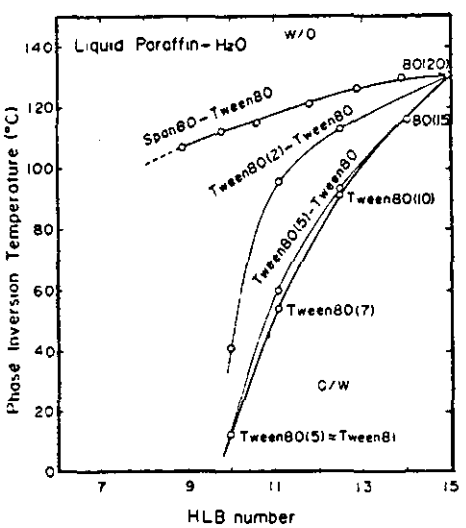

FIGURE 1.10 - The PIT in emulsions composed of water/paraffin (1:1 wt ratio) containing 2wt% of polyoxyethylene(N) sorbitan monooleates and their mixtures (Shinoda 1986).

Surfactant	HLB
Tween 80(20)	15
Tween 80(15)	14
Tween 80(10)	12.3
Tween 80(7)	11.1
Tween 80(5)	10
Tween 80(2)	7.2
Span 80(0)	4.4

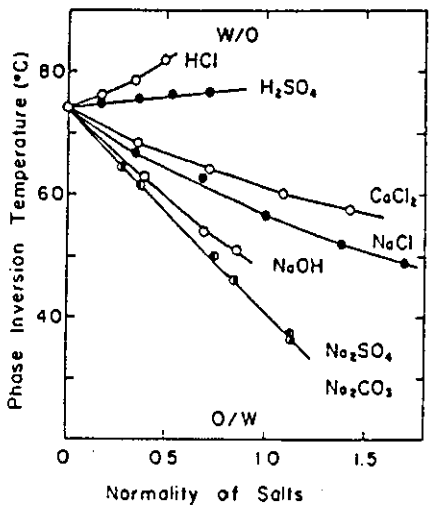

FIGURE 1.11 - The effect of added salts, acid and alkali on the PIT of a cyclohexane/water emulsion (1:1 volume ratio) containing 3wt% NPE9.7 in water (Shinoda 1986).

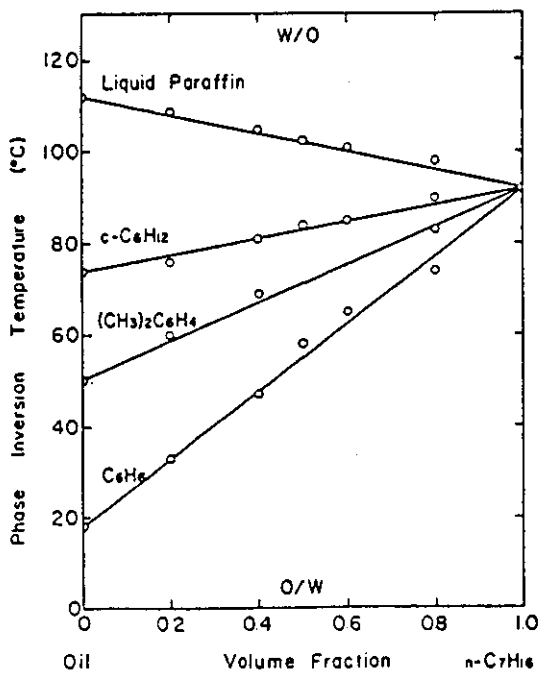

FIGURE 1.12 - The effect of mixing n-heptane with various oils on the PITs of emulsions stabilised with NPE9.6 (1.5wt%) (Shinoda 1986).

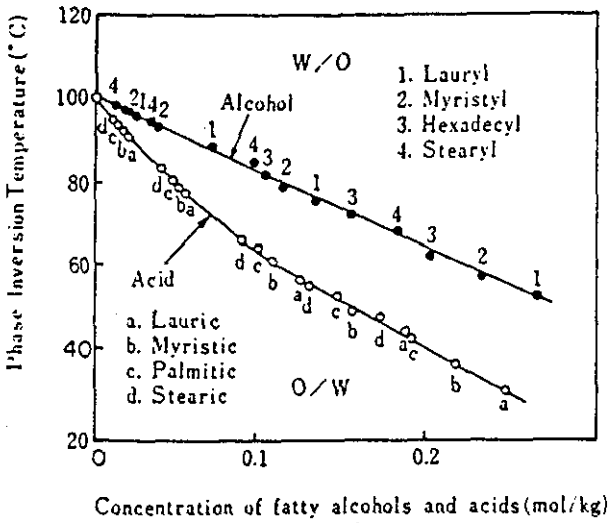

FIGURE 1.13 - The effect of added fatty acids and alcohols on the PIT of (1:1 wt ratio) paraffin/water 3wt% NPE6.3.

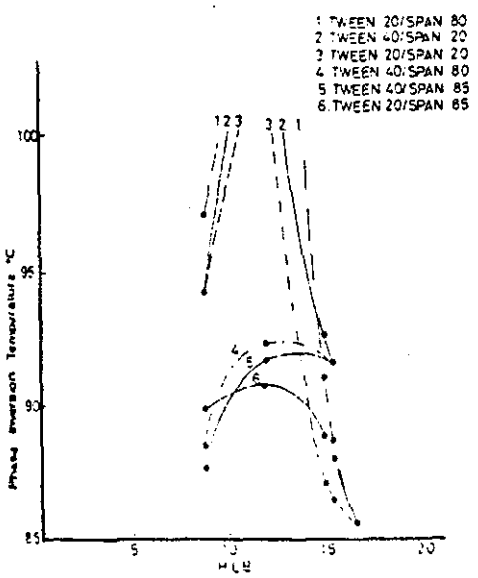

FIGURE 1.14 - The PIT of emulsions stabilised by Tween-Span surfactants (Parkinson 1972).

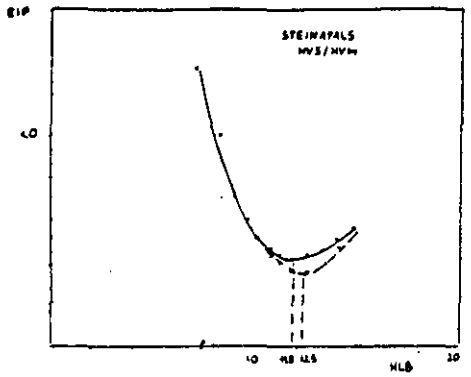

FIGURE 1.15 - EIP as a function of HLB for a mixture of NPE3 and NPE14 surfactants. ——— all surfactant initially in oil and ------ NPE14 initially in water (Marszall 1975).

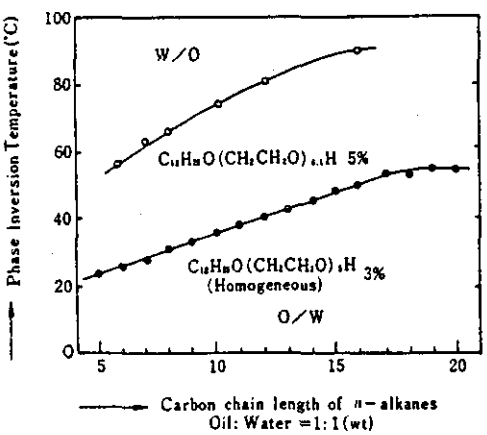

FIGURE 1.16 - The correlation between the hydrocarbon chain length of n-alkanes and the PIT (Shinoda 1986).

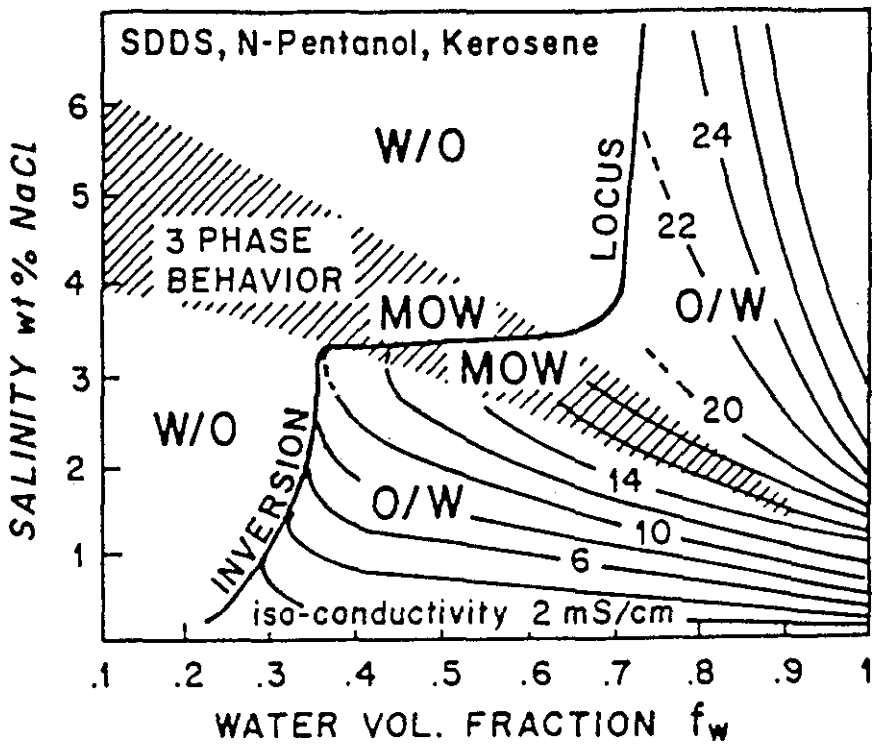

FIGURE 1.17 - Bidimensional formulation/WOR map showing the nSOW phase behaviour, the inversion locus and the emulsion types in each region (Salager 1983b).

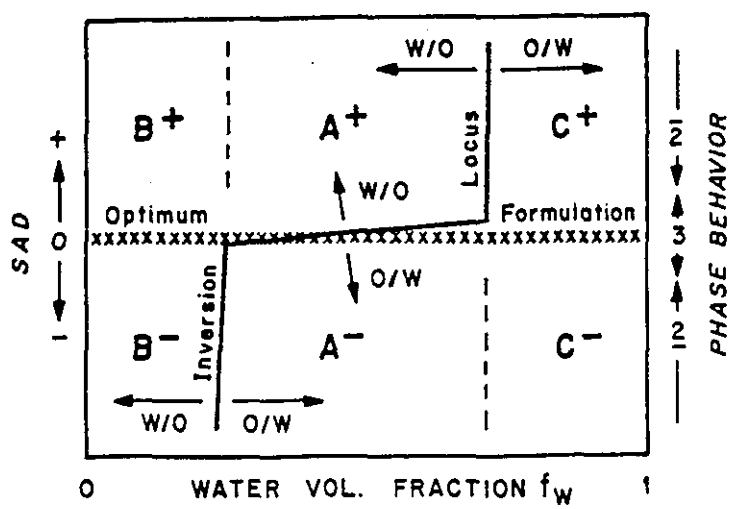

FIGURE 1.18 - Schematic WOR map showing the inversion locus and the different emulsion type regions (Salager 1983b).

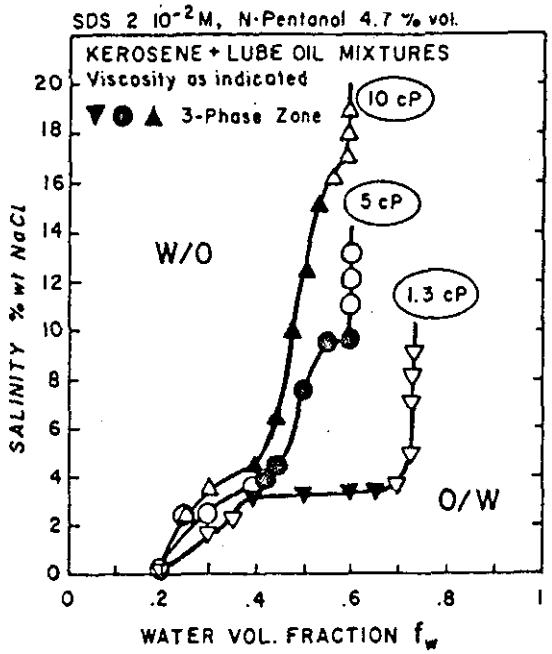

FIGURE 1.19 - Affect of the oil phase viscosity on the inversion locus (Salager 1983b). As the oil viscosity increases the A^+/C^+ boundary shifts to lower values of f_w, while the A^-/B^- boundary remains unaltered.

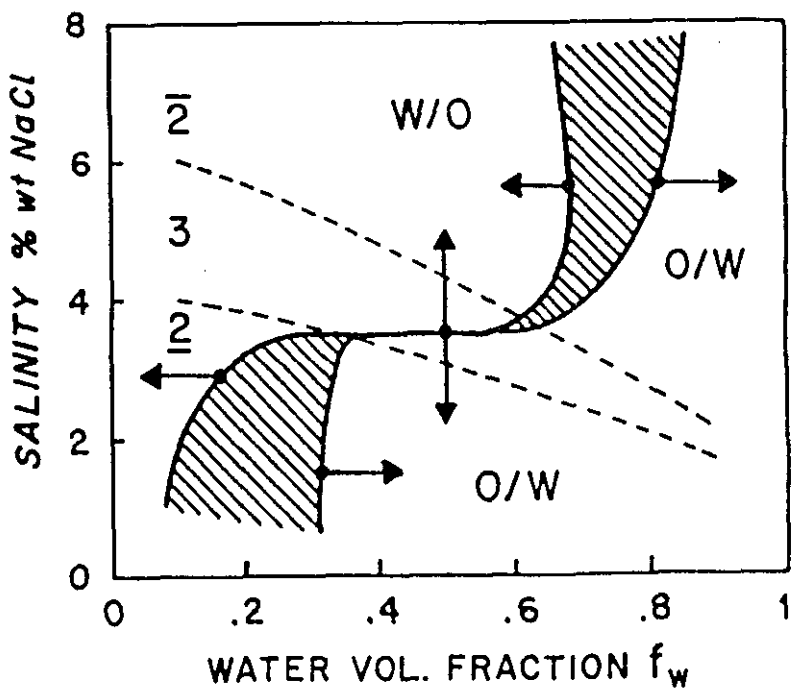

FIGURE 1.20 - Dynamic inversion locus showing the hysterisis zones (shaded). The arrows indicate the direction of change (Salager 1988).

CHAPTER 2
DYNAMIC INVERSION MAPS

2.1 INTRODUCTION

The literature review of chapter 1 highlights the fact that phase inversion of emulsions of nSOW systems is closely related to the system's phase behaviour. nSOW phase behaviour is dependent on the surfactant's affinity for the oil and water phases. Dynamic inversions can be brought about by changing either the surfactant's affinity, or the system's WOR. Hence, in order to predict the effect of a dynamic composition change on a system, a "dynamic inversion map" relating surfactant affinity and WOR has been devised here. The map will be used as an experimental framework for the drop size studies of chapters 5 and 6.

Notation

Depending on the surfactant's affinity, nSOW phase behaviour can be Type 1, Type 2 or Type 3. The water phase of a Type 1 system (which contains surfactant micelles) has quite different properties from a Type 3 or Type 2 water phase. Differences in behaviour of Type 1 water phases with surfactant concentration $>CMC_w$ and $<CMC_w$ are also seen. Hence, in the course of the work which is presented here, we have found the usual emulsion terminology (O/W or W/O) to be inadequate for describing all emulsion types because it does not indicate the surfactant's affinity. Also, no set notation exists for describing the microemulsion phases (surfactant phase) of Type 3 systems. Therefore, a simple notation was devised. For all three Winsor systems, O will denote oil containing surfactant at a concentration $<CMC_o$ and W will denote water containing surfactant at a concentration $<CMC_w$. For Type 1 and Type 2 systems the micelle-containing phase is given the suffix m. Bancroft (1913) stated that "a hydrophile colloid will tend to make water the dispersing phase while a hydrophobe colloid will tend to make water the disperse phase." Experience from the present study has shown that, for Bancroft's rule to be obeyed, the surfactant must be capable of producing a stable emulsion and that micelles must be present (this fact will help explain some "abnormal" results discussed by other workers - see discussion of this chapter). Therefore, agitation of Type 1 mixtures is expected to produce O/W_m (oil-in-water) emulsions whereas Type 2 is expected to produce W/O_m (water-in-oil) emulsions. For Type 3 systems 1, 2 or 3 phases can be present:

(i) a surfactant microemulsion M_s,

(ii) an oil phase containing surfactant monomers at CMC_o and an aqueous microemulsion M_w,

(iii) a water phase containing surfactant monomers at CMC_w *and an oleic* microemulsion M_o,

(iv) a water phase containing surfactant monomers at CMC_w, an oil phase containing surfactant monomers at CMC_o and a surfactant phase M_s.

The M_w notation is provided to differentiate between a Type 3 aqueous microemulsion phase and a Type 1 aqueous micellar phase (W_m). Similarly, the M_o notation is provided to differentiate between a Type 3 oleic microemulsion phase and a Type 2 oleic micellar phase (O_m). Note, a M_w phase can contain more oil than water despite the M_w phase being the water phase.

Characterisation of Phase Inversion

There are many apparent contradictions to be found in phase inversion literature. Some of these contradictions have been explained by Salager's observation that there are two types of phase inversion - Transitional inversion induced by changing the nSOW phase behaviour and Catastrophic inversion induced by changing the system's WOR. In Salager's SAD-WOR equilibrium map technique, surfactant affinity (and nSOW phase behaviour) is plotted against the volume fraction of water. Surfactant-Affinity-Difference (SAD) was used to describe phase behaviour types - see chapter 1). Therefore, a SAD vs WOR map provides a good framework for studying dynamic phase inversions because the variables connecting both inversion types are included in the map.

Shinoda et al's PIT work and Marszall's EIP work are studies of dynamic inversions. PIT inversions (induced by change in temperature altering the surfactant affinity) can now be seen to be transitional inversions, while EIP inversions (induced by adding dispersed water phase to a continuous oil phase) are dynamic catastrophic inversions.

WOR maps are limited to examining one surfactant concentration per map. Phase behaviour changes with composition in three phase systems are usually represented on triangular diagrams (these have been used for surfactant-oil-water systems by Smith(1985) and (1990)). However, triangular diagrams can only apply to nSOW systems when the surfactant is a single species. When commercial distributed nonionic surfactants are used (or the surfactant is made up from a mixture of surfactants), triangular diagrams are inappropriate because the surfactant's affinity depends on the HLB of the interfacial surfactant, not on the overall weight-average HLB (this will be discussed in detail in chapter 3). In the case of a distributed surfactant, the HLB of the interfacial

surfactant varies with WOR and with surfactant concentration. Hence, the construction of a meaningful triangular phase diagram (which can only show one surfactant affinity condition) is impossible with mixed surfactants.

In chapter 3 it will be shown how the effect of surfactant concentration on the WOR map phase behaviour can be eliminated (so that the map is the same for all surfactant concentrations >CMC), by refering to the affinity of the interfacial surfactant only.

In order to construct a WOR map Salager et al (1983) checked the phase behaviour of pre-equilibrated mixtures (at known WOR and SAD) before emulsification. After emulsification, emulsion type was determined by electrical conductivity. Salager noted that large deviations from the generalised WOR map could occur. In the work reported here, reasons for such deviations will be explored and it will be shown that, when non-ionic surfactants are used, the sequence of events can have important effects on observed behaviour. This will lead to the development of "Dynamic Inversion Maps"

2.2 EXPERIMENTAL

2.2.1 Experimental procedures

To examine the effect of oil type on phase inversion, a number of different hydrocarbon oil phases were used:

The oil phase was either toluene, cyclohexane or n-heptane. These were Standard Laboratory Grade reagents supplied by Fisons. The aqueous phase was distilled water which contained 0.5% potassium chloride (to enhance electrical conductivity). Pairs of surfactants were used to prepare mixtures with a range of HLB values. It should be noted that, although HLB is used in presenting the results which follow, the weight fraction of either surfactant could have been used equally well. In accordance with accepted practice, HLB values are used for convenience with a particular system; they are not meant to be used for comparing different systems. The mixtures were made either from surfactants based on polyoxyethylenenonylphenylether (NPE) or from surfactants containing polyoxyethylenesorbitanmonolaurate (SML). In the first group were NPE2 - Igepal co210®(HLB 4.6), NPE5 - Igepal co520® (HLB 10.0) and NPE12 - Igepal co720® (HLB 14.2). In the second group were Span 20® (HLB 8.6), Tween 21® (HLB 13.3) and Tween 20® (HLB 16.7). These materials were supplied by Aldrich and Sigma Chemical Company respectively. In subsequent discussion the hydrocarbons will be referred to as "oil".

Phase inversions were induced either by varying surfactant compositions (to alter the HLB) or by changing phase ratios. Thus all experiments could be carried out at room temperature (20°C). During inversion, all mixtures were located in an unbaffled, dished glass vessel (diameter 10 cm capacity 0.75 dm^3). A 4-cm diameter propeller was used for agitation. The stirrer speed was set at 500 rpm in all the experiments of this chapter unless stated otherwise. A more detailed examination of the effects of agitation conditions are given in chapters 5 and 6. Changes in continuous phase from non-aqueous to aqueous (or vice-versa) were detected by changes in electrical conductivity (the water phase conductivity >> oil phase conductivity).

2.2.2 Choice of SAD variable

The surfactant HLB was chosen as the SAD variable in this study because, unlike other surfactant affinity variables, in this case:

(i) The surfactant affinity is varied by altering the surfactant only,

(ii) the surfactant affinity can be altered isothermally.

Hence, the oil and water phases remain physically unchanged with variation of surfactant affinity and therefore, their physical properties (eg. CMC_w, CMC_o) remain unaltered. This has advantages for comparing different oil-water systems containing the same surfactant type (see chapter 3).

2.2.3 Transitional inversions in Type 3 systems

A standardised procedure was used to construct inversion maps. For each system (water, oil and surfactant type) a suitable pair of lipophilic and hydrophilic surfactants was chosen and a titration process was used to locate accurately the transitional inversion line (where SAD = 0). A water phase containing a known weight % of the hydrophilic surfactant was added to a W/O_m emulsion containing the same weight % of the lipophilic surfactant until phase inversion occurred. The value of f_w was noted and the HLB was calculated. Here, f_w is the volume fraction of the aqueous phase. Since the amount of surfactant is very small its contribution to values of f_w is neglected in subsequent discussion. In oil-water systems containing NPE surfactants, at any given value of f_w, the transitional inversion was usually found to be reversible. Hence, these inversions established the transitional inversion boundary in the system. However, in oil-water systems containing SML surfactants, transitional inversions could only be induced if the dispersed phase fraction (of the initial emulsion type) was greater than 0.7, at the transitional inversion point. Therefore, transitional inversions W/O_m to O/W_m could be used to locate points on the transitional inversion boundary at high values of f_w, and inversions O/W_m to W/O_m at low values of f_w.

In order to characterise the events which occurred during a transitional inversion, from SAD positive to SAD negative, a detailed study of phase behaviour was made using cyclohexane/NPE(2 wt%) with $f_w = 0.5$ at 22°C. After electrical conductivity had been measured, samples of the dispersions were allowed to settle for a month. When the HLB was <10 it was noted that the system showed Type 2 behaviour, the emulsion structure being W/O_m. As the HLB increased to 10.58, the oil phase solubilised a much larger volume of water and became cloudy; the system now Type 3 and the emulsion structure W/M_o. Over a narrow range of HLB values (<0.3) the mixture split into 3 phases O,W and M_s. It was noted that the electrical conductivity rose sharply when HLB values changed by 0.1 within this range but there was not a large step increase at a precise HLB value. Above HLB = 10.86, the mixture separated into a clear oil and a cloudy water phase (O/M_w). As the HLB was increased further to values >11.5, the water phase became clear; the phase behaviour was now Type 1 and the emulsion structure was O/W_m. The change in the settled phase volumes is shown schematically on figure 2.1, together with the notation introduced here and the possible emulsion structure before phase separation. Hence, the transitional inversion boundary (where SAD = 0) indicates an important division between types of phase behaviour on the inversion map. The system shows Type 3 phase behaviour close to the lines where SAD = 0, Type 2 behaviour when HLB values are lower than those required for SAD = 0 and Type 1 behaviour when HLB values are higher than those required for SAD = 0.

2.2.4 Catastrophic inversions in Type 2 and Type 1 systems

Investigation of phase changes by altering f_w at constant HLB (remote from SAD = 0) showed that the sequence of events was important. It was noted that addition of water to oil with SAD negative ("high" HLB) or addition of oil to water with SAD positive ("low" HLB) produced distinct phase inversions which could be detected easily by measuring changes in electrical conductivity. Note, in some catastrophic inversions, violent fluctuations in the electrical conductivity were seen near the inversion point, however, the electrical conductivity reached a stable value after a short period of agitation. The exact values of f_w required for these inversions were found to depend on agitation intensity and on phase addition rates during the mixing process. Therefore, a uniform procedure was used for changing f_w. In all experiments, separate oil and water phases were prepared so that each contained the same amount of a given surfactant mixture. One phase was put into the agitated vessel initially and the second phase was added in 5 cm^3 aliquots. In most experiments, these aliquots were added at 1 minute intervals with a stirrer speed of 500 rpm. In some cases, drops of the dispersed phase

(before inversion) contained very small drops of the continuous phase. e.g. a transition could be $W_m/O \rightarrow O/W_m/O \rightarrow O/W_m$. Photographs of this $O/W_m/O$ system are shown in figure 2.2.

When phase changes were induced by adding oil to water with SAD negative ("high" HLB) or by adding water to oil with SAD positive ("low" HLB) changes in electrical conductivity were not very sharp and transition points (at low f_w and high f_w respectively) were difficult to detect. In these cases, distinct phase inversion was not observed and complex mixtures were formed. For example, the addition of water to oil with SAD positive produced very large aqueous drops which contained very small oil drops within them. Volume fractions of the continuous phase were very low and the mixtures had a porridge-like consistency. For any given value of HLB, the phase change which resulted from the addition of oil to water and the phase change which resulted from the addition of water to oil occurred at different values of f_w.

The formation of drops with complex structure can facilitate inversions which are not expected with simple drops. At very low values of f_w, the formation of a continuous aqueous phase, in accordance with Bancroft's rule, may not occur because the volume of the oil phase is too large (this is equivalent to the B^- region on Salager's schematic SAD-WOR map, see figure 1.18). The exact minimum value of f_w that is required for a W_m/O emulsion to invert to a O/W_m emulsion may be less than 0.26 (at closest packing of oil drops) because drops may have a range of sizes or may be distorted from spherical. However, with a two-phase system the critical value of f_w is not expected to be much less than 0.2. Thus, with reference to figure 1.18, mixtures with compositions corresponding to the region B^- may be expected to form W_m/O dispersions. When such a mixture, e.g. water (f_w = 0.1), cyclohexane and NPE (2%) was agitated a W_m/O dispersion was actually obtained (the HLB was 14.2). However, on settling, a O/W_m dispersion sedimented underneath a clear cyclohexane layer. A further cycle of agitation and settling produced a larger lower layer (of O/W_m) and a smaller cyclohexane layer. Repeated cycles eventually produced a O/W_m dispersion. Microscopic examination of the O/W_m layer in the intermediate stages (after the first settling step) showed that the aqueous drops which were dispersed in the continuous hydrocarbon phase contained small drops of oil, as described above. Thus, the effective volume of the aqueous phase had been increased. Since the final volume fraction of the dispersed phase was so high (f_w=0.1), the drops could not be an assembly of uniform spheres. Prolonged agitation of the original W_m/O dispersion, without settling, produced no phase inversion - see note below. The sequence of events is shown in figure 2.3 and the drop structure is as shown figure 2.2.

Note: A cyclohexane/NPE12, W_m/O emulsion (f_w=0.2), was found to invert after 25 minutes constant agitation without the need for a agitation-sedimentation cycle, or the need to add more water phase. This suggests that $O/W_m/O$ drops were formed during agitation and that the continuous oil phase was gradually incorporated into the $O/W_m/O$ drops with time. Hence, a sufficient length of prolonged agitation time may not have been allowed in the f_w=0.1 emulsion case.

2.3 RESULTS

The dynamic inversion maps , for a number of nSOW systems, derived using the procedures described above are shown in figures 2.4 to 2.9. Inversion point data are given in tables A2.1 to A2.6 of appendix 2. The oil phase was either, cyclohexane, n-heptane or toluene and the surfactant was NPE type or SML type. In all cases the locus for the transitional inversion was found to be a straight line. In the diagrams, these lines are extrapolated to $f_w = 0$ and to $f_w = 1$. The HLB of surfactant mixtures were taken as weight averages (note the comment above).

In Figures 2.4 to 2.9, the regions labelled in parenthesis are those observed before catastrophic inversion when oil was added to water with SAD positive or when water is added to oil with SAD negative. The values of f_w at which the inversion $W_m/O \rightarrow O/W_m$ occurred (with HLB constant) depended on stirrer speed. At a stirrer speed of 200 rpm, the injected aqueous phase was not dispersed evenly but tended to settle near the bottom of the vessel. This aided inversion when an O/W_m emulsion formed at the bottom of the vessel and the upper oil layer became incorporated into this layer. Figure 2.10 demonstrates the movement of the inversion boundary with stirrer speed and Figure 2.11 shows how this inversion boundary moved when the addition rate was varied with the stirrer speed constant.

2.4 DISCUSSION

The dynamic inversion maps of this chapter provide a framework for studying dynamic inversions in nSOW systems.

2.4.1 Comparison with other studies

The map derived in this study combines dynamic inversion with equilibrium phase behaviour. The inversion phenomena observed in PIT, EIP and SAD studies are all incorporated within the map framework.

In Salager et al's SAD map studies, samples were equilibrated prior to emulsification to determine the nSOW phase behaviour. In the maps produced in this study, the systems phase behaviour was determined by the position of the transitional inversion line. It may be assumed that equilibrium phase behaviour was achieved between each stage of the dynamic inversions because, the time between aliquot additions >> the time required for transfer of surfactant across the interface (note, the interfacial area in an emulsion is extremely large). The inversion locus shown on Salager et al's SAD maps, shows the emulsion types that form on emulsifying the pre-equilibrated samples and hence, these are not dynamic studies. The inversion locus will represent one emulsification procedure only.

Shinoda et al's PIT inversions are dynamic studies of transitional inversion. The PIT inversion line is usually a straight, nearly horizontal line, over a wide range of f_w (much wider than shown in Salager et al's SAD maps). Similar results were obtained in this study using HLB as the surfactant affinity variable. In Shinoda et al's studies, the surfactant used was generally the NPE type. Other authors (eg. Parkinson 1972), have used SML surfactants and have found different trends from those found by Shinoda et al. A linear transitional inversion line was obtained in this study when using NPE surfactants and when using SML surfactants. However, transitional inversion was only observed in SML systems if the dispersed phase fraction was >0.7. It may be that in Parkinson's study that the transitional inversion was "missed" and a catastrophic inversion was observed. This shows the benefit of having a map of nSOW phase behaviour when examining dynamic inversions.

In Marszall's EIP studies, NPE surfactants were again used. In EIP studies, water is added to the oil phase containing surfactant, hence, EIP studies are studies of dynamic catastrophic inversions. A plot of EIP against HLB usually gives a curve with a minimum EIP value at the required HLB of the oil. Examination of the catastrophic inversion boundaries at SAD^-, obtained in the NPE systems studied here, reveals that these boundaries are similar to EIP curves. In each NPE system map, the catastrophic inversion point occurs at a lower value of f_w as the HLB increases. It may be that if higher HLB values had been studied, a minimum value of f_w at inversion would have been obtained. Hence, Marszall's findings in EIP studies may apply to catastrophic inversion boundaries. Note, catastrophic inversion boundaries at SAD^- in SML systems did not show the same trends as NPE systems.

2.4.2 Effects of changing surfactant affinity

The results show that transitional phase inversion, which is induced by changing the HLB, occurs over a very narrow range of conditions. Within the precision of most experimental procedures, these conditions could be regarded as corresponding to an "inversion point".

Previous work (Shinoda 1986) suggests that the boundary corresponding to SAD = 0 (where transitional inversion occurs) might be represented by a horizontal line in the phase transition diagram. When surfactant mixtures are used, it can be seen that this boundary slopes from left to right. This can be explained in the following way. The creation of a surfactant phase requires the existence of micelles but the lipophilic component of the surfactant mixture has a higher CMC in the oil than does the hydrophilic component. Therefore, when f_w is low, less lipophilic surfactant is available to contribute to the surfactant phase. The calculated weight-average HLB of the mixtures will be less than the actual HLB of the surfactant phase. As f_w increases, a lower proportion of the lipophilic component exists in non-micellular form in the oil. The boundary at SAD=0 remains a straight line, reasons for this will be discussed chapter 3. As noted by Shinoda (1986), the effect described above, is amplified at lower surfactant concentrations. As the surfactant concentration increases, the SAD=0 line will move towards the horizontal. A full investigation of the effect of surfactant concentration is given in chapter 3.

In the case of toluene, transitional inversion with NPE surfactants could not be observed at low f_w when the surfactant concentration was 2 wt%. Even when the concentration was 5 wt% it can be seen from Figure 2.6 that a somewhat distorted "map" is obtained. This may occur because the CMC of NPE surfactants in toluene is relatively high. It should be noted that Shinoda(1986) found that PITs of aromatic hydrocarbons showed "abnormal" behaviour and that the PIT was sometimes dependent on the "way of shaking". The slope of PIT with WOR found by Shinoda for these oils may be explained in terms of a high CMC in the oil phase, however, the fact that the PIT was dependent on the agitation conditions, suggests that some of the PIT inversions were catastrophic inversions (the results of this study showed that transitional inversion points were unaffected by agitation conditions, however, catastrophic inversion points were).

Note, CMCs of commercial surfactants must be discussed with caution because they are assigned an average chain size but their constituents have a range of molecular sizes. Each component has its individual CMC which makes a separate contribution to the HLB of the surfactant phase. It should be noted that, in surfactant mixtures, the CMC values for individual components are not manifested. Mixed micelles are formed at a distinct CMC for each mixture. Graciaa (1982) showed that the HLB of a surfactant's

micelle phase increases as $f_w \rightarrow 0$ or as the surfactant concentration decreases. Hence, with f_w constant, a complete transition from SAD- to SAD+ can occur as the concentration of a "lipophilic" surfactant rises. The transition is seen only when the micelle concentration is relatively low. When NPE surfactants are used with toluene or cyclohexane, HLB values were varied by altering the ratio of Igepal co520® to Igepal co720®. An apparent discontinuity in the SAD=0 line occurred as the proportion of Igepal co720® approached 0 (i.e. when the HLB approached 10.0). Inversion at HLB = 10.0 is shifted to lower values of f_w.

Electrical conductivity measurements in the cyclohexane/NPE system showed that the oleic phase was continuous at low HLB and the aqueous phase was continuous at high HLB. When three phases were present, the rise in conductivity which accompanied the increase in HLB suggests that the surfactant phase was continuous because the surfactant phase is mostly oil at low HLB but becomes mostly water at high HLB.

A schematic representation of the "settled" phases which are present during sequential stages of transitional inversion from $O/W_m \rightarrow W/O_m$, with NPE surfactants, is shown in Figure 2.1 together with possible emulsion structures. The progression shown in Figure 2.1 applies for surfactant concentrations up to about 8wt% but, at concentrations above this, the system does not become three-phase but a single M_s phase can exist. In these circumstances the sequence becomes:

$$W/O_m \rightarrow W/M_o \rightarrow M_s \rightarrow O/M_w \rightarrow O/W_m$$

As shown above, the definition of an invariant inversion point may be inappropriate for a transitional change. In the experiments reported here, an inversion at SAD=0 was deemed to have occurred when a large change in electrical conductivity resulted from a small change in HLB (0.05, the approximate accuracy of the titration). However, the system may still be three-phase at this stage. For example, with inversions at high f_w, an emulsion could show high conductivity but still appear to have a large dispersed phase. This suggests that a surfactant phase (mainly water) was still continuous; with further rises in HLB the emulsion "thinned" suddenly and became O/M_w. The measured inversion point may be naturally in the three-phase region near the condition where the system changes from W/M_o to $(O+W)/M_s$.

When SML surfactants were used it was noted that complete transitional inversion did not occur unless the dispersed phase fraction was >0.7; it may be that the surfactant phase does not become continuous with dispersed phase fractions <0.7. The change from SAD+ to SAD- could possibly be via a double emulsion:

$W/O_m \rightarrow (W+O)/M_s/O \rightarrow W_m/O + O/W_m/O$

In this section an understanding of transitional inversion mechanisms has been developed. In chapter 5, optical microscopy techniques are used to investigate the change in drop sizes across the phase transition SAD+ to SAD-. Photomicrographic evidence from this analysis will be used to further clarify the mechanism of transitional inversion in NPE systems and SML systems.

2.4.3 Effects of changing phase ratio

For conditions remote from the region where SAD = 0, it can be seen that the term "phase inversion" must be used with care. With a negative SAD, addition of water to oil produced a phase inversion which could be identified clearly. The same observation was made when oil was added to water with SAD positive. These changes could be described as "catastrophic". The other transitions, which were induced by changing f_w (as described above), cannot be regarded as phase inversions in the same way. These changes are not sharp and changes in electrical conductivity must be interpreted carefully. The pattern of these changes can be recognised with experience when they are examined in conjunction with visual observation of the mixtures. For these transitions, it could be that available surfactant is only sufficient to cover the surface of the dispersed phase and that further additions of DISPERSED PHASE WOULD lead to an excess of this phase.

From the results of changing the phase ratio at a particular HLB, it can now be seen that a true phase inversion can be induced only when the ratio is changed in one direction. This may appear to be incompatible with other studies which do not show such wide hysteresis zones (Smith 1990). However, it should be noted that the surfactants used in this study produced stable emulsions whereas those used in some other studies (Smith 1990) did not. Also, investigation of complex drops was not always made in previous studies. The direction of changing WOR for a true catastrophic inversion, is determined by the surfactant and is related to the stability of the emulsion drops before catastrophic inversion (see below).

Comparisons of the two types of surfactants showed that the double emulsions ($O/W_m/O$ or $W/O_m/W$) formed in agitated mixtures when NPE surfactants were used. Double emulsions could form with sorbitan monolaurate surfactants but far fewer small drops were located within the large drops. It can be seen that, as SAD approaches 0, the value of f_w required for "catastrophic" inversion with SML surfactants is close to a value which corresponds to f_{cp} (the actual value for closest packing will vary slightly because drops are not monosized or may distorted from spherical). This is to be expected if only a few small drops exist within the large drops. With NPE mixtures the range of f_w values

for catastrophic inversion near SAD = 0 was relatively wide. Structured drops could be obtained with SML mixtures if stirring stopped and settling occurred (see above). Under these conditions, the volume fraction of dispersed phase in the settled dispersion became relatively high.

From the observations made from the agitation-settling experiment, it is apparent that the $W_m/O+O/W_m/O$ drops, formed on initial agitation, are unstable as these rapidly coalesce when agitation is removed. After phase separation had taken place, the lower layer was an O/W_m emulsion, hence, the oil drops from within the water drops are stable. It was shown that a true catastrophic inversion could not be induced when the initial emulsion was O/W_m or W/O_m (which are stable states). Therefore, a catastrophic inversion can only take place when the initial emulsion state is unstable.

The results showed that the location of boundaries for catastrophic inversions depended markedly on dynamic conditions. At high stirrer speeds the inversion boundary approached a constant position but with poor agitation conditions the inversion locus moved noticeably with stirrer speed (see Figure 2.10). Greatest movement was noticed where the tendency to form $O/W_m/O$ drops was pronounced. When the addition rate of the aqueous phase was reduced the value of f_w for the phase inversion was reduced also (see Figure 2.11) because more time was available for the formation of $O/W_m/O$ drops.

This section has introduced some of the variables affecting catastrophic inversion points. A detailed examination of the effects of agitation conditions on the drop sizes of various nSOW emulsions before and after catastrophic inversion is given in chapter 6.

2.4.4 Use of dynamic inversion maps

The result of changing HLB and f_w in a particular system can be predicted from the path on the inversion map (providing that the start condition is known). This is illustrated in Figure 2.12 which shows a schematic map with the unstable conditions marked in parenthesis.

Detailed studies of the drop types and sizes present along a path on a dynamic inversion map, are the subject of chapter 5 and 6. The dynamic inversion map developed in this chapter contains two SAD variables - HLB and surfactant concentration. In chapter 3, it will be shown how the effect of surfactant concentration on SAD can be removed from the map structure by considering interfacial surfactant only. A surfactant partitioning model is derived and the results of the model used, to show how surfactants may be classified, based on thermodynamic parameters.

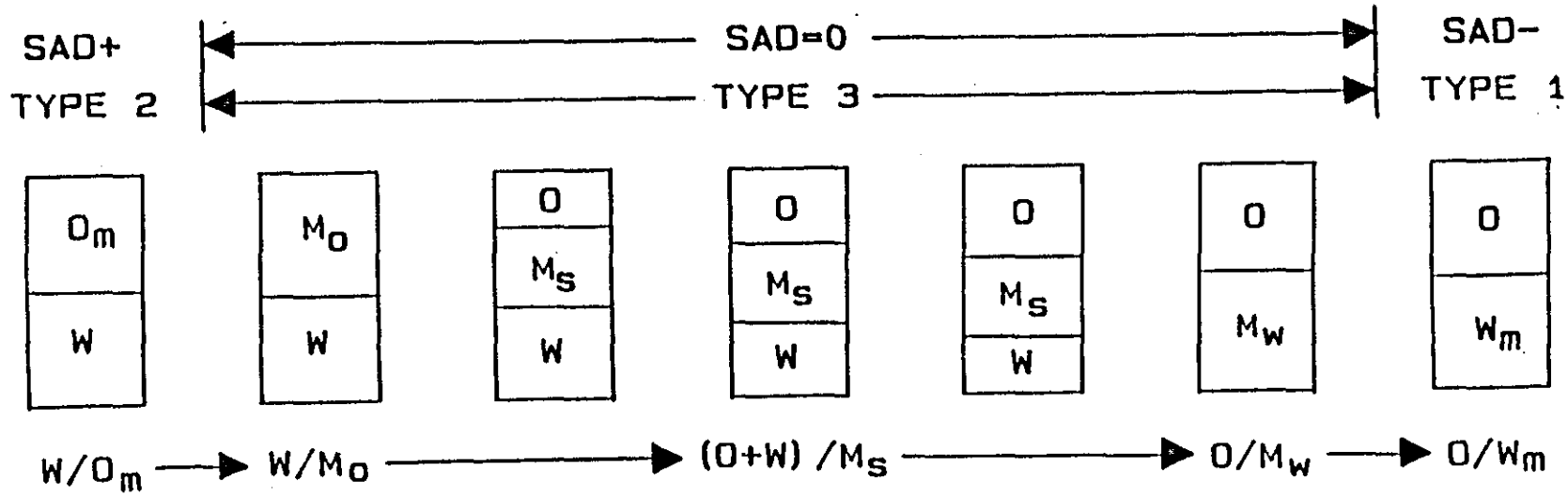

FIGURE 2.1 - Schematic representation of transitional inversion from W/O_m to O/W_m.

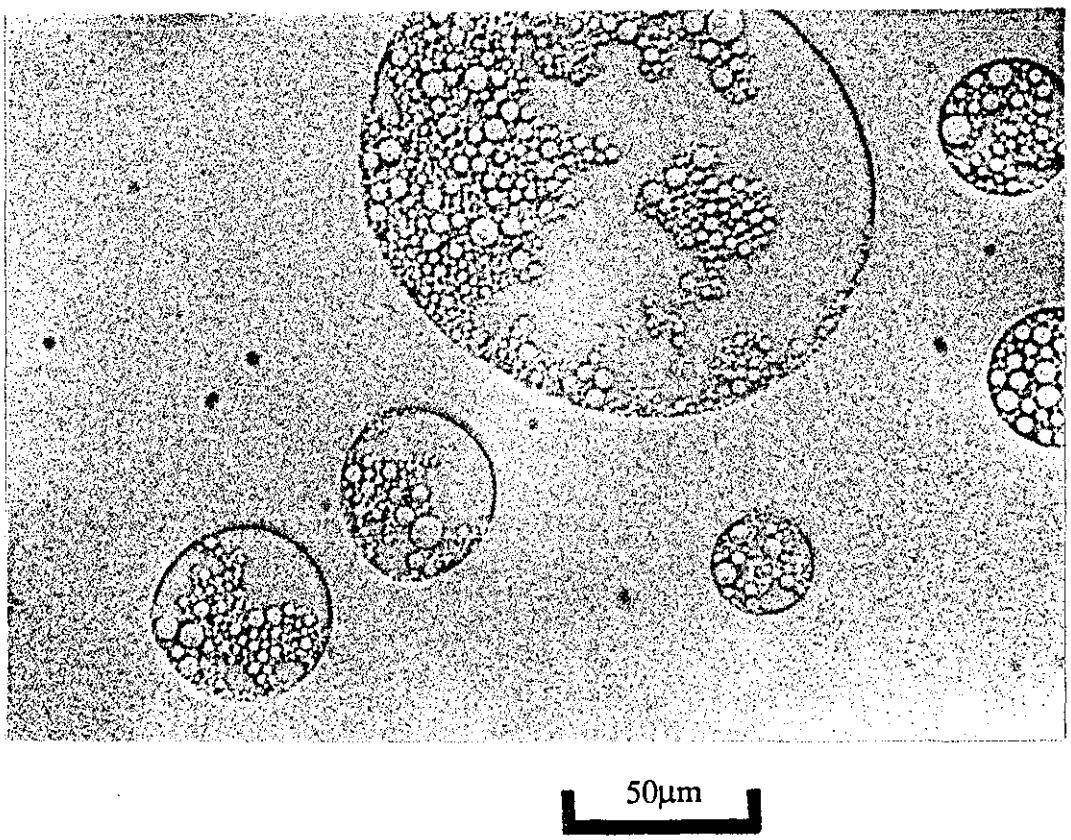

FIGURE 2.2 - O/W_m/O drops formed during catastrophic inversion of aqueous NPE surfactant in cyclohexane (see text for details) magnification x 500

SCHEMATIC REPRESENTATION OF AGITATION-SETTLING PROCEDURE

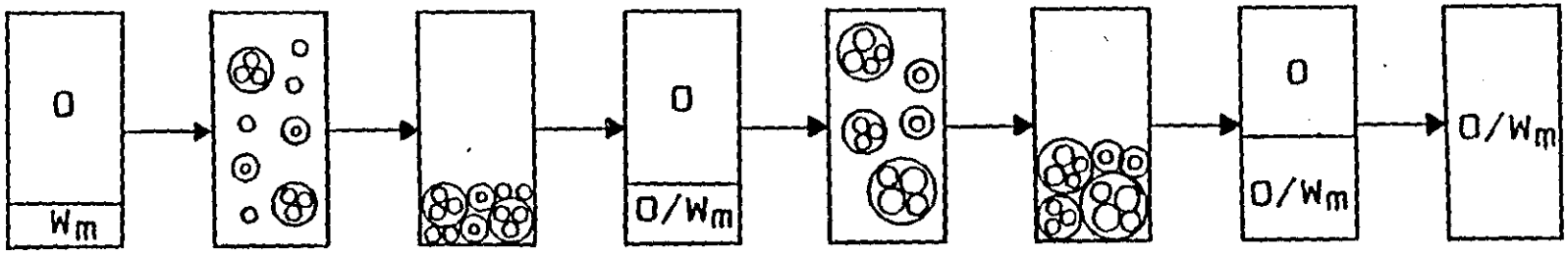

INITIALLY BEFORE AGITATION

ON AGITATING $W_m/O - O/W_m/O$ FORMED DUE TO LARGE OIL PHASE VOLUME

REMOVING AGITATION DROPS SEDIMENT AND COALESCE FORMING AN O/W_m EMULSION

AGITATION PRODUCES $O/W_m/O$ EMULSION

CYCLE OF SEDIMENTATION-COALESCENCE-AGITATION REPEATED; O/W_m EMULSION VOLUME INCREASES EACH TIME UNTIL ALL THE OIL IS EMULSIFIED.

PHOTOGRAPHS OF SETTLED STAGE BETWEEN AGITATIONS:

CYCLOHEXANE/2wt% NPE, f_w=0.1, HLB=14.2

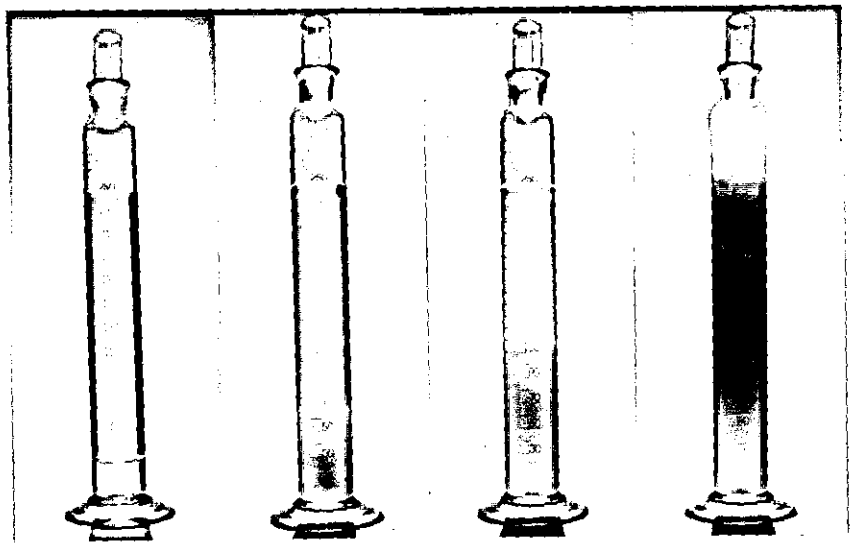

FIGURE 2.3 - Sequence of events during agitation and settling.

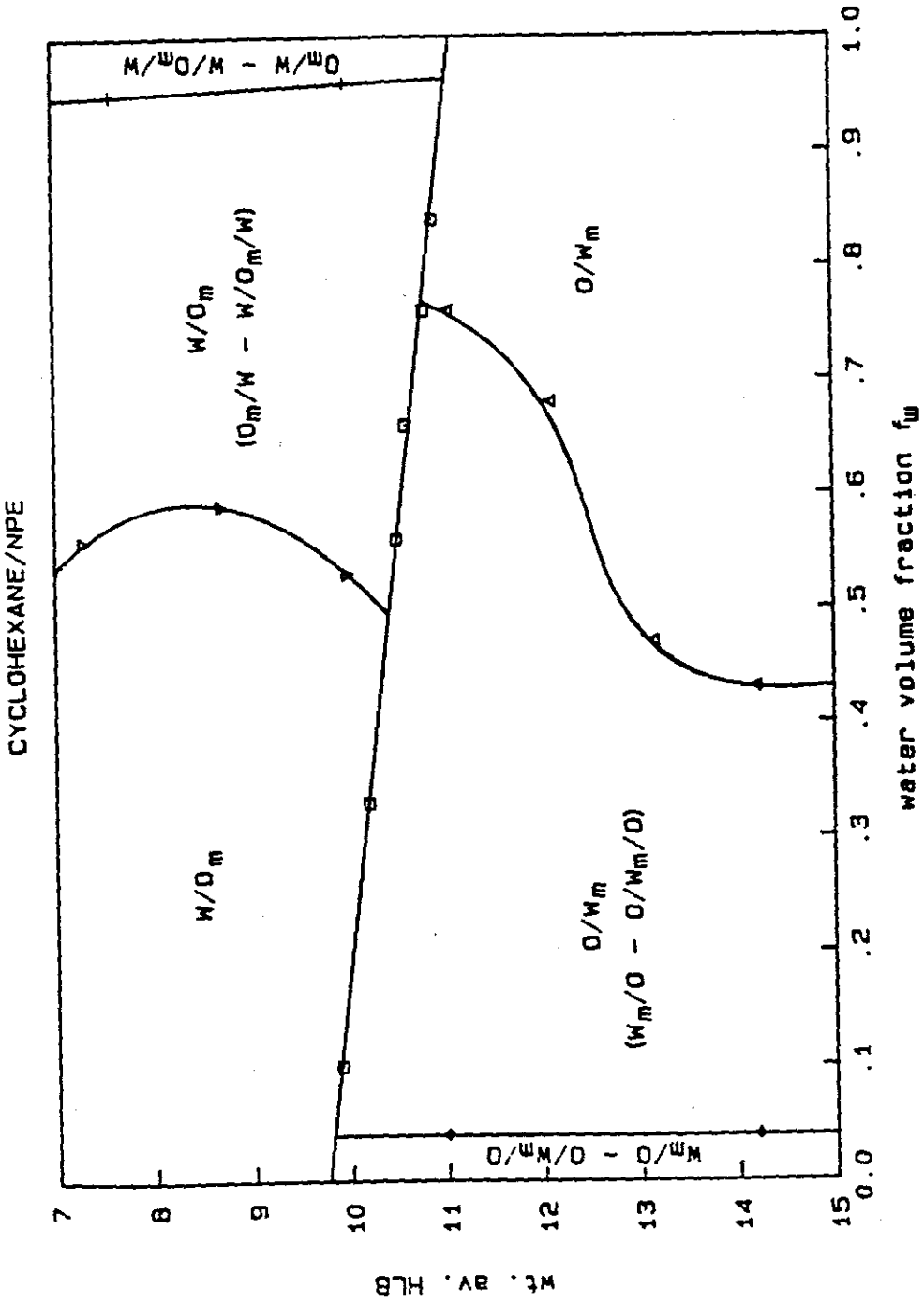

FIGURE 2.4 - Phase inversion map for cyclohexane and NPE surfactants (2 wt %).

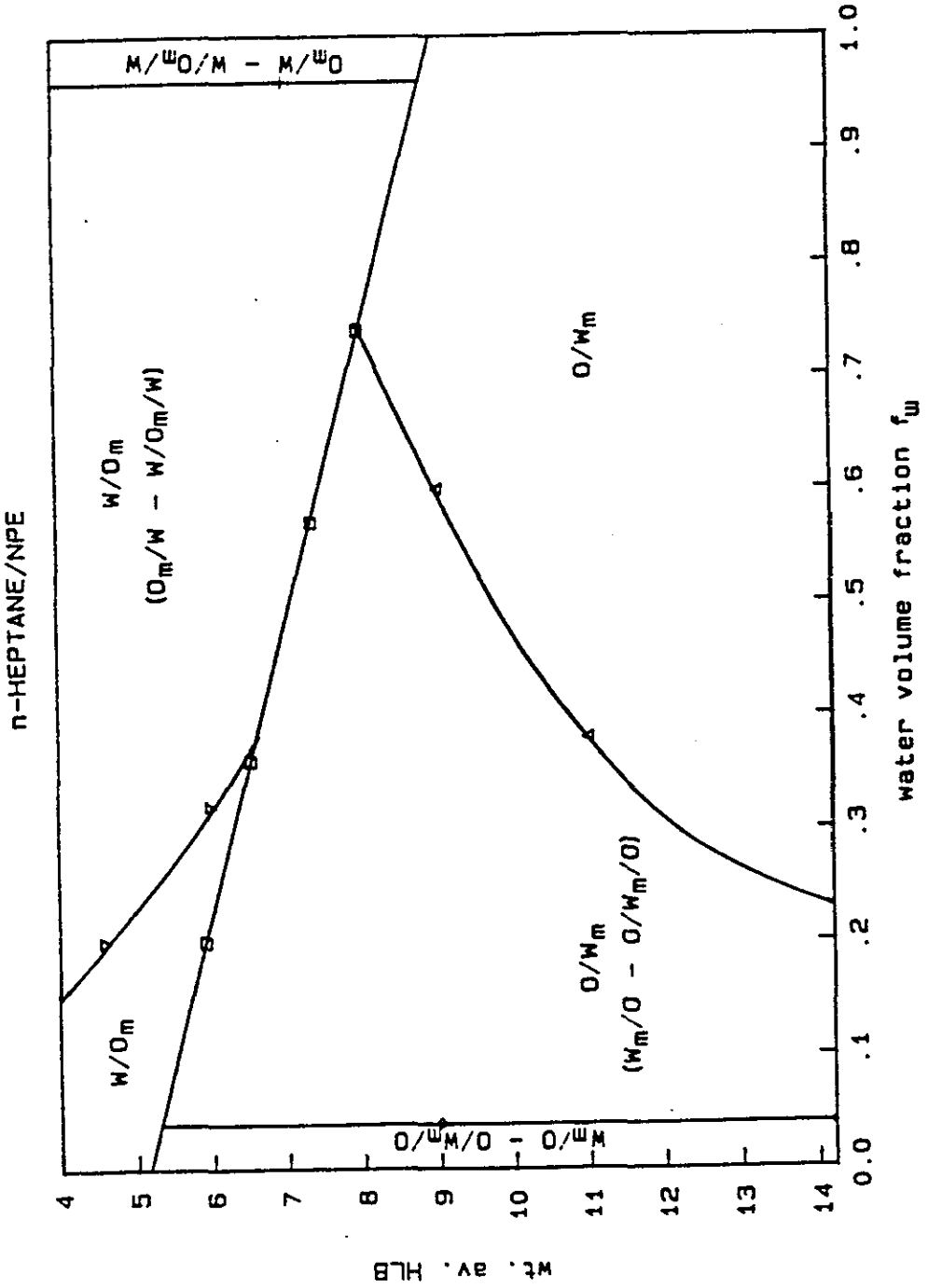

FIGURE 2.5 - Phase inversion map for heptane and NPE surfactants (2 wt %).

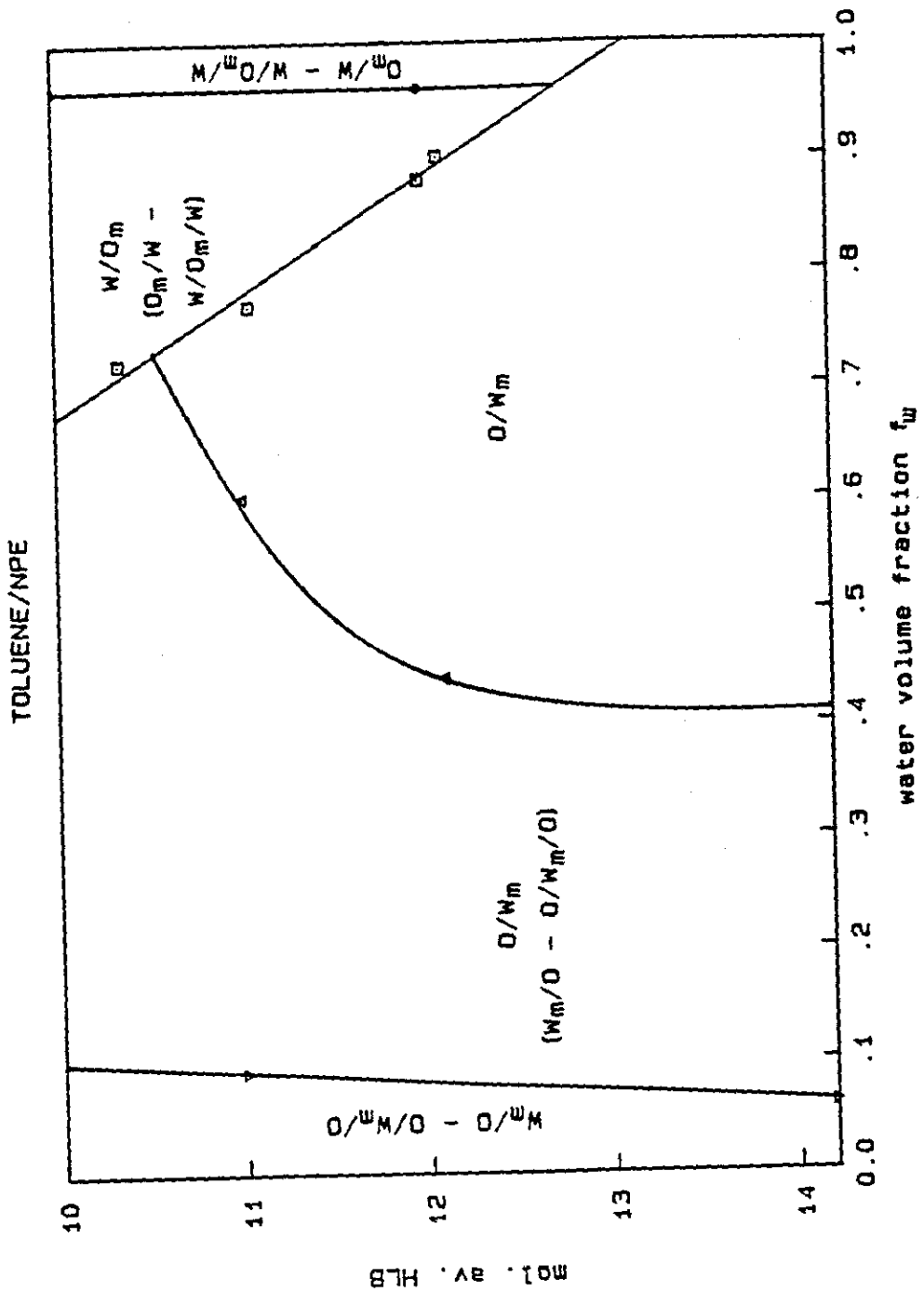

FIGURE 2.6 - Phase inversion map for toluene and NPE surfactants (5 wt %).

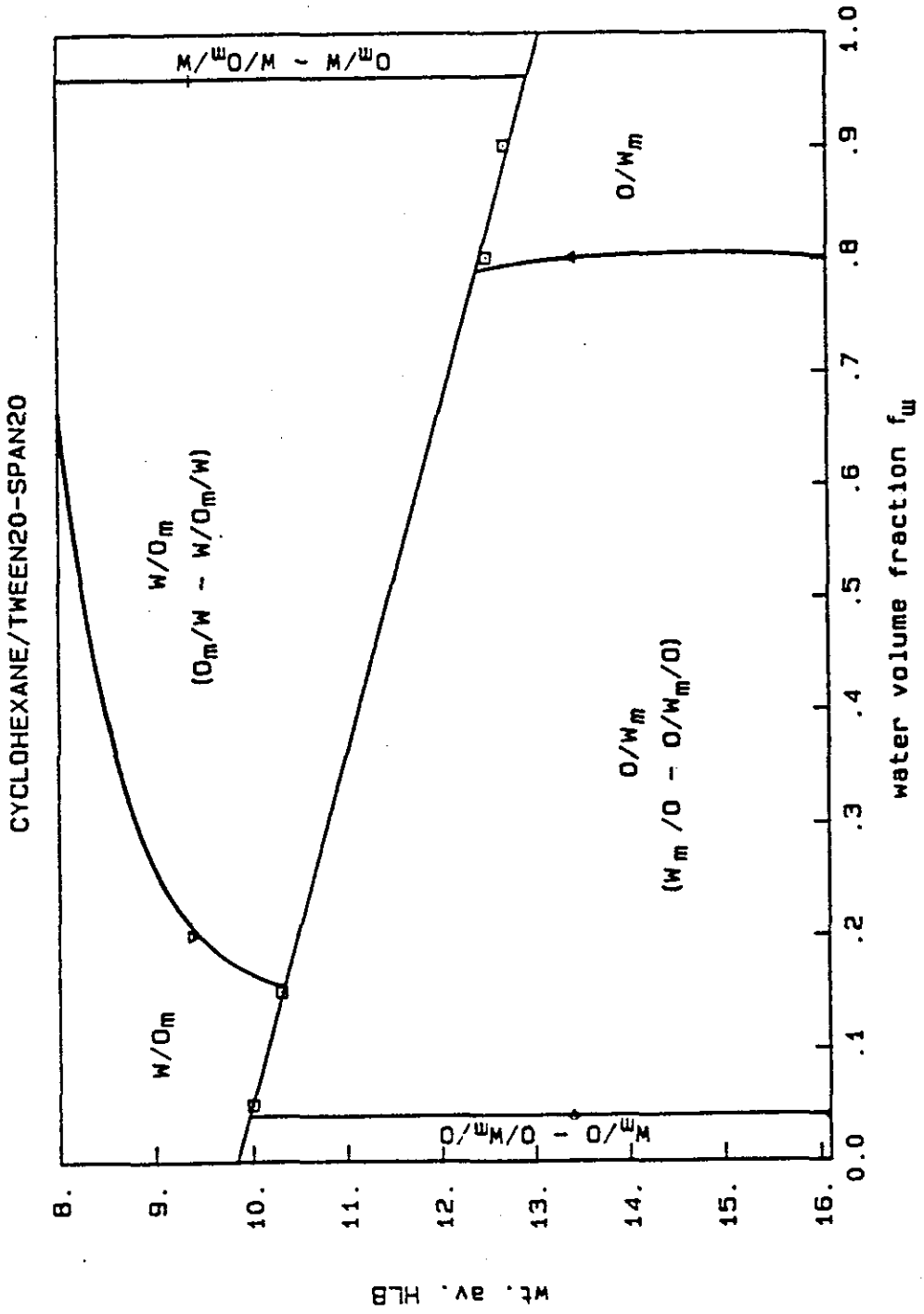

FIGURE 2.7 - Phase inversion map for cyclohexane and SML surfactants (2 wt %).

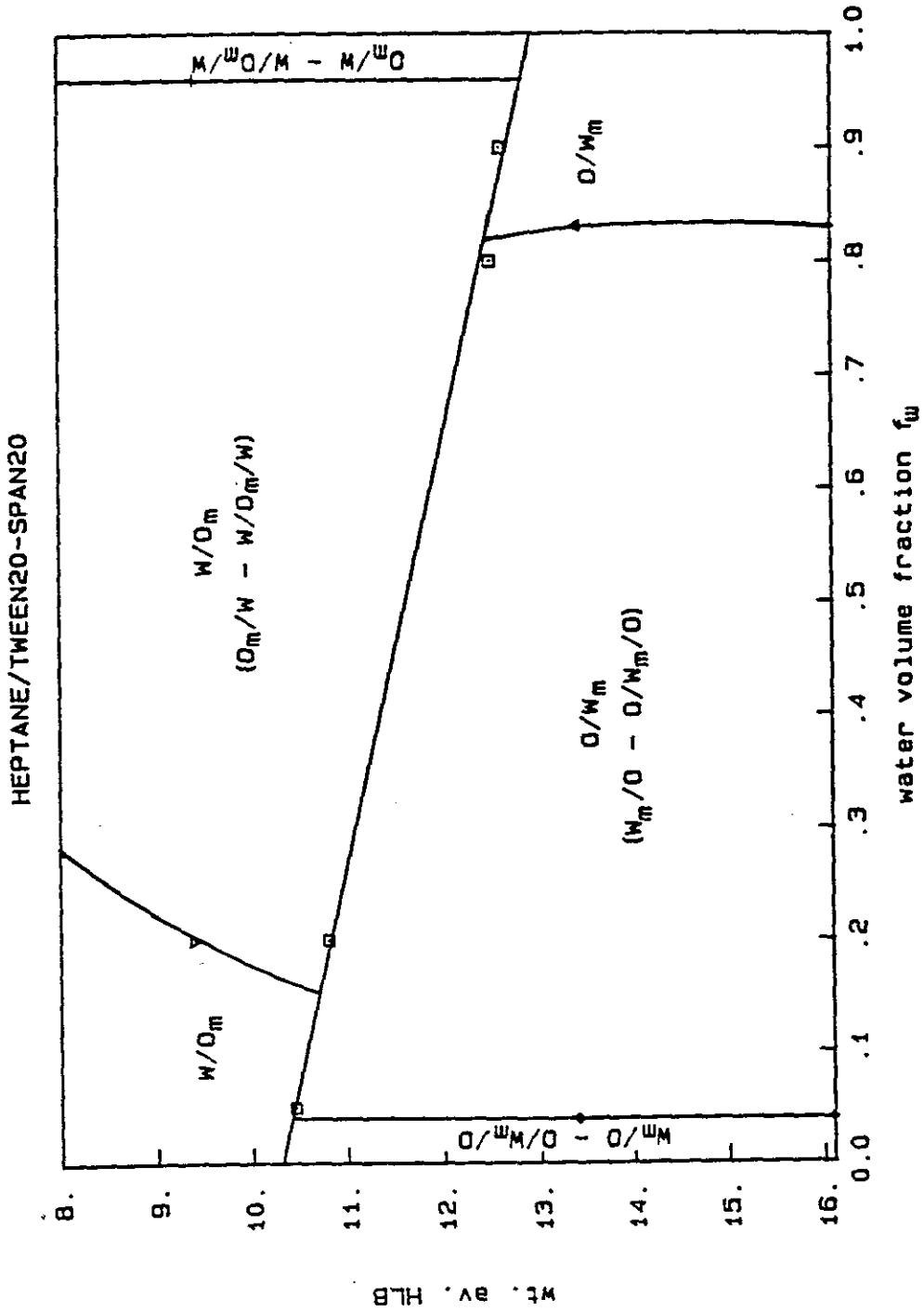

FIGURE 2.8 - Phase inversion map for heptane and SML surfactants (2 wt %).

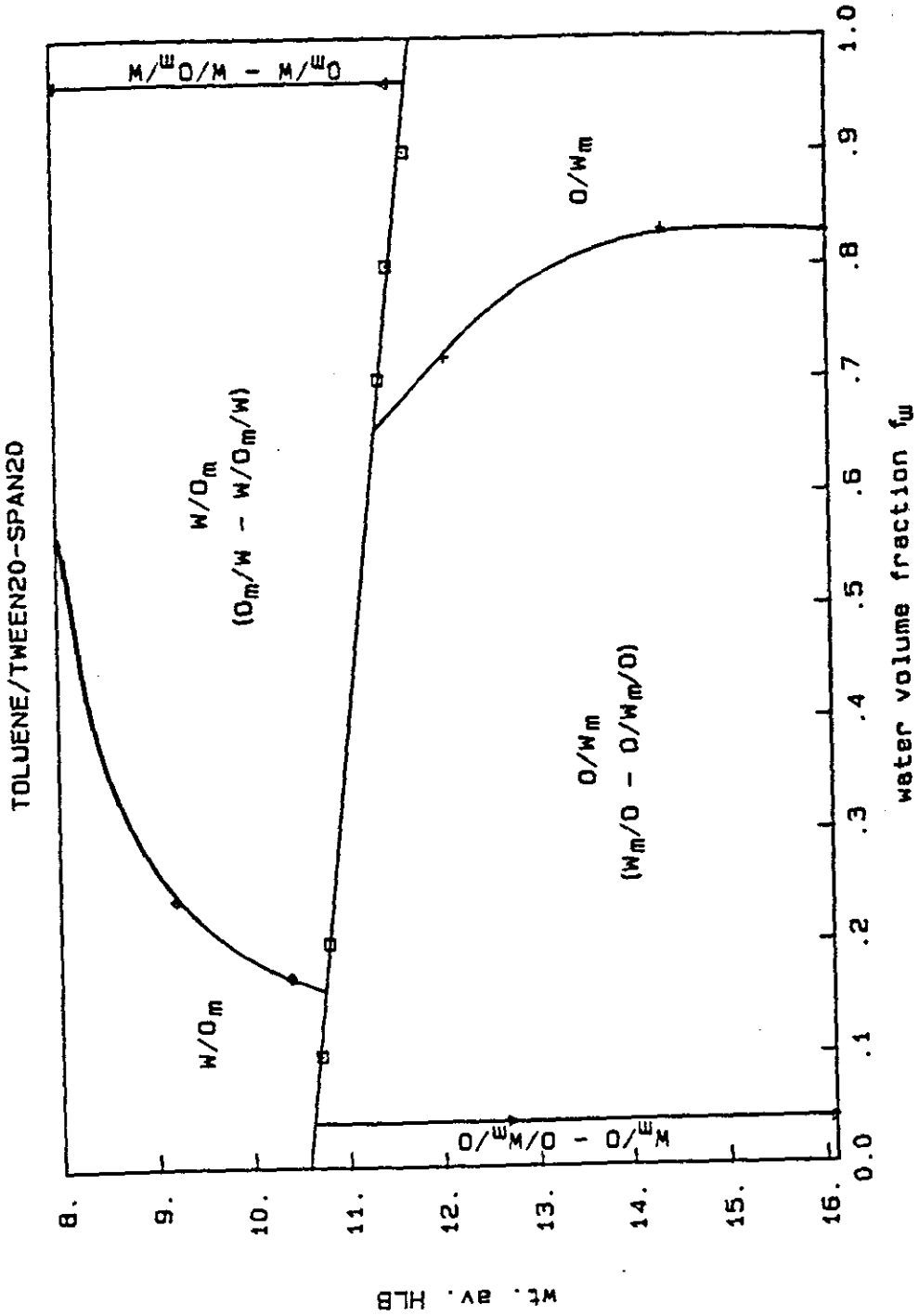

FIGURE 2.9 - Phase inversion map for toluene and SML surfactants (2 wt %).

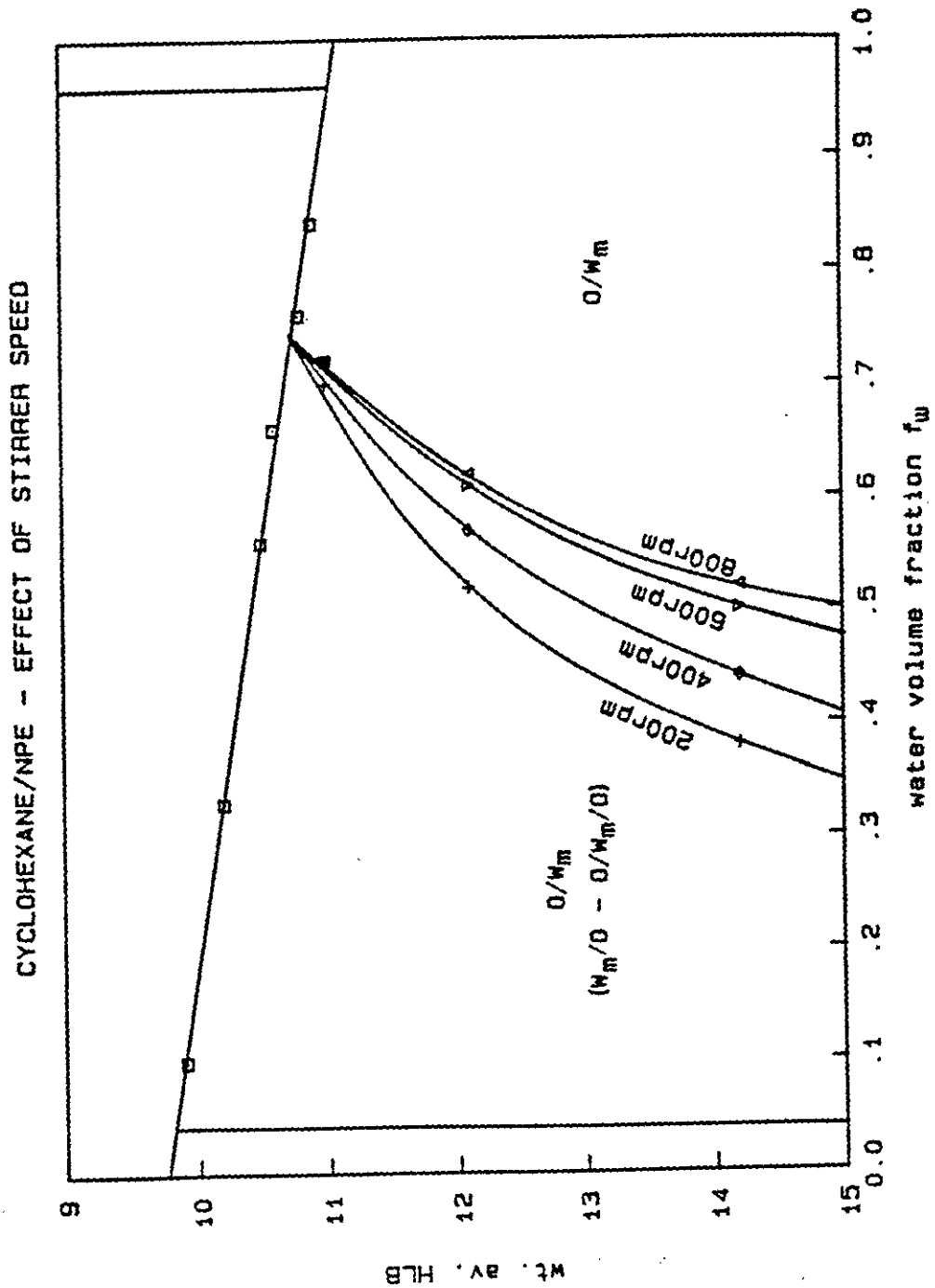

FIGURE 2.10 - Effect of stirrer speed on the phase inversion boundary for cyclohexane and NPE surfactants (2 wt %).

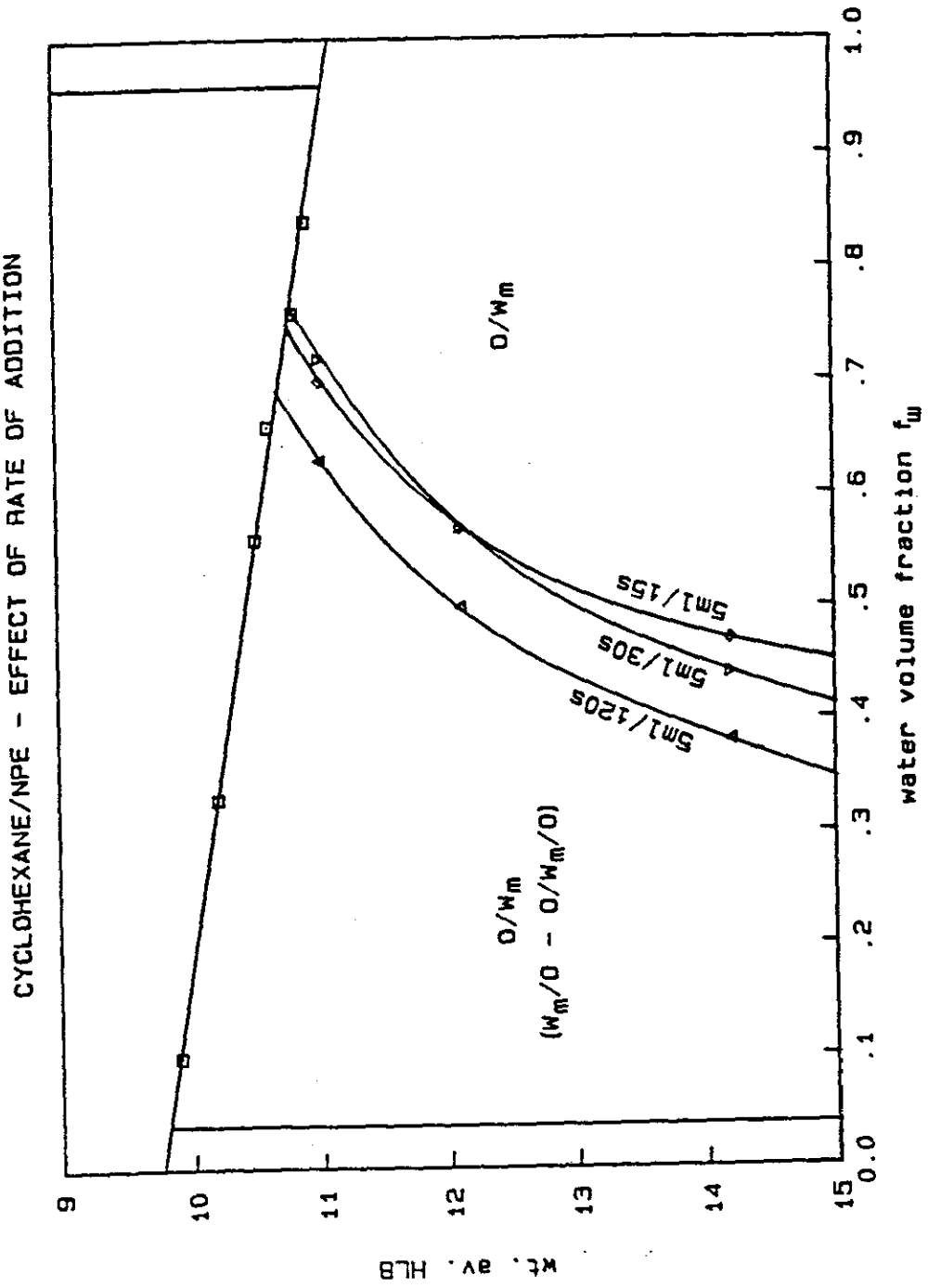

FIGURE 2.11 - Effect of addition rate on the phase inversion boundary for cyclohexane and NPE surfactants (2 wt %).

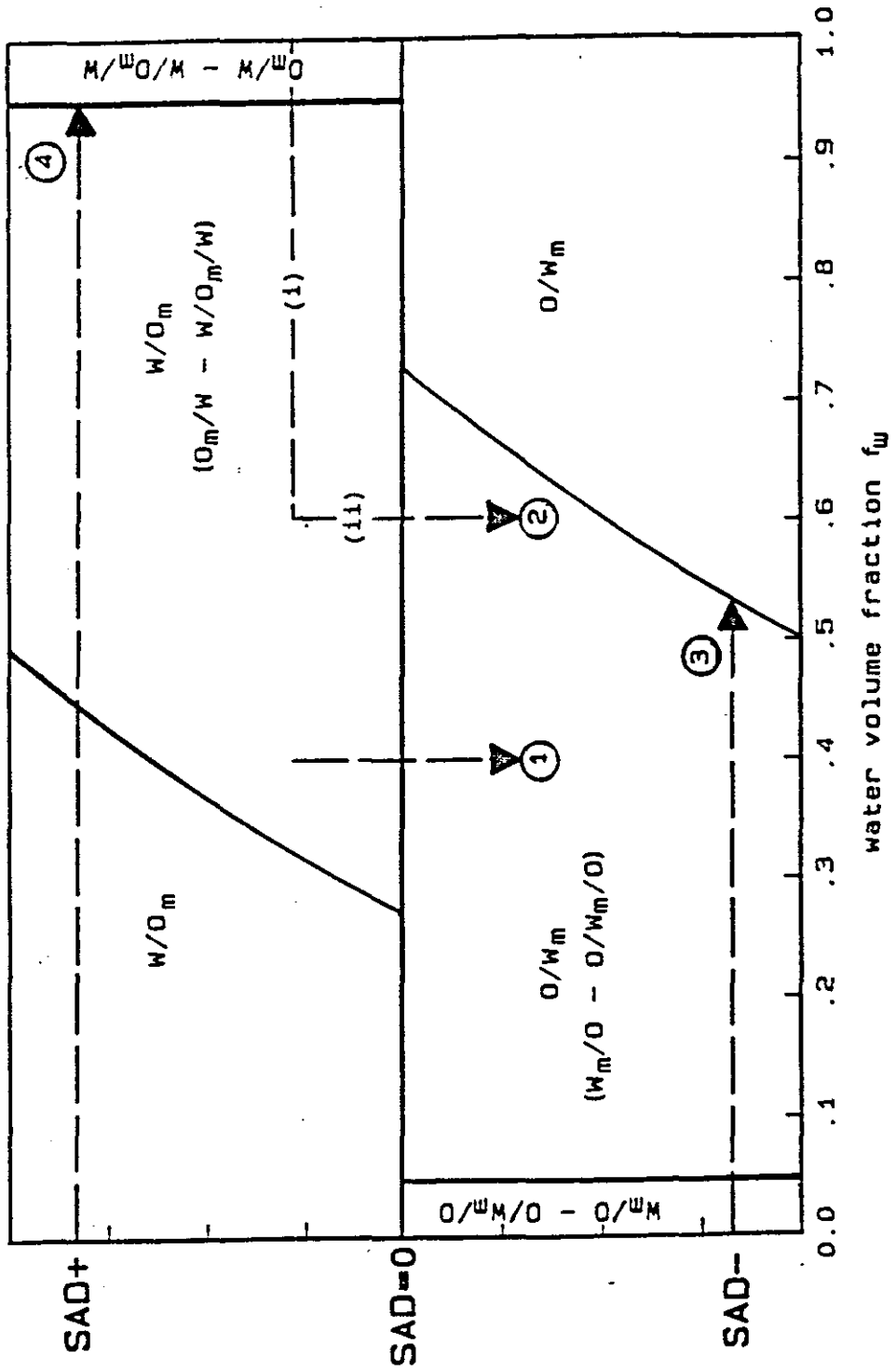

FIGURE 2.12 - Use of phase inversion map for NPE systems.

Path	Start condition	Path condition	End condition
1	W/O_m	$W/M_o \rightarrow (O+W)/M_s \rightarrow O/M_w$	O/W_m
2(i)	W	$O_m/W + W/O_m/W$	-
2(ii)	$O_m/W + W/O_m/W$	$W/M_o/W \rightarrow (O+W)/M_s \rightarrow O/M_w$	O/W_m
3	O	$W_m/O + O/W_m/O$	O/W_m
4	O	W/O_m	$W/O_m/W$

CHAPTER 3 - The Relationship Between nSOW Phase Behaviour and the Partitioning of Surfactant Between Phases

3.1 INTRODUCTION

In this chapter the partitioning of surfactant between the oil phase, water phase and the interface is considered, with particular reference to transitional inversion. The chapter is split into two parts. In the first part a model is derived which can be used to predict CMC_o values from transitional inversion SAD=O lines. In the second part, surfactant partitioning results are used to show how nSOW phase behaviour is related to thermodynamic parameters.

From the results of chapter 2 it is apparent that the SAD=0 line is usually a straight line sloping down from left to right across the map. The slope of the line, as was shown by Shinoda et al (1986) in PIT work, is affected by the surfactant concentration. The line slopes because the surfactant present will have a distribution of chain lengths. The CMC of the more lipophilic short chain length molecules in the oil phase is far greater than the CMC of the longer chain length molecules. Also for the short chain length molecules, their CMC in the oil phase >> their CMC in the water phase. Hence, at lower values of f_w more of the short chain surfactant molecules will be dissolved as monomers in the oil phase, leaving the longer chain surfactant molecules at the oil-water interface. Therefore, the actual HLB of the surfactant at oil-water interfaces increases as $f_w \rightarrow 0$ and will be higher than the overall mole average HLB of all the surfactant in the system.

In the construction of the inversion maps presented in chapter 2, a titration between a lipophilic and hydrophilic surfactant at different values of f_w was used to locate the SAD=0 line at constant temperature, in an oil-water system. This isothermal technique for changing SAD allows a simple surfactant partitioning model developed here to be applied to transitional inversion as the SOW system properties (eg. CMC) remain constant.

The model derived here uses mixed surfactant theory to predict the slope of the SAD=0 line with surfactant concentration (at constant temperature), for transitional inversion induced by varying the amounts of a homogeneous lipophilic and a homogeneous hydrophilic surfactant in an oil-water system. It is further shown that the same model can in some (usual) cases be used to calculate mixed CMCs to predict transitional inversion boundaries in systems containing surfactants having chain length distributions.

3.1.1 PART 1 - MIXED MICELLE THEORY

A number of studies have been reported that use a phase separation model of micellisation to describe the partitioning of surfactant between oil-water-surfactant phases. Harusawa et al (1981), investigated the partitioning of nonylphenylether (NPE) surfactants between water and cyclohexane. Graciaa et al (1983) and Allan et al (1989), looked at the partitioning of surfactants having a distribution of chain lengths using, ethoxylateoctylphenols (EOP) in water/iso-octane and NPE in water/hexane systems respectively. All these models assume ideal mixing, thermodynamic equilibrium and that the system can be split into three constituent parts:

(i) water phase containing surfactant monomers at a mixed CMC_w ,

(ii) oil phase containing surfactant monomers at a mixed CMC_o ,

(iii) a pseudo surfactant phase, which represents the surfactant in micelle form and surfactant at oil-water interfaces.

The phase separation model representation, together with the different emulsion structures and phase behaviour present across a transition from SAD+ to SAD- is shown in figure 3.1.

It is assumed that microemulsion phases (O_m, W_m, M_s, M_o, M_w) despite being single thermodynamic phases, are composed of submicroscopic regions of oil and water separated by an interfacial layer of surfactant (Graciaa 1989), hence, each of the different microemulsion phases can be constructed from the three phase elements (i), (ii) and (iii). The pseudo surfactant phase contains micelle interfaces in Type 1 and Type 2 systems and it contains the surfactant layer bounding the bicontinuous oil and water structure of the surfactant phase (M_s) in Type 3 systems. Solubilised oil and water in surfactant micelles are regarded as "emulsified" in the form described by (i) and (ii). Hence, the pseudo surfactant phase contains all the surfactant (and only surfactant), in the system which is not dissolved as monomers in the oil and water phases (i) and (ii). At normal (low) surfactant concentrations the pseudo surfactant phase can be assumed to have negligible volume as solubilised material is not included in it.

Note, phase separation models alone cannot be used to determine the phase behaviour of the emulsion system because they cannot show which phase the surfactant micelles will form in.

Basis of phase separation models:

[I] At surfactant concentrations below that at which the pseudo surfactant phase separates (ie. below either CMC), it has been shown by experiment that the partition coefficient for surfactant monomer i between oil and water can be written as (Harusawa 1981):

$$K_i = \frac{CMC_{oi}}{CMC_{wi}} \qquad [3.1]$$

[II] For conditions above the CMCs, using an analogy to Raoult's law, it is shown below that for ideal solution:

$$C_{oi} = x_i CMC_{oi} \qquad [3.2a]$$

$$C_{wi} = x_i CMC_{wi} \qquad [3.2b]$$

where: x_i = mole fraction of surfactant i in the pseudo surfactant phase,

C_{oi} , C_{wi} = concentration of monomeric surfactant dissolved in the oil and water phases respectively.

Derivation

Let C_o and C_w be the total number of moles of surfactant in one litre of oil and water phase respectively, to be used as local reference values. The chemical potentials of component i in the oil and water phases can be written as:

$$\mu_{oi} = \mu^*_{oi} + RT\ln(C_{oi}/C_o) \qquad [3.3]$$

$$\mu_{wi} = \mu^*_{wi} + RT\ln(C_{wi}/C_w) \qquad [3.4]$$

where the activity coefficient is assumed to be unity. Assuming the micelles behave as an ideal mixture, we can write for component i in the mixed micelles:

$$\mu_{mi} = \mu_{moi} + RT\ln x_i \qquad [3.5]$$

When applying a phase separation model to micellisation in equilibrated two phase systems, it may be assumed that when micellisation occurs, a saturation (CMC) is reached in both phases (Harusawa 1980). Therefore, considering the equilibrium condition between oil, water and micelle phases - for component i in pure micelles:

$$\mu_{oi} = \mu^*_{oi} + RT\ln(CMC_{oi}/C_o) \qquad [3.6]$$

$$\mu_{moi} = \mu^*_{wi} + RT\ln(CMC_{wi}/C_w) \qquad [3.7]$$

At equilibrium $\mu_{mi} = \mu_{oi}$ for the micelle and oil phases and $\mu_{mi} = \mu_{wi}$ for the micelle and water phases. Therefore, by rearrangement of equations [3.3] to [3.7] the results, equation [3.2a] and [3.2b], are obtained.

These equations can now be used in mass balances and applied to transitional inversion.

3.1.2 THEORY APPLIED TO TRANSITIONAL INVERSION

Isothermal transitional inversion is thought to occur at a specific value of HLB of the pseudo surfactant phase, this was proven by Graciaa et al (1989) for the iso-octane/EOP system using CMC data. The HLB of the pseudo surfactant phase was calculated from the mole average of each chain length in the phase (commercial nonionic surfactants have a distribution of chain lengths and each chain length must be treated separately). The main problem with phase separation models is that they require a large amount of cmc data. However, a simple method for determining the HLB of the pseudo surfactant phase and slope of the SAD=0 line that requires only a minimum of inversion data is shown below:

$$x_i = \frac{\text{Total number of moles of surfactant i present in all phases - number of moles of i dissolves as monomer in the oil and water phases}}{\text{Total number of moles of surfactant in the pseudo phase}}$$

$$x_i = \frac{C_i V - C_{oi} V_o - C_{wi} V_w}{\sum_{i=1}^{N} (C_i V - C_{oi} V_o - C_{wi} V_w)} \qquad [3.8]$$

where, V = total volume of the system ($V_o + V_w$),

V_o = volume of the oil phase,

V_w = volume of the water phase,

C_i = effective overall concentration of surfactant i.

$$x_i = \frac{C_i - (1 - f_w) C_{oi} - f_w C_{wi}}{\sum_{i=1}^{N} (C_i - (1 - f_w) C_{oi} - f_w C_{wi})} \qquad [3.9]$$

When considering transitional inversion there are advantages in splitting the surfactant into hydrophilic and lipophilic groups. Hence, we will consider the simple case of isothermal transitional inversion brought about by varying the ratio of a homogeneous lipophilic and a homogeneous hydrophilic surfactant in an oil-water system.

For a two surfactant system:

Subscript 1 will denote lipophilic surfactant and
h will denote hydrophilic surfactant.

Again, in common with accepted practice, the mole average HLB of the pseudo surfactant phase will be calculated in accordance with equation [3.10] below. However, it should be noted that for a two surfactant system the value of HLB_{act} is entirely dependent on x_h and x_l. Hence, the pseudo surfactant phase composition is the important variable.

The actual HLB of the pseudo surfactant phase:

$$HLB_{act} = \sum_{i=1}^{N} x_i HLB_i \qquad [3.10]$$

$$\begin{aligned} x_h + x_l &= 1 \\ C_{ol} &= x_l CMC_{ol} \\ C_{wl} &= x_l CMC_{wl} \\ C_{oh} &= x_h CMC_{oh} \\ C_{wh} &= x_h CMC_{wh} \\ C_t &= C_h + C_l \end{aligned}$$

Substituting these equations into [3.9] we arrive at the following quadratic equation:

$$-x_h^2[(1-f_w)(CMC_{ol}-CMC_{oh})+f_w(CMC_{wl}-CMC_{wh})] \quad +$$

$$x_h[(1-f_w)(CMC_{ol}-CMC_{oh}+f_w(CMC_{wl}-CMC_{wh})-(C_h+C_l)] \quad +$$

$$C_h = 0 \qquad [3.11]$$

Equation [3.11] applies to a rather artificial surfactant case because commercial nonionic surfactants have a distribution of chain lengths and are sold as having an average chain length, for which its HLB is calculated. However, there are certain cases when equation [3.11] can be applied to isothermal transitional inversion in systems containing distributed surfactants.

3.1.3 LUMPING OF DISTRIBUTED SURFACTANT TERMS

Deriving a mixed surfactant model for isothermal transitional inversion in systems containing distributed surfactants becomes very complex and requires a large amount of experimental data because each chain length has to be treated separately. However, it has been noted that, to a first approximation, the CMC of a Poisson distributed surfactant is the same as that of a homogeneous surfactant of the same chain length as the distributed surfactant's average chain length (Allan 1989). It has been shown that the average ethylene oxide chain length of the surfactant molecules, in the pseudo surfactant phase of a system containing a distributed surfactant, approaches a constant above a certain

overall surfactant concentration (Graciaa 1983) (see figure 3.2). Hence, the distributed surfactant above a certain overall concentration in an oil-water system may then be regarded as a single component. Therefore, in the case of transitional inversion in systems containing distributed surfactants, if the overall surfactant concentration is such that each of the surfactant pair may be regarded as single components then equation [3.11] can also be applied to these systems. To discuss this it is first necessary to show how the CMC terms of a distributed surfactant may be lumped together.

Crook et al (1965) made the assumption, for dissolved surfactant monomers in the oil and aqueous phase, that there are "weak interactions between molecules of varying ethylene oxide chain length". This assumption is not unreasonable because the CMCs of surfactant monomers are normally of the order 10^{-5} to 0.1 moles/l and the molecules are nonionic.

The partition coefficient of a distributed surfactant between oil and water can be defined as (note equation [3.1]):

$$K_{o/w} = \frac{\sum_{i=1}^{N} C_{oi}}{\sum_{i=1}^{N} C_{wi}} \qquad [3.12]$$

Equation [3.12] was shown to be in good agreement with experimental results (Crook 1965).

This technique of lumping CMC values can be used to derive expressions for each of the terms in equation [3.11]. For each of the surfactant pair we are concerned only with the number of moles of that surfactant dissolved in each phase, hence:

$$x_l = \sum_{i=1}^{N} x_{li} \qquad [3.13]$$

$$CMC_{ol} = \frac{\sum_{i=1}^{N} x_{li}.CMC_{oi}}{x_l} \qquad [3.14]$$

where, x_{li} = lipophilic surfactant's contribution to the overall mole fraction of chain length i in the pseudo phase,

CMC_{oi} = the CMC of chain length i in the oil phase.

Similar expressions can be derived for x_h, CMC_{oh}, CMC_{wh}, CMC_{wl}.

3.1.4 LINEAR TRANSITIONAL INVERSION LINE

Equation [3.11] can now be applied to isothermal transitional inversion in systems containing distributed surfactants, but it should be remembered that the x and CMC terms are now variables governed by equations of the form of [3.13] and [3.14]. However, there is a special case of equation [3.11] in which there is a linear variation of C_h with f_w at a set C_t. In this case the lumped parameters must be constant for quadratic equation [3.11] to reduce to a linear form. Hence, if a linear isothermal transitional inversion line is obtained for a range of conditions studied, we are then justified in using lumped parameters for the distributed surfactant and the surfactant can be regarded as a single component for that range of conditions.

In this part, it will be shown how equation [3.11] can easily be applied to inversion data and used to predict the variation of slope of the SAD=0 inversion line with surfactant concentration at constant temperature.

In part 2, the effect of carrying out the inversion titrations at different temperatures and the subsequent changes in the surfactant CMC values will be examined. A link between transitional inversion and CMC values is proposed and the subsequent possibility of a surfactant classification system based on thermodynamic relationships discussed.

3.2 EXPERIMENTAL

The surfactants and hydrocarbon oil phases used in this part of the study were as described in the experimental section of chapter 2.

3.2.1 Setting SAD=0 lines

Titrations as described in chapter 2 were used to determine the SAD=0 lines at different surfactant concentrations and temperatures. The titrations give $HLB_{mol.av.}$ and f_w values at the transitional inversion point, where:

$$HLB_{mol.av.} = \frac{C_l}{C_t}.HLB_l + \frac{C_h}{C_t}.HLB_h \qquad [3.15]$$

3.2.2 Measurement of CMC_o of a 3 phase system

The mixed CMCs of a distributed surfactant will vary with surfactant concentration and WOR, however, the mixed CMC at each surfactant concentration will be of the same order. An attempt was made here to measure the CMC_o of NPE5 (Igepal co520) in cyclohexane at 25°C. Gas chromatography has been used to measure CMC values of distributed surfactants by Allan (1989) and Graciaa (1983). However, accurate determination of the CMC of each chain length of the surfactant is difficult (especially

for CMC_w values because these are generally very low $<10^{-4}$ moles/l). The surfactant is sometimes chemically modified before GC analysis (Allan 1989). GC analysis is generally restricted to shorter chain length surfactants. The experimental procedure and sample preparation method used here are described below:

Sample preparation

The system cyclohexane/NPE5 was chosen for analysis because the average chain length of the surfactant is low and the system can show three phase behaviour at room temperature. 100 ml of water containing 2 wt% NPE5 was added to 100 ml of cyclohexane also containing 2 wt% NPE5, in an agitated vessel. The system formed a W/O_m emulsion. Cyclohexane was then added to the system until the transitional inversion point was reached (as f_w decreases and the surfactant concentration decreases, the surfactant will become more hydrophilic). The agitation was then stopped and the emulsion was allowed to phase separate over a period of 2 weeks. In its phase separated state the emulsion was 3-phase. Hence, the surfactant micelles formed a surfactant phase and the oil phase will contain surfactant monomers at CMC_o.

GC analysis

The mixed CMC_o was determined using a PYE-Unicam series 304, temperature programmable gas chromatograph. A 12 m Bonded phase/ 1 vitreous silica capillary column of internal diameter 0.22 mm was used with a flame ionisation detector (FID) operated at 300°C. The column was initially held at 60°C for 2 minutes, then increased at a rate of 4°C/min to 300°C, where it was held for 1 hour. Gas flow rates used for the FID were 300 cm^3/min at 60 psi of air, 33 cm^3/min at 60 psi of hydrogen and 30 cm^3/min at 60 psi of nitrogen. Helium was used as the carrier gas, at a velocity of 40 cm/s and with a pressure drop of 20 psi across the column. Chromatograms were recorded and the peak areas determined on a PYE-Unicam PU4810 computing integrator.

A 0.5 µl sample was injected directly onto the column. Each sample contained 0.4 g/l of xylene as a marker.

3.3 RESULTS

SAD=0 lines:

(i) Inversion data for the cyclohexane/NPE5-NPE12 system at 20°C is tabulated in table A3.1 of appendix 3 and plotted on figure 3.3.

(ii) Inversion data for the cyclohexane/NPE2-NPE12 system at 20°C is tabulated in table A3.2 of appendix 3 and plotted on figure 3.4.

(iii) Inversion data for the toluene/NPE5-12 system at 22°C is tabulated in table A3.3 of appendix 3 and plotted on figure 3.5.

(iv) Inversion data for the n-heptane/NPE2-NPE12 system at 20°C is tabulated in table A3.4 of appendix 3 and plotted on figure 3.6.

(v) Inversion data for the SML systems at 20°C are tabulated in table A3.5 of appendix 3 and plotted on figure 3.7.

(vi) Inversion data for the cyclohexane/NPE5-NPE12 system at 20°C, 40°C and 60°C are tabulated in table A3.6 of appendix 3 and plotted on figure 3.8.

(vii) Inversion data for the n-heptane/NPE systems at 30°C and 50°C are tabulated in table A3.7 of appendix 3 and plotted on figure 3.9.

CMC_o measurement

Good separation between the cyclohexane and xylene peaks was obtained with the GC. Seven separate peaks due to the surfactant were obtained, hence, the distributed NPE5 surfactant was composed of 7 chain lengths. From the xylene peak area and the sum of the surfactant chain length peak areas, a mixed $CMC_o = 0.07$ mol/l, was calculated for NPE5 in cyclohexane at room temperature.

3.4 ANALYSIS

To gain an idea of the expected order of the CMC_o and CMC_w values of the average chain length of Igepal® Co210 (NPE2), Igepal® Co520 (NPE5) and Igepal® Co720 (NPE12) in cyclohexane and water, we can use the results of Harusawa et al (1981) for homogeneous NPE6 and homogeneous NPE8 surfactants in the same system and at a similar temperature. It has been noted (Crook 1963), that there is a linear relationship in a series of homogeneous surfactants between the ethyleneoxide chain length and the logarithm of its CMC. The expected order determined for the average chain length of Igepal® co210, Igepal® co520 and Igepal® co720 derived from the data of (Harusawa 1981) is shown in Table 3.1.

TABLE 3.1 - ESTIMATED CMC DATA

SURFACTANT	EON	CMC_o mole/l	CMC_w mole/l
Igepal ® co210	2	0.30	1×10^{-5}
Igepal ® co520	5	0.03	2×10^{-5}
Igepal ® co720	12	10^{-4}	1×10^{-4}

Note, the CMC_o value for NPE5 in cyclohexane derived from Harusawa et al's data, is lower than, but of the same order as the experimental CMC_o determined here by GC analysis, for a distributed NPE surfactant (average chain length = 5) in the same oil.

HLB_{act} value of the pseudo surfactant phase is constant at the transitional inversion point (constant temperature), therefore, in the proposed model, x_h and x_l must also be constant when the surfactant concentration is such that the distributed surfactants can be regarded as single components.

Figures 3.3, 3.4 and 3.5 show quite clearly that SAD=0 inversion lines, produced by varying the surfactant concentration at constant temperature, converge at f_w=1. This is to be expected as CMC_w values are of a much smaller order than the total surfactant concentration used and, therefore, at f_w=1 approximately all the surfactant present in the system is in the pseudo surfactant phase. Hence, the overall mole average HLB at f_w=1 is approximately equal to HLB_{act} of the pseudo surfactant phase. Therefore, values of x_l and x_h for the systems at inversion (x_{linv}, x_{hinv}) can be calculated from the HLB value at the intercept of the SAD=0 at f_w=1, using figures 3.3, 3.4 and 3.5 and equation [3.10]. Furthermore, in the isothermal inversion technique used, $CMC_o >> CMC_w$ and equation [3.11] can be reduced to a simpler form:

$$-x_h^2(1-f_w)(CMC_{ol}-CMC_{oh})+x_h[(1-f_w)(CMC_{ol}-CMC_{oh})-C_t]+C_h = 0 \quad [3.16]$$

A value for (CMC_{ol}-CMC_{oh}) can be calculated for each system by choosing suitable combinations of inversion data (f_w,mole average HLB - used to calculate C_h) and substituting values for x_{hinv} in equation [3.16]. Note, (CMC_{ol}-CMC_{oh}) $\cong CMC_{ol}$. Hence, the necessary data required by the model is easily calculated from the value of the intercept of SAD=0 line at f_w=1 and the concentration of the surfactant pair at a particular f_w.

The values of x_h and [CMC_{ol}-CMC_{oh}] calculated at each surfactant concentration for the three systems (i), (ii) and (iii) are tabulated in table 3.2.

TABLE 3.2 - MODEL RESULTS

SYSTEM	Line	C_t mol/l	HLB_{act}	x_{hinv}	CMC_{ol}-CMC_{oh} mol/l
C/NPE5-NPE12	1	0.0227	10.70	0.17	0.068
	2	0.0454	10.76	0.18	0.070
	3	0.0681	10.76	0.18	0.076
	4	0.1135	10.76	0.18	0.076
C/NPE2-NPE12	1	0.1135	10.17	0.58	0.424
	2	0.2270	10.05	0.57	0.434
T/NPE5-NPE12	1	0.1135	12.94	0.70	1.080
	2	0.2270	12.81	0.67	1.004

3.5 PARTITION MODEL DISCUSSION

From figures 3.3, 3.4 and 3.5 it can be seen that SAD=0 lines are linear for the range of surfactant concentrations examined and hence, the surfactant pair used can be regarded as individual lumped components for each surfactant concentration. The linearity of the SAD=0 lines justifies the use of equation [3.16] to calculate lumped (CMC_{ol}-CMC_{oh}) values.

In each of the cyclohexane/NPE systems the (x_{hinv},CMC_{ol}-CMC_{oh}) values calculated are reasonably constant, therefore, the overall surfactant concentration used in each of these experiments is sufficiently high, for the system to have reached its plateau region condition (see figure 3.2). These values can be used to predict the position of SAD=0 lines on inversion maps at higher surfactant concentrations. In the case of the Toluene/NPE system, higher surfactant concentrations than those used would be needed for consistency in (x_{hinv},CMC_{ol}-CMC_{oh}) values to be obtained.

The values of (CMC_{ol}-CMC_{oh}) $\cong$ CMC_{ol} found for the cyclohexane/NPE systems are higher than, but of the same order as, that suggested by Harusawa et al's (1981) data, for the average chain lengths. The value of CMC_{ol} for NPE5 in cyclohexane determined by equation [3.16] is in good agreement with the CMC_{ol} value found by GC analysis. The lumped CMC_{ol} value is governed by equation [3.14] and it may be higher than that of the average chain lengtth because it is affected by the relatively high CMCs (>molar) of its short chain length components. The fact that the lumped CMC value is of the same order as the CMC of its average chain length is in good agreement with the "to a first approximation" finding of Allan et al (1989).

Care must be taken to ensure that the SAD=0 line is linear before applying equation [3.16]. It should be noted that the predictions of equation [3.16] may be less accurate at low surfactant concentrations and at low f_w values.

An illustration of distributed surfactants deviating from single component behaviour can be found when examining a discontinuity in the model equation [3.16] if the predicted SAD=0 line passes through the HLB of the lipophilic surfactant in the range f_w=0 to 1 (eg. in figure 3.3 where the lipophilic surfactant is Igepal® co520, HLB=10). At these points x_h=0, hence, $C_{ol} = CMC_{ol}$. The model suggests that there is no lipophilic pseudo surfactant phase to be balanced by hydrophilic surfactant ie. the surfactant concentration is lower than the CMC. In real cases there will be pseudo surfactant phase present, however, the lipophilic surfactant's pseudo surfactant phase concentration will now be so low that the distributed surfactant no longer shows single component behaviour ie. the pseudo surfactant concentration will reduce as f_w decreases. This effect is similar to a decrease in the overall surfactant concentration; hence, the system will move away from the plateau region shown in figure 3.2, towards 0. If f_w is further reduced at HLB=10 by adding more oil phase, the pseudo surfactant phase will become progressively more hydrophilic (see note in introduction) and there may be a transitional inversion point to the left of the predicted point on figure 3.3. It should be emphasised that this deviation from single component behaviour is only found at extrapolated points close to an intersection of the SAD=0 line, with the HLB of the lipophilic surfactant.

3.6 PARTITION MODEL CONCLUSIONS

1) A simple model has been derived that can easily be applied to isothermal transitional phase inversion in nonionic surfactant systems.

2) The model provides a relatively easy way of obtaining mixed surfactant CMC data for lipophilic nonionic surfactants. The model and CMC data can be used to predict the position of SAD=0 lines on inversion maps at higher surfactant concentrations.

3) Distributed nonionic surfactants in oil-water systems can be regarded as single components above a certain surfactant concentration and over a wide oil-water ratio range.

3.7 PART 2 - surfactant partitioning results

In part 1 of this chapter a model was derived which can be used to calculate mixed surfactant CMCs and transitional inversion point HLB_{act} values from linear isothermal transitional inversion lines on a SAD map (HLB_{act} is the HLB of a pseudo surfactant phase). In this part the model is applied to several more systems at varying temperatures; the results are discussed in terms of a nonionic surfactant classification system based on thermodynamic relationships.

The most widely used surfactant classification system is the Hydrophile-Lipophile balance (HLB) - an empirical approach for measuring surfactant affinity. The "balance" is seen as a measure of the surfactant's attraction to water against its attraction for oil. The HLB value assigned to a surfactant is based on analytical or composition data. Attempts have been made to equate HLB with thermodynamic quantities (Davies 1963). However, the limitations of the HLB concept are fully recognized; many researchers have found no correlation between HLB and the type of emulsion formed and have also found variations with water to oil ratio and surfactant concentration. The main failing of the HLB concept, stems from the fact that it takes no account of the oil phase type ie. the HLB concept does not allow a surfactant to have different affinities for different oils.

In a move towards incorporating oil type, Graciaa et al (1983) showed that it is the HLB of a pseudo surfactant phase (termed HLB_{act} here) rather than the weight average HLB that is the important variable. The pseudo surfactant phase refers to interfacial surfactant only ie. it represents all the surfactant in the system that is not dissolved as monomers in the oil and water phases. It was shown that isothermal transitional inversion occurs at a specific HLB_{act} value in the iso-octane/ethoxyphenol (EOP) system for each of a number of combinations of differing chain length EOP surfactants. The HLB_{act} value was calculated from the mole average HLB of the components of the pseudo surfactant phase. The pseudo surfactant phase refinement to the HLB concept merely shows that, for one class of surfactants, SAD is dependent on the average chain length of the surfactant molecules in the pseudo surfactant phase, however, it cannot be used to compare surfactants of different chemical type because this still relies on the HLB concept. Hence, it is unlikely that even HLB_{act} values could be used to compare surfactants of different chemical type.

3.8 BASIS FOR A SURFACTANT CLASSIFICATION SYSTEM

nSOW phase behaviour can only be predicted accurately by reference to the SOW system at its transitional inversion condition, where the surfactant's affinity is balanced. This can be used as a basis for a surfactant classification system. HLB_{act} at SAD=0 (HLB_{inv}) can be used as a reference in a series of surfactants of the same chemical type

- (ie. $HLB_{act}<HLB_{inv}$ will produce Winsor Type 2 systems, $HLB_{act}=HLB_{inv}$ will produce Winsor Type 3 systems and $HLB_{act}>HLB_{inv}$ will produce Winsor Type 1 systems) - but a scale of surfactant chain length would have been equally appropriate. Changes in two SAD variables eg. HLB and temperature, would require a reference HLB_{inv} for each temperature. However, changes in the system's physical properties (eg. CMC affected by all SAD variables) would seem to be a more direct link as a measure of SAD and these can be related to thermodynamic quantities as will be shown later in this chapter.

3.9 SURFACTANT TYPE

The deficiencies of the HLB concept, even when HLB_{act} values of the pseudo surfactant phase are considered, can be discussed by applying the model derived in part 1 to all the systems studied in this chapter. Results are summarised in table 3.3 below (results from part 1 included):

TABLE 3.3 - CMC AND HLB_{act} RESULTS FOR SYSTEMS AT 20°C

SYSTEM	x_{hinv}	CMC_{ol}-CMC_{ob} (moles/l)	MOLE AV. HLB_{act}
Cyclohexane/NPE2-NPE12	0.58	0.424	10.17
Cyclohexane/NPE5-NPE12	0.18	0.070	10.76
Cyclohexane/SML*	0.30	0.097	11.03
Toluene/NPE5-NPE12	0.70	1.080	12.94
Toluene/SML*	0.19	0.052	10.13
nHeptane/NPE2-NPE12*	0.24	0.099	6.90
nHeptane/SML*	0.27	0.084	10.80

*weight average data recalculated to mole average.

Examination of table 3.3 reveals that the HLB_{act} values in the cyclohexane/NPE systems are in fairly good agreement with each other. This is in accordance with the findings of Graciaa et al (1983) for HLB_{act} at inversion at a set temperature using Octylphenol (EOP) surfactants in isoOctane. The HLB_{act} value of SML in cyclohexane is also reasonably close to the cyclohexane/NPE value, however, there is no consistency between SML and NPE results in both the toluene and n-heptane systems.

Therefore, table 3.3 shows that systems containing different oils or different chemical type surfactants, but having the same HLB_{act} value of the pseudo surfactant phase cannot be expected to show similar behaviour. Hence, the HLB concept for surfactant classification becomes meaningless even when considering the HLB_{act} value of the pseudo surfactant phase.

3.10 TEMPERATURE EFFECT

Applying the model to the data of table A3.6 and figure 3.8 and table A3.7 and figure 3.9, the effect of temperature on x_h and (CMC_{ol}-CMC_{oh}) of the cyclohexane/NPE system and n-heptane/NPE system can be examined. Results are tabulated in table 3.4.

TABLE 3.4 - TEMPERATURE EFFECT

SYSTEM - TEMPERATURE/°C	HLB_{act}*	x_h	(CMC_{ol}-CMC_{oh}) moles/l
Cyclo/NPE5-NPE12 20	10.76	0.18	0.070
Cyclo/NPE5-NPE12 40	11.65	0.39	0.086
Cyclo/NPE5-NPE12 60	12.70	0.64	0.146
nHept/NPE2-NPE12 20	6.90	0.24	0.099
nHept/NPE2-NPE12 30	9.40	0.50	0.184
nHept/NPE2-NPE12 50	10.90	0.66	0.263
nHept/NPE5-NPE12 50	10.80	0.19	0.049

* value at 25°C.

As might be expected values of (CMC_{ol}-CMC_{oh}) ≡ CMC_{ol} rise with temperature. In both the cyclohexane/NPE5-NPE12 system and n-heptane/NPE2-NPE12 system the SAD=0 lines tend to converge near the HLB of the lipophilic surfactant, suggesting that C_{ol} at the transitional inversion point remains reasonably constant with temperature variation. Note in the two n-heptane/NPE systems at 50°C, the values of HLB_{act} at inversion are in good agreement with each other (see table 3.4), again in accordance with the findings at 20°C in the cyclohexane/NPE systems.

3.11 CMC AND INVERSION POINT

From the calculated model data of Tables 3.3 and 3.4 it can be seen that:

For NPE surfactants the CMC_o values rise in the oils studied in the order - nheptane < cyclohexane < toluene and correspondingly the value of the inversion HLB_{act} rises in the same order.

For SML surfactants the CMC_o values rise in the order - toluene < nheptane < cylclohexane and the values of HLB_{act} rise in the same order.

It was noted by Shinoda et al (1986), that the higher the HLB of a surfactant in a system the higher the PIT would be. As CMC_o values rise with temperature it may now be proposed that Shinoda's observation is part of a more general rule:

"For a given temperature, the higher the CMC_o for a particular surfactant chain length in an oil the higher the HLB_{act} at transitional inversion will be."

A consequence of rising temperature is rising CMC_o, hence, PIT is a subcase of the above rule. For any given temperature, the better the solvent the higher CMC_o will be, hence, from the rule above, the higher the HLB will be at inversion. In figure 1.6, plots of HLB vs PIT for a number of different oils are shown. From figure 1.6, it can be seen for the oils shown, that for any particular temperature, the HLB at the inversion point decreases in the order: $(CH_3)_2C_6H_4 > C_6H_{12} > nC_7H_{16} > nC_{16}H_{34}$. Therefore, from the above rule, it may be expected that CMC_o values would also decrease in the same order; given the nature of the oils listed, this would seem reasonable (note, the CMC_{ol} values of NPE surfactants in toluene, cyclohexane and n-heptane calculated in this study).

Note also, that HLB_{act} values at inversion are similar in the cyclohexane/SML and nHeptane/SML systems, as are the slopes of the SAD=0 lines and hence, the CMCs.

Hence, it appears that transitional inversion (SAD=0) points in different oil-water systems may be related to each other by the partitioning of the surfactant between oil and water phases.

3.12 GIBBS FREE ENERGY OF PHASE TRANSFER

3.12.1 THEORY

It has already suggested that there may be a connection between transitional inversion and surfactant CMC values for particular environment conditions affecting the surfactant's affinity eg. Oil type and temperature. The thermodynamic variable Gibbs free energy of phase transfer of surfactant from bulk phase to interface is dependent on surfactant type and affinity and hence, changes in the Gibbs free energy of phase transfer will show changes in nSOW phase behaviour.

The Gibbs free energy of phase transfer is defined by equation [3.17] below:

$$\Delta G = -RT \ln K_{o/w} \qquad [3.17]$$

Note changes in other SAD variables eg. salt concentration, can also be related to ΔG.

$K_{o/w}$ was defined by equation [3.12]: For the distributed lipophilic-hydrophilic two surfactant system equation [3.12] becomes:

$$K_{o/w} = \frac{x_l CMC_{ol} + x_h CMC_{oh}}{x_h CMC_{wh} + x_l CMC_{wl}} \qquad [3.18]$$

Note also:

$$\Delta G = \Delta H - T\Delta S \qquad [3.19]$$

If ΔH and ΔS can be regarded as constant for the temperature range studied, (Allan et al (1989) showed that this was a reasonable assumption for a hexane/NPE system) substitution of [3.19] in [3.17] gives:

$$\ln K_{o/w} = \frac{-\Delta H}{RT} + \frac{\Delta S}{R} \qquad [3.20]$$

3.12.2 VARIATION OF $K_{o/w}$ WITH SURFACTANT CHAIN LENGTH

Before proceeding further it is first necessary to have an idea of how $K_{o/w}$ values change with surfactant chain length. In part 1, we used Harusawa et al's data (1981) to determine the order of CMC values of NPE2, NPE5 and NPE12 surfactants in cyclohexane (at 20°C) by assuming that there is a linear relationship between lnCMC and chain length. We can use a similar approach to determine $K_{o/w}$ values for chain lengths 1 to 12; the calculated results are tabulated in table 3.5.

TABLE 3.5 - VARIATION OF $K_{o/w}$ WITH SURFACTANT CHAIN LENGTH AT 20°C

Ethylene oxide Chain length	CMC_o moles/l	CMC_w moles/l	$K_{o/w}$	$\ln K_{o/w}$
1	0.61	10^{-5}	61000	11.0
2	0.30	10^{-5}	30000	10.3
3	0.14	10^{-5}	14000	9.5
4	0.060	2×10^{-5}	3000	8.0
5	0.030	2×10^{-5}	1500	7.3
6	0.013	3×10^{-5}	481	6.2
7	0.006	3×10^{-5}	200	5.3
8	0.003	4×10^{-5}	70	4.3
10	6×10^{-4}	6×10^{-5}	10	2.3
12	10^{-4}	10^{-4}	1	0.0

Table 3.5 shows that $K_{o/w}$ values for surfactant partitioning between an oil and water phase decrease dramatically with increasing surfactant chain length. Hence, it can be seen for a SOW system at any temperature, that ΔG rises with rising HLB of the surfactant. Also, as isothermal transitional inversion occurs at a specific HLB_{act} value in any system, then it follows that isothermal transitional inversion occurs at a specific

ΔG value (ΔG_{inv}) in any one system. Furthermore, if transitional inversion does occur when a certain combination of CMC values is reached, ΔG_{inv} will be constant for the surfactant in all oil/water systems.

If for any temperature there is a specific value of ΔG at which the surfactant's affinity is balanced (SAD=0) then we have the basis for a surfactant classification system: Each surfactant type could be assigned a reference value of ΔG at SAD=0 (ΔG_{inv}). In any SOW system, the free energy of phase transfer for a set of conditions can then be calculated using equation [3.17] and the surfactant's affinity determined by comparison with ΔG_{inv} in accordance with the three phase behaviour possibilities below:

$\Delta G > \Delta G_{inv}$ Type 1 system
$\Delta G = \Delta G_{inv}$ Type 3 system
$\Delta G < \Delta G_{inv}$ Type 2 system

3.12.3 APPLICATION AND RESULTS

To be able to apply the data calculated in this study some assumptions must first be made:

(i) For all the systems studied $CMC_{ol} >> CMC_{oh}$, therefore, $C_{oi} = x_i(CMC_{ol}-CMC_{oh})$,

(ii) Similarly, $CMC_{wh} >> CMC_{wl}$, therefore, $C_{wi} = x_h CMC_{wh}$. This will be true for the NPE2-NPE12 systems and the SML systems where the difference in HLB numbers is large and will be approached in the NPE5-NPE12 systems.

(iii) The third assumption required is that the CMC_{wh} values of NPE12 (Igepal® 720) and SML (Tween® 20) are unaffected by the oil phase. Harusawa et al (1981), noted that the application of the CMC values in pure water, to nonpolar hydrocarbon-water systems will not lead to large errors. With the possible exception of toluene systems this is a valid assumption, hence, CMC_{wh} will be regarded as constant for each of the oil-water systems studied.

Applying the assumptions, equation [3.18] becomes:

$$CMC_{wh}.K_{o/w} = \frac{x_l}{x_h} \quad (CMC_{ol} - CMC_{oh}) \qquad [3.21]$$

Table 3.6 summarises the $CMC_{wh}.K_{o/w}$ values at SAD=0 calculated using equation [3.21] from the data of Table 3.3 and Table 3.4:

TABLE 3.6 - Values of $CMC_{wh}.K_{o/w}$ at SAD=0

SYSTEM	TEMP/°C	$CMC_{wh}.K_{o/w}$
cyclohexane/NPE2-NPE12	20	0.31
cyclohexane/NPE5-NPE12	20	0.32
n-heptane/NPE2-NPE12	20	0.31
toluene/NPE5-NPE12	22	0.46
cyclohexane/SML	20	0.23
n-heptane/SML	20	0.23
toluene/SML	20	0.22
cyclohexane/NPE5-NPE12	40	0.13
cyclohexane/NPE5-NPE12	60	0.08
nHeptane/NPE2-NPE12	30	0.18
nHeptane/NPE2-NPE12	50	0.13
nHeptane/NPE5-NPE12	50	0.21

Both the NPE systems at 20°C and the SML systems at 20°C show remarkable consistency in $CMC_{wh}.K_{o/w}$ values at SAD=0.

3.12.4 OTHER TRANSITIONAL INVERSION STUDIES - ISO-OCTANE/EOP SYSTEM

Graciaa (1989) showed that for isothermal conditions, the HLB_{act} value at the transitional inversion point was constant, when the surfactant was a mixture of differing chain length molecules of the same chemical type. In Graciaa et al's study, mixtures of a lipophilic distributed surfactant and a hydrophilic distributed surfactant were used to set SAD=0 at different WOR. Hence, we can apply the model derived here to Graciaa et al's data, to calculate mixed CMC_{ol} values. Graciaa (1989) also gave values for the CMC_w and CMC_o for each chain length of the surfactant in the oil-water system. We shall use the CMC_w values for the average chain length of Graciaa et al's distributed surfactants, together with the mixed CMC_{ol} calculated from equation [3.16], to calculate the expected order of $K_{o/w}$ for the iso-octane/EOP system at the transitional inversion point. Note, an accurate determination of $K_{o/w}$ is not possible by this method because the mixed CMC_w values of a distributed surfactant are not equal to the average chain length CMC_w value - but they will be of the same order.

Graciaa et al's inversion data are tabulated in table A3.8 of appendix 3 and plotted on figure 3.10. From figure 3.10, it can be seen that the SAD=0 lines converge at f_w=1, in agreement with the earlier discussion (although the number of data points is somewhat limited). HLB_{act} and CMC_{ol} values calculated from the SAD=0 lines using equation 3.16 are tabulated in table 3.7 below (Graciaa (1989) data for the CMC_o value for the average chain length is also shown for comparison):

TABLE 3.7 - mixed CMC_{ol} and HLB_{act} values calculated from SAD=0 data (Graciaa 1989) - Iso-octane/EOP system (overall surfactant concentration =0.0341moles/l).

SYSTEM surfactant pair	HLB_{act}	x_{hinv}	CMC_{ol} from eqn[3.16] (moles/l)	CMC_{ol} Graciaa data (moles/l)
1. EOP3-EOP9	10.0	0.41	0.05	0.033
2. EOP3-EOP7	10.0	0.525	0.05	0.033
3. EOP1.5-EOP9	10.0	0.63	0.15	0.14*
4. EOP1.5-EOP7	10.0	0.72	0.14	0.14*

* the average value of EOP1 and EOP2 is given.

The mixed CMC_o values of the EOP3 surfactant derived from system (1) and system (2) are in good agreement with each other, as are the two EOP1.5 values from system (3) and system (4). In each case the mixed CMC_{ol} value is of the same order as Graciaa et al's experimentally determined value for the average chain length. In the case of the EOP1.5 surfactant good agreement is found between the values of the calculated mixed CMC_{ol} and Graciaa et al's CMC_{ol} for the average chain length. This is because the distribution of chain lengths of a EOP1.5 surfactant cannot be very wide.

The values calculated for the partition coefficient at the transitional inversion point are tabulated in table 3.8 below:

TABLE 3.8 - Iso-octane/EOP partition coefficient at SAD=0 (25°C)

SYSTEM surfactant pair	x_{hinv}	CMC_{ol} moles/l	CMC_{oh} moles/l	CMC_{wl} moles/l	CMC_{wh} moles/l	$K_{o/w}$	ΔG SAD+ to SAD-
EOP3-EOP9	0.41	0.05	$2.1x10^{-4}$	$1.03x10^{-4}$	$3.04x10^{-4}$	160	-13.0
EOP3-EOP7		0.05	$1.5x10^{-3}$	$1.03x10^{-4}$	$2.68x10^{-4}$	130	-12.5
EOP1.5-EOP9	0.525	0.15	$2.1x10^{-4}$	$6.3x10^{-5}$	$3.04x10^{-4}$	250	-14.1
EOP1.5-EOP7	0.63	0.14	$1.5x10^{-3}$	$6.3x10^{-5}$	$2.68x10^{-4}$	180	-13.3
	0.72						

The values for $K_{o/w}$ for each case are of the same order. The differences in the exact values is due to the fact that the values used for CMC_{oh}, CMC_{wh} and CMC_{wl} were not mixed CMC values.

Hence, from the analysis of sections 3.12.3 and 3.12.4, it appears that for a given temperature, if CMC_{wh} can be regarded as constant, that isothermal transitional inversion in nonionic surfactant-oil-water systems occurs when $K_{o/w}$ acquires a particular value - a characteristic of the surfactant type.

We will now examine changes in ΔG_{inv} with temperature.

3.12.5 TEMPERATURE CHANGE

CMC_w values of nonionic surfactants usually initially decrease with temperature increase (a $\ln CMC_w$ vs $1/T$ relationship has been noted (Meguro 1984)) and then increase above 50°C (Rosen 1989). However, over a 40°C increase CMC_w values will typically decrease by some 20% of the initial value and hence, for the purpose of this analysis, CMC_{wh} (for NPE12) will be considered constant with temperature.

From equation [3.20] if ΔH_{inv} and ΔS_{inv} remain reasonably constant with rising temperature, then $K_{o/w}$ values must decrease at the inversion point as the temperature rises (Note: ΔH is negative). If CMC_{wh} can be regarded as reasonably constant for each system at each temperature, then refering to Table 3.6 it can be seen that, for both the cyclohexane/NPE5-NPE12 system at 20°C, 40°C and 60°C and the nHeptane/NPE2-NPE12 system at 20°C, 30°C and 50°C, that the $K_{o/w}$ at the transitional inversion point do indeed decrease with rising temperature.

Substituting $CMC_{wh} = 10^{-4}$ moles/l (from Harusawa's data) into equation [3.21], values of $K_{o/w}$ can be calculated and $\ln K_{o/w}$ vs $1/T$ plotted (see Table 3.9 and Figure 3.11).

TABLE 3.9 - VALUES OF $LnK_{o/w}$ AT SAD=0 VS 1/T

SYSTEM	TEMP/ C	$K_{o/w}$	$lnK_{o/w}$	1/T (K^{-1})
toluene/NPE5-NPE12	22	4500	8.4	0.00340
cyclo/NPE2-NPE12	20	3200	8.1	0.00341
cyclo/NPE5-NPE12	20	3300	8.1	0.00341
cyclo/NPE5-NPE12	40	1300	7.2	0.00319
cyclo/NPE5-NPE12	60	800	6.7	0.00300
nHept/NPE2-NPE12	20	3100	8.0	0.00341
nHept/NPE2-NPE12	30	1800	7.5	0.00330
nHept/NPE2-NPE12	50	1300	7.2	0.00310
nHept/NPE5-NPE12	50	2100	7.6	0.00310

Allowing for the constant CMC_{wh} assumption, the plot $lnK_{o/w}$ vs 1/T is remarkably linear, also, the spread of the data at any temperature is not significantly wide. Hence, the results are in good agreement with equation [3.20]. Figure 3.11 can be used to calculate values for ΔH and ΔS at the transitional inversion point, ΔH_{inv} and ΔS_{inv}. The results of this study show that ΔH_{inv} and ΔS_{inv} may be constant for NPE surfactants in all oil-water systems, when the systems are at their transitional inversion point. Therefore, the phase behaviour (Type 1, Type 2, Type 3) of a nSOW system (and hence, the stable emulsion type) can be determined at any temperature, by referencing the partition coefficient of the surfactant monomers between the oil and water phases with K_{inv} calculated from substitution of ΔH_{inv} and ΔS_{inv} in equation [3.20].

Figure 3.11 can be used to gain an idea of the magnitude of the thermodynamic phase transfer parameters at the transitional inversion point.

From the $K_{o/w}$ value at 20°C ie. for a transitional inversion SAD+ to SAD-:

$$\Delta G_{inv} = -19.6 \text{ kJ/mole}$$

3.13 SAD CORRELATIONS

In the literature review of chapter 1, optimum formulation correlations were discussed. Bourrel (1980) showed for ethoxylated nonionic surfactants that SAD was a linear function of temperature, oil EACN, surfactant chain length (EON) and salinity. In the section above, a thermodynamic basis for SAD was established ie. SAD=0 when

$\Delta H=\Delta H_{inv}$ and $\Delta S=\Delta S_{inv}$. The relationship between oil EACN, temperature and the surfactant chain length at the transitional inversion point (EON_{inv}) is derived below, from a thermodynamic basis:

The affinity of a distributed surfactant or a mixture of surfactants is related to the mole average chain length of the surfactant in the interfacial monolayer. The CMC of a surfactant in oil and water has been shown (Crook 1963) to have an approximately logarithmic relationship with the mole average chain length of a distributed surfactant (at constant temperature). Hence, it follows that the partition coefficient of a surfactant mixture between oil and water can be approximated by an expression of the form:

$$\ln K_{o/w} = k_1 EON + k_2 \qquad [3.22]$$

where, EON = mole average chain length of the pseudo surfactant phase,
k_1 and k_2 are constants depending on the oil type.

Allan et al (1989) examined the temperature dependence of the partition coefficent of NPE surfactants in hexane. They showed that ΔH and ΔS are linear functions of EON. Hence:

$\Delta H = k_3 EON + k_4 \qquad \Delta S = k_5 EON + k_6$

where, k_3 to k_6 are constants depending on the oil type,

$\Delta G=\Delta H-T\Delta S = EON(k_3-Tk_5) + k_4-Tk_6$

Hence,

$$EON = \frac{\Delta H-k_4}{k_3-Tk_5} - \frac{T(\Delta S-k_6)}{k_3-Tk_5} \qquad [3.23]$$

Allan et al's data for the constants k_3 to k_6 for the hexane/NPE system showed considerable scatter: k_3=7 ($\pm$4.4) and k_5=13 ($\pm$15). However, from the data it is reasonable to assume that $k_3 << Tk_5$, then equation [3.23] can be rewritten:

$$EON = -\frac{\Delta H-k_4}{k_5}\left[\frac{1}{T}\right] + \frac{\Delta S-k_6}{k_5} \qquad [3.24]$$

If ΔH_{inv} and ΔS_{inv} can be regarded as constant at the transitional inversion point for a particular surfactant type in any oil-water system, then equation [3.24] can be used to calculate EON_{inv} - the mole average chain length of the pseudo surfactant phase of a system at the transitional inversion point at any temperature.

To test the validity of equation [3.24], values of EON_{inv} vs T for the cyclohexane/NPE5-NPE12 system can be calculated from the HLB_{act} values of table 3.4. The PIT for two more EON_{inv} values were determined for the same system under conditions of f_w=0.8 and surfactant concentration = 0.1 moles/l (for these conditions the overall mole average HLB≡HLB_{act}). The data is summarised in table 3.10 and plotted on figure 3.12.

TABLE 3.10 - SURFACTANT CHAIN LENGTH AT SAD=0 VS 1/T

EON_{inv}	PIT (°C)	$1/T\ (K^{-1})\times10^3$
5.8	20.0	3.41
6.2	30.5	3.29
7.0	40.0	3.19
8.1	49.5	3.10
8.7	60.0	3.00

Figure 3.12 shows that again there is good agreement between result and theory. The constants k_3 to k_6 will depend on the oil type. As oil type can be correlated by EACN, then there must be a relationship between EACN and the values of the constants. Hence, the variation of EON_{inv} with EACN could be included in equation [3.23].

3.14 CONCLUSIONS - Surfactant partitioning

This study has shown how the SAD variables - mole average chain length of a pseudo surfactant phase (HLB_{act}) and temperature relate to each other in terms of thermodynamic parameters, based on the partitioning of surfactant between oil and water phases. It was shown that at any one temperature transitional inversion in NPE systems occurs at a specific ΔG value - independent of the oil type. The variation of the PIT with surfactant chain length can be determined by considering ΔH and ΔS to be constant at the transitional inversion point; this can then be used to show that EON_{inv} varies with 1/T.

Previous studies (Salager 1988) have shown which variables affect the surfactant's affinity and linear correlations have been derived to link SAD variables together (Bourrel 1980). Future work could now concentrate on the effects different SAD variables have on the surfactant's partitioning between oil and water and hence, their effect on ΔG, ΔH and ΔS. It is only with studies of this type that we will move from the correlation approach of HLB, PIT and optimum formulation equations, to a clearer understanding of nSOW phase behaviour based on thermodynamic principles.

This completes the discussion on nSOW phase behaviour. Chapter 4, 5 and 6 to follow, are concerned with the drop sizes of emulsions present before and after inversion.

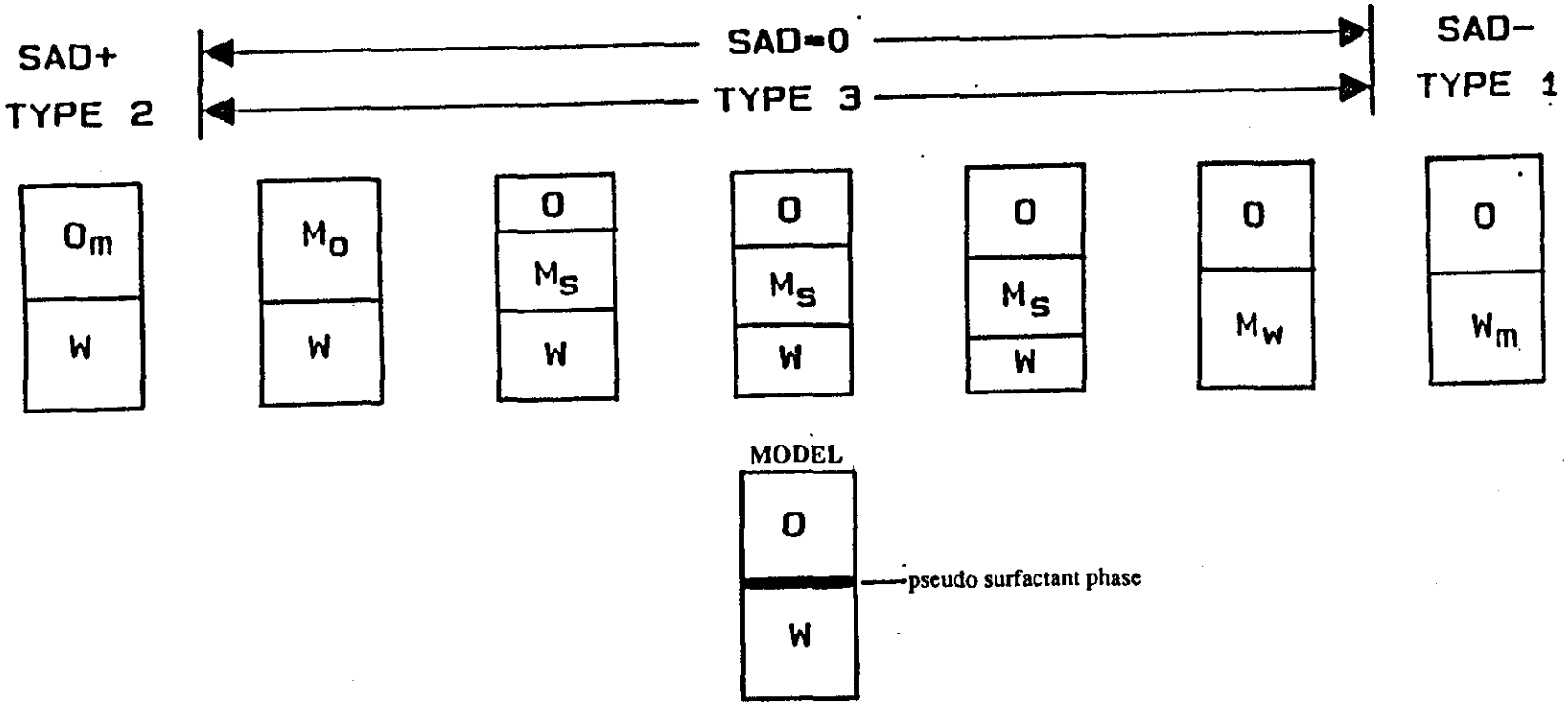

FIGURE 3.1 -Surfactant partitioning model structure and the settled volumes present for each possible nSOW phase behaviour condition.

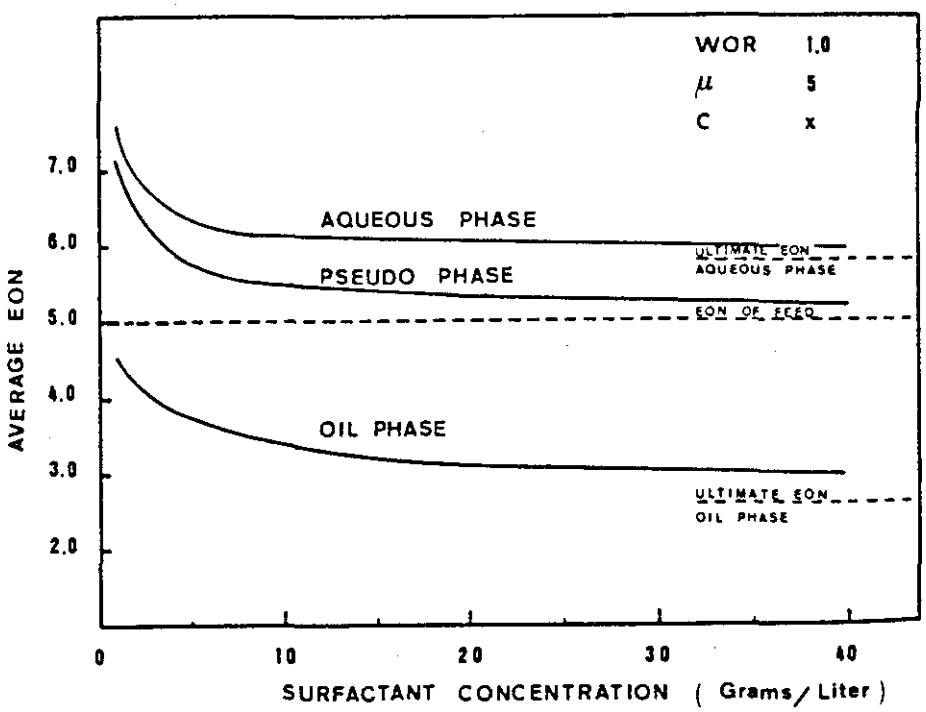

FIGURE 3.2 -Effect of surfactant concentration on the average EON in each phase (reproduced from Graciaa 1983).

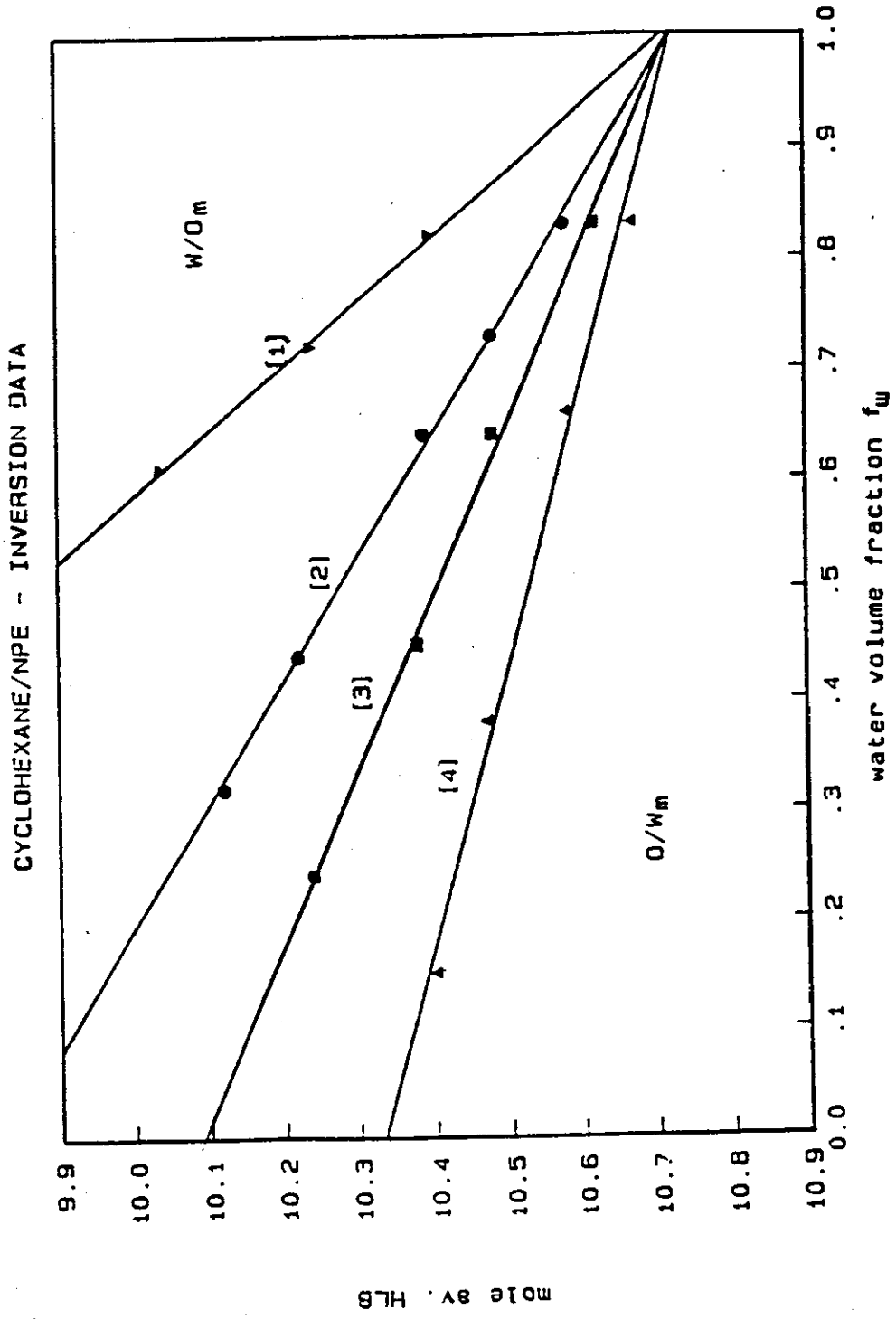

FIGURE 3.3 -Transitional inversion lines - Cyclohexane/NPE5-NPE12 system at surfactant concentrations: [1] 0.0277 moles/l, [2] 0.0454 moles/l, [3] 0.0681 moles/l, [4] 0.1135 moles/l.

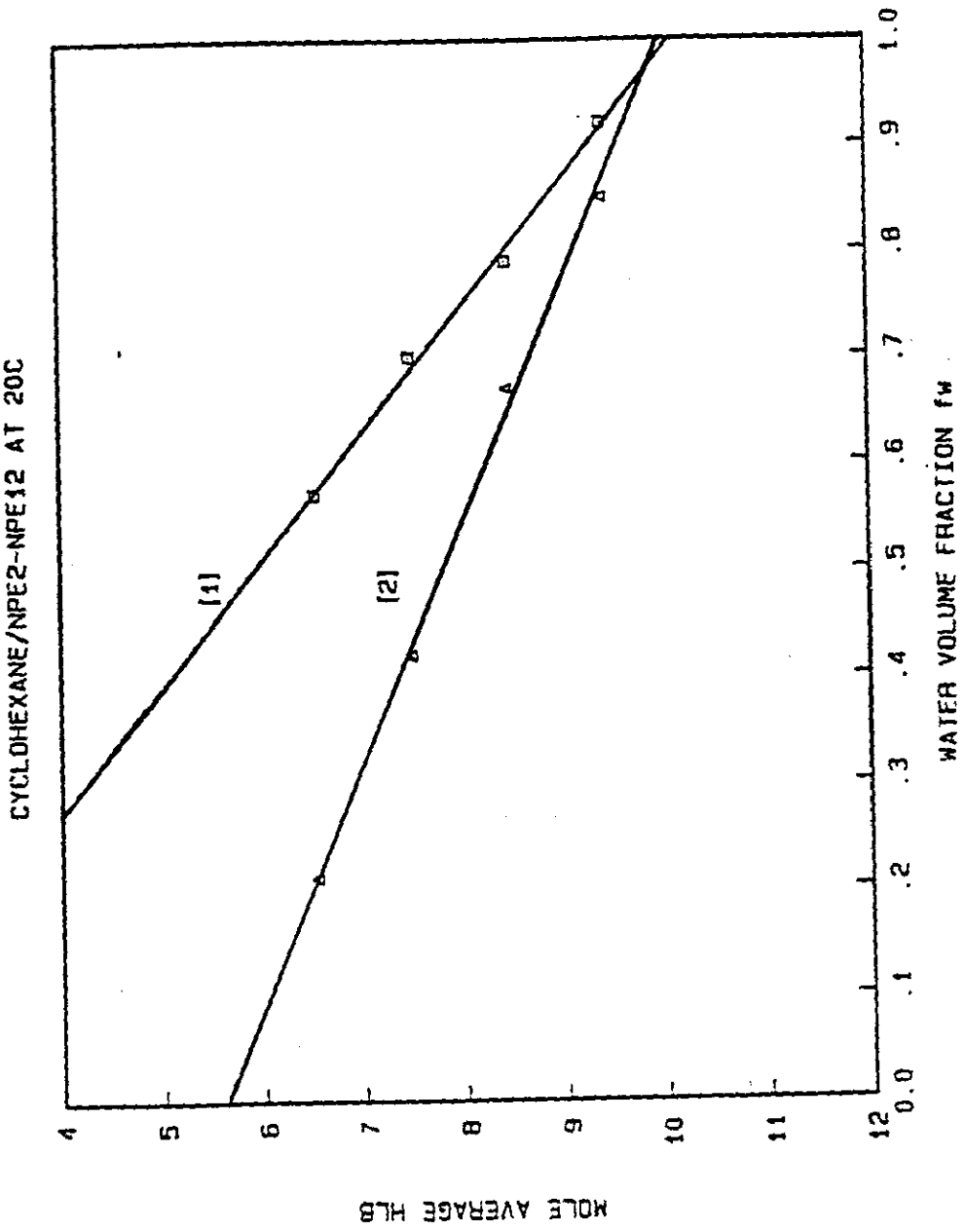

FIGURE 3.4 -Transitional inversion lines - Cyclohexane/NPE2-NPE12 system at surfactant concentrations: [1] 0.1135 moles/l, [2] 0.227 moles/l.

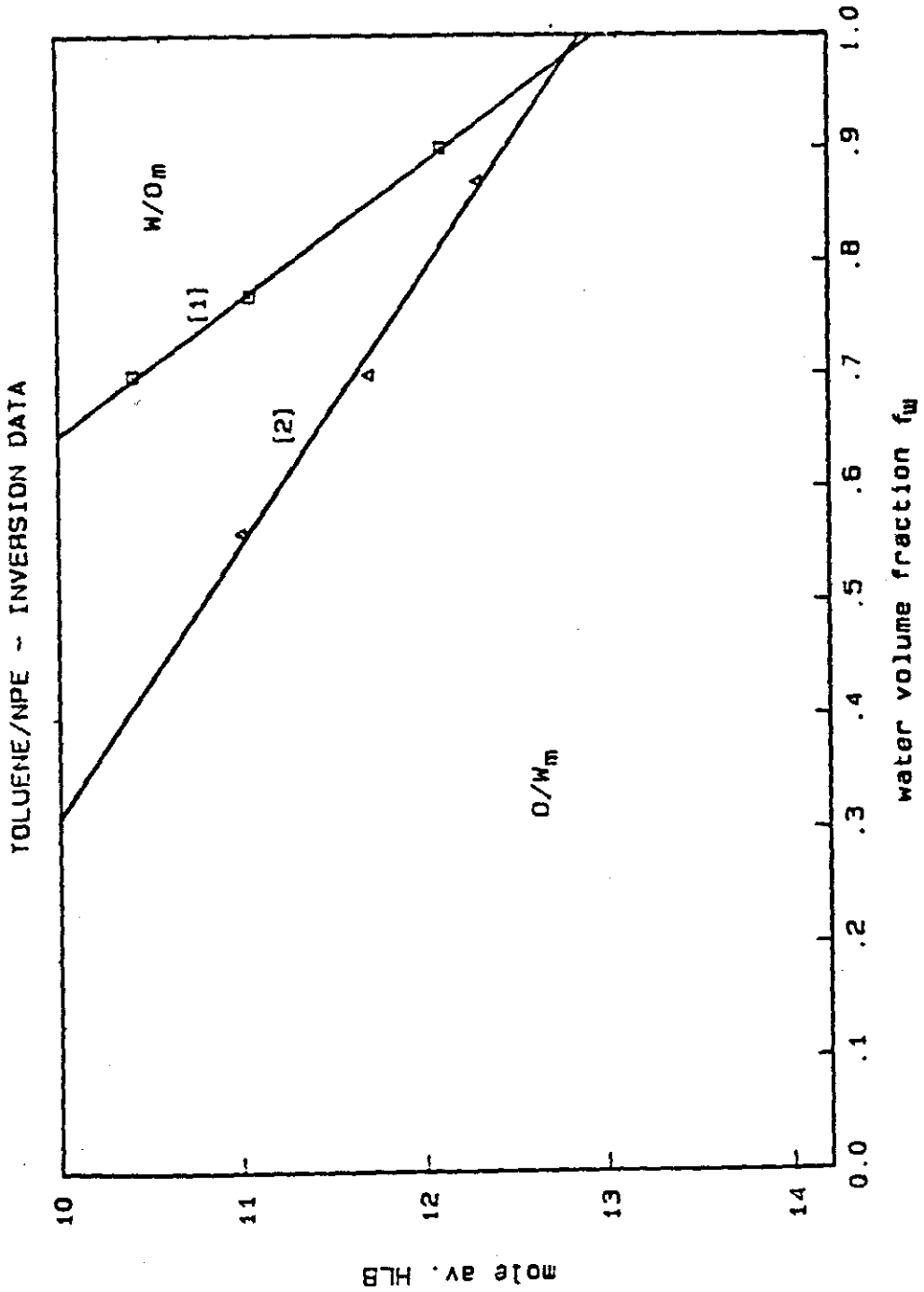

FIGURE 3.5 -Transitional inversion lines - Toluene/NPE5-NPE12 system at surfactant concentrations: [1] 0.1135 moles/l, [2] 0.227 moles/l.

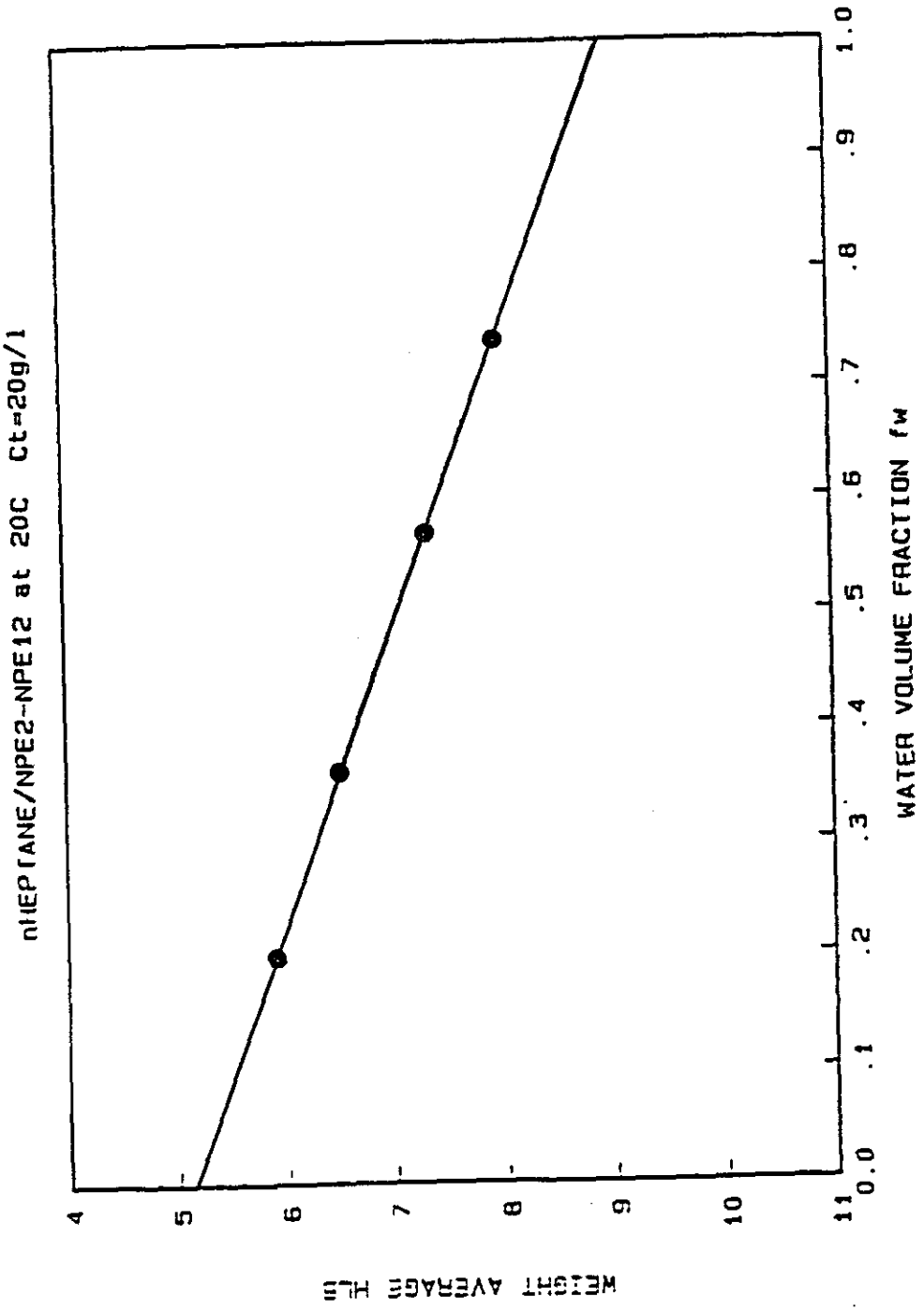

FIGURE 3.6 -Transitional inversion line nHeptane/NPE2-NPE12 system 20°C, surfactant concentration = 20g/l.

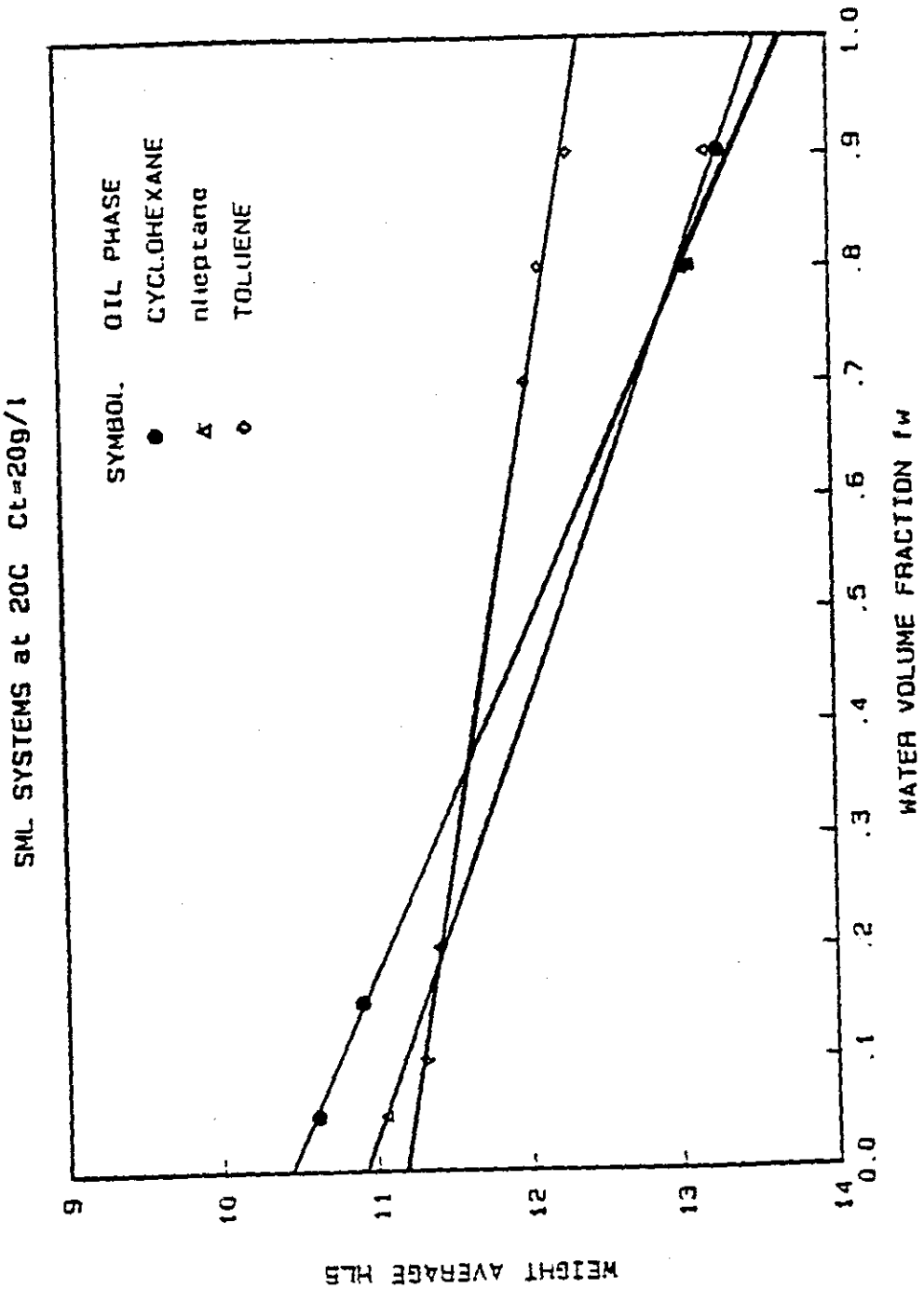

FIGURE 3.7 -Transitional inversion lines in SML systems 20°C, surfactant concentration 20g/l.

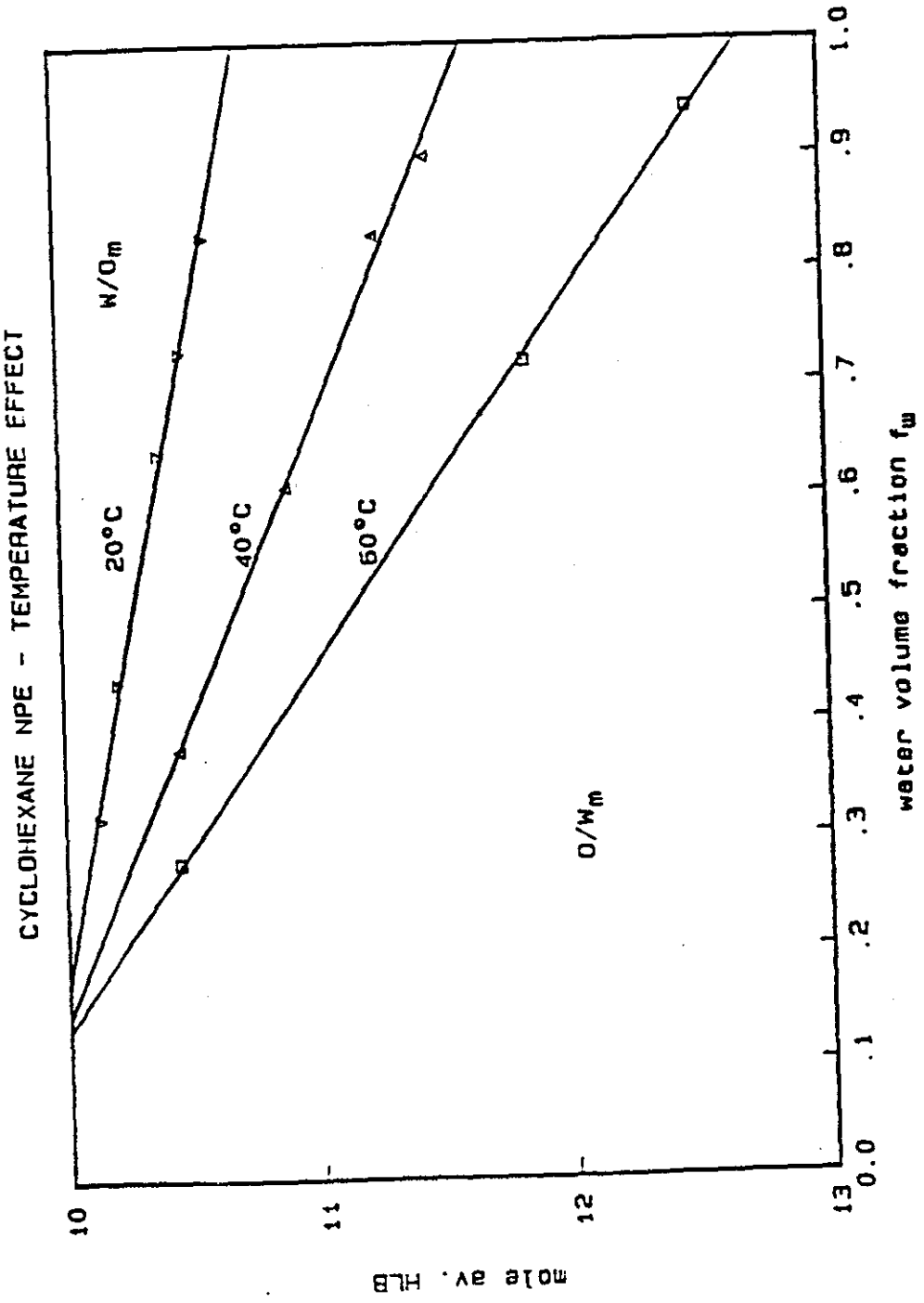

FIGURE 3.8 -Temperature effect on transitional inversion,
Cyclohexane/NPE5-NPE12 system, surfactant concentration = 0.0454 moles/l.

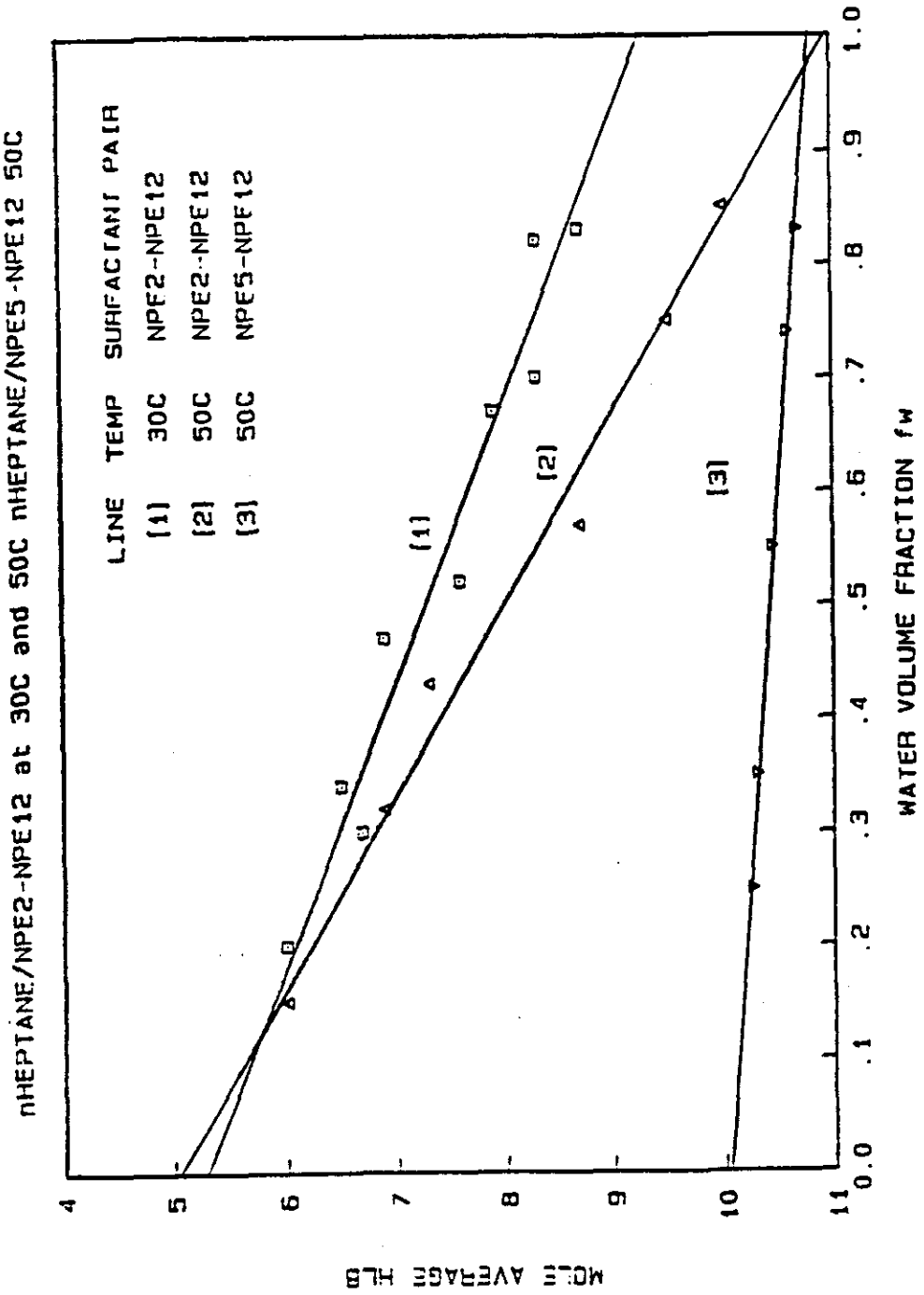

FIGURE 3.9 -Temperature effect on transitional inversion, nHeptane/NPE systems, surfactant concentration = 0.0454 moles/l.

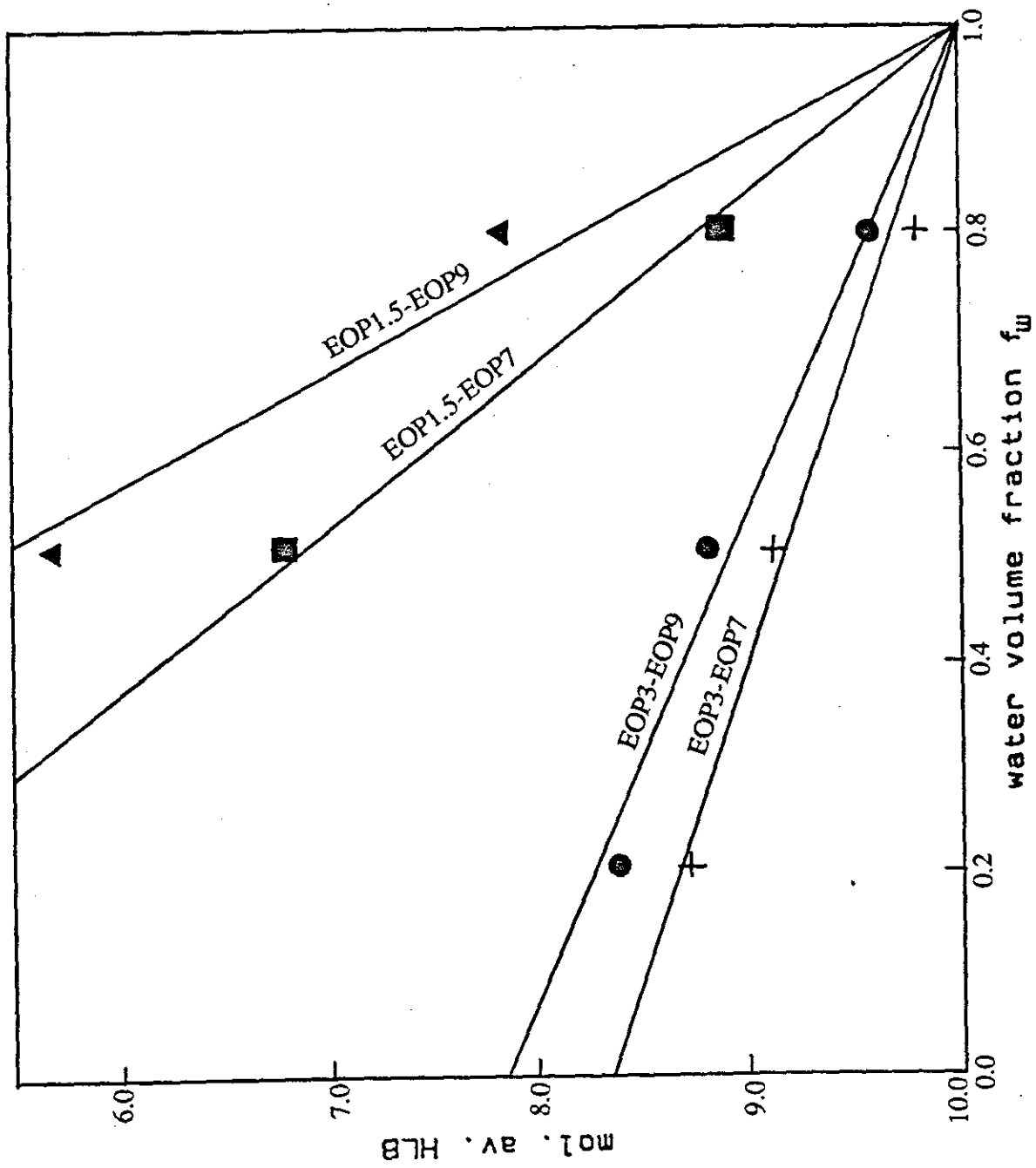

FIGURE 3.10 -Transitional inversion lines - iso-octane/EOP systems at 25°C, surfactant concentration = 0.034 moles/l (Data from Graciaa 1989).

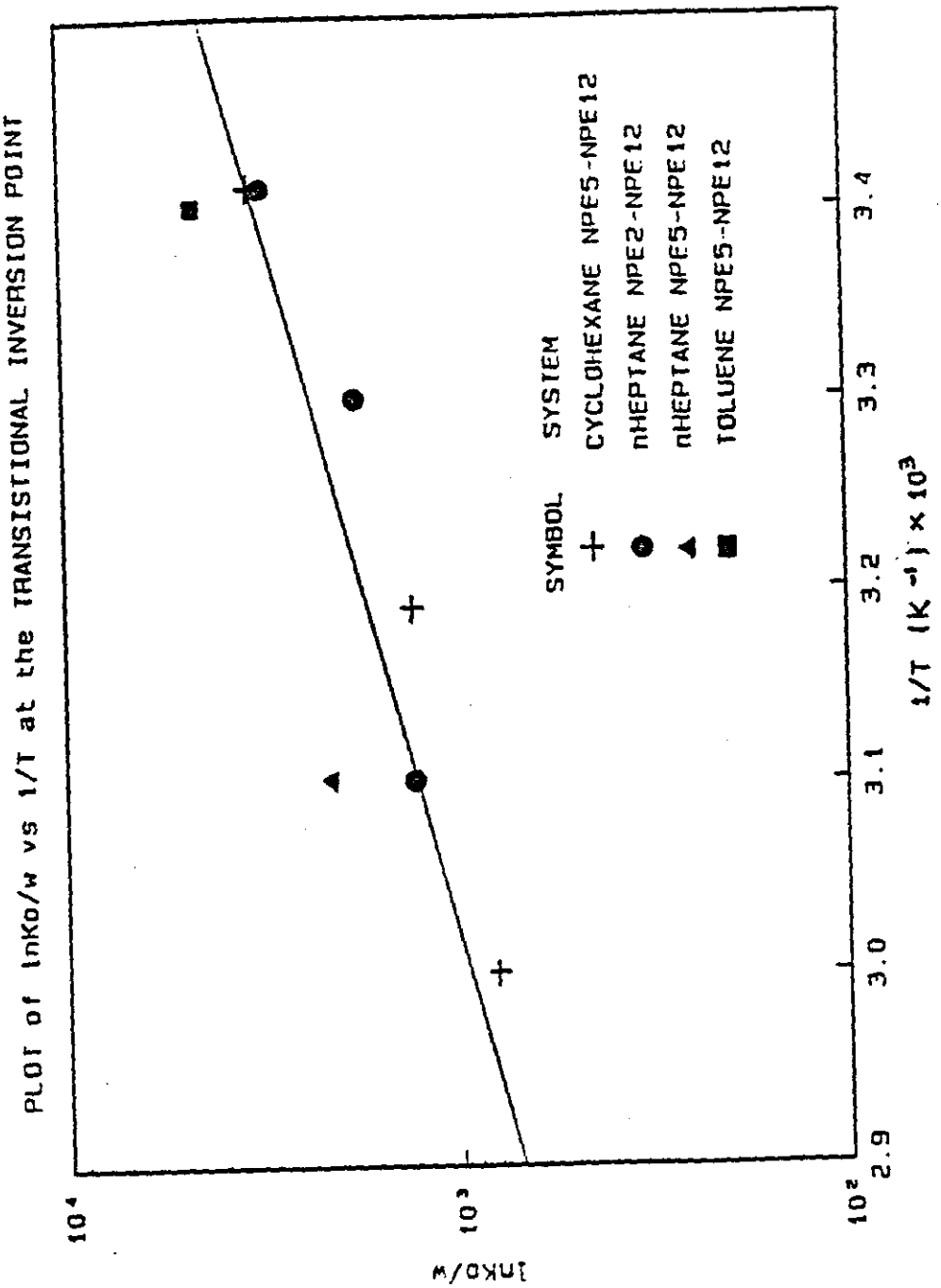

FIGURE 3.11 -Plot of $\ln K_{o/w}$ vs 1/T for all the systems studied at their transitional inversion points.

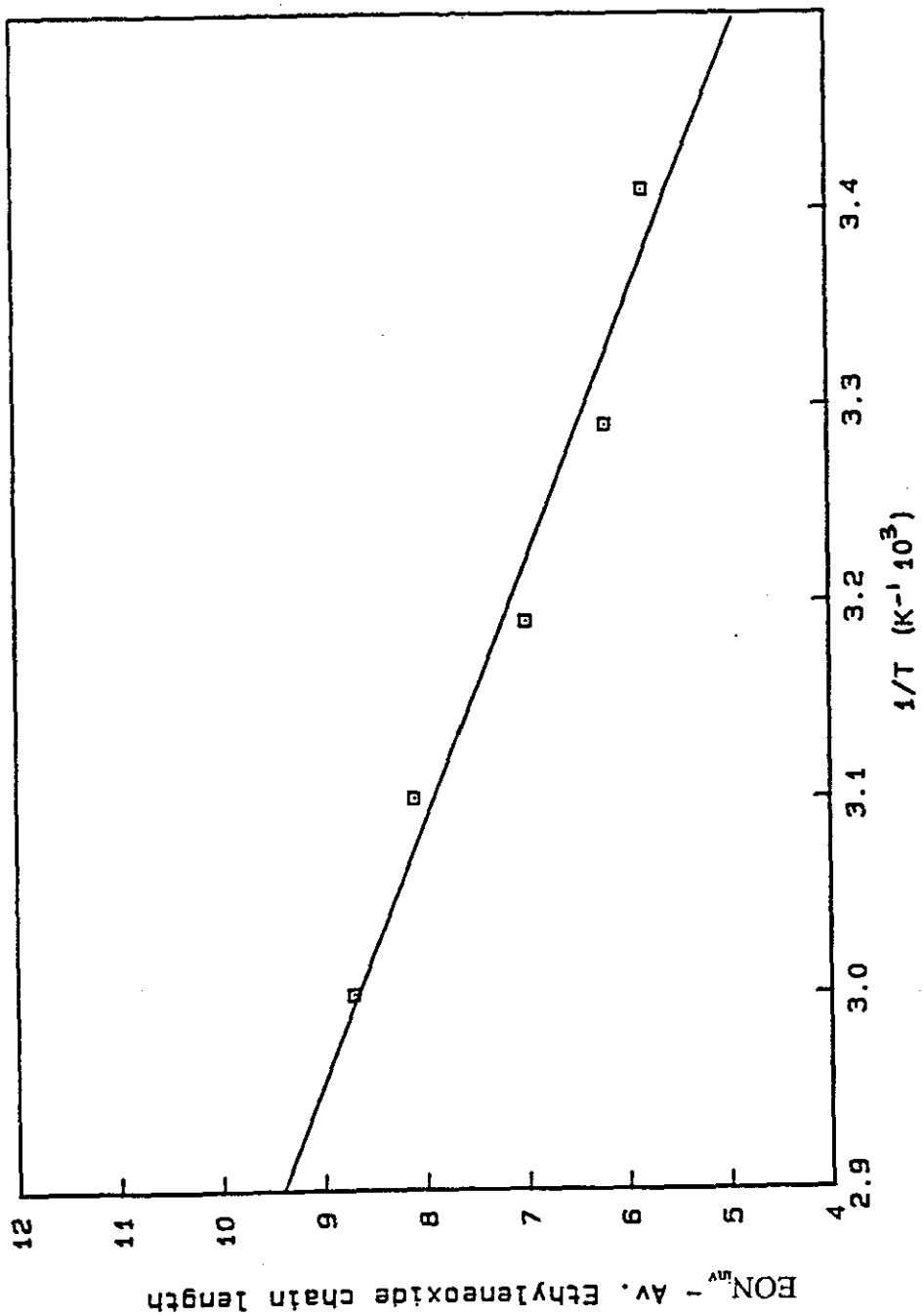

FIGURE 3.12 -Plot of EON_{inv} - mole average chain length of interfacial surfactant at the transitional inversion point vs 1/T (Cyclohexane/NPE5-NPE12 system).

CHAPTER 4
LITERATURE REVIEW OF DROP BREAKAGE AND DROP COALESCENCE IN AGITATED VESSELS

4.1 INTRODUCTION

Chapters 5 and 6 to follow are studies of the emulsion drop types and sizes present before and after inversion. In order to be able to discuss the results of these chapters, it is necessary to have an understanding of drop breakage and drop coalescence in agitated vessels. The relevant literature is briefly reviewed in this chapter (comprehensive reviews are to be found in the literature, see Nagata 1975, Coulaloglou 1976, Mersman 1982 and Tavalrides 1981).

4.2 DROP SIZE STUDIES - STANDARD TANK GEOMETRY

In the majority of drop size studies in agitated vessels, a stirrer and vessel of "standard geometry" are used. The standard geometry (Nagata 1975) of a vessel and 6-blade turbine stirrer are shown in figure 4.1. The effect of the vessel dimensions, stirrer dimensions and baffle dimensions were discussed by Nagata (1975) and Oldshue (1983).

4.3 DYNAMIC DROP SIZE EVENTS IN A STIRRED VESSEL

Emulsions agitated in a stirred vessel are in a constantly changing dynamic state, with drops being broken up and drops coalescing at any one time. The emulsion's drop size distribution can be modelled by the following population balance equation for all drops of volume v (Stamatoudis 1985):

$$r_b(v')\alpha(v')\beta(v,v')\,dv' + F(v-v',v')\,dv' = r_b(v) + F(v,v')\,dv' + d[N(t)A(v)]/dt \qquad [4.1]$$

where, $r_b(v)$ is the number of drops of size v breaking per unit volume per unit time,
$F(v,v')\,dv'$ is the number of pairs of drops of size v and v' coalescing per unit volume of dispersion per unit time,
$\alpha(v')$ is the number of daughter drops resulting from a breakage of a drop of volume v',
$\beta(v,v')\,dv'$ is the fraction of drops with volume v formed by the breakage of a drop of volume v',

A(v) dv is the volume fraction of drops of size v,

N(t) is the number of drops of all sizes per unit time t,

L is the maximum drop size present in the dispersion.

The terms on the left hand side represent the contribution of drops of volume v by breakage of larger drops and by coalescence of smaller drops, respectively. The first two terms on the right hand side represent the loss of drops of size v due to breakage and coalescence. The last term on the right hand side is an accumulation term.

The drop breakage rate $r_b(v)$ depends on the interfacial tension and on the flow field outside the drops. The drop coalescence rate F(v,v'), again is a function of the flow field and also, the collision efficiency between colliding drops. The collision efficiency is dependent on the time that two drops remain in contact and the time for the continuous phase film between the drops to drain out to achieve film rupture and hence, coalescence.

An emulsion's drop size distribution at any time is the result of the dynamics of drop breakage rates and coalescence rates. Although equation [4.1] is useful for describing the events affecting the drop sizes of an agitated emulsion, in practice, no complete solution of equation [4.1] has been attempted because of the complexities of drop break up and drop coalescence.

4.4 FLOW FIELD - REYNOLD'S NUMBER

The difficulty in the calculation of drop sizes of emulsions in stirred vessels stems from the fact that in a stirred vessel a wide range of shear rates exist. There is a dispersing zone around the impellor and a coalescing zone through the rest of the tank. Park et al (1975), examined drop breakage at different points in a baffled stirred vessel, they found that for low dispersed phase systems (f_{disp}<0.1), drop breakage did not occur in regions of the vessel beyond distances of 1/6 impellor diameter from the impellor tip ie. break up was confined to the region swept out by the impellor - approximately 10% of the tank volume. Through the other 90% of the tank volume, drops coalesced, but did not break up. The maximum impellor zone shear rate is of most interest for drop break up as all drop s will eventually enter that zone (Oldshue 1983).

In a similar way to that used in pipe flow, mixing conditions in agitated vessels can be determined from Reynold's number (Re). Where for an agitated vessel:

$Re = ND^2\rho_{eff}/\mu_{eff}$ _____[4.2] where, N = stirrer speed (rev/s),
D = stirrer diameter (m),
ρ_{eff} = effective emulsion density (kg/m^3),
μ_{eff} = effective emulsion viscosity (Pa.s).

For emulsions of low dispersed phase fraction, the density and viscosity of the continuous phase are used as the effective emulsion density and effective emulsion viscosity respectively. However, for emulsions of high dispersed phase fraction (as will be present in catastrophic inversions), the dispersed phase fraction (f_{disp}) and dispersed and continuous phase viscosities (μ_d, μ_c) affect the effective emulsion viscosity. There are many correlations for μ_{eff} to be found in the literature, these were reviewed by Guilinger et al (1988) for low and high dispersed phase emulsions. These authors found that a correlation by Vermeulen et al (1955) best fitted their results:

$$\mu_{eff} = \left[\frac{\mu_c}{1 - f_{disp}}\right]\left[1 + \frac{1.5\mu_d f_{disp}}{\mu_d + \mu_c}\right] \quad \text{[4.3a]}$$

Also,

$$\rho_{eff} = \rho_c(1-f_{disp}) + \rho_d f_{disp} \quad \text{[4.3b]}$$

where, ρ_c is the continuous phase density and ρ_d, is the dispersed phase density.

Generally, for turbine impellors in agitated vessels, Re and mixing conditions are correlated as follows (Perry 1974):

Re	Flow Field
>10000	Turbulent
10000>Re>10	Transitional (turbulent at impellor, laminar in regions remote from the impellor.
<10	Laminar.

Note, for laboratory scale mixers, Leng (1982), found that the transition to turbulent flow occurred at Re=1000.

Laminar flow is usually avoided in agitated vessels because of phase separation below a certain minimum rotational speed of the impellor (for critical agitator speed required for dispersion see equation [4.4] below). Hence, the literature reviewed here mainly concerns turbulent and transitional regimes. Those aspects of laminar shear flow relevant to this study will be reviewed in the discussion of the drop size results of chapters 5 and 6.

The critical agitator speed (N_c) required to disperse a lighter liquid in a more dense liquid using a paddle, in a flat bottomed cylindrical vessel, with a liquid depth, $H=D_t$, can be calculated from equation [4.4] (Nagata 1975):

$$N_c = KD_t^{-2/3} (\mu_c/\rho_c)^{1/9} [(\rho_c-\rho_d)/\rho_c]^{0.26} \quad [4.4]$$

(Conditions - $D=D_i/3$, $B=0.06D_t$, number of paddles=4, $T=D_i/2$, $K=750$ for agitator located at the vessel centre.)

4.5 DROP DEFORMATION

Drops are formed by stress being imparted to a primary drop, causing elongation of all or part of it, followed by the development of surface wave growth to the point where the primary drop breaks into droplets and smaller satellite droplets (see figure 4.2, Stephenson (1974)). The factors important to this process are:

(a) Viscous and elastic properties of the disperse and continuous phases,
(b) the interfacial properties,
(c) the flow conditions.

For drop break up to be achieved, the drop's Laplace pressure which opposes the deformation must be overcome. The Laplace pressure occurs because the pressure on the concave side of a curved interface with interfacial tension σ, is higher than that at the convex side by an amount:

$$\Delta P = \sigma(1/r_1+1/r_2) \quad [4.5]$$

where, r_1 and r_2 are the principal radii of curvature (for a spherical drop equation [4.5] becomes $\Delta P=2\sigma/r$).

Drops can be broken up either by turbulence causing pressure gradients across the drop or by viscous shear exerted by the surrounding liquid.

4.6 TURBULENT FLOW

The complexity of turbulent flow in agitated vessels makes analysis extremely difficult. In all but qualitative discussions, treatment is confined to isotropic turbulent flow ie. the velocity fluctuations have no preferred direction. Much of the theory of isotropic turbulence is due to Kolmogoroff (1941 and 1949).

Kolmogoroff Length Scale

Turbulent motion is considered as a superpostion of a spectrum of velocity fluctuations and eddy sizes on an overall mean flow. Large eddies (of the size of the impellor diameter, D) have large velocity fluctuations of low frequency. These are not isotropic and contain the bulk of the kinetic energy imparted by the impellor to the system. The large eddies interact with slow moving streams producing smaller eddies of high frequency, which further disintergrate to a size λ_k. In the range ($D>>\lambda>>\lambda_k$) energy passes from large to small eddies without dissipation. This is known as the inertial subrange and the eddy sizes in this range are similar to the drop sizes in a typical emulsion (Walstra 1983). Below λ_k energy is dissipated as heat by viscous forces - the viscous subrange. If the drop diameter exceeds λ_k drop breakage is caused by turbulent pressure fluctuations, drop sizes below λ_k may be produced by viscous shear (see note below). With the transfer of kinetic energy down the scale of eddies the directional elements of the main flow are lost. In isotropic turbulence the root-mean-square velocity fluctuations in each dimension must be equal. The intensity of the flow can be determined by a single parameter ε, the energy dissipated per unit volume of fluid.

NOTE: Davies (1985) discussed the drop breakage processes in high intensity agitation equipment. He showed that the smallest drop sizes were produced by turbulent pressure fluctuations and not by viscous shear. Leng (1982) has shown (for a low viscosity system) that viscous shear forces controlled the drop sizes of emulsions when the drop sizes were >200μm and, turbulent pressure fluctuations controlled the drop sizes, when the emulsion drop sizes were <200μm.

The Kolmogoroff length scale was derived from dimensional reasoning and is defined as:

$$\lambda_k = (\upsilon^3/\varepsilon)^{1/4} \quad \text{[4.6]}$$

and the velocity scale u_k, associated with it is:

$$u_k = (\upsilon\varepsilon)^{1/4} \quad \text{[4.7]}$$

where, υ is the kinematic viscosity.

The mean square of the relative velocity in an isotropic turbulent flow between two points separated by a distance r, is given by:

$$u^2(r) = c_1\varepsilon^{2/3}r^{2/3} \quad \text{[4.8a] for } (r>\lambda_k)$$

$$u_2(r) = c_2\varepsilon r^2/\upsilon \quad \text{[4.8b] for } (r<\lambda_k)$$

where, c_1 and c_2 are universal constants.

Stirred Vessel

The drop size distribution of a dispersion agitated in a stirred vessel can be modelled at any point by equation [4.2]. Drops will be constantly breaking up and coalescing in the vessel, however, after a certain time a dynamic equilibrium will be achieved and a steady-state drop diameter found for the dispersion (the result of a balance between break up and coalescence). Investigators usually assume there is either a maximum drop diameter d_{max}, above which no drop is stable (drop breakage control), or, a minimum drop diameter d_{min}, below which no drop is stable (coalescence control).

(a) Maximum Stable Drop Diameter in Isotropic Turbulence

Hinze (1955) obtained the minimum value of the Weber number (We, defined as the ratio of the deforming stress to the restoring stress) when drop breakage occurs in isotropic turbulence, by considering the forces acting upon isolated drops. The basic assumption was that in order for a drop to become unstable and break, the kinetic energy of the drop oscillations must be sufficient to provide the gain in surface energy necessary for break up. The kinetic energy of the drop oscillations is proportional to $\rho_c u(d)^2 d^3$, where d is the drop diameter. The gain in surface energy is proportional to σd^2, hence:

$$We = c_3\rho_c\sigma^{-1}u^2(d)d \quad \text{[4.9]}$$

We has a critical value above which the drop becomes unstable (We_{crit}). Therefore, for a drop diameter $d>\lambda_k$, substituting equation [4.8a] in equation [4.9]:

$$We_{crit} = c_4\rho_c\sigma^{-1}\varepsilon^{2/3}d_{max}^{5/3} = \text{constant} \quad \text{[4.10]}$$

Energy dissipation ε, can be closely estimated from power consumption/unit volume of dispersion. Experiments (Bates 1963) and Rushton (1950), show that for high Re (>10000), the average energy input of the impellor/unit volume of dispersion is independent of the properties of the liquid and is a function only, of the vessel and impellor geometries:

$$\varepsilon = c_5 N^3 D^2 \quad [4.11]$$

Using equations [4.11] and [4.10], Shinnar (1961) derived the following relation for d_{max} in a turbulent agitated vessel:

$$d_{max} = c_6 We_{crit}^{-0.6} \text{ or } d_{max} = c_6 \rho_c^{-0.6} \sigma^{0.6} N^{-1.2} D^{-0.8} \quad [4.12]$$

D

(for $d>\lambda_k$).

Values for We_{crit} found in the literature range from 11×10^{-3} (Van Heuven 1968) to 7.4×10^{-3} (Sprow 1967) and 7.5×10^{-3} (Chen 1967).

In the case of drops, diameter $D<\lambda_k$, drop breakage is by viscous shear forces. Taylor (1932) derived an expression for We_{crit} (for the maximum stable drop diameter) when drop break up is by viscous shear forces:

$$We_{crit} = \mu_c(\delta u/\delta r)(d/\sigma) = f(\mu_d/\mu_c) \quad [4.13]$$

Shinnar (1961), using the relation for locally isotropic flow $(\delta u/\delta r) = 2\varepsilon/15\upsilon$, derived the following expression:

$$d_{max} = c_7 \sigma \upsilon^{0.5} \mu_c^{-1} N^{-1.5} D^{-1} f(\mu_d/\mu_c) \quad [4.14]$$

(for $d<\lambda_k$).

(b) Minimum Stable Drop in Isotropic Turbulence

In an agitated dispersion drops will be constantly colliding with each other. If the drops stay together for a sufficient time, drainage of the continuous phase film between the drops will occur and the drops will coalesce. Shinnar (1961) assumed there to be an adhesive force between drops, which tends to hold colliding drops together and he assumed that this force would be a function of the drop diameter. The adhesion energy can be defined as:

$$E_{ad} = A(h)d \quad [4.15]$$

where, A(h) is a constant.

A balance between the kinetic energy of the dispersion drops and the adhesion energy is then used to find a minimum drop diameter below which, the eddies will not be able to separate two colliding drops and therefore, will not be able to prevent their coalescence. Hence:

$$We_{crit} = c_8\rho_c u^2(d)d_{min}^3/E_{ad} \quad \text{[4.16]}$$

Substituting equations [4.11] and [4.8a] in equation [4.16], Shinnar obtained:

$$d_{min} = c_9\rho_c^{-3/8}\varepsilon^{-0.25}A(h)^{3/8}$$

$$d_{min} = c_{10}\rho_c^{-3/8}N^{-3/4}D^{-0.5} \quad \text{[4.17]}$$

(for $d>\lambda_k$).

When viscous shear is the force preventing coalescence ie. when $d_{min}<\lambda_k$, Sprow (1967) determined We_{crit} as:

$$We_{crit} = (\mu_c\nabla u d^2)/F = \text{constant} \quad \text{[4.18]}$$

where, ∇u = the local velocity gradient = $c_{11}\varepsilon^{1/2}\upsilon_c^{-1/2}$ (Sprow 1967),

F = the adhesion force,

Hence:

$$d_{min} = c_{12}F^{1/2}\mu_c^{-1/2}\upsilon^{1/4}\varepsilon^{-1/4}$$

$$d_{min} = c_{13}F^{1/2}\mu_c^{-1/2}\upsilon^{1/4}N^{-3/4}D^{-0.5} \quad \text{[4.19]}$$

(for $d_{min}<\lambda_k$).

(c) Minimum and Maximum Drop Diameters Derived From Drop Breakage Rate and Drop Coalescence Rate Models.

The maximum and minimum stable drop diameter derivations above relate to steady-state drop size conditions, hence, they do not give any information about the rates of drop breakage and drop coalescence. Rate models to be found in the literature were reviewed by Tavlarides (1981), more recent models include those by Das (1987) and

Laso (1987). Rate models are complex and beyond the scope of this study. Those aspects of drop breakage and coalescence rate models concerning this study, will be reviewed in the discussion of the drop size results of chapters 5 and 6 to follow.

Drop breakage and drop coalescence rate models have been used to derive expressions for steady-state d_{max} and d_{min} for dispersions in transitional and laminar flow conditions, for $d>\lambda_k$ (Tavalrides 1981):

Laminar Flow

$$d_{max} \propto \mu_c^{-1}\sigma N^{-1}D^{-1}D_t^{2} \quad [4.20]$$

$$d_{min} \propto \mu_c^{-0.5}N^{-0.75}D^{-1.25}\sigma^{0.5}D_t^{0.5} \quad [4.21]$$

Transitional Flow

$$d_{max} \propto \mu_c^{m}\rho_c^{-(m+1)}\sigma N^{-(m+2)}D^{-(2m+3)}D_t^{-2} \quad [4.22]$$

$$d_{min} \propto \mu_c^{-(m-1)/4}\rho^{-(m+1)/4}N^{-(m+4)/4}D^{-(2m+7)/4}D_t^{0.5} \quad [4.23]$$

m is found from the gradient of a plot of log. power number vs log. Re (see figure 4.3, Metzner 1961). With increasing Re, m continuously increases from -1 (Re=15) to 0.16 (Re=300) and then decreases, approaching 0 (Re=11000).

4.7 DROP SIZE CORRELATIONS

In many real systems the measured average diameter of a drop size distribution (usually the Sauter mean diameter (D_{sm}) or volume/area diameter, defined by equation [4.24] below) is a linear function of d_{max} (Sprow 1967).

$$D_{sm} = \Sigma d_i^{3}.p_i/\Sigma d_i^{2}.p_i \quad [4.24]$$

where, d_i = diameter of size range i,

p_i = fraction of the total number of drops in size range i.

Equation [4.13] has been verified with a large number of dispersions (see review by Coulaloglou 1976), where the volume fraction of the dispersed phase is low (<0.2). It has been found that the constant c_6 in equation [4.12] can depend on the dispersed phase fraction f_{disp} (where an increase in the drop sizes is found with increase in f_{disp}) because of turbulence damping by the dispersed phase and increased coalescence rates. c_6 is often replaced by a function of the form:

$$c_{14}(1+c_{15}f_{disp})$$

which has been found to be in agreement with results for low dispersed phase fraction dispersions ($f_{disp}<0.2$). This leads to the well established form of We correlations for D_{sm}, in a dispersion produced by a turbine agitator:

$$\frac{D_{sm}}{\overline{D}} = c_{14}(1+c_{15}f_{disp}).We^{-0.6} \qquad [4.25]$$

Note, equation [4.25] has no dependency on μ_c ie. μ_c has no effect on drop sizes unless it is high enough to prevent turbulence (Walstra 1983). However, an extensive study of the effect of the dispersed phase viscosity on the drop sizes of dispersions has been made by Arai (1977), Calabrese (1986a), (1986b) and Wang (1986) and these authors have shown that increased viscous resistance to break up with increasing μ_d, can cause a rise in dispersion drop sizes.

Calabrese et al (1986b) suggested a dispersed phase viscosity group should be added to We correlations. Their final We correlation is shown below:

$$\frac{D_{sm}}{\overline{D}} = 0.054(1+3f_{disp})We^{-3/5}.[1+4.42(1-2.5f_{disp})V_i(D_{sm}/D)^{1/3}]^{3/5} \qquad [4.26]$$

where, $V_i=(\rho_c/\rho_d)^{0.5}\mu_d ND/\sigma$ = tank viscosity group
The effect of the dispersed phase viscosity can be ignored if $V_i<<0.65We^{0.2}$ (Wang 1986).

4.8 DROP SIZE DISTRIBUTIONS

We number correlations give an average D_{sm} value for a dispersion, but they do not give any information as to the dispersion's drop size distribution. The effect of stirrer speed and interfacial tension on the drop sizes of dispersion has been shown by Nagata (1975) (see figure 4.4). As the stirrer speed increases the dispersion's drop size distribution moves from a wide normal distribution to a much less broad log.-normal distribution. A similar effect is obtained with decrease in the dispersion's interfacial tension.

Calabrese et al (1986a) examined the effect of the dispersed phase viscosity on the drop size distribution of dispersions. They found that the drop size distribution broadens as μ_d increases and that it contained more smaller drops, however, an increase in D_{sm} was found because D_{sm} values are determined by the largest drops.

Another factor affecting the drop size distribution results is the sampling position in the tank (see figure 4.5 Sprow 1967). Hence, a constant sampling position should be used when comparisons are made between experiments. The variations occur due to differences in localised values of dispersed phase fraction (which affects coalescence rates); the dispersed phase fraction is larger at the top of the vessel if $\rho_d<\rho_c$ and larger at the bottom when $\rho_d>\rho_c$ ie. the variations are due to the effect of the bouyancy of the dispersed phase.

The literature reviewed in this chapter will be applied to the drop size results of chapters 5 an 6.

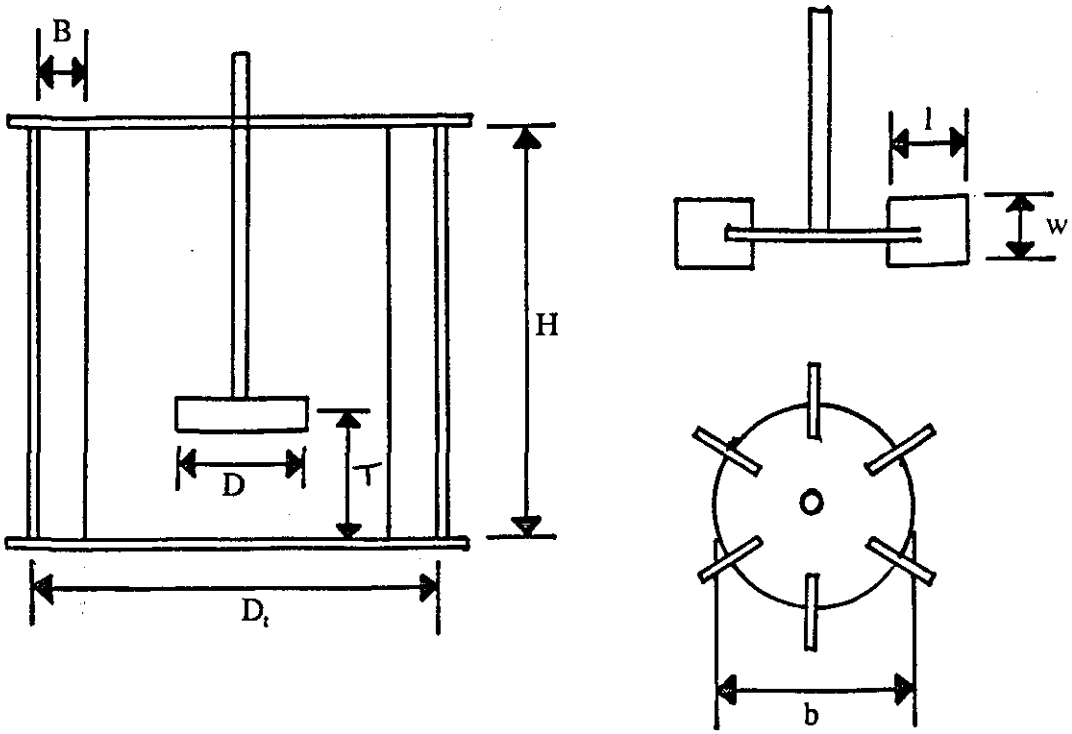

SYMBOL	STANDARD GEOMETRY
D_t = vessel diameter, D = Agitator diameter, H = Height of liquid in the vessel, B = Baffle width, T = Height of the stirrer above the vessel bottom,	D_t $D = 0.4D_t$ $H = D_t$ $B = 0.1D_t$ $T = D_t/3$
w = blade width, l = blade length, b = disc diameter.	w = D/5 l = D/4 b = 2D/3

FIGURE 4.1 - Standard vessel and 6-Blade Turbine Agitator Geometry (Nagata 1975).

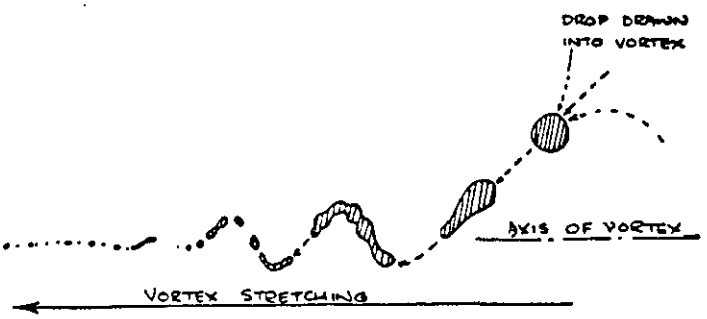

FIGURE 4.2 - Drop break up in a stretched vortex (Stephenson 1974).

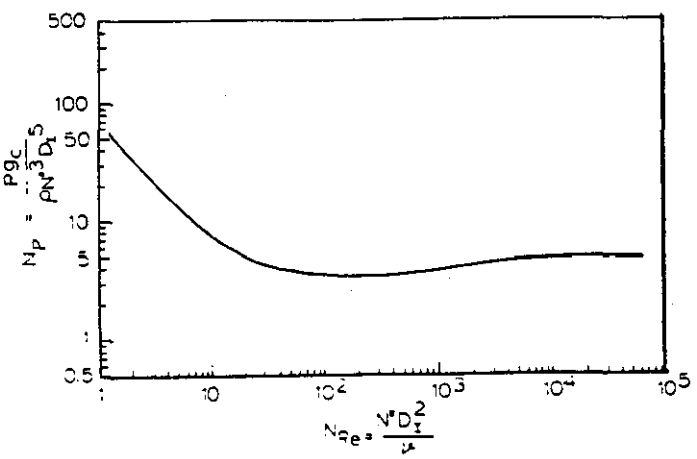

FIGURE 4.3 - Power number-Reynold's number correlation in Newtonian fluids, for a 6-blade turbine impellor (Metzner 1961).

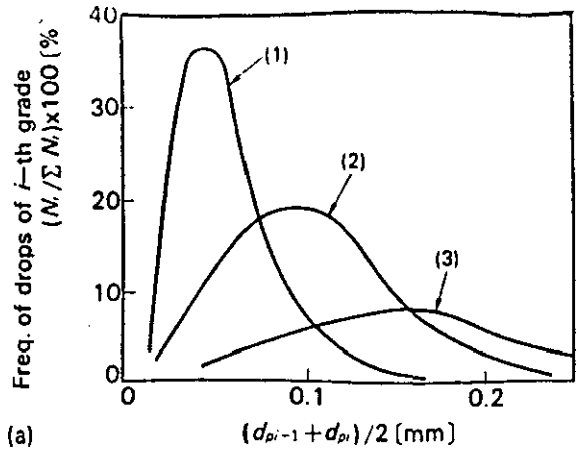

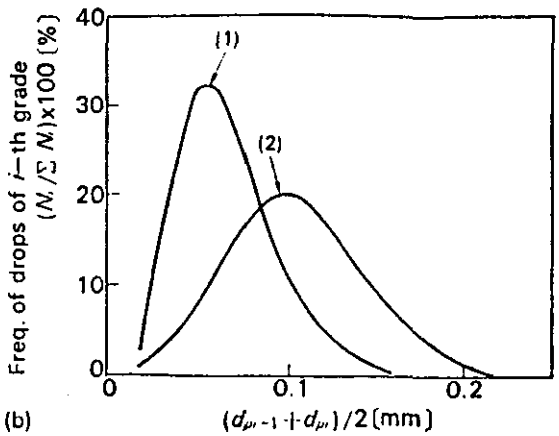

FIGURE 4.4(a) - The effect of agitator speed on the drop size distribution of toluene-water dispersions (Nagata 1975).

FIGURE 4.4(b) - Effect of interfacial tension on the drop size distribution of dispersions (Nagata 1975).
(1) i-amyl alc.-water, σ=4.91 dynes/cm, N=330rpm.
(2) n-hexane-water, σ=51/1 dynes/cm, N=625rpm.

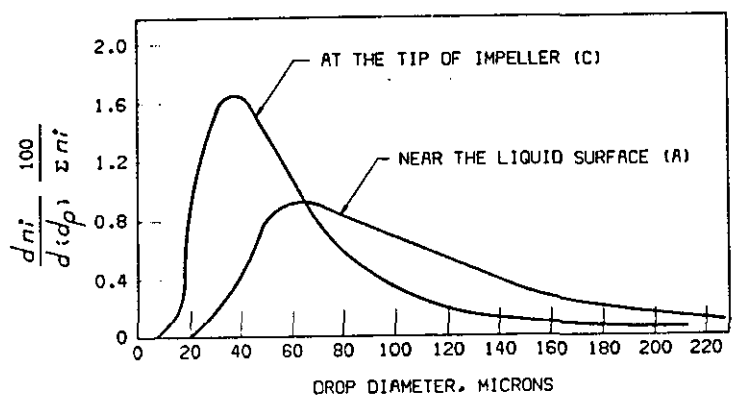

FIGURE 4.5 - Drop size distribution at two different sampling points (Nagata 1975).

CHAPTER 5
THE EFFECT OF TRANSITIONAL INVERSION ON EMULSION DROP SIZES

5.1 INTRODUCTION

In chapter 2 it was shown how transitional inversion is directly related to the surfactant-oil-water phase behaviour. It was further shown in chapter 3 how transitional inversion occurs when certain thermodynamic conditions are met (dependent on the surfactant chemical type) and how this can be used to classify surfactants. This chapter will concentrate on the effects dynamic conditions have on drop sizes across the phase transition.

Shinoda et al (1986) investigated how the drop sizes of cyclohexane/NPE9.7 3wt% O/W_m emulsions vary with temperature, for temperatures up to the Phase Inversion Temperature (PIT). Shinoda et al's work can now be seen as an investigation of the effect of an SAD change SAD- to SAD=0 on the drop sizes of O/W_m emulsions, where SAD=0 is located at the PIT. In the study, O/W_m emulsions were made up at varying temperatures up to the PIT and their drop sizes were measured immediately after agitation was stopped and also 5 hours after agitation was stopped. From the resulting size distributions number-average diameters were calculated (keeping the temperature constant during each experiment). The results of that study are summarised on figure 5.1(a) (Shinoda 1986).

Figure 5.1(a) shows that the mean drop diameters of the emulsions in that study decrease as the temperature approaches the PIT; Shinoda (1986) states that this reflects the change of the oil/water interfacial tension and the fraction of surfactant phase being present in this system as a function of temperature. Figure 5.1(a) also shows that 5 hours after agitation, the drop diameter of emulsions close to the PIT rise rapidly with time because coalescence is facilitated due to the ultralow interfacial tension (Shinoda 1986).

Measurements of the change in interfacial tension across the phase transition have been made by:

(i) Kunieda and Shinoda (1982), who used a sessile drop technique. This study showed that an Antonoff relationship for the interfacial tensions, that were possible between the three phases, held for conditions near the PIT (change in SAD with temperature).

(ii) Cayais et al (1974), measured the interfacial tension across a phase transition directly using a spinning drop apparatus. They used change in oil carbon number for a homologous series of hydrocarbons (similar to the equivalent alkane carbon number EACN used by Cash et al (1977) - discussed in chapter 1) was the SAD variable. The

results of Cayais et al's study are shown in figure 5.2: EACN=8 is equivalent to SAD=0, EACN<8 is equivalent to SAD+ conditions and EACN>8 is equivalent to SAD- conditions.

As can be seen from figure 5.2, values as low as 10^{-3} dynes/cm have been measured for the SAD=0 condition: Note some authors (Salager 1988) have quoted values as low as 10^{-4} dynes/cm.

Shinoda et al's results for emulsion stability across the phase transition (figure 5.1(b)), show that for O/W_m emulsions, the drainage rate was low at temperatures about 20-40°C below the PIT and low for W/O_m emulsions at temperatures about 20-40°C above the PIT. This led to Shinoda's rule that "the HLB numbers of surfactants whose HLB temperatures in an oil/water system are 25-70°C higher than the emulsion's storage temperature are the required HLB numbers for emulsification of that system" (1986).

Figure 5.1(b) also shows that the stability of emulsions reduces to a minimum in Type 3 systems. Many other studies have shown stability maxima either side of a stability minimum in the three phase region (Graciaa 1982), (Bourrel 1979) and (Salager 1980) although there has been much conjecture as to the relevance of the measurement of stability used in some studies (Milos 1982).

The emulsion stability findings of the workers summarised above are shown schematically on figure 5.3 in terms of the notation used in this study, along with a recapitulation of the transitional inversion mechanism proposed in chapter 2.

The facts that small drops could be produced near the PIT and that emulsion stability was highest 20-70°C below the PIT, led Shinoda to a further study where emulsions were produced at temperatures below the PIT, at the PIT and above the PIT and then rapidly cooled to aid stability. The drop diameter and stability results of the O/W_m emulsions produced are shown on figure 5.4 (Shinoda 1986). Figure 5.4(a) shows that the drop sizes of emulsions produced at the PIT are retained in the final cooled emulsion. Shinoda noted that emulsions with the finest drops were produced by emulsifying 2-4°C below the PIT and then cooling. Shinoda termed this emulsification method "emulsification by the PIT method". The study also showed that "emulsification by the inversion method" ie. emulsification above the PIT as a W/O_m emulsion and then cooling, did not result in such small drops.

Friberg (1978) performed similar experiments to Shinoda and found that at temperatures above the PIT there was no surfactant phase present and there was "no reduction in drop sizes". However, at temperatures below the PIT when the system was 3-phase and the emulsion volume contained 20% and 50% surfactant phase, there was a large reduction

in the emulsion's drop sizes. Hence, it was concluded that as the surfactant phase separated on cooling it will produce extremely small drops. These extremely small drops skew the average droplet size to smaller values (Shinoda 1986).

Parkinson and Sherman (1972) looked at the drop sizes at the "PIT" of systems stabilised by Tween-Span mixtures and found only small differences in the drop sizes of emulsions made at the PIT with those produced at other temperatures. The results of these workers may again be explained by noting that transitional inversion points in systems stabilised by these surfactants, may be missed if the dispersed phase fraction is <80% as the surfactant phase may not become continuous. Hence, the inversion observed by these workers may have been a catastrophic inversion.

The literature review above highlights the observations of the workers in this field. It will be noted that most of the work has concerned change in drop size and stability with phase behaviour. Studies which have examined drop sizes have paid little or no attention to agitation conditions, surfactant concentration, water-oil-ratio or phase viscosities. This study will attempt to discover which variables are important for determining drop sizes at the transitional inversion point. The results should then lead to a clearer picture as to the mechanism of transitional inversion and the emulsion structures that exist at each point across the transition.

5.2 EXPERIMENTAL

5.2.1 System Components

All experiments for this chapter were carried out on the Cyclohexane/NPE system and Cyclohexane/SML system; the system components were used as described in chapter 2. Polyisobutene (PIB) was added to the cyclohexane in some experiments to examine the effects of changes in the oil phase viscosity on transitional inversion. The polyisobutene was low molecular weight (average molecular weight = 380000) and was used as supplied by Aldrich chemical company. A calibration of oil phase viscosity against concentration of polyisobutene in cyclohexane was made, the results are tabulated in table A4.1 of appendix 4 and plotted on figure 5.5. The oil phase viscosity was measured using a Brookfield rotary viscometer, the calibration of which, was checked before use. Measurements were made of the change in the oil phase density with increasing polymer concentration; the cyclohexane density (0.007 poise system Weast 1982) was measured as 762 kg/m^3 at 25°C and the PIB-cyclohexane (2 poise system) was measured as 766 kg/m^3 at 25°C, hence, there is little change in the oil phase density with increasing polymer concentration. Attempts were also made to measure the change in the interfacial tension of the PIB-cyclohexane/NPE12 system with rising polymer concentration (see below).

However, even for this system (where the interfacial tension will be much greater than at SAD=0), the interfacial tension was far too low to be measured by conventional methods eg. pendant drop, sessile drop and Du Nouy ring. A spinning drop apparatus would be required to measure such low interfacial tensions, however, such apparatus is expensive and was not available to this study. Other studies have investigated the effect of rising viscosity of one phase on the drop sizes of dispersions by adding polymer to a phase:

Arai (1977) - polystyrene in xylene solutions - upto 25% polymer in xylene was used and no change in the interfacial tension was seen (viscosities in the range 0.78 to 1500 cpoise were examined).

Stamatoudis (1985) - water in glycerol solutions - a small change (approximately 10%), was found between a 223.1 cpoise water phase and a 3.6 cpoise water phase.

In the above studies no surfactant was present, hence, the interfacial tensions were relatively high, however, the results indicate that there will be little change in the interfacial tension between high and low oil phase viscosity systems, when the oil phase viscosity is altered by adding a polymer.

The polyisobutene dissolved in the cyclohexane may affect the partitioning of surfactant between oil and water phases, which will affect the interfacial tension. However, as will be seen in the results section of this chapter, little change in the HLB_{act} value at the transitional inversion point (dependent on the surfactant partitioning, see chapter 3), was found between low and high oil phase viscosity systems. Hence, it may be concluded for the PIB-cyclohexane systems examined (where the polymer in oil concentration was <10% in all experiments), that the interfacial tension will remain reasonably constant at each oil phase viscosity (for the same HLB_{act} value).

Changing HLB brought about by varying the ratio of a lipophilic surfactant to a hydrophilic surfactant in the oil/water system was again used as the SAD variable. Hence, all the experiments could be performed isothermally at 25°C. In each experiment 500ml surfactant-oil-water mixtures were located in a 0.75 dm^3 dished bottomed vessel (diameter 10 cm) and agitation was supplied by either, a 6 blade Rushton turbine with variable speed drive, or by an Ultra Turrax rotor-stator device. Detailed experimental procedures are given in each section to follow.

All experiments were carried out with the system in its stable state ie. Type 1 systems were made up as O/W_m emulsions and Type 2 systems were made up as W/O_m emulsions.

5.2.2 Measurement of Drop Diameters

Two techniques for measuring drop diameters of emulsions were used:

(i) Optical Microscopy - as all the emulsions examined were in their stable state (see exceptions in Type 3 systems below), normal slide and cover slip methods could be used. Optical microscopy can be used to measure drop diameters greater than 0.5 microns.The information observed on each slide was stored on video tape. Hard copies of still frames were then used for drop diameter measurments. The diameters of at least 300 drops were measured to obtain a statistically accurate size distribution, from which the Sauter Mean Diameter (D_{sm}) for the sample was calculated (note, in subsequent discussion D_{sm} will refer to drop sizes determined by optical microscopy). For each set of experiments, a check on the accuracy of the calculated D_{sm} was made; in one experiment per set, after determining the D_{sm} from the diameter measurements of approximately 300 drops, a further 150 drops were measured and the D_{sm} re-calculated. In the case of each set of experiments described in chapters 5 and 6, little or no change in the D_{sm} was found. Hence, the measurement of 300 drop diameters produced a reasonably accurate drop size distribution.

(ii)Photon-Correlation-Spectroscopy was used for drop sizes in the range 10^{-8}m to approximately 3 microns (this technique becomes very inaccurate for drop sizes above this). The PCS was similar to that used by Davies et al (1988), to measure drop sizes in water/cyclohexane microemulsions. The apparatus comprised of a Malvern spectrometer (Type 144), a helium-neon laser (Model 124B Spectra-Physics Stabilite) and a Malvern K7025 real time multibit correlator. Data storage and analysis were carried out by an on-line microcomputer.

The technique calculates a mean diameter for a dispersion sample as follows:

An estimate of the drop polydispersity factor (Q) (for mondisperse emulsions Q=0) is made, where:

$$Q = \mu_2/CF^2 \qquad CF=D_{eff}K^2$$

and,

$$\mu_2= \int P(CF)(CF-CF)^2\, dCF$$

CF is the mean value of the correlation function decay rate, having a distribution P(CF) which reflects the drop size distribution. μ_2 is the second moment of P(CF), K is the scattering vector and D_{eff} is the effective (mean) droplet diffusion coefficient from which the mean drop diameter d is calculated.

$$D_{eff}= kT/3\pi\mu_c d$$

where, μ_c = continous phase viscosity,
T = sample temperature,
k = constant.

Note this technique requires that each sample be diluted until the dispersed phase was <5% of the emulsion volume. To test the consistency of the results at least 3 samples were analysed 5-10 times for each emulsion condition examined and the average result was recorded.

Comparisons were made between each sizing technique when the drop sizes of a sample were within the range 0.5 microns to 3 microns.

5.2.3 Limitations

The drop size measuring techniques described above are limited in that they can only be used to measure drop sizes of two phase systems. Hence, we can measure oil drop diameters in Type 1 systems, water drop diameters in Type 2 systems and O/M_w and W/M_o in Type 3 systems (although as will be shown later the drop sizes for these Type 3 systems are small and drop diameter measurements can only be made when the dispersed phase fraction is low). However, in Type 3 systems where the surfactant phase is continuous $(O+W)/M_s$, direct measurement of oil and water drop diameters is not possible with either drop sizing technique because:

(a) In the case of optical microscopy the drop diameters are very small and the dispersed phase fraction is very large, this makes the emulsion quite opaque when viewed with a microscope.

(b) As was stated earlier, Photon Correlation Spectroscopy requires the sample to be dilute - this is never the case for these Type 3 conditions. Dilution of a sample with surfactant phase is not possible as this could only be achieved by adding more surfactant, which as will be seen in the results of this chapter, has a great effect on the drop sizes of Type 3 emulsions.

Therefore, to measure the drop diameters of (O+W)/M_s emulsions (for both drop sizing techniques), the system must be shifted from its SAD=0 condition. The oil drop diameters were measured by diluting a sample with water containing hyrophilic surfactant so that the system became O/W_m. Similarly, the water drop diameters were measured by diluting a sample with oil phase containing lipophilic surfactant so that the system became W/O_m.

It is questionable as to whether using this dilution technique, the drop diameters measured bear any relation to the actual drop diameters of an (O+W)/M_s emulsion. However, as will be seen consistent variations in the drop diameter results were obtained (especially with rising surfactant concentration). Also, if the desired resultant emulsion is to be a stable O/W_m or a stable W/O_m emulsion, then refering to Shinoda et al's (1986) work, a shift in HLB would be required, firstly to get the emulsion into the desired physical state and secondly to aid stability by raising the interfacial tension.

To be able to assess the drop sizes produced by transitional inversion, it is first necessary to investigate how the drop size distributions of emulsions vary with agitation time and SAD across a transition on a SAD map.

5.3 RESULTS

5.3.1 VARIATION OF DROP SIZES ACROSS A PHASE TRANSITION

Chapter 2 showed that transitional inversion boundaries are easily located in systems containing NPE surfactants, however, in systems containing SML surfactants, locating the transitional inversion boundary can be difficult as the surfactant phase may not become continuous unless the dispersed phase fraction is large. Also, most of the literature refering to transitional inversion has been concerned with systems containing NPE surfactants. Therefore, this study has concentrated on transitional inversion in NPE systems, so that comparisons could be made with the results of other workers and also,

for ease of location of the various stages across the phase transition. A brief study of transitional inversion in systems containing SML surfactants was also made, to examine any changes in the inversion mechanism.

CYCLOHEXANE/NPE SYSTEMS

Direct emulsifications were performed on the cyclohexane/NPE system (f_w=0.8, temperature = 25°C and stirrer speed 600rpm) at constant HLB_{act} values at varying points across the transitional inversion line, in accordance with figure 5.6. Samples of emulsion were analysed by optical microscopy at regular time intervals through each run, until a stable drop size distribution was obtained. The Sauter mean drop diameter was calculated for each distribution.

As discussed in Chapter 3, mole average HLB_{act} values (the HLB of a pseudo surfactant phase) rather than mole average overall HLB, should be used as a measure of surfactant affinity. Hence, the concentration of each of the surfactant pair in the surfactant-oil-water system was calculated to achieve a set HLB_{act} value and to keep the concentration of the pseudo surfactant phase constant. Details of the calculations are given in table A4.2 of Appendix 4.

5.3.1(a) Time to Achieve a Stable Drop Size Distribution

The change in the Sauter mean diameter (D_{sm}) of O/W_m emulsions with time at four different HLB_{act} values is shown by figure 5.7. The drop size distribution results are tabulated in table A4.3, Appendix 4. In figure 5.8, plots are made of the change in the drop size distributions with time at 3 different HLB_{act} values. Figures 5.7 and 5.8 show that the time taken to reach a stable drop size distribution reduces and also, the D_{sm} reduces, the closer the HLB_{act} value is to the transitional inversion point HLB_{act} value.

5.3.1(b) A Detailed Study of Drop Sizes in Type 3 map Regions

A more detailed study was made of drop sizes in agitated Type 3 systems. The three possible emulsion types in Type 3 systems were examined ie. W/M_o, $(O+W)/M_s$ and O/M_w. Note $(O+W)/M_s$ emulsions were shifted to O/M_w and W/M_o emulsions by altering the HLB of the surfactant phase, to measure the oil and water drop diameters as explained in the experimental section. The effect of a rapid shift in HLB to achieve the transitions $O/M_w \rightarrow W/O_m$ and $W/M_o \rightarrow O/W_m$ was also examined. The O/M_w and W/M_o conditions were located accurately by the following procedure:

(i) The system was first made up as an $(O+W)/M_s$ emulsion at HLB_{act}=10.5.

(ii) To locate the O/M_w condition, hydrophilic surfactant (Igepal co720) was then added gradually (1 drop every 2 minutes to allow equilibrium to be achieved) until the emulsion suddenly thinned on moving from an $(O+W)/M_s$ state to a O/M_w state.

(iii) Similarly, the W/M_o condition was located by adding lipophilic surfactant (Igepal co210) until the emulsion suddenly thinned out on moving from the $(O+W)/M_s$ state to the W/M_o state.

Table 5.1 below summarises the results of this part - optical microscopy and Photon-Correlation-Spectroscopy (PCS) results are shown for comparison. The full drop size data is tabulated in table A4.4 of Appendix 4.

TABLE 5.1 - Variation of drop sizes across the Type 3 region at f_w=0.8.

Start HLB_{act}	Start Emulsion Structure	O/W_m Shift* D_{sm} μm	PCS μm	W/O_m Shift* D_{sm} μm	PCS μm
10.00	W/M_o	1.2	3.5	1.2	2.0
10.25	$(O+W)/M_s$	1.4	0.9	1.3	2.0
10.50	$(O+W)/M_s$	1.0	1.6	1.0	1.8
11.00	O/M_w	<0.5	0.35	1.1	2.0

* O/W_m shift refers to a SAD change inducing the transition $(O+W)/M_s \rightarrow O/W_m$, similarly, W/O_m shift refers to a change in SAD inducing the transition $(O+W)/M_s \rightarrow W/O_m$. D_{sm} refers to optical microscopy result.

Comparisons of the D_{sm} and PCS results show that generally, PCS diameters > D_{sm}. This is because PCS becomes inaccurate when drop sizes >1 μm are present in the emulsion sample.

Similar experiments to those in section 5.3.1(b) were performed at f_w=0.2. Table 5.2 below summarises the results. Full drop size distribution data is tabulated in table A4.5 of Appendix 4.

TABLE 5.2 - Variation of drop sizes across the Type 3 region at f_w=0.2.

Start HLB_{act}	Start Emulsion	O/W_m Shift D_{sm} (μm)	W/O_m Shift D_{sm} (μm)
10.00	W/M_o	1.2	<0.5
10.25	$(O+W)/M_s$	1.0	1.2
10.50	$(O+W)/M_s$	1.0	1.0
11.00	O/M_w	1.0	1.0

Note: Cyclohexane/NPE system at HLB_{act}=10.0 with the system in its W/M_o state, at f_w=0.2. For this system microscopy gave the result, D_{sm}<0.5μm (ie. no single drops were visible), however, PCS gave a result of 2.0μm. Photomicrographs of the W/M_o emulsion revealed that flocculation occured between drops. This may explain the large difference in the microscopy and PCS results.

Tables 5.1 and 5.2 show that the drop sizes of "shifted" Type 3 emulsions are affected by the initial start condition:

(i) Only W/M_o and O/M_w emulsions appear to be affected by f_w - if the micelle concentration is kept constant.

(ii) The shift of $(O+W)/M_s$ emulsions to SAD- and SAD+ is used to measure the oil and water drop sizes respectively. The tables show that the oil and water drops of $(O+W)/M_s$ emulsions are of a similar size to each other.

(iii) Shifting emulsions from O/M_w state to O/W_m state produces finer emulsions than a shift across the inversion boundary ie. from $(O+W)/M_s$ to O/W_m (refer to Table 5.1).

5.3.1(c) Steady Drop Sauter Mean Diameter D_{sm} Results at points either side of the Phase Transition

The results of steady drop size distributions for W/O_m emulsions at HLB_{act}=8.0 and HLB_{act}=6.0 are tabulated in Table A4.6, Appendix 4. Table 5.3 below summarises the Sauter mean diameters of emulsions at each HLB_{act} value examined once a steady drop size distribution was achieved. Figure 5.9 is composed of photomicrographs of steady state emulsions produced at varying HLB_{act} values across the phase transition. Figure 5.10, is a plot of steady drop size distribution D_{sm} vs HLB_{act}; compare with figure 5.2, Cayais et al (1974) interfacial tension plot across the phase transition and with figure 5.3, derived from stability studies. Figure 5.11 shows plots of the steady state size distributions at different points either side of the phase transition.

TABLE 5.3 - Summary of steady state drop size results across the phase transition.

HLB_{act}	Emulsion Structure	f_w	D_{sm} (μm)
6.00	W/O_m	0.8	4.4
8.00	W/O_m	0.8	4.2
10.00	W/M_o	0.8	1.0
10.00	W/M_o	0.2	0.35*
10.25	$(O+W)/M_s$	0.8	1.2
10.25	$(O+W)/M_s$	0.2	1.0
10.50	$(O+W)/M_s$	0.8	1.0
10.50	$(O+W)/M_s$	0.2	1.0
11.00	O/M_w	0.8	0.35*
11.00	O/M_w	0.2	1.0
11.50	O/W_m	0.8	8.0
12.10	O/W_m	0.8	11.0
14.20	O/W_m	0.8	13.0

* PCS result.

Having now shown how drop sizes vary across the phase transition, this chapter will now concentrate on investigating variables that may affect the drop sizes at the transitional inversion point.

5.3.2. THE EFFECT OF AGITATION CONDITIONS, SURFACTANT CONCENTRATION AND OIL PHASE VISCOSITY ON DROP SIZES AT THE TRANSITIONAL INVERSION POINT

In the following experiments the system was initially made up as an $(O+W)/M_s$ emulsion before being shifted to an O/W_m state. The drop size results refer to the emulsion in its final O/W_m state.

5.3.2(a) Agitation Conditions

Varying levels of agitation were examined, from simple shaking through to a high speed rotor-stator device. All experiments were carried out on the cyclohexane/2wt%NPE system. When the agitation was supplied by a stirrer or Ultra-Turrax, the emulsion and tank volumes were as described in the experimental section of this chapter. Samples were removed for drop size analysis after 1 to 2 minutes

agitation time (this was approximately the time taken for adjusting the HLB of the system to the exact transistional inversion HLB). The "simple shaking" result applies to a 20 ml volume of emulsion in a sample tube, shaken by hand once every 5 seconds over a period of 1 minute. It was noted that spontaneous emulsification took place as soon as the oil and water phases were contacted. The results of these experiments are summarised in table 5.4 below, full size distribution results are given in table A4.7 of Appendix 4.

TABLE 5.4 - Effect of agitation conditions.

Agitation Method	D_{sm} (μm)
Simple Shaking	1.4
Rushton turbine 200rpm	1.6
Rushton turbine 800rpm	1.0
Ultra-Turrax 5000rpm	1.2

5.3.2(b) Effect of Surfactant Concentration

500ml volumes of cyclohexane/NPE (f_w=0.8) system were agitated at 600 rpm at the system's transitional inversion point for a range of overall surfactant concentrations. Samples were removed for drop size analysis after appproximately 5 minutes agitation time. The results of this section are summarised in table 5.5 below - full drop size distribution results are tabulated in table A4.8, Appendix 4. Figure 5.12 is a plot of D_{sm} vs surfactant concentration.

TABLE 5.5 - Effect of Surfactant Concentration.

Overall surfactant concentation (g/l)	D_{sm} (microns)
10	3.20
20	1.00
50	0.24
80	0.15
120	0.07

5.3.2(c) Effect of Oil Phase Viscosity

The oil phase (cyclohexane) viscosity was raised by adding polyisobutene; for calibration of concentration of polyisobutene in cyclohexane vs phase viscosity, see figure 5.5). For a number of different oil viscosities, transitional inversions were

performed under conditions of: Surfactant concentration 20 g/l, water volume fraction f_w=0.8 and a stirrer speed of 600 rpm. Changes in drop size distribution with time were examined when moving to the transitional inversion point from each direction:

ie. (i) $W/O_m \rightarrow (O+W)/M_s \rightarrow O/W_m$

(ii) $O/W_m \rightarrow (O+W)/M_s \rightarrow O/W_m$

The introduction of polyisobutene into the oil phase had little effect on the HLB_{act} value at the transistional inversiom point.

(i) Transitions $W/O_m \rightarrow (O+W)/M_s \rightarrow O/W_m$

Figure 5.13 is a plot of D_{sm} vs agitation time at 4 different oil phase viscosities. Evidence of variations in drop sizes between samples becomes apparent at oil phase viscosities >5 poise, as shown by the examples in table 5.6. This indicates that mixing throughout the tank was far from homogeneous in these cases. Full drop size distribution data for figure 5.13 are given in table A4.9, Appendix 4.

TABLE 5.6 - Examples of sampling variations.

Oil Phase viscosity	Agitation time/ min	D_{sm} (microns)
10 poise	15	4.2
	15	10.0
30 poise	20	4.1
	20	7.2

(ii) Transitions $O/W_m \rightarrow (O+W)/M_s \rightarrow O/W_m$

In these experiments the system was made up as an O/W_m emulsion (HLB_{act}=11.5) and then stirred for 10 minutes before shifting it to its transitional inversion point (HLB_{act}=10.5). After 1 minutes further agitation the system was shifted back to an O/W_m state (HLB_{act}=12.0) and samples were taken immediately for drop size analysis. The results are summarised in table 5.7 below and full drop size distribution data is tabulated in table A4.10, Appendix 4.

TABLE 5.7 - Effect of oil phase viscosity (Drop sizes after agitation at SAD=0)

Oil Phase Viscosity poise	D_{sm} (microns)
0.007	1.0
1.0	1.4
2.0	1.9
5.0	2.3
10.0	2.1
30.0	1.9

5.3.3 DIRECT EMULSIFICATION COMPARISON

Direct emulsifications were performed using a number of different oil phase viscosities, on the polyisobuteneXwt%-cyclohexane/2wt%NPE system at HLB_{act}=12.0, water volume fraction f_w=0.8 and stirrer speed 800 rpm. Samples were removed at regular time intervals to monitor the change in drop size distribution with time. The Sauter mean diameter was calculated for each size distribution and these were compared with the D_{sm} values of emulsions made at the transitional inversion point and then shifted to HLB_{act}=12.0. Figure 5.14 summarises the direct emulsification D_{sm} vs time results and compares direct emulsification and transitional inversion results. Full drop size distribution results are given in Table A4.11, Appendix 4. Note that the 0.007 poise Sauter mean diameter values used in figure 5.14 (N=800rpm), were calculated from the data of figure 5.7 (N=600rpm) assuming $D_{sm} \propto N^{-1.2}$. On figure 5.14, the points on the transitional inversion line, for oil phase viscosities >0.007poise, are taken from table 5.7.

5.3.4 CYCLOHEXANE/SML SYSTEMS

Isothermal transitional inversions were performed on the cyclohexane/SML 2wt%, f_w=0.8 system. For this system, transitional inversion when moving from SAD+ to SAD- is possible, but it is not possible when moving from SAD- to SAD+ (see chapter 2). Two experiments were performed:

(i) A transitional inversion SAD+ to SAD- : The change in drop sizes and drop structures were tracked across the phase transition. Photomicrographs were taken at various stages and these revealed different drop structures from those found in transitional inversion in systems containing NPE surfactant, as shown in figure 5.15.

(ii) The system was initially made up as an O/W_m emulsion (in the SAD- map region), this emulsion was then subjected to a change in SAD induced by direct injection of the lipophilic surfactant (Span20), so its composition now lay in the SAD+ region of the SAD map. No inversion was observed or could be induced and no significant change in drop sizes was found between the initial O/W_m emulsion and the final O_m/W emulsion.

5.4 DISCUSSION

The results of this chapter show which parameters affect drop sizes in transitional inversion. Comparisons have been made between the drop size distributions of emulsions produced by transitional inversion and the drop size distributions of emulsions produced by direct emulsification. Firstly, to revise the visualisation of the emulsion structures present at the various stages of a transitional inversion, the mechanism of transitional inversion in NPE systems will be discussed:

CYCLOHEXANE/NPE SYSTEMS

5.4.1 MECHANISM OF TRANSITIONAL INVERSION

Figure 5.9 shows photomicrographs of steady state emulsions at different SAD states across the phase transition. It can be seen that the drop sizes of emulsions in SAD- and SAD+ regions reduce as the SAD=0 inversion boundary is approached; this is probably due to the interfacial tension change across the phase transition (see figure 5.2 Cayais 1974).

The mechanism of transitional inversion proposed in Chapter 2 was described by the existance of 5 emulsion structures (**Dynamic Inversions SAD+ to SAD-**):

Mechanism - $W/O_m \rightarrow W/M_o \rightarrow (O+W)/M_s \rightarrow O/M_w \rightarrow O/W_m$

The M_o phase was proposed to differentiate between a Type 2 and a Type 3 oil phase. The only physical difference between W/O_m and W/M_o emulsions is that the drop sizes of the W/M_o emulsions will be much smaller because of the ultra-low interfacial tension existing in Type 3 systems.

A break point in the mechanism occurs when the system moves from a W/M_o structure to a $(O+W)/M_s$ structure, where the surfactant phase becomes continuous. No attention has yet been paid as to how the surfactant phase becomes continuous: The photomicrographic examination of a dynamic transitional inversion revealed the existance of complex drops containing smaller drops, as a precursor to the surfactant phase becoming continuous - such a structure is shown in Figure 5.16. These drops maybe dispersed surfactant phase in oil. The complex drops are large in comparison with the drops within them, this may indicate that the complex drops are unstable to coalescence, but the drops within them are stable. In Chapter 6 it will be shown that in true catastrophic inversions of the type $W_m/O+O/W_m/O \rightarrow O/W_m$, the initial water drops are unstable to coalescence, however, after inversion the oil drops formed are stable. Hence, the complex drops may be composed of oil and water drops in a surfactant phase (in oil), where the surfactant phase "wants" to become the overall continuous phase.

It was noted in chapter 2 that electical conductivity rose gradually over a 0.5 HLB number SAD change within the Type 3 region. It was concluded that this was because the surfactant phase was continuous (the M_s phase is mainly oil moving to mainly water as the system moves through the 3 phase region). However, the existance of (O+W)/M_s/O structures identified in this chapter indicates another possible reason for the gradual rise in conductivity: The rise may be due to dynamic changes in the dispersed phase caused by the "growth" of (O+W)/M_s/O structures.

Once the surfactant phase becomes continuous the emulsion becomes thick and quite viscous. The emulsion structure can no longer be visualised as drops within a continuous phase, as is shown by the photomicrograph of an SAD=0 emulsion structure, Figure 5.9. Theoretically, the oil-water interface should be flat at the inversion point (Shinoda 1986); this led Shinoda to represent a Type 3 surfactant phase as a bicontinuous state (see Figure 1.3). This bicontinuous structure of a surfactant phase cannot be observed as the bounded "strands" of oil and water are solubilised in surfactant micelles and therefore, have a size of the order of 10^{-8}m. Figure 1.3 and the SAD=0 photomicrograph in Figure 5.9 (the structure of a Type 3 emulsion ie. surfactant phase including excess oil and water phases) do show some simalarities in structure. Hence, it may be that an agitated 3 phase system, also, consists of a bicontinuous oil and water "strands" separated by a surfactant layer. The excess oil and water phases will swell the size of the oil and water "strands" of the surfactant phase and the bicontinuous structure will now be observable.

The transitional inversion is completed as the system moves into the SAD- map region and the emulsion structure becomes O/W_m. The break of the emulsion from an (O+W)/M_s state to an O/M_w state may also be achieved via complex drops ie. (O+W)/M_s $\rightarrow$ (O+W)/M_s/W $\rightarrow$ O/M_w. Figure 5.9 shows that in dynamic transitional inversions, the small drops produced in the Type 3 region are retained in the final O/W_m emulsion.

Having now reviewed the transitional inversion mechanism in NPE systems, the change of drop size with time across the SAD map will be discussed.

5.4.2 DROP SIZE VARIATION WITH AGITATION TIME ACROSS A PHASE TRANSITION

There are discrepancies to be found in the literature concerning the change in drop size of an emulsion with agitation time; some authors state that there is no significant reduction in the drop sizes of emulsions after 5 minutes agitation time (Gopal 1968), others however, have shown that agitation times in excess of 1 hour are required before an emulsion obtains a steady drop size distribution (Lee 1984).

The purpose of this section is not to investigate all parameters which may affect emulsification rates at each point on a SAD map, its purpose is more to show how emulsification rates at the transitional inversion point fits into the general overview of the map. However, emulsification rates have been shown to be dependent on the following (from a summary by Walstra 1983):

(i) Surfactant concentration - generally higher surfactant concentrations give smaller drops, hence, a greater number of disruptions is necessary and therefore, a longer agitation time is required. It should be noted that no decrease in the final drop size is found when the surfactant concentration exceeds the CMC. However, some researchers have shown that even in systems containing surfactant above the CMC, the higher the surfactant concentration is, the longer the agitation time required to achieve a stable drop size distribution will be.

(ii) Surfactant Type. Note that this variable is taken into account within the SAD map.

(iii) Stirring rate, where an increase in emulsification rate has been found with revolution number. As the results section of this chapter has shown, agitation conditions have little effect on drop sizes at the transitional inversion point, therefore, detailed studies of the effects of stirrer speed will not be attempted in this chapter. Detailed studies of the effects of agitation conditions will be given in chapter 6 when discussing catastrophic inversion.

The time required to achieve a stable drop size distribution at different HLB_{act} values is shown by figure 5.7. Figure 5.7 together with figure 5.8 (plots of size distibution changes with time) show that:

(a) For the emulsion in its "steady state" form, the further the HLB_{act} value of the surfactant is from the HLB_{act} value at SAD=0, the larger the drop sizes and the wider the distribution of drop sizes of the emulsion will be.

(b) The further the HLB_{act} value of the surfactant from the SAD=0 value, the longer the agitation time required to achieve a stable drop size distribution.

The results (a) and (b) are consequences of rising interfacial tension as the HLB_{act} moves further from its HLB_{inv} value.

Analysis

The disruption of droplets is often treated as a first order reaction (Gopal 1968, Hong 1983):

$$\frac{dZ}{dt} = kZ \qquad [5.1]$$

where, Z = number of drops per unit volume,

t = agitation time,

k = rate constant (t^{-1}).

Assuming a final number of drops Z_∞ (since there is a final average diameter $D_{sm\infty}$) leads to:

$$D_{sm} = \frac{D_{sm\infty}}{(1- \exp(-kt))} \quad [5.2]$$

However, many researchers have found that equation [5.2] does not fit their results (Walstra 1983). Reasons for the difference in theory and experimental results have been forwarded:

(i) There is probably a whole spectrum of reaction rates depending for instance on drop size (Walstra 1983).

(ii) Turbulence is not uniform throughout a stirred vessel (disruption zones exist at the impeller and coalescence zones exist near the tank walls) and there will be a delay time before all the volume elements of the emulsion pass through the drop disruption zone (Oldshue 1983).

It is often assumed that the final drop mean diameter of an emulsion is the result of a balance of disruption and coalescence (Tavlarides 1981). Hence, a coalescence term is sometimes added to equation [5.1]. The simplest theories (Gopal 1968), assume that the decrease in the number of drops Z, is proportional to Z^2 (the binary collision theory approximation). Therefore, equation [5.1] becomes:

$$dZ/dt = k_1Z - k_2Z^2 \quad [5.3]$$

However, for systems containing a stabilising surfactant it has been found that coalescence rate is not a strong function of collision rate (van Boekel 1981). It was concluded that coalescence was probably only of importance for drops that have just been formed and have not yet aquired an equilibrium surfactant adsorption layer. Hence, for the systems studied in this chapter equation [5.1] may be appropriate.

Rearrangement of equation [5.2] gives:

$$\ln[(D_{sm}-D_{sm\infty})/D_{sm}] = kt \quad [5.4]$$

Plots of $\ln(D_{sm}-D_{sm\infty}/D_{sm})$ vs t at different HLB_{act} values can be made from the data of Figure 5.7 (plots of D_{sm} vs t). The calculations are summarised in Table A4.12 of Appendix 4 and plotted on Figure 5.17.

Figure 5.17 shows that the results of this study for the cyclohexane/NPE system are in good agreement with equation [5.4], hence, drop disruption in this system can be treated as a first order reaction. As the addition of a coalescence term is not necessary (see equation [5.3]), it may be concluded that the drop sizes of emulsions with a stabilising surfactant present, at a concentration >>CMC, may not be affected by coalescence. Also, it is possible that the reasons forwarded by other workers in discussing discrepancies between theory and experimental results ((i) and (ii) above), may not apply to the systems studied here because in this study, the continuous phase was of low viscosity (water), the dispersed phase fraction was low (f_w=0.8) and the stirrer speed was 600 rpm, therefore, a large turbulent region will be present in the stirred vessel and the rate of movement of material around the vessel will be high.

It was obvious from figure 5.7 that the drop disruption rate must increase rapidly as the HLB_{act} of the system approaches its HLB_{inv} value. From figure 5.17, values can be calculated for the rate constant (k) for disruption at each HLB_{act} value. These are tabulated in Table 5.8 below.

TABLE 5.8 - Values for the rate constant for drop disruption for a range of HLB_{act} values.

HLB_{act}	k (min^{-1})
14.2	0.043
12.1	0.097
11.5	0.115
10.5	>2.500*

*Note: For this system at its SAD=0 condition (HLB_{act}=10.5), it is impossible to assign an accurate k value as the emulsion drop size distribution reaches a stable state almost instantaneously. The k value at HLB_{act}=10.5 is included to show that the drop disruption rate in Type 3 systems is an order of magnitude greater than in Type 1 systems. As will be seen later, the sizes of the drops of Type 3 emulsions are controlled by a different mechanism from that controlling drop sizes of Type 1 emulsions, hence, equation [5.4] may not apply to Type 3 systems.

Some authors have stated, that the effect of the dispersed phase fraction on drop sizes is unclear and that its effect is small if the surfactant concentration is kept constant (Walstra 1983). Hence, the final drop diameter at any HLB_{act} may be independent of f_w for the low viscosity systems studied which have stabilising surfactant present at a concentration >CMC. However, it will be shown in chapter 6, that turbulence damping by the dispersed phase, will cause a rise in the emulsion's drop sizes as the dispersed phase fraction increases. Therefore, it may be possible to estimate drop disruption rates at all points of the SAD- side of the cyclohexane/NPE map, from equation [5.2] and the data of Table 5.8, but allowance must be made for turbulence damping.

5.4.3 STABLE DROP DIAMETERS ACROSS THE PHASE TRANSITION

The results of this chapter have shown that the SAD shifting technique used to measure Type 3 system emulsion drop sizes does produce reasonable and consistent results.

For Type 3 systems table 5.3 shows that only the drop sizes at the O/M_w and W/M_o conditions are affected by f_w; reasons for this will be discussed in section 5.4.6 of this discussion. Tables 5.1 and 5.2 show that the drop sizes of emulsions made up at Type 3 conditions and then shifted to SAD+ or SAD- are affected by the precise condition of the initial emulsion. Emulsions initially made up as an O/M_w emulsion produced smaller drops in the shifted O/W_m emulsion than emulsions initially made up as $(O+W)/M_s$ or W/M_w. This would seem to be consistent with the findings of Shinoda et al (1986), who found that O/W_m with the smallest drops were produced by emulsifying at 2-5°C below the PIT, rather than at the PIT or just above the PIT. However, the fact that the smallest drops were produced in the O/M_w emulsion state does not fit with Friberg's (1978) explanation of Shinoda's findings ie. that the smallest drops of the emulsion are produced by the separation of the surfactant phase on cooling (again this will be discussed further in section 5 of this discussion).

When changing SAD to cross the phase transition from SAD+ to SAD-, the oil/water interface moves from concave towards the water phase in Type 2 systems, to effectively straight in Type 3 systems when the surfactant's affinity for oil and water is balanced, to convex towards the water phase for Type 1 systems (Shinoda 1986). Hence, whatever shape the oil and water drops may be in the $(O+W)/M_s$ emulsion, it can be argued that for surfactant present in the monolayer at oil/water interfaces:

area of a surfactant molecule's coverage on the oil side of the interface	=	area of a surfactant molecule's coverage on the water side of the interface

This may therefore provide an explanation as to why for each condition examined, the oil and water drops of (O+W)/M_s emulsions are of a similar size (see Tables 5.1 and 5.2).

Figure 5.10 is a plot of stable drop Sauter mean diameter vs HLB_{act}, this can be compared with figure 5.2 (Cayais 1974), which shows how interfacial tension varies during a phase transition. Interfacial tension becomes ultra-low in Type 3 systems (values as low as 0.001 dynes/cm have been recorded - Salager 1988) and reduces to a minimum effectively 0 dynes/cm at the transitional inversion point (Shinoda 1986). However, figure 5.10 shows that stable Sauter mean drop diameters do not pass through a minimum value within the Type 3 3-phase region, instead a reasonably constant value for both the oil and water drops is found. However, two minima in the drop size vs SAD plot appear at the edges of the Type 3 region (the presence of which depends on f_w), corresponding to O/M_w and W/M_o conditions (see figure 5.10).

Hence, it appears that interfacial tension is not the limiting factor for determining drop diameters at the transitional inversion point.

5.4.4 AGITATION CONDITIONS

Table 5.4 shows that the type or level of agitation employed in emulsification of Type 3 mixtures (for the low oil viscosity case examined) has little or no effect on the drop sizes of emulsions produced by transitional inversion. This is not too surprising as again the interfacial tension is so low that even the mildest agitation conditions can reduce drop sizes to their minimum value. Note spontaneous emulsification was observed as soon as Type 3 system components were added together.

As drop sizes at the transitional inversion point are not determined by agitation conditions or interfacial tension, this minimum value must therefore be primarily determined by the system's composition.

5.4.5 EFFECT OF SURFACTANT CONCENTRATION

Figure 5.12 clearly shows that the drop sizes produced by transitional inversion are extremely dependent on the surfactant concentration. The fact that large and consistent differences were seen in the oil drop sizes of (O+W)/M_s emulsions at different surfactant concentrations, indicates that the drop measuring technique used gives valid answers.

The drop sizes would therefore, seem to be limited by the area of surface coverage of the surfactant.

In Type 1 and Type 2 systems drop stability depends on surfactant forming a monolayer at the oil-water interface. When drop disruption occurs the new surface produced is stabilised by surfactant moving from micelle form to the new interface. Therefore, micelles can be seen as the form that excess surfactant takes that is not required at oil-water drop interfaces. In chapter 2, it was argued that the transitions $O/W_m \rightarrow O/W_m/O$ and $W/O_m \rightarrow W/O_m/W$, could only occur because there was no more surfactant in excess micelle form to stabilise new interface and, hence, these transitions normally occur at high dispersed phase fractions.

Up to this point we have pictured an agitated three phase Type 3 system as a dispersion of oil and water drops in surfactant phase ie. $(O+W)/M_s$, in common with other studies found in the literature (Shinoda 1986). This picture of a stirred Type 3 emulsion stems from what is known about the Type 3 systems phase separated state. However, the surfactant phase is quite unlike an oil or water phase and the idea that it behaves as a "phase" in an agitated state is probably incorrect. Its behaviour is probably similar to micelle behaviour in Type 1 and Type 2 systems.

In Type 1 systems surfactant present above the CMC forms micelles in the water phase. A phase separated Type 1 system whose water-oil ratio is such that its emulsified state would be on the $O/W_m \rightarrow O/W_m/O$ transition boundary, can therefore, be pictured as an oil phase containing surfactant at CMC_o and a water phase containing surfactant monomers at CMC_w and also surfactant micelles which contain solubilised oil. In an agitated state this system would contain no micelles and therefore, no solubilised oil because all the surfactant would be employed at the oil-water interface.

A Type 3 system in its phase separated state can be pictured as three phase:

(i) An oil phase containing surfactant monomers at CMC_o,

(ii) a water phase containing surfactant monomers at CMC_w,

(iii) a micelle phase containing cosolubilised oil and water (a surfactant phase).

Applying the above description to this system: As the interfacial tension is essentially zero in a Type 3 system, then in an agitated state, the drop sizes of this system will easily be reduced until the area of surfactant micelle coverage is maximised. Hence, an agitated Type 3 system should not be pictured as drops of oil and water in surfactant phase ie. $(O+W)/M_s$, but rather, drops of oil and water between surfactant monolayers ie. $(O+W)/S$. This reasoning is summarised in figure 5.18. Note, the earlier discussion in section 5.4.1 when comparing an $(O+W)/M_s$ structure (from figure 5.9) with Shinoda's schematic surfactant phase diagram (figure 1.3).

Note: The visualisation of an agitated Type 3 system described in figure 5.18, has similar components to that used (with some success) in Chapter 3, in the development of a partitioning model of surfactant between oil, water and a pseudo surfactant phase.

The validity of this picture of an agitated Type 3 system can be tested by examining surfactant area of coverage. The results calculated from the surfactant partitioning model of Chapter 3 for surfactant CMCs in the cyclohexane/NPE system, can be used to calculate the surfactant micelle concentration; this together with drop size distribution results for systems at the transitional inversion can then be used to calculate the area of coverage/surfactant molecule.

5.4.6 SURFACTANT COVERAGE ANALYSIS

The interface between the phases of surfactant-oil-water is often pictured as oil and water phases separated by a surfactant monolayer. Each nonionic surfactant molecule is taken to be composed of a hydrophilic chain and a lipophilic head; the hydrophilic chain and lipophilic head occupy a specific area at the water side and the oil side of the interface respectively.

Values of the area of coverage of the hydrophilic chain of nonionic surfactants are often estimated by plotting surface tension of water phase against air vs the logarithm of the surfactant concentration in the water phase, for conditions below the CMC. For nonionic surfactants the Gibbs adsorption isotherm can be written (see section 1.2):

$$\Gamma = \frac{1}{RT} \cdot \frac{d\pi}{d\ln C} \qquad [5.5]$$

where, Γ = surface excess surfactant,

π = surface pressure,

C = surfactant concentration.

Also:

$$A_s = \frac{1}{\Gamma N_A} \qquad [5.6]$$

where, A_s = area of coverage per surfactant molecule (m^2),

N_A = Avogadro's Number = 6.022×10^{23}.

Using the method described above Hsiao et al (1956), calculated the molecular area of the average hydrophilic chain length for a range of NPE surfactants. Their results are tabulated in Table 5.9 below:

TABLE 5.9 - Results of Hsiao et al (1956) - surfactant coverage

EON	A_s (Å^2)	$A_s.EON^{-1/2}$
9.5	55	17.8
10.5	60	18.5
15.0	72	18.6
20.0	82	18.3
30.0	101	18.4
100.0	172	17.3

Average=18.15

where, EON = average hydrophilic chain number of the NPE surfactant.

Lange (1967) showed that $A_s.EON^{-1/2}$ was constant for Hsiao et al's results, this is in accordance with the findings of van Voorst Vader (1960) for polyoxyethylene compounds. Hence, it is possible to estimate the area of coverage/surfactant molecule, for the average hydrophilic chain length at the transitional inversion point in the cyclohexane/NPE system from Hsiao et al's data.

In Chapter 3, it was shown that isothermal transitional inversion occured in a system at a specific average chain length (or HLB_{act}) of the surfactant in a pseudo surfactant phase. The pseudo surfactant phase refers to interfacial surfactant only, therefore, the average chain length of the surfactant at the interface can be calculated directly from its composition.

For the cyclohexane/NPE system the fraction of the lipophilic surfactant (chain length=5) and the fraction of the hydrophilic surfactant (chain length=12) in the pseudo surfactant phase was 0.82 and 0.18 respectively. Hence,

$$EON_{inv}=0.82x5+0.18x12 = 6.26$$

Therefore, for the cyclohexane/NPE transitional inversion point at 25°C the area of coverage of the surfactant hydrophilic chain can be estimated as:

$$A_s = 18.15x6.26^{1/2} = 45 \text{ Å}^2$$

Analysis

In the preceeding discussion it was argued that the surfactant area of coverage is maximised in agitated Type 3 systems ie. all surfactant present above the CMC is located at oil-water interfaces. The area of coverage per surfactant molecule in Type 3 system emulsions, can be estimated from conditions at the transitional inversion point by equating the available surfactant maximum area of coverage to the surface area of the oil and water drops.

The different emulsion structures present in Type 3 regions were discussed earlier in the mechanism of transitional inversion in NPE systems. The analysis below will consider only the O/M_w, $(O+W)/M_s$ and W/M_o emulsion forms.

TYPE 3 - 3 PHASE SYSTEMS

The following analysis is similar to that used by Baker and Tadros (1987) when examining water drop sizes in water/Xylene microemulsions. Baker and Tadros's study was concerned only with water drops in oil and also, no allowance was made in the model to distinguish between interfacial surfactant and dissolved surfactant monomers. Hence, a number of refinements are made here to allow for the more complex emulsion structures found at the transitional inversion point and to allow for dissolved surfactant.

A number of assumptions are required:

(i) The oil and water drops within the surfactant phase are to be of a similar size and that the area of coverage of a surfactant molecule at the oil side of the interface is equal to the area of coverage of a surfactant molecule on the water side of the interface (note earlier discussion on the surfactant having equal affinity for each phase and also, the drop size data of tables 5.1 and 5.2).

(ii) That the surface area/volume of the spherical drops measured by shifting the system to an O/W_m or W/O_m state is equivalent to the surface area/volume of the oil and water drops in an (O+W)/S emulsion (whatever the shape of the drops at a SAD=0 condition may be).

Let d_i = the average diameter of interval i of a size distribution,

p_i = the fraction of the total number of drops in interval i.

Then:

$$\frac{\text{Total Emulsion volume}}{\text{Total drop surface area}} = \frac{1\Sigma d_i^3.p_i}{6\Sigma d_i^2.p_i} = \frac{1}{6}.D_{sm}$$

Surface area of oil and water drops/litre
of emulsion=$6x10^{-3}/D_{sm}$ _____[5.7]

The surfactant will have a distribution of differing chain length molecules and each chain length will have different coverage areas, however, an average area of coverage per surfactant molecule can be calculated for the isothermal transitional inversion condition because isothermal transitional inversion occurs at one HLB_{act} value and hence, the make up the surfactant is the same for this condition for any surfactant concentration.

The maximum area of surfactant interface/ litre of emulsion=

Moles of surfactant interfacial phase per litre	x	area of coverage per surfactant molecule	x	number of molecules per mole

$= C_m.A_s.N_A$_____[5.8]

Where, C_m = surfactant interfacial phase concentration (moles/l),

From Chapter 3:

$$C_m = C_t-(1-f_w)(x_lCMC_{ol}+x_hCMC_{oh})-f_w(x_lCMC_{wl}+x_hCMC_{wh})$$

Substituting the calculated and estimated data from Chapter 3:

CMC_{ol}=0.07 moles/l $CMC_{wl}=2x10^{-5}$ moles/l
$CMC_{oh}=10^{-4}$ moles/l $CMC_{wh}=10^{-4}$ moles/l
x_l=0.82 x_h=0.18 f_w=0.8

$C_m = C_t$-0.0115 moles/l_____[5.9]

Equating equations [5.7] and [5.8] and substituting in equation [5.9] we arrive at the following equation which can be used to estimate the area of coverage per surfactant molecule:

$$A_s = \frac{6x10^{-3}}{(C_t-0.0115).D_{sm}.N_A}$$ _____[5.10]

The D_{sm} values calculated from microscopy data at surfactant concentrations of 10 g/l and 20 g/l can be used with equation [5.10] to estimate the surfactant's area of coverage per molecule. The drop diameters determined for higher surfactant concentrations by photon-correlation-spectroscopy (PCS) cannot be used with equation [5.10] as these drop diameter values are not volume/area diameters. However, we can predict D_{sm} values at higher surfactant concentrations from the surfactant coverage values calculated at 10 g/l and 20 g/l and compare these with the PCS results.

The results of calculated for A_s from D_{sm} from the experimental results at surfactant concentrations of 10 g/l and 20 g/l are summarised in Table 5.10 below:

TABLE 5.10 - Estimation of surfactant area of coverage/molecule

Surfactant Conc. (g/l)	HLB_{inv}	C_m (moles/l)	D_{sm} μm	$\mathring{A}_s$ (A^2)
10	10.4	0.008	3.2	39
20	10.5	0.028	1.0	36

If we take an average value of A_s=37.5$\mathring{A}^2$, we can estimate D_{sm} at higher surfactant concentrations using equation [5.10]. Results are tabulated in Table 5.11 below (PCS results are shown for comparison):

TABLE 5.11 - Comparison of calculated and experimental drop diameter values at varying surfactant concentrations.

Surfactant Conc. (g/l)	HLB_{inv}	C_m (moles/l)	D (μm) PCS	D_{sm} (μm) calculated*
20	10.53	0.028	2.0	1.00
50	10.63	0.106	0.24	0.30
80	10.70	0.158	0.15	0.17
120	10.76	0.274	0.073	0.10

* using equation [5.8].

The value estimated for a surfactant molecule's area of coverage is in reasonable agreement with that estimated from Hsiao et al's data. Good agreement is found between the calculated drop diameter values and the PCS results (note PCS becomes relatively

inaccurate for measuring drop diameters above 1 micron). Hence, the argument of an (O+W)/S emulsion structure for 3 phase Type 3 systems and the theory that drop size is determined by surfactant coverage, would seem valid. It is also, worth noting that the (O+W)/S structure ties in well with the surfactant partitioning model derived in Chapter 3.

As oil and water drops have been found here to be of an equal size in an (O+W)/S emulsion, then the area of coverage of surfactant on oil would seem to be the same as that on water. If this is the case then providing C_m is kept constant, rather than C_t kept constant (note variation with f_w discussed in Chapter 3), then the ratio of oil and water in the system will have no effect on drop sizes eg. a surfactant-oil-water system with a C_m of 20 g/l will always have an approximately 98% dispersed phase, whatever the value of f_w. This is in agreement with the results for (O+W)/M_s systems in Tables 5.1 and 5.2.

TYPE 3 - TWO PHASE SYSTEMS

The surfactant coverage analysis developed above can be extended further to Type 3 systems of 2 phases only ie. W/M_o and O/M_w. For these Type 3 systems not all of the oil or water phase volumes are dispersed in the surfactant. If again the surfactant micelle area of coverage is maximised for these systems then:

For O/M_w systems equation [5.10] becomes:

$$D_{sm} = \frac{6\times10^{-3}.(1-f_w)}{(C_t-0.115).A_s.N_A} \qquad [5.11]$$

For W/M_o systems equation [5.10] becomes:

$$D_{sm} = \frac{6\times10^{-3}.f_w}{(C_t-0.115).A_s.N_A} \qquad [5.12]$$

If again we take A_s=37.5Å^2, we can estimate D_{sm} values for O/M_w and W/M_o emulsions at surfactant concentrations of 20g/l and compare with the experimental results of Table 5.1 and 5.2.

TABLE 5.12 - Comparison of calculated and experimental drop diameter values.

Emulsion Type	f_w	calculated D_{sm} (μm)	experimental D_{sm} (μm)
O/M_w	0.8	0.2	0.35*
$(O+W)/M_s$	0.8	1.0	1.0
W/M_o	0.8	0.8	1.0
W/M_o	0.2	0.2	<0.5

*PCS result

Reasonable agreement is found between result and theory. Hence, this theory may explain the two minima seen on the drop diameter vs SAD graph (Figure 5.3). The important observation is that the drop sizes of O/M_w and W/M_o emulsions are dependent on f_w, whereas, those of (O+W)/S emulsions are not.

The theory based on surfactant coverage derived above is consistent with experimental observations. It also indicates that the mechansism of transitional inversion in NPE systems proposed in Chapter 2:

ie. $W/O_m \rightarrow W/M_o \rightarrow (O+W)/M_s \rightarrow O/M_w \rightarrow O/W_m$

may be correct, as the surfactant coverage-drop size analysis fits well with each of the emulsion structures proposed for each phase behaviour type.

5.4.7 EFFECT OF OIL PHASE VISCOSITY AND TRANSITIONAL INVERSION - DIRECT EMULSIFICATION COMPARISON

Figure 5.14 shows the variation of D_{sm} with time for direct emulsifications of polyisibutene Xg/l cyclohexane/NPE (HLB_{act}=12.0) O/W_m emulsions at f_w=0.8 and stirrer speed of 800rpm. The D_{sm} results at each viscosity all correspond to the same curve - this is in agreement with Weber number correlations for emulsions with low dispersed phase fractions. The data for an oil phase viscosity of 0.007 poise was calculated from the data of figure 5.7 for the same system agitated at 600rpm. It was assumed that $D_{sm} \propto N^{-1.20}$ (the correlation for drop breakage control in isotropic turbulence (Shinnar 1961)); this was found to be in good agreement with the results for higher oil viscosities. Hence, it is reasonable to assume that, isotropic turbulence was developed in the tank, in the direct emulsifications.

Note, Calabrese et al (1986) made an extensive examination of the effect of dispersed phase viscosity on drop sizes of dispersions. They suggested a function should be added to Weber number correlations to account for the effect of increased viscous resistance to drop break up in higher dispersed phase viscosity systems (see chapter 4). However, the addition of a dispersed phase viscosity group would not seem necessary for the results presented on figure 5.14.

To compare the drop sizes of emulsions produced by transitional inversion with those of emulsions produced by direct emulsifications, refer to figure 5.14 and figure 5.13 - the variation of drop diameter at the transitional inversion point at different oil phase viscosities and also the data of Table 5.7. It was already shown on figure 5.7 how drop sizes vary with time at the transitional inversion point for low viscosity oil phases (0.007 poise); in these systems the emulsion droplets were rapidly reduced to a minimum size allowed by the surfactant concentration, from whichever side of the SAD=0 line the transition was approached (ie. no difference was seen when the required result was an O/W_m emulsion, between moving $W/O_m \rightarrow (O+W)/S \rightarrow O/W_m$ or $O/W_m \rightarrow (O+W)/S \rightarrow O/W_m$).

For oil phase viscosities of 1 to 2 poise, figure 5.13 shows that if SAD=0 is approached from the oil continuous side (from SAD+, W/O_m emulsion state), then a mixing time of approximately 20 minutes is required until a stable drop size distribution is achieved. At oil phase viscosities of 5, 10 and 30 poise and again approaching SAD=0 from an oil continuous SAD+ state, large variations between different samples were found, even after 20 minutes of agitation. Hence, the oil phase viscosity can prevent the drop sizes of emulsions produced by transitional inversion becoming small because mixing through the stirred vessel may become far from homogeneous (see table 5.6).

However, if the SAD=0 state was approached from the water continuous SAD- side of the inversion map, then the mixing conditions in the vessel will be turbulent. It was found when approaching the SAD=0 line from this side that drop sizes of emulsions at the transitional inversion point were rapidly reduced, so that the D_{sm} of the drop size distribution was <2 μm, in the case of all of the oil phase viscosities examined.

These experiments highlight good practice for making emulsions with small drop sizes by the transitional inversion method: Approach the SAD=0 condition with the low viscosity phase continuous to enable premixing of the system's components.

5.4.8 CYCLOHEXANE/SML SYSTEMS

The two experiments performed on the cyclohexane/SML system revealed several differences between transitional inversion in systems containing SML surfactants and systems containing NPE surfactants. Transitional inversion was only possible in SML

systems when the dispersed phase fraction was >0.7. Hence, for the system under study (cyclohexane/SML f_w=0.8) inversion was only possible moving from SAD+ to SAD-. Taking each experiment in turn:

(i) SAD+ to SAD=0 to SAD-

Figure 5.15 shows photomicrographs taken at each stage of the transition. The effect of the change SAD+ to SAD=0 is similar to transitional inversion in the cyclohexane/NPE system. As the system's SAD moves closer to SAD=0 the water drop sizes of the W/O_m emulsions become smaller reflecting the reduction in interfacial tension.

In systems containing NPE surfactant a discontinuity occurs in the Type 3 region, as the system moves from a W/M_o to a $(O+W)/M_s$ condition. A discontinuity was also seen in the cyclohexane/SML system Type 3 region, however, a difference in the systems structure was obvious (compare SAD=0 conditions, Figure 5.9 and Figure 5.15). Whereas, at the NPE system inversion point the emulsion was thick and highly viscous, at the SML system inversion point the emulsion thinned and the water phase became continuous. Within the water phase complex drop structures (large drops containing very small drops) were present. These drops may be oil and water drops in surfactant phase.

The complex drops are large in comparison with the drops within them, this may indicate that the complex drops are unstable to coalescence, but the drops within them are stable. Hence, in a similar manner to that discussed in the mechanism of transitional inversion for systems containing NPE surfactants, the complex drops seen in this transitional inversion may be composed of the phase that "wants" to become continuous, but in this instance is unable to because the water volume is too large.

On further shift in SAD towards SAD-, after stirring for some time for a new equilibrium to attain, the complex drops broke down and the emulsion became O/W_m, however, the drop sizes (1-10 μm range) resulting from this transitional inversion process were not significantly smaller than those that could be produced by direct emulsification. This is in agreement with the findings of Parkinson and Sherman (1972), for systems containing SML surfactants.

(ii) SAD- to SAD+

Inversion was not possible changing SAD from SAD- to SAD+ in this system. The rapid change in SAD induced on the system produced no significant changes in the drop sizes of the emulsion. The step change across the SAD=0 boundary moved the emulsion from an O/W_m to a O_m/W state. This experiment shows the value of SAD maps for interpreting the results of dynamic changes on a system - the final emulsion in this

experiment may appear no different from the initial emulsion. However, once equilibrium is achieved the final emulsion will be far more unstable than the initial emulsion as the surfactant micelles will now have moved into the dispersed phase.

The two experiments discussed above show the differences in mechanism of transitional inversion in NPE systems and SML systems:

(a) In chapter 2 it was stated that for transitional inversion in SML systems the surfactant phase may not become continuous unless the dispersed phase fraction was >0.7. Having now examined drop changes across the transition, it is possible to clarify the mechanism of transitional inversion in SML systems further; it appears that the surfactant phase never becomes continuous for these inversions. Although the transitional inversion point is dependent on the surfactant (the inversion is still induced by phase behaviour change), it is only achieved physically when a large dispersed phase fraction is present, which becomes an excess continuous phase in the 3-phase region ie. excess water that is not emulsified in the surfactant phase. Hence, transitional inversion in SML systems containing a large water volume fraction can be written as:

INVERSION PATH	**MECHANISM**
SAD+ to SAD-	$W/O_m \rightarrow (O+W)/M_s/W \rightarrow O/W_m$
SAD- to SAD+	$O/W_m \rightarrow (O+W)/M_s/W \rightarrow O_m/W$

(b) The W/O_m drop sizes did decrease in size as SAD moved towards SAD=0, therefore, use of the O/M_w and W/M_o emulsion states to make fine emulsions may still be possible using SML surfactants. However, the smallest water drops observed before the SAD=0 condition in experiment (i) were not as small as those found in the cyclohexane/NPE system for a similar pseudo surfactant phase concentration. It may be that interfacial tension in Type 3 SML systems does not reduce to such ultra-low values as have been observed in NPE systems.

This chapter has dealt with the mechanisms and drop sizes of emulsions subjected to transitional inversion. Chapter 6 will now examine the variables which may affect drop sizes and inversion points in catastrophic inversions, brought about by changing f_w.

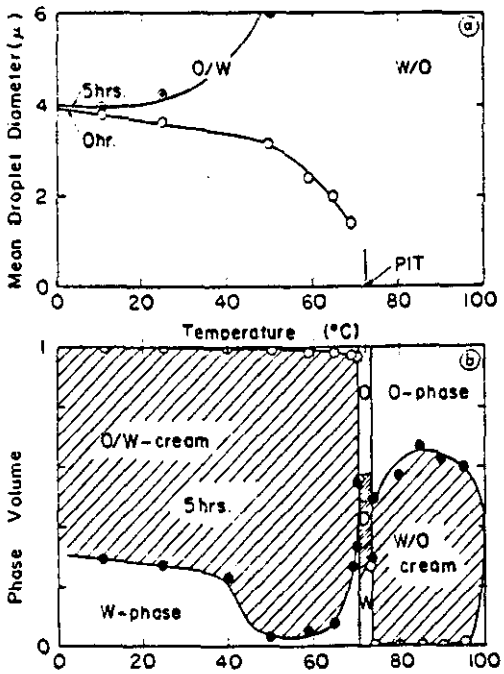

FIGURE 5.1 - (a) The effect of temperature on the mean volume diameter of emulsions containing, 48.5% cyclohexane, 48.5% water and 3% NPE9.7, after 0 hours and 5 hours after emulsification. (b) the effect of temperature on the volume fraction of oil, cream and water phases in the same system. After emulsification with a single surfactant, the system was maintained at the temperature indicated for 5 hours. (Reproduced from Shinoda 1986).

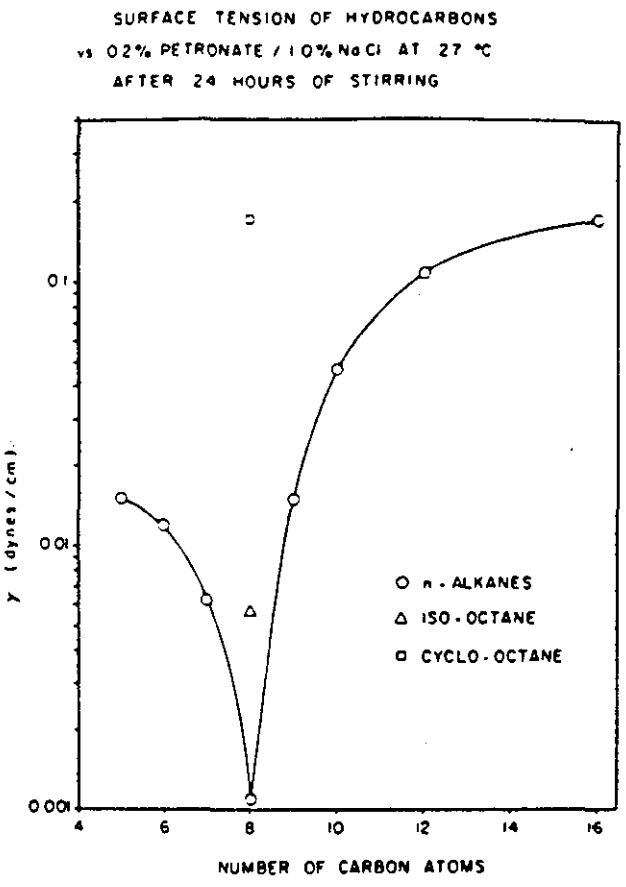

FIGURE 5.2 - The variation of interfacial tension across an SAD transition, measured using a spinning drop apparatus (reproduced from Cayias 1974).

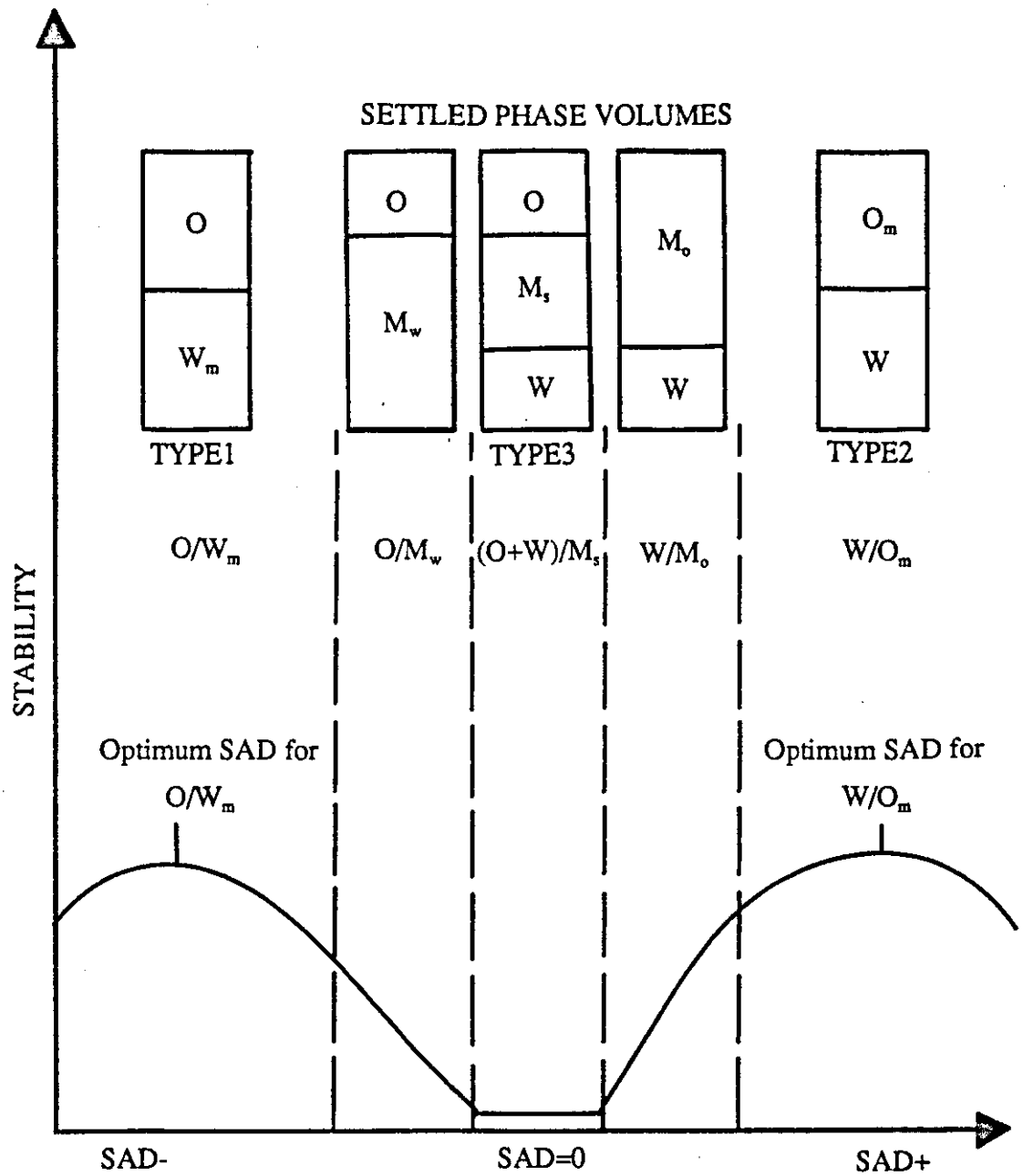

FIGURE 5.3 - Schematic representation of emulsion stability variation across the phase transition.

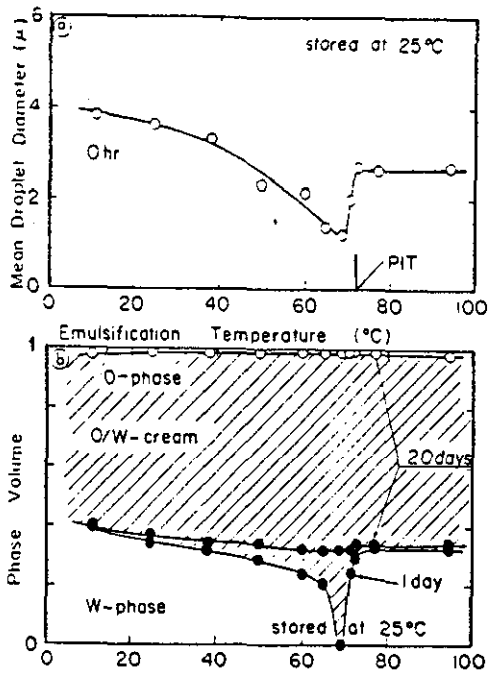

FIGURE 5.4 - (a) The effect of the emulsification temperature on the mean volume diameter of emulsions containing, 48.5wt% cyclohexane, 48.5wt% water and 3wt% NPE9.7. (b) The effect of the emulsification temperature on the volume fractions of oil, cream and water phases, of the same emulsion 20 days after agitation. After emulsification with a single surfactant, the system was stored at 25°C (reproduced from Shinoda 1986).

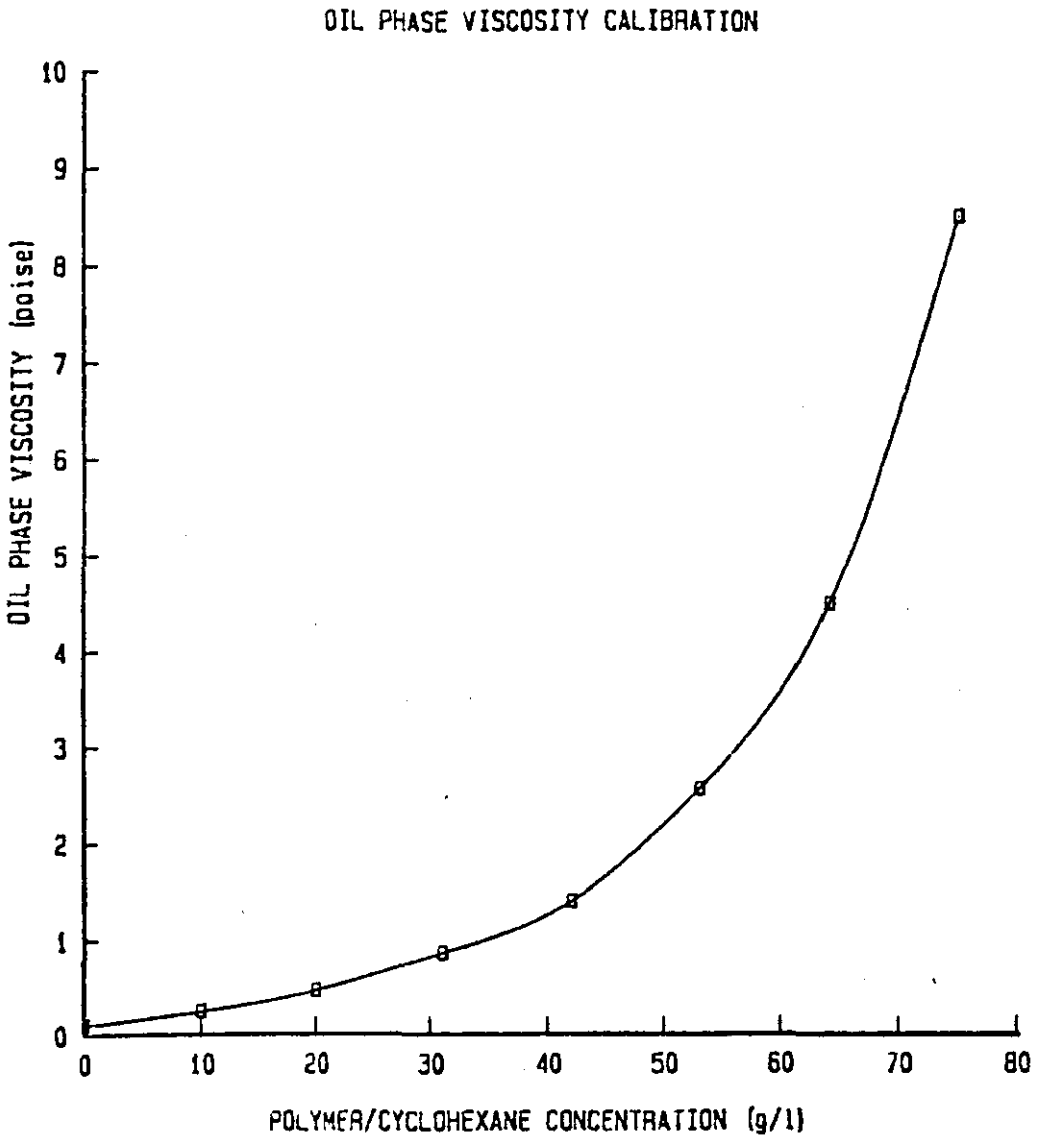

FIGURE 5.5 - *Oil Phase polymer concentration/ viscosity calibration at 20°C.*

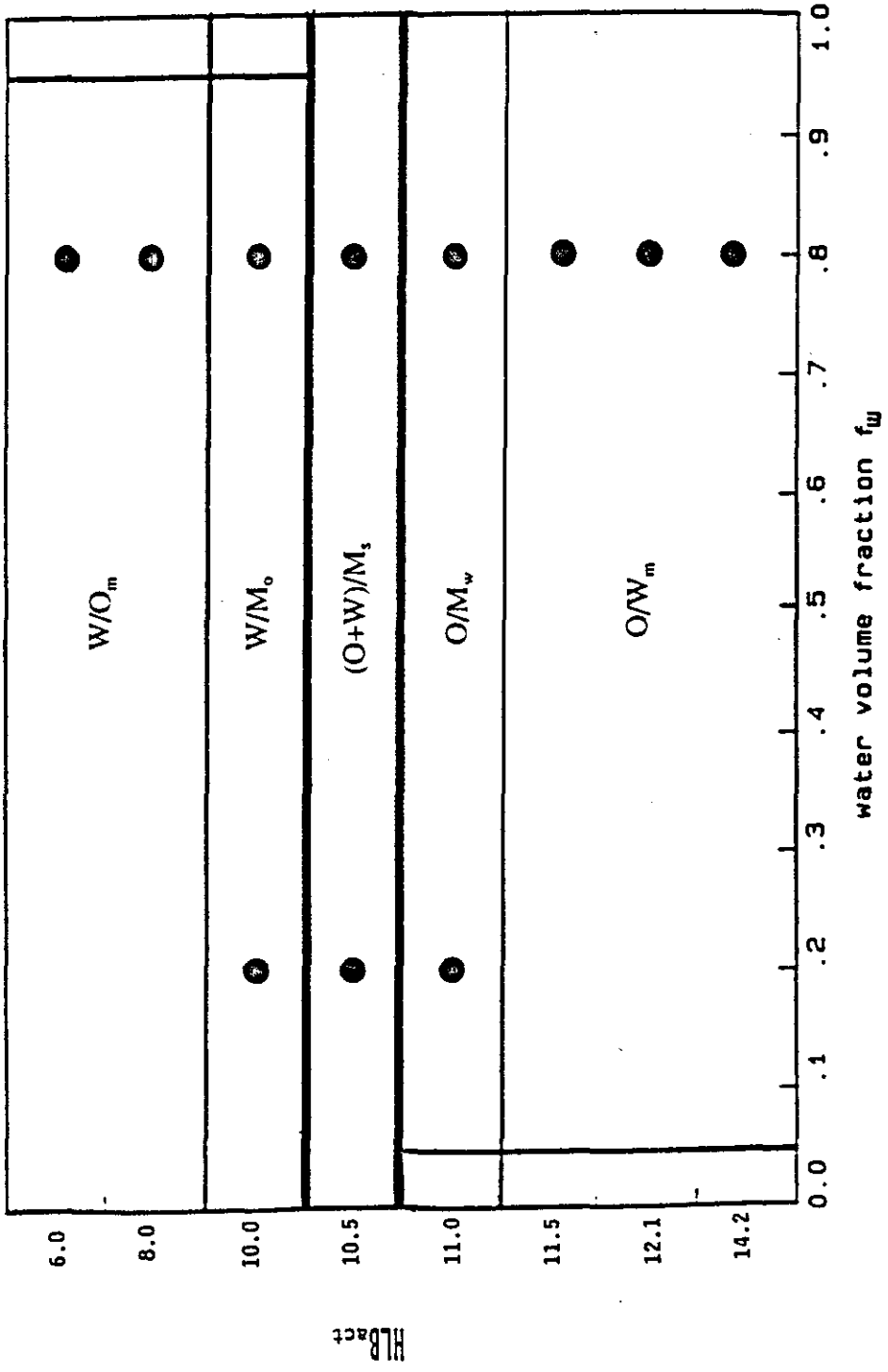

FIGURE 5.6 - The position and emulsion type at each point examined across the SAD transition (cyclohexane/NPE5-NPE12 system at 25°C).

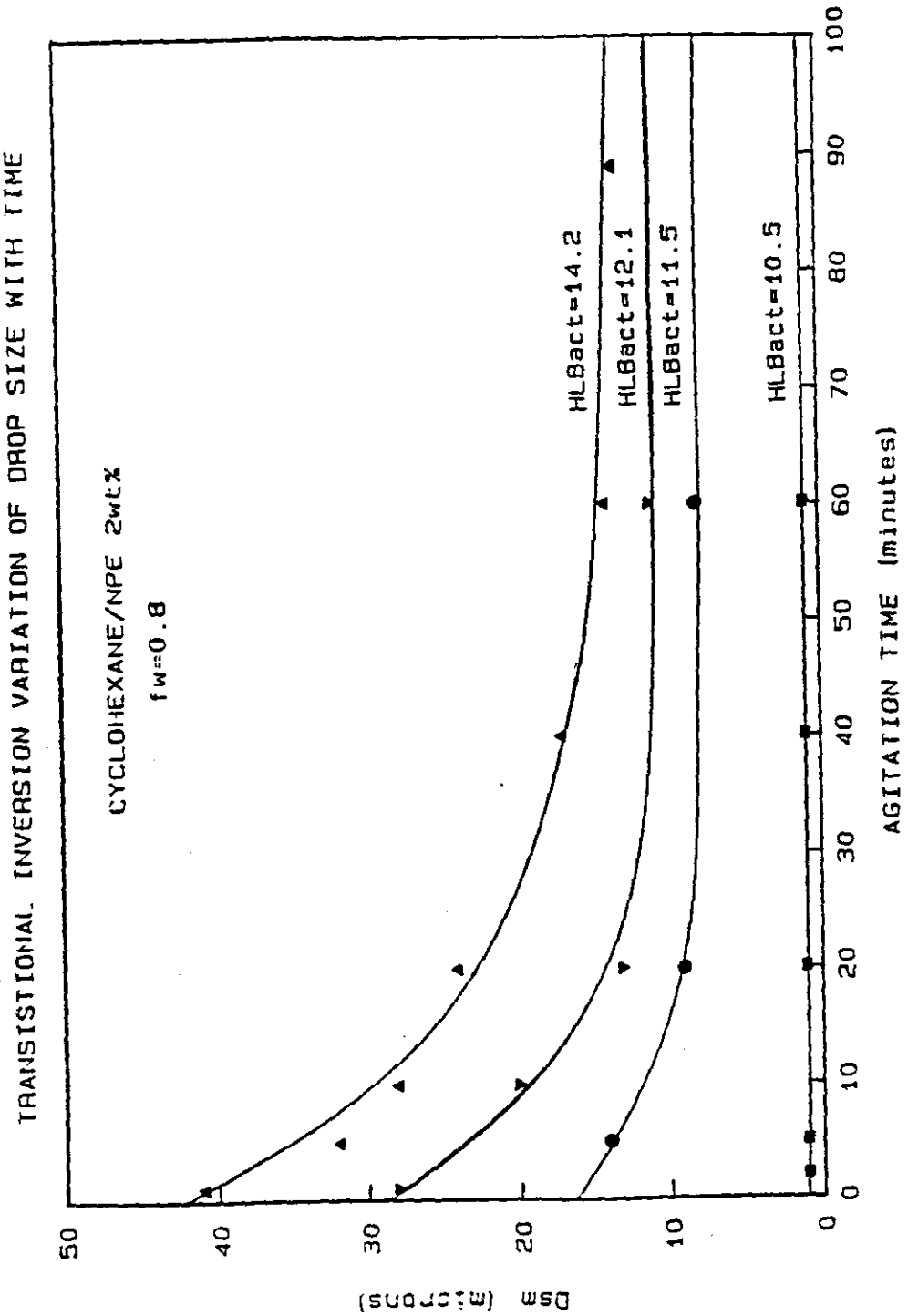

FIGURE 5.7 - The variation of drop sizes with agitation (600rpm) time at different SAD-conditions (cyclohexane/NPE5-NPE12 system at 25°C).

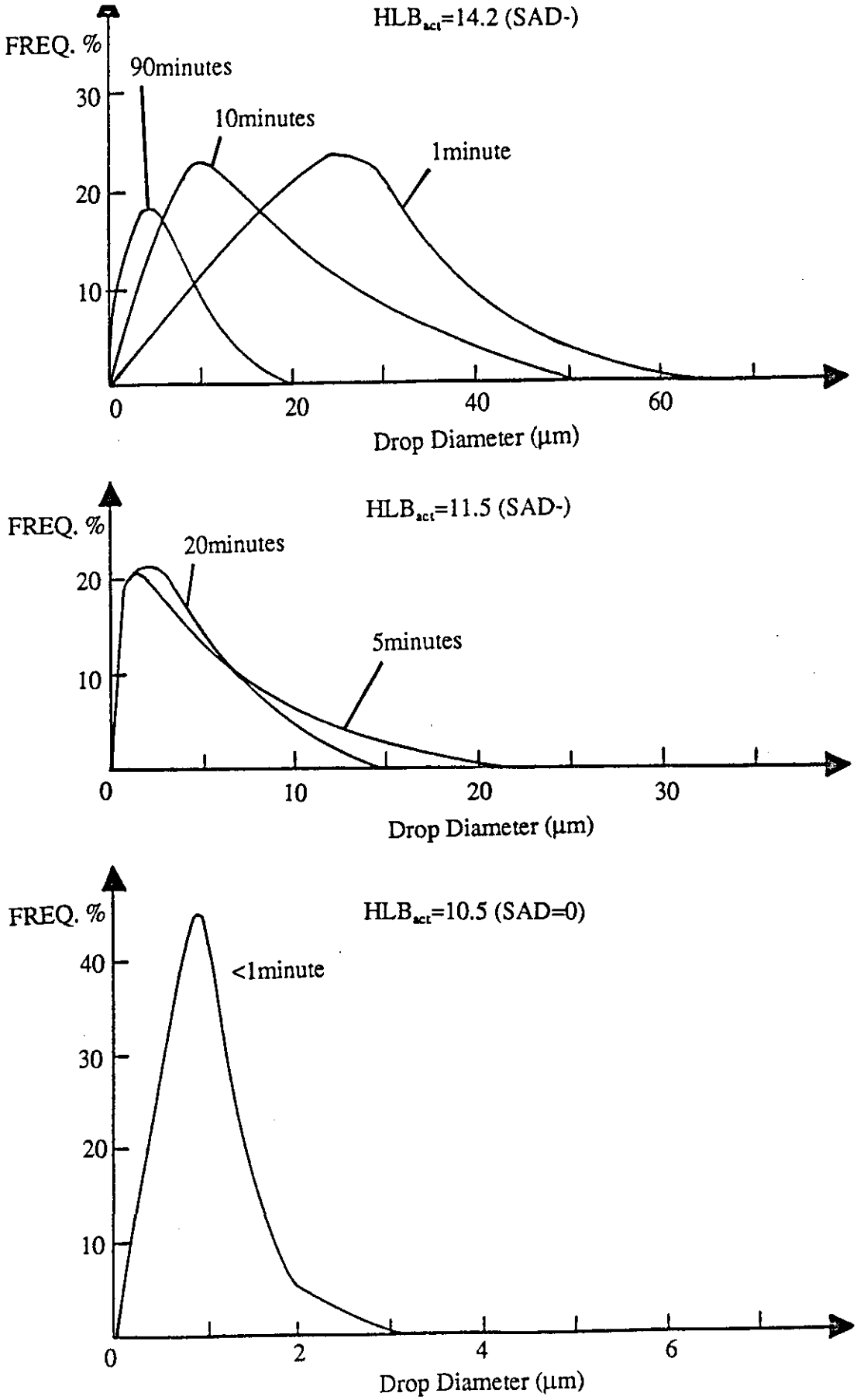

FIGURE 5.8 - The change in the O/W$_m$ emulsion's drop size distribution with agitation time (600rpm), at three HLB$_{act}$ values (SAD- condition: cyclohexane/NPE5-NPE12 system at 25°C). The mean diameter of each size distribution interval was used to produce a continuous curve.

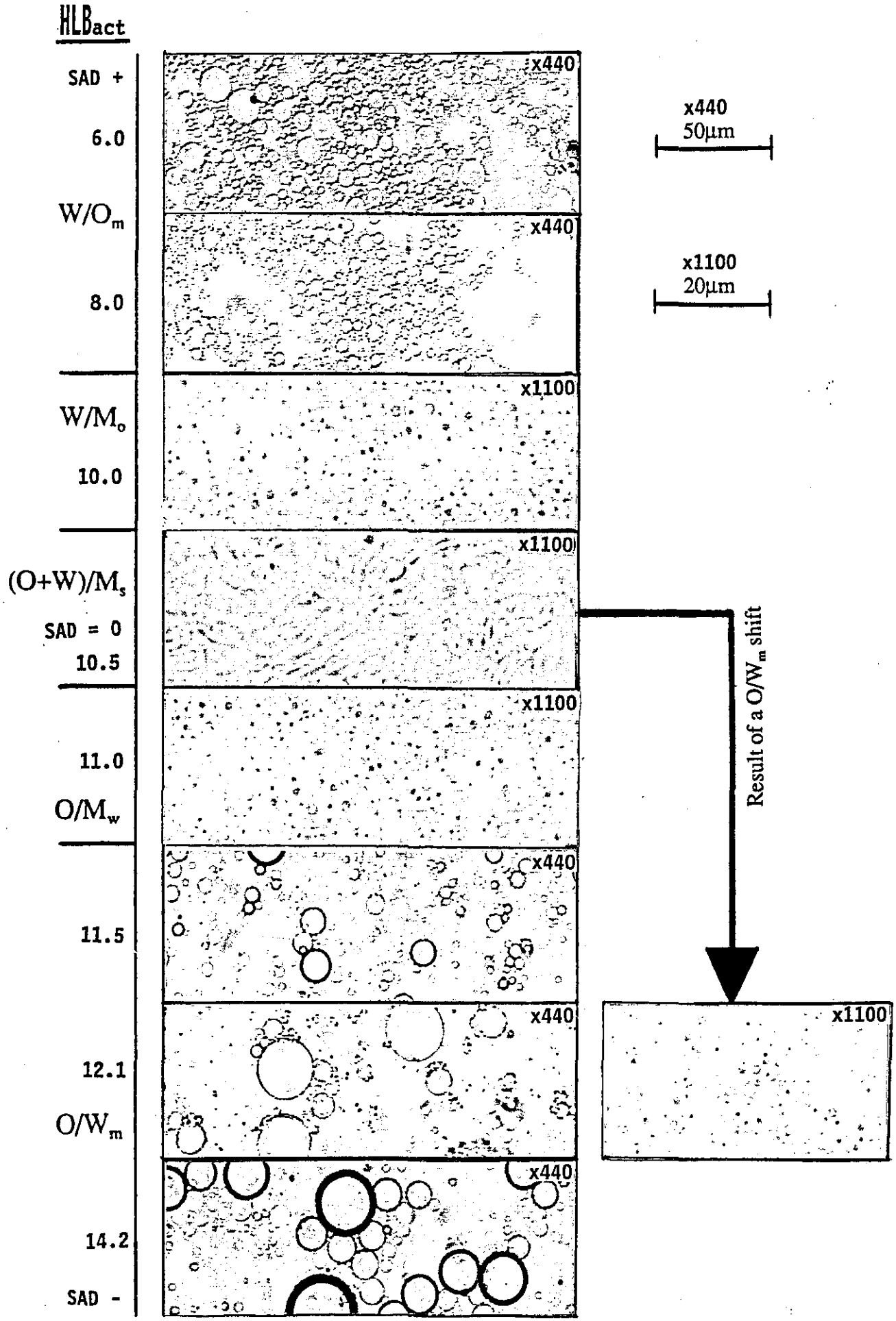

FIGURE 5.9 - Photomicrographs of steady-state emulsions produced at points across the phase transition (cyclohexane/NPE systems at 25°C).

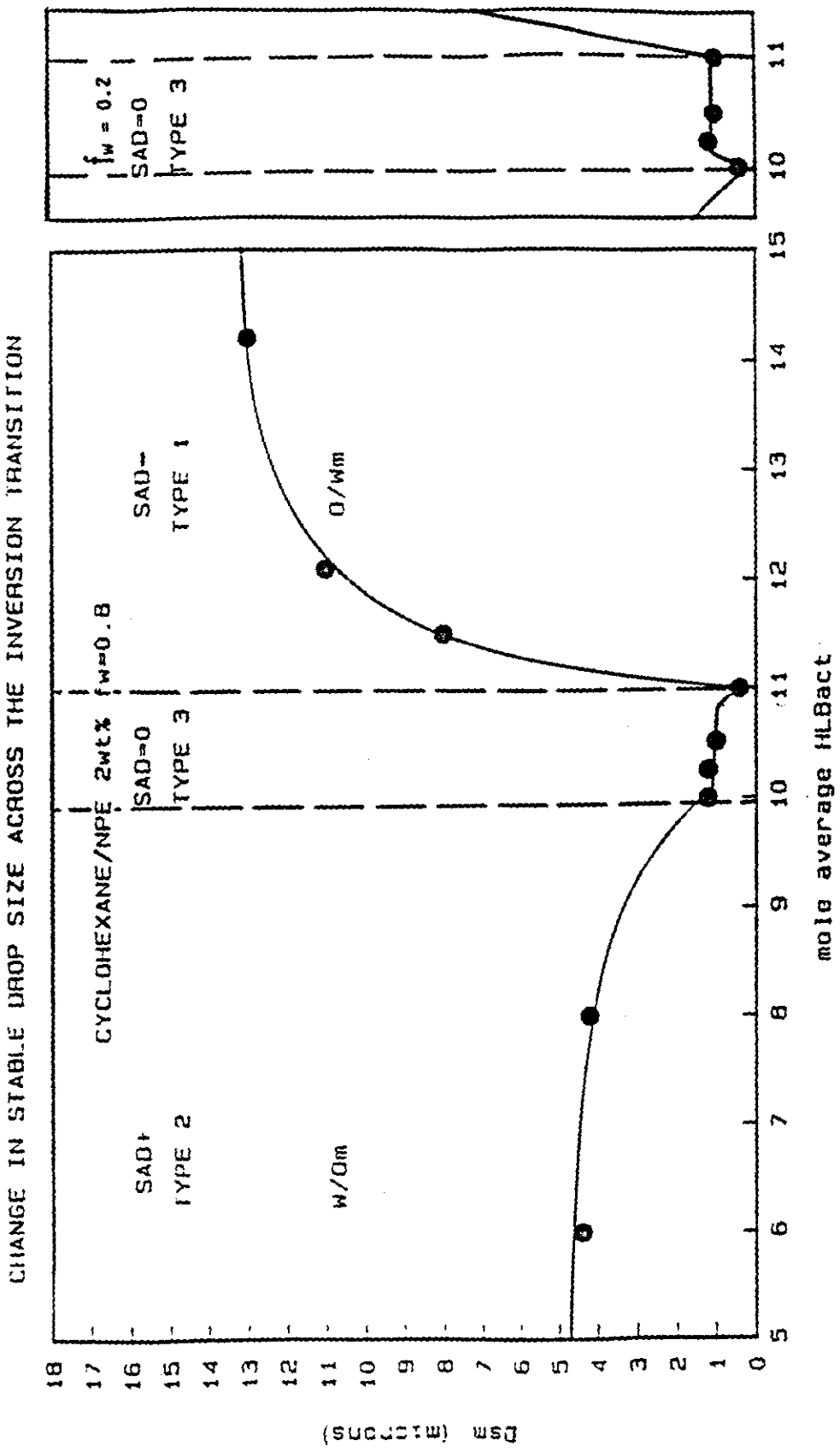

FIGURE 5.10 - Change in the steady-state drop diameter (D_{sm}) across the phase transition (cyclohexane/NPE systems at 25°C).

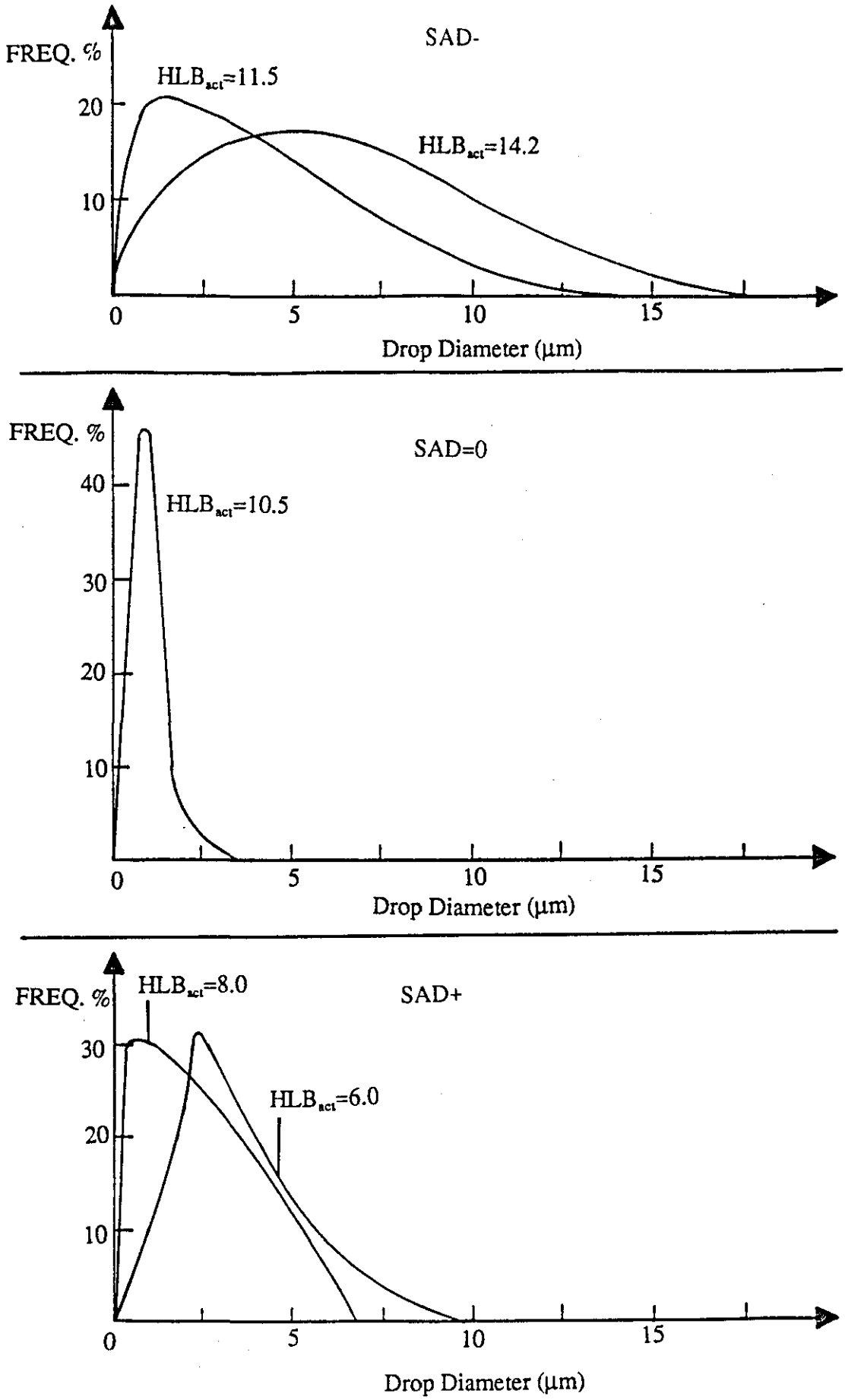

FIGURE 5.11 - Steady-state drop size distributions of O/W$_m$ emulsions at SAD-, (O+W)/M$_s$ emulsions at SAD=0 and W/O$_m$ emulsions at SAD+ (cyclohexane/NPE systems at 25°C).

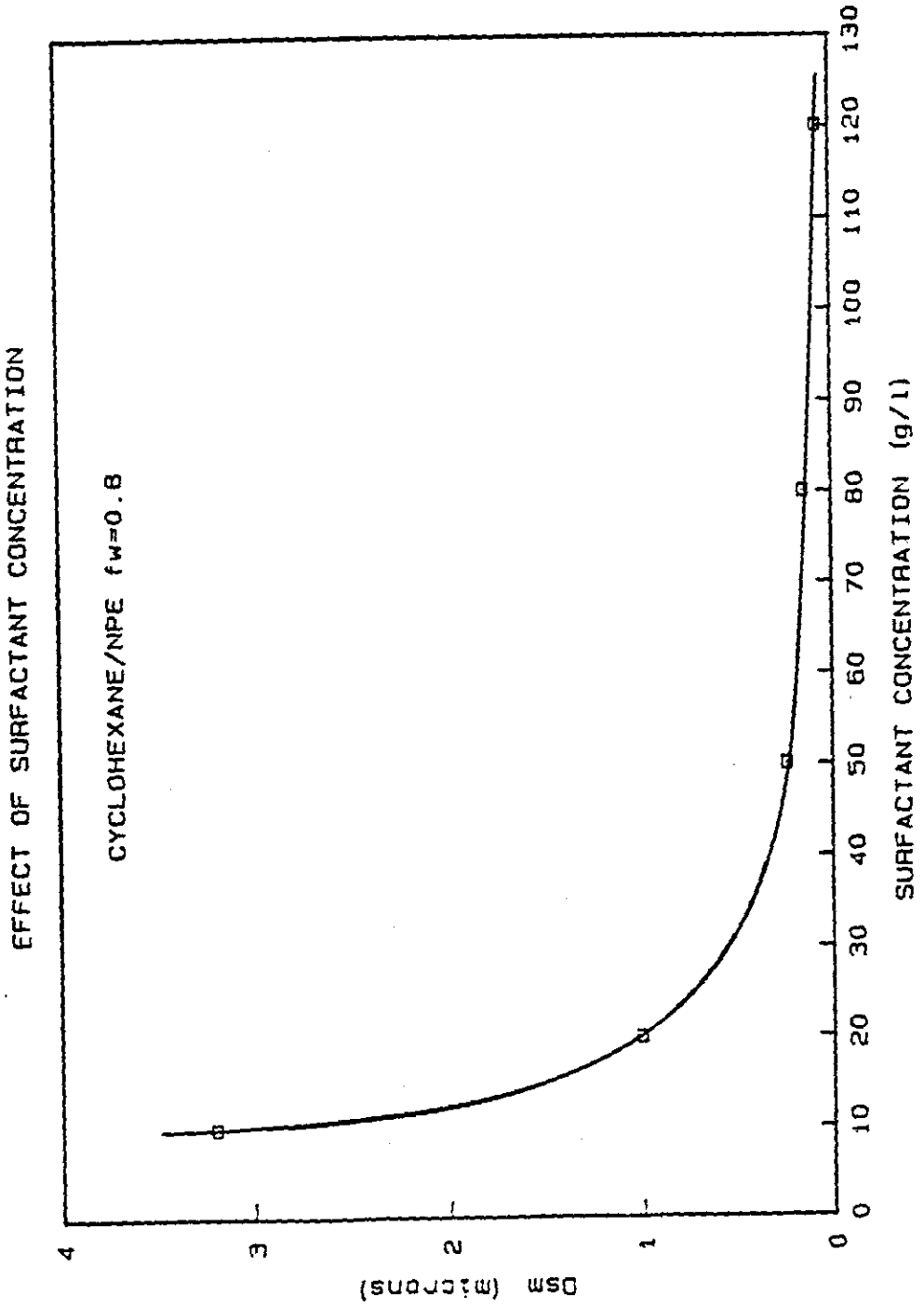

FIGURE 5.12 - Variation of drop size at the SAD=0 point, with surfactant concentration (cyclohexane/NPE5-NPE12 system at 25°C).

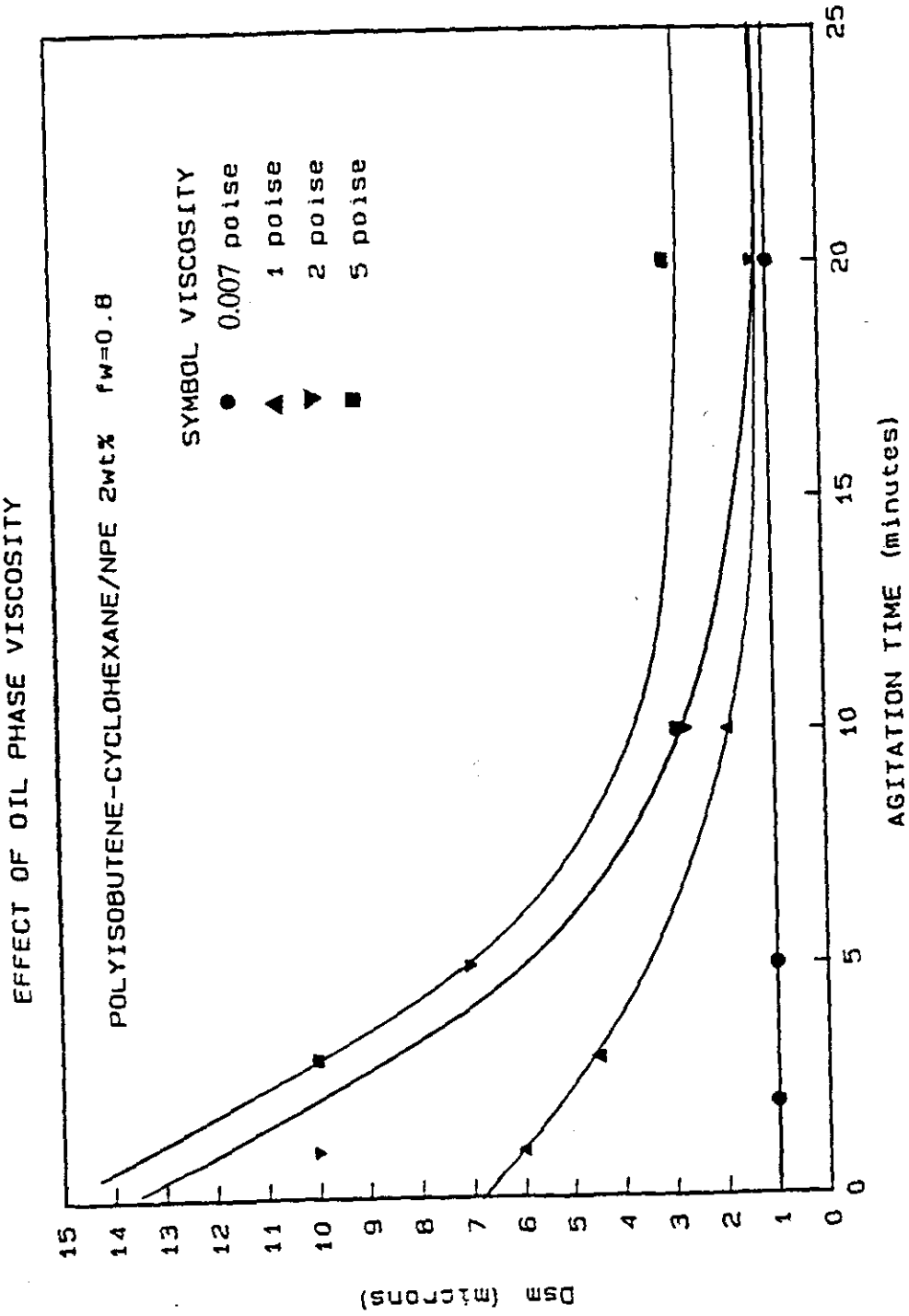

FIGURE 5.13 - Effect of the oil phase viscosity on the time required to achieve a steady-state drop diameter at the transitional inversion point, approaching SAD=0 from an oil phase continuous condition (PIB-cyclohexane/NPE5-NPE12 system at 25°C).

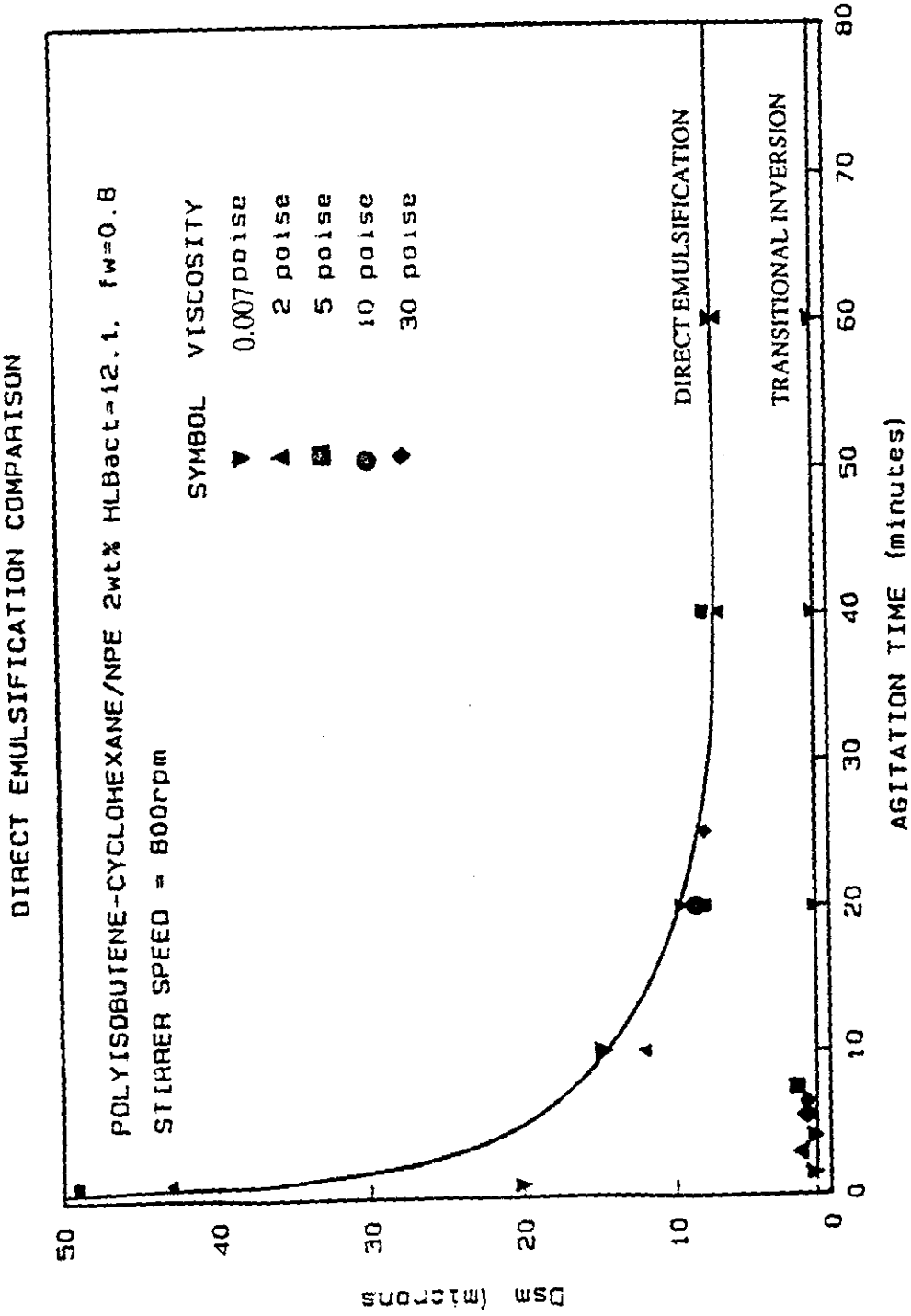

FIGURE 5.14 - Transitional inversion - Direct emulsification comparison (PIB-cyclohexane/NPE5-NPE12 system at 25°C).

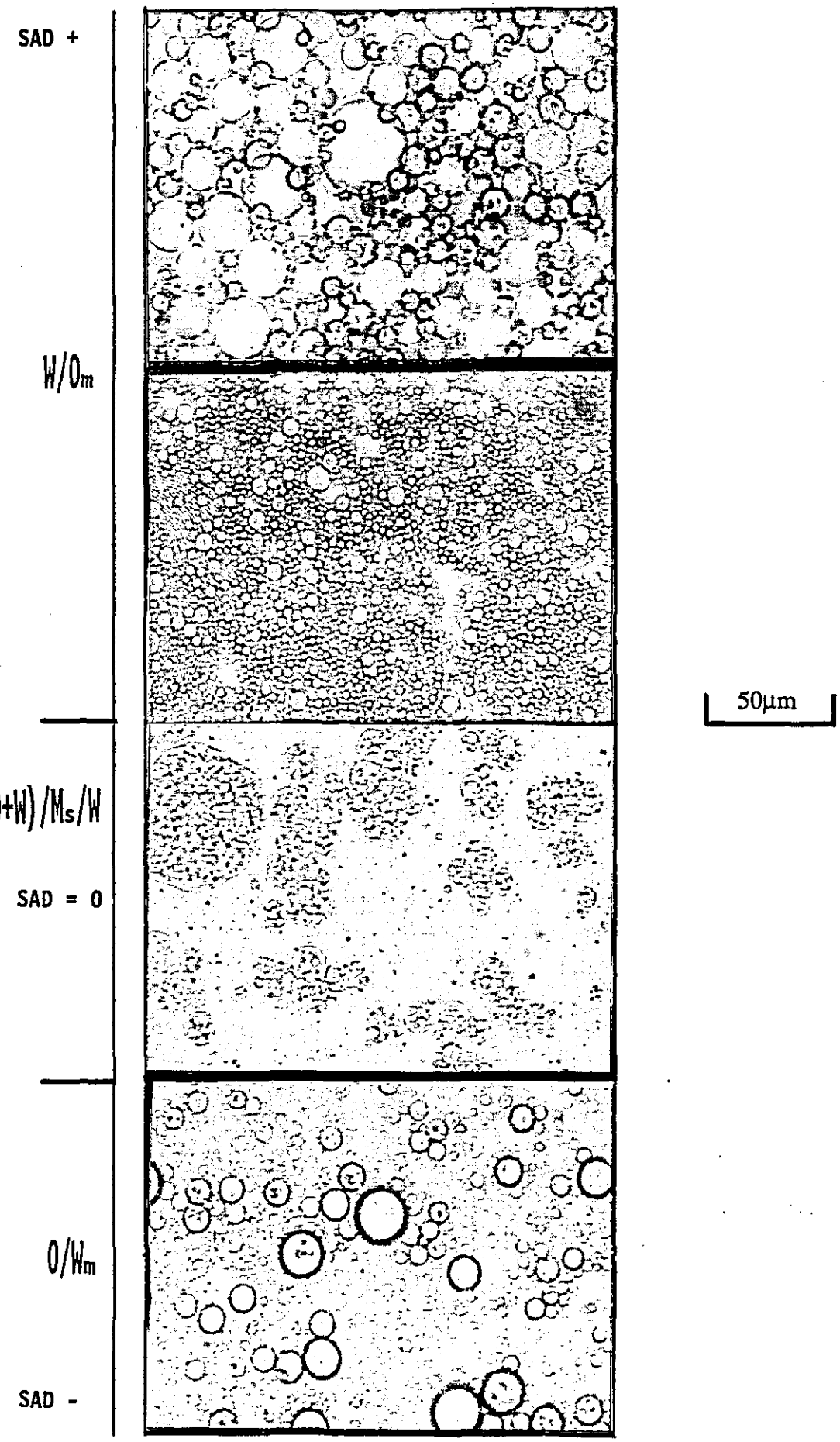

FIGURE 5.15 - Photomicrographs (x440) taken at points during a transition from SAD+ to SAD- (cyclohexane/SML system at 25C).

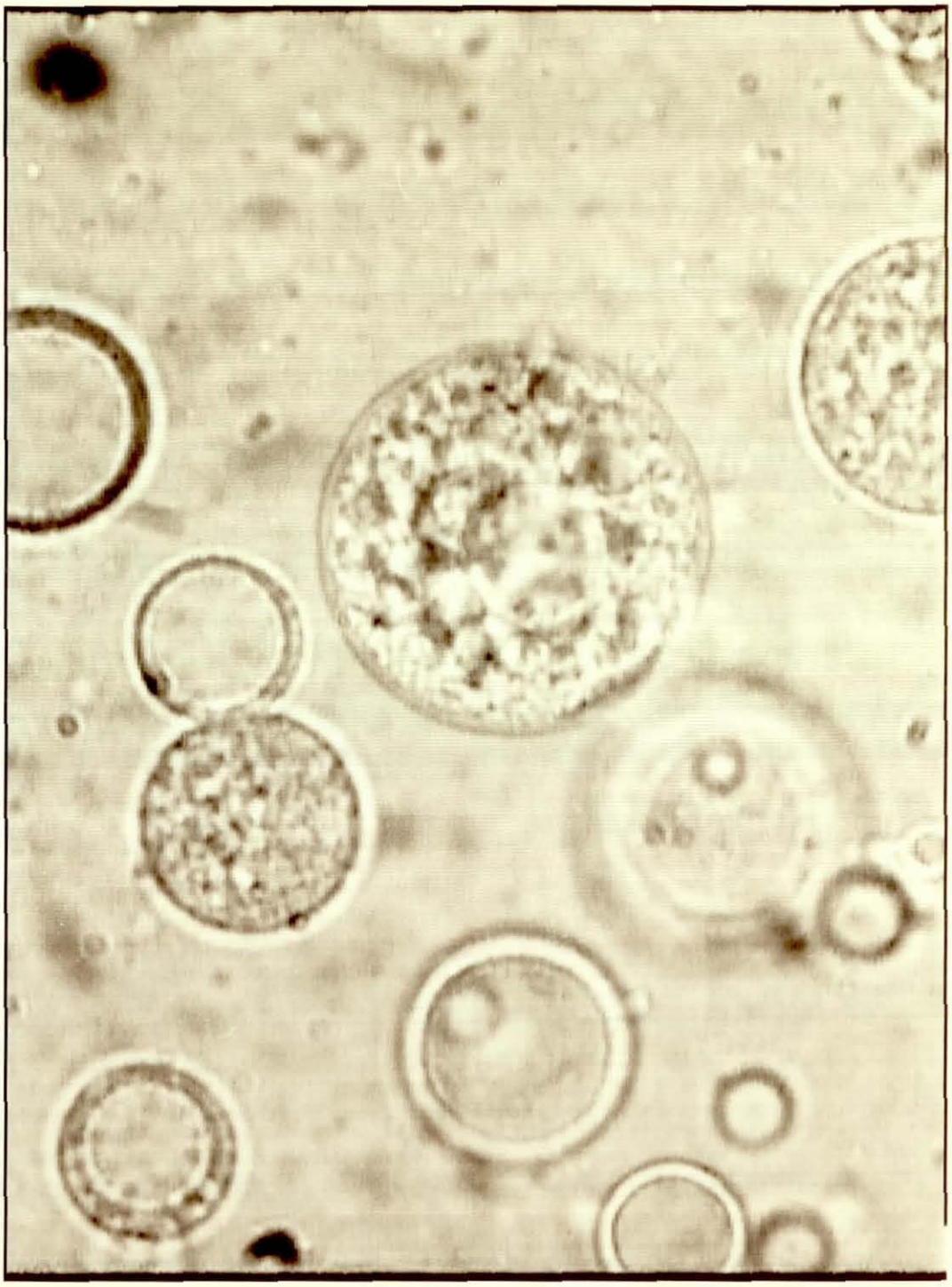

FIGURE 5.16 - Photomicrograph (x2200) of a (O+W)/M_s/O drop structure (cyclohexane/SML).

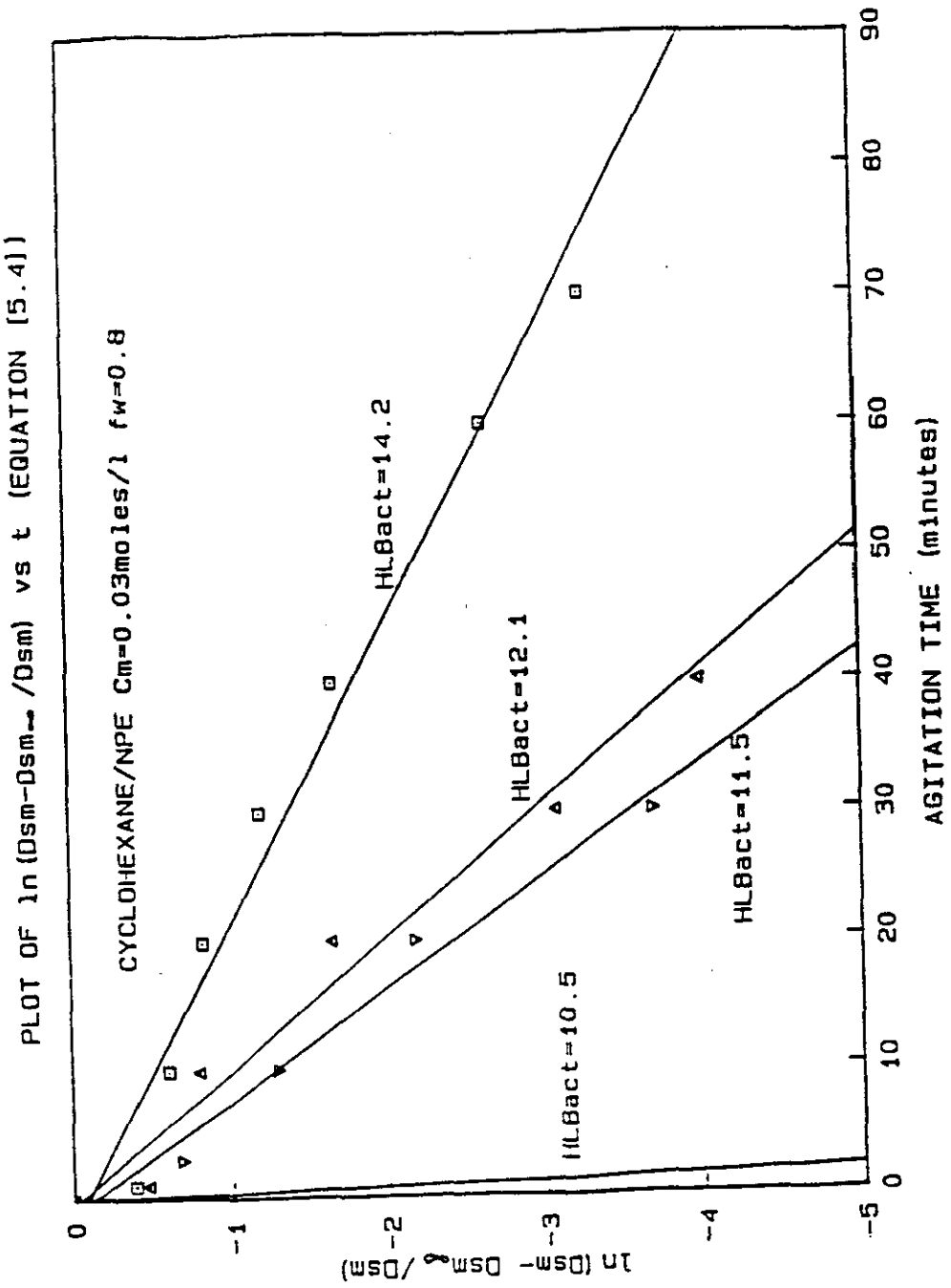

FIGURE 5.17 - Plot of $\ln[(D_{sm}-D_{sm\infty})/D_{sm}]$ vs agitation time, results of equation [5.4].

APPENDIX 6 - ACRONYMS

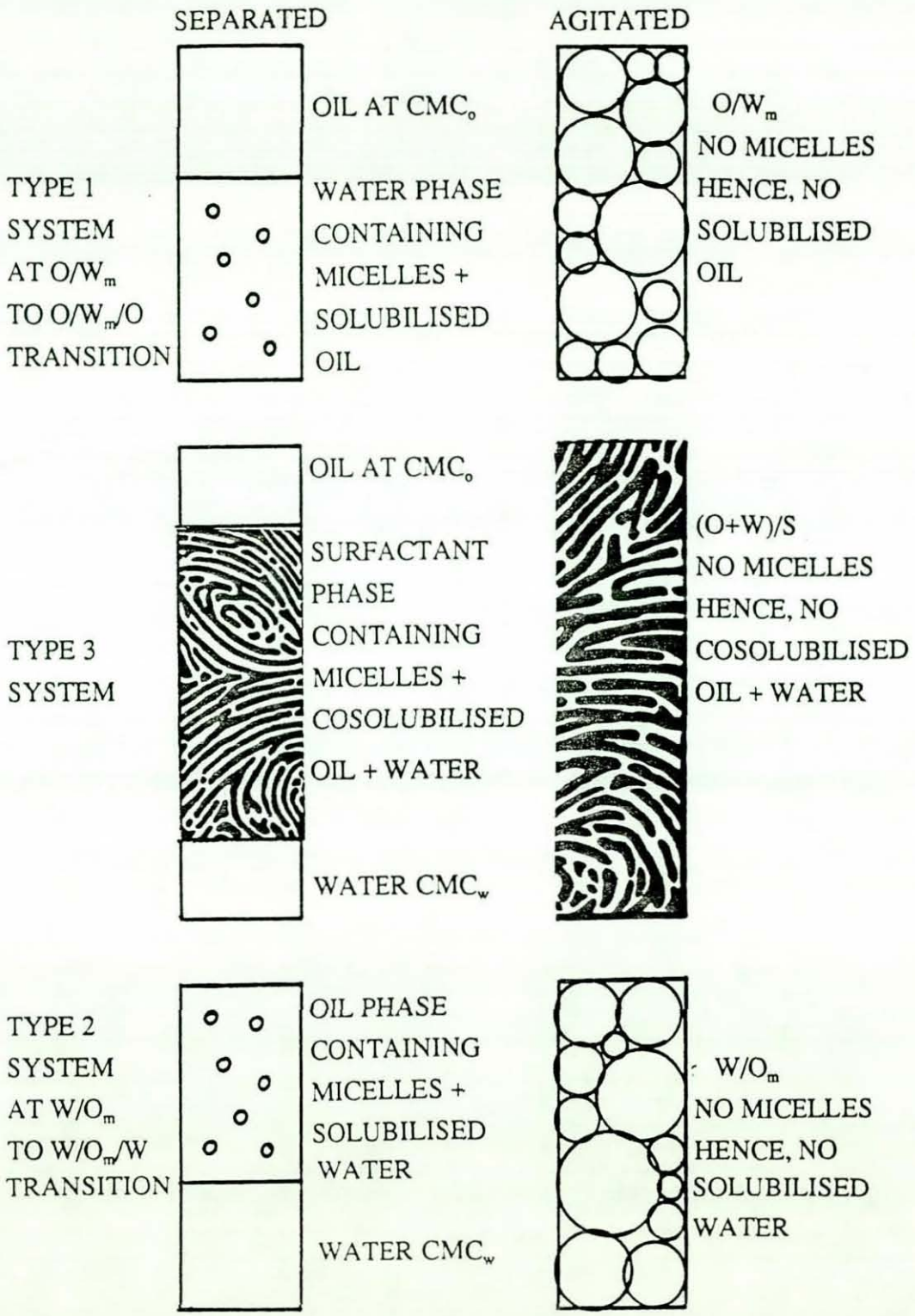

FIGURE 5.18 - Schematic representation of phase separated and emulsified nSOW systems, where in an emulsified state, the surfactant micelles are "used up" forming a monolayer at the oil-water interface.

CHAPTER 6

CATASTROPHIC INVERSION - DROP SIZE STUDIES

6.1 INTRODUCTION

This chapter is concerned with the factors affecting the drop sizes in nSOW systems before and after catastrophic inversions of the type ($W_m/O+O/W_m/O$) to O/W_m; where inversion is brought about by further addition of water to the oil phase. In this chapter, unless stated otherwise catastrophic inversion will relate mainly to inversions of this type. However, a brief study will also be made of catastrophic inversions of the type ($O_m/W+W/O_m/W$) to W/O_m.

There are a number of different drop types present at different stages of a catastrophic inversion (see chapter 2). Therefore, in order to help the reader's understanding of this chapter, the drop types studied and drop notation used, are described below:

Drops present before Catastrophic Inversion

Three drop types can be present before inversion - (i) unstable water drops containing surfactant micelles, in a continuous oil phase ie. W_m/O drops, (ii) unstable water drops containing stable oil drops and surfactant micelles, in a continuous oil phase (these will be denoted as $O/W_m/O$ drops in subsequent discussion), and (iii) stable oil drops in unstable water drops (denoted as oil drops in $O/W_m/O$ drops, in subsequent discussion).

Drops present after Catastrophic Inversion

After catastrophic inversion has taken place the resulting emulsion consists of stable oil drops in a continuous water phase containing surfactant micelles ie. O/W_m drops.

Ostwald (1910a,1910b) first modelled catastrophic inversions as being caused by the complete coalescence of the dispersed phase at a closest packed condition (corresponding to a dispersed phase fraction of 0.74 in Ostwald's uniform hard sphere model). Other studies eg. (Marszall 1975), have shown that catastrophic inversions (though these inversions were not recognised as being catastrophic inversions by the author) can occur over a wide range of f_w. It has been suggested (Becher 1966) that this may be due to the formation of double emulsion drops ($O/W_m/O$), boosting the actual volume of the dispersed phase.

Chapter 2, on dynamic inversion maps, showed how the nature of the surfactant (when the surfactant is able to stabilise the emulsion) dictates that catastrophic inversions can occur by changing f_w in one direction only, because a requirement for catastrophic inversion, is that the drops of the initial dispersed phase are unstable. Hence, the term inversion hysterisis (Becher 1966) is misleading in systems of this type. It was also

shown in Chapter 2, that catastrophic inversion boundaries on a SAD map, are affected by agitation conditions eg. stirrer speed and rate of dispersed phase addition. Changes in the position of catastrophic inversion boundaries may be due to the extent of double emulsion drop formation. For inversions $O/W_m/O$ to O/W_m, the boundaries shifted to lower values of f_w as the stirrer speed decreased and as the rate of addition of water phase decreased. Through the formation of $O/W_m/O$ drops a delayed catastrophic inversion can be brought about without changing f_w by using a sedimentation/agitation cycle, or in the case of systems containing certain NPE surfactants, even by prolonged agitation of an $O/W_m/O$ emulsion, providing there is sufficient water phase present.

There are only a few studies of dynamic factors affecting catastrophic inversions to be found in the literature. Virtually all studies have been concerned with the movement of inversion boundaries with either, changes in the systems composition, or changes in the systems dynamics. EIP studies are studies of catastrophic inversions in nSOW systems (these were reviewed in chapter 1), however, EIP studies have not been concerned with the systems dynamics. Those studies that have looked at the effect of agitation conditions on catastrophic inversion boundaries, have been concerned with oil-water systems with no surfactant present.

In the case of systems that do not contain a stabilising surfactant, inversion hysterisis has been shown to occur (Clarke 1978). The region between the hysterisis boundaries is sometimes called the "ambivalence region" (Clarke 1978). Those studies that have looked at the effect of the system's composition include: (Clarke 1978) - the effect of additives in the oil and water phases and (Selker 1965) - who noted that as the viscosity of the oil phase increased the more likely it was to become the dispersed phase. Many studies have examined the effect of stirrer speed on catastrophic inversion boundaries: (Quinn 1963), (Selker 1965) showed that inversion was shifted to higher dispersed phase fractions as stirrer speed increased, this was also noted by (Arashmid 1980) and (Guilinger 1988). In batch mode the location of the impellor can be critical (Rodger 1956), (Quinn 1963), (Selker 1965) and (Kato 1991) - generally, it was found that for a certain range of WOR, the phase in which the impellor was initially immersed became continuous. Guilinger et al (1988), examined catastrophic inversions in a continuous mixer system, they found that the height of the agitator above the vessel bottom had no affect on inversion and also, that the rate of addition of feed to the mixer had little effect on the inversion point. Catastrophic inversion in batch systems has also been found to occur on increase in agitation strength (Clarke 1978), (Rodger 1965) and (Kato 1991), hence, it has been concluded that the difference between the coalescing rates of the oil drops and those of the water drops, is the controlling factor which dominates dispersion types (Kato 1991).

Some studies (Guilinger 1988), have discussed the effects of the materials of construction of the stirred vessel on catastrophic inversion points. However, in the systems to be studied here, these effects will be negligible as surfactant will be present.

In oil-water systems with no surfactant present the formation of O/W/O and W/O/W drops may be limited (Gilchrist 1989), however, some authors have noted the presence of these drop types (Kato 1991), (Rodger 1956) in oil-water dispersions. Delayed catastrophic inversion can also occur in oil-water dispersions over a narrow range of f_w (Gilchrist 1989). During the delay time there is a rise in the drop sizes of the dispersion; the growth is controlled by the relative rates of drop break up and coalescence (Gilchrist 1989). Hence, catastrophic inversion although it may be controlled by the presence of a surfactant, is ultimately dependent on the drop types and size distribution of the emulsion. Therefore, its understanding requires a detailed knowledge of the drop sizes produced at the catastrophic inversion point and how these are related to the drop sizes prior to the inversion.

Catastrophic Inversion Drop Size Studies

Catastrophic inversion by its very nature occurs at high dispersed phase fractions. For these conditions the measurement of drop sizes is very difficult, as will be discussed in section 6.3 of this chapter. It was noted in chapter 4, that the vast majority of drop size (breakage-coalescence) studies in the literature, refer only to dispersions having very low dispersed phase fractions (in the range 0.025-0.2 see review Tavlarides 1981). Hence, as part of this catastrophic inversion study we shall attempt to see if correlations for systems of low dispersed phase fractions, can be applied to systems having a high dispersed phase fraction.

Arashmid and Jeffreys (1980), developed a model to predict catastrophic inversion points in oil-water systems. They suggested that catastrophic inversion occurs when the drop collision frequency = drop coalescence frequency; good agreement was found between result and theory. They modelled the change of drop size with dispersed phase fraction using a correlation by Thornton et al (1967). This correlation predicted a linear variation of D_{sm} with dispersed phase fraction. Arashmid and Jeffreys gave experimental results for the variation of D_{sm} with f_{disp} for a system agitated at 400rpm. They indicate that D_{sm} did vary linearly with f_{disp} upto f_{disp}=0.5, however, above this D_{sm} was shown to rise rapidly with f_{disp}. As far as the author is aware this is the only study in the literature that has tracked the change of D_{sm} with f_{disp} up to a catastrophic inversion point.

6.2 EXPERIMENTAL

All the experiments described in this chapter were carried out on the Cyclohexane/NPE system and Cyclohexane/SML system; the system components were as described in chapter 2. The oil phase viscosity was again altered by dissolving polyisobutene in the cyclohexane (for concentration - viscosity calibration see figure 5.5).

All the experiments were carried out at 25°C in a $0.75dm^{-3}$ dished bottomed glass vessel (diameter=10cm). Agitation was supplied by either a stainless steel 6 blade Rushton turbine (as described in chapter 4) with variable speed drive, or by an Ultra-Turrax rotor-stator device. In certain experiments 4 stainless steel baffles were inserted at the vessel walls, each being of standard geometry (1/10 tank diameter - see figure 4.1).

At the start of each experiment a specified concentration of a surfactant mixture (with a set HLB) was added to each of the oil and water phases, hence, the surfactant concentration was kept constant in each run. Note that as the mole average HLB values used were high (usually HLB=14), then the HLB_{act} value of the interfacial surfactant will remain reasonably constant over the entire range of f_w.

500ml volumes of nSOW were used in each run. The WOR was altered by adding aliquots (of specified volume) of dispersed phase at regular specified time intervals. An approximately constant volume of emulsion was used throughout each run; this was achieved by withdrawing a sample of emulsion equal to the volume of the aliquot of dispersed phase to be added. The sample was taken just before each dispersed phase addition and was used for drop size analysis. More detailed experimental procedures are given in each results section to follow.

6.3 MEASUREMENT OF DROP DIAMETERS

Preliminary tests showed that the sizes of the drops before and after inversion (for the range of agitation conditions used) were in the range 1 - 500 microns, hence, optical microscopy could be used to obtain drop size distribution data. As described in the introdution of this chapter, in catastrophic inversions there are 3 different drop types present through a run:

(i) stable oil drops within the water drops (present in some systems before a catastrophic inversion) ie. oil drops in $O/W_m/O$ drops,

(ii) stable oil drops in the inverted O/W_m emulsion and,

(iii) Unstable double emulsion $O/W_m/O$ drops and unstable water drops before catastrophic inversion.

The techniques developed in this study to measure each drop type outlined above are described below:

(i) and (ii), stable oil drops within $O/W_m/O$ drops (present before inversion) and in the final (inverted) O/W_m emulsion

The fact that these drop types are stable makes them easy to size. Normal microscope slide and cover slip techniques can be used to size both drop types. In the case of the oil drops within $O/W_m/O$ drops, once a sample is placed between a slide and cover slip, the large $O/W_m/O$ drops will spread out and coalesce ie. the sample will invert to an O/W_m emulsion. Therefore, the unstable $O/W_m/O$ drops disappear leaving the stable oil drops from within the $O/W_m/O$ drops. Note it is recognised that the coalescence of the $O/W_m/O$ drops on the slide may produce new oil drops from oil trapped inbetween the coalescing drops. However, with choice of a nSOW system in which the water drops contain a large number of oil drops, then using drop counting methods, these slide produced oil drops will then be small in number and hence, they will be statistically insignificant.

All information observed on each slide was stored on video tape and hard copies were taken from this to produce drop size distributions for each sample. At least 300 drops/distribution were measured, the accuracy of the distribution was checked as described in chapter 5.

(iii) Unstable Water and Unstable $O/W_m/O$ Drops Present Before Inversion

There are two main problems in sizing drops of this type:

(a) In chapter 2, it was shown that in true catastrophic inversions, the drops present before inversion are unstable. It is because of this that normal microscope slide and cover slip techniques cannot be used, as the $O/W_m/O$ drops rapidly coalesce if agitation is removed.

(b) Catastrophic inversion usually occurs at high dispersed phase fractions; there are great difficulties in sizing drops in a closest packed situation due to overlap of drops in different layers and even when slide and cover slip techniques can be used, a sample often has to be diluted first.

Previous photographic techniques for sizing unstable drops in dispersions can be divided broadly into two groups: (a) Insitu measurement, and (b) Sample withdrawal measurement. Techniques in group (b) involve either the addition of surfactant to stabilise the dispersion eg. Shinnar (1961), or encapsulating the drops of a sample by interfacial polymerisation (Mlynek 1972). Phase inversion is extremely dependent on nSOW phase behaviour, hence, techniques of this sort involving addition of surfactants are inappropriate for this study.

Insitu measurements have been made using photographs taken either, through a window in the tank wall - Chen (1967), Collins (1970), Keey (1969), Rodger (1956), Schindler (1968) and Gilchrist (1989), (note these studies are limited to looking at drops very close to the tank wall), or by using a microscope probe built into the vessel - Mlynek (1972), Hong (1983), Coulaloglou (1976) and Park (1975). Various refinements have been made by researchers so that their probes can be used to investigate drop sizes in different regions of the stirred vessel. In insitu studies of this sort, illumination is usually supplied by a flash lamp placed in the vessel close to the probe tip (or vessel wall); the short duration flash (1-100 μs) is used to "freeze" the motion of the drops passing in the region between the probe and lamp.

Insitu techniques have the advantage that all measurements of the dispersion are made under the actual dynamic conditions.

Developing a photomicrographic technique to measure unstable $O/W_m/O$ drops (present before a catastrophic inversion) has complexities in addition to those present in normal dispersion drop size studies:

(i) In dispersion studies where insitu probes have been used the disperse phase fraction is very low (generally <0.2), however, in catastrophic inversion studies the sizing technique must function at dispersed phase fractions >0.7.

(ii) $O/W_m/O$ drops disperse light to a much greater extent than drops of one phase.

(iii) Previous studies using insitu measurement techniques have been used to size drops of the order of 1mm; as will be seen the $O/W_m/O$ drops in this study are much smaller than this.

The effects, these added difficulties have, on developing a photomicrographic technique to size $O/W_m/O$ drops, became apparent when attempts were made to use an optical probe. A schematic diagram of the probe initially designed in this study is shown in figure 6.1. The essential features in the design of the probe are:

(a) A protective lens cap which could be adjusted so that the plane of focus of the objective lens was directly in front of the cap's cover slip glass. This feature eliminated distortion of the image caused by drops moving between the lens and its plane of focus.

(b) To improve the "quality" of the light source a condenser lens was fitted in the lamp housing section of the probe.

(c) The gap y between the cover slip and glass slide (available for flow of emulsion through the probe) was adjustable.

In initial trials the probe was found to work well at low dispersed phase fractions, however, as the dispersed phase fraction increased the quality of the image was reduced and also the brightness of the image was reduced. Apart from some adjustments that could be made to the camera and light source, the only way to resolve these problems was to reduce the gap y. At very high dispersed phase fractions the gap y had to be reduced so much that the flow of emulsion through y was severly restricted, so much so that the hydrodynamics of the observed emulsion could not be representative of the hydrodynamics of the tank - the motion of the drops through y was so slow that drop coalescence could not be prevented. When the system was close to a closest packed condition, no image could be obtained even when the gap was reduced to a minimum.

Improvement of the probe to be able to observe the drops at high dispersed phase fraction, with a sufficient gap y to allow flow of material through the probe, could possibly be achieved by improving the optics and light source of the probe. This would mean the virtual construction of a high quality bench microscope within the tank, which was not feasible. It was decided to use a sample withdrawal method to observe the $O/W_m/O$ drops using a flow cell mounted on a bench microscope as described below:

Sample Withdrawal Flow Cell Arrangement

The arrangement used is shown schematically on figure 6.2. It consisted of a video camera attached to an Olympus BH2 microscope which had a high power (100 Watt) light source, a glass/brass flow cell (figure 6.2(b)), a 50ml glass syringe and polyethylene connecting pipes. The connection of the sample collection tube to the stirred vessel was so arranged that the point in the stirred vessel where the sample was withdrawn was adjustable. Note previous studies (Nagata 1975) have shown that the drop size distribution of samples taken at different heights in a stirred tank can vary greatly. However, a detailed study of the effect of sample position was not made in this study and therefore, the sample position was kept constant in each run. In all experiments the sample position used was - vertically, half the emulsion height (0.5H) and horizontally one quarter tank diameter distance in from the tank wall (note, a constant emulsion volume was used in all of the experiments of this chapter, hence, the sampling position was always constant with respect to the agitator).

The microscope was focussed on a plane just below the cover slip. The flow cell consisted of (see figure 6.2(b)) a brass body attached to a normal microscope slide, a central circular block with a cover slip attached at its centre and inlet and outlet tubes. The central block screwed (on a fine thread) into the body of the cell, hence, the gap y between the cover slip and slide glass was adjustable. After a few test runs an optimum

gap y was found that allowed free flow of sample through the cell, but was not too large to prevent a good image being obtained when emulsions of high dispersed phase fraction were sampled.

In order to achieve the high illumination required when the emulsion's dispersed phase fraction was large, a continuous light source was employed. Therefore, the shutter speed of the camera (1/1000 s) was relied upon to "freeze" the motion of the drops through the cell.

The use of a sample withdrawal technique was easily incorporated into the experimental technique used for adjusting f_w: Before each aliquot of dispersed phase was added to the stirred vessel, a sample equal to the volume of the aliquot was withdrawn through the sample cell using the syringe. The withdrawn sample volume was measured using the syringe.

To reduce the risk of coalescence altering the size distribution of a sample, during its flow time through the collector pipe, the sample was withdrawn as quickly as possible. NOTE: It is impossible to compare precisely the levels of turbulence developed in the collector pipe to that developed in the stirred tank. Turbulence levels are usually measured by Reynold's number; if we calculate the Reynold's number for the flow through the collector tube at maximum possible throughput that could be achieved using the experimental set up and compare this with a stirred tank Reynold's number, then the turbulence level in the collector pipe is approximately equivalent to a stirrer speed of 600rpm in the stirred vessel used. Tank Reynold's number and pipe Reynold's number are not strictly interchangeable as a measure of turbulence and it should be remembered that turbulence is far from uniform throughout a stirred vessel. However, the calculation does show that the order of turbulence developed in the collector pipe is the same as that developed in the stirred vessel. In chapter 4, it was shown that at the levels of turbulence developed in the stirred vessel, long periods of agitation time are required for drop break up to greatly affect the drop sizes of an emulsion. The residence time of a sample in the collector tube is short (<0.5 s), hence, with the sample withdrawal technique used, drop breakage in the collector tube will be negligible.

However, at the maximum rate that a sample could be withdrawn through the cell, the motion of the drops could not be "frozen" by the camera's 1/1000 s shutter speed. The fact that the syringe plunger was manually operated, meant that a pulse motion to the sample flow could be induced so that the sample was removed quickly (to move it to the observation point), then its motion was slowed (for the camera to obtain distinct images) and then its flow was increased again. A pulse could be induced for every 10ml of sample (10 ml = approximate volume of the collector tube and sample cell). The

slowing of the sample's flow increased the risk of coalescence (providing an environment similar to a stagnant region of a stirred tank), however, with choice of the right system to study (see part 6.4 of this chapter) this risk was small if the drops are still in motion.

The video camera signal was stored on video tape, hard copies of stills were taken from the tape and these were used to produce drop size distribution results for each sample. At least 300 drops/distribution were measured to produce a statistically accurate size distribution (see chapter 5). The use of frame by frame advance on the video recorder enabled selection of frames to be made for the hard copies. To again minimise the risk of coalescence altering the size distribution of a sample, hard copies were taken of frames from the slowing down part of a pulse, as soon as the flow was slow enough for the camera to produce distinct clear images.

This sample withdrawal method has the disadvantage that the drops in the sample are in a completely different hydrodynamic state to that of the actual emulsion. However, it does offer the advantage over some other sizing techniques in that the drop sizes at any point in the vessel can be examined. Although drop breakage may not be significant during the emulsion sample's transit from the tank to the observation point, droplet coalescence may take place, if the emulsion's dispersed phase fraction is large, especially when the flow through the cell is slowed down. However, in certain nSOW systems coalescence is more likely than in others, hence, the choice of system to study becomes important (see section 6.4 of this chapter).

6.4 CHOICE OF SYSTEMS

It is obvious from the proceeding section that certain nSOW systems are more appropriate for studying each of the different drop types present during a catasrophic inversion run.

(i) Inverted O/W_m Emulsion Studies

The final inverted O/W_m emulsion is stable, hence, these drops can easily be measured whichever system is used and therefore, we are not restricted in our system choice.

(ii) Oil Drops Within $O/W_m/O$

To study these drops, it is necessary to choose a system which produces a large number of oil drops within the water drops, to allow for inaccuracies in the drop sizing technique (and also so that there are enough oil drops to study). As was seen in chapter 2, generally systems containing NPE surfactants invert at much lower values of f_w to systems containing SML surfactants. This is because very densely packed $O/W_m/O$ drops are formed in NPE systems. Therefore, the cyclohexane/NPE12 (HLB=14.2) system was chosen for this part of the study. Note, the purpose of this study is to determine the

mechanism(s) of formation of the oil drops within water drops and to examine the effect of dynamic variables. The results of the cyclohexane/NPE12 system are expected to apply to oil drops within $O/W_m/O$ drops in all nSOW systems.

(iii) $O/W_m/O$ Drops

To study these drops we should choose a system in which drop coalescence rates are relatively low, so that the sample withdrawal method to be used, will not lead to large errors. Again it is expected that the results of this part of the study will apply to $O/W_m/O$ drops present before catastrophic inversion in all nSOW systems.

Photomicrographs taken using the sample withdrawal method, of the cyclohexane/NPE and cyclohexane/SML system with low and high dispersed phase fractions respectively, are shown in figure 6.3. As can be seen from figure 6.3, the $O/W_m/O$ drops of the NPE system disperse the transmitted light (the drops appearing black) compared to those in the SML system. It was found that the $O/W_m/O$ drops of the NPE system are densely packed with oil drops. The large number of oil drops within the $O/W_m/O$ drops in this system, suggests that coalescence rates are very high in NPE systems (see Discussion, part 6.6 of this chapter) and therefore, NPE systems are inappropriate for studying $O/W_m/O$ drops by the sample withdrawal method. Note: At slightly higher values of f_w to that of the NPE system of figure 6.3, very large drops (>3mm) pass through the sample cell; it is impossible to say if these large drops are present in the stirred vessel or are a product of the sizing technique.

It was seen in chapter 2 that catastrophic inversions in the cyclohexane/SML (HLB=14) system did not take place until f_w=0.8; this suggests that coalescing rates before catastrophic inversion in this system are comparitively low. Preliminary tests watching a video taken of the motion of the drops through the sample cell frame by frame, showed that, even when f_w was high (>0.7), coalescence was almost unseen unless the flow of the drops was very low (slower than that required by the camera) or nonexistant. For this system the number of oil drops within the $O/W_m/O$ drops is also comparitively low, which aids light availability at high dispersed phase fractions. Therefore, the Cyclohexane/SML (HLB=14) system, is a convenient system to study $O/W_m/O$ drops, present before a catastrophic inversion.

6.5 RESULTS
CYCLOHEXANE/NPE12 2wt% HLB=14.2 SYSTEM

6.5.1 The Events Occuring and, Changes in the Drop Size Distribution of the Oil Drops Present Before and After Catastrophic Inversions

600 ml of cyclohexane containing 2 wt% of Igepal Co720 (note that the surfactant was not dissolved/dispersed completely in the cyclohexane first) was agitated in a glass vessel (described in section 4.3). A stirrer speed of 600 rpm was used and 4 baffles were fitted in the tank. f_w was altered by adding water containing 2 wt% of Igepal Co720, in 20ml aliquots at 2 minute intervals (20 ml of emulsion were removed before each addition and used for drop size analysis). The diameters of the oil drops within the $O/W_m/O$ drops present before catastrophic inversion were measured as described in section 6.3. After catastrophic inversion had taken place the resulting emulsion was agitated further until a stable drop size distribution was achieved.

Inversion Events and Description

Photomicrographs taken at different stages of the inversion run are shown in figure 6.4.

In the early stages of a run at low f_w (=0.03), there were only a few oil drops present within the water drops together with a gel-like substance. A photomicrograph of the gel is shown in figure 6.4(a). As f_w increased this gel gradually disappeared, which coincided with the appearance of small (1 μm) oil drops. These are shown in figure 6.4(b) together with much larger oil drops formed at higher f_w. Figure 6.4(c) is a photomicrograph of the oil drops within $O/W_m/O$ drops just prior to inversion and figure 6.4(d), shows the oil drops present at the catastrophic inversion point (O/W_m emulsion). Note that figure 6.4(c) is similar to figure 6.4(d), however, there are a few larger drops in figure 6.4(d), that were formed at the catastrophic inversion point.

The changes in the drop size distribution of the oil drops within the water drops at different values of f_w are shown in figure 6.5. The drop size distribution of the inverted O/W_m emulsion at the catastrophic inversion point and after further agitation for 1 hour is also shown. Full drop size distribution data is tabulated in table A5.1 of Appendix 5.

Figure 6.5 shows that at low f_w (=0.07) the size distribution of the oil drops in the $O/W_m/O$ drops is reasonably narrow (1 to 55 μm) and has a pronounced peak at 2 μm. At f_w=0.24 the size distribution is bimodal - there is still a large peak at 2 μm and there is now a second peak at 5 μm. The distribution is also wider (1 to 80 μm). At the catastrophic inversion point the distribution is still bimodal with peaks at 2 μm and 5 μm, however, the distribution is much wider 1 to 250 μm. After 20 minutes further agitation, the inverted O/W_m emulsion's size distribution is trimodal and the large oil

drops formed at the catastrophic inversion point have been broken up. When a stable drop size distribution is achieved (after 1 hours further agitation after inversion), the distribution is once again bimodal, with peaks at 2 μm and 5 μm. However, the 5 μm peak is much larger, hence, it appears that the size distribution peak caused by further agitation coincides with the secondary peak first seen at f_w=0.24. Table A5.1 of Appendix 5 gives size distribution data at intermediate values of f_w to those shown in figure 6.5. From table A5.1 it can be seen that the width of the size distribution of the oil drops in the $O/W_m/O$ drops increases and also the proportion of the larger drops increases as f_w increases.

6.5.2 Effect of Stirrer Speed on the Size Distribution of Inverted O/W_m Emulsions

Similar experiments to that described in 6.5.1 were carried out on the Cyclohexane/NPE12 system at stirrer speeds of 400 rpm and 800 rpm. The size distribution results of the inverted O/W_m emulsion at each stirrer speed are tabulated in table A5.2 of Appendix 5 and plotted on Figure 6.6. Note in the experiment at 800 rpm, time was allowed for the surfactant to disperse uniformly in the oil and water phases. Table A5.3 of appendix 5 gives the drop size distribution data of the inverted O/W_m emulsion after 1 hours direct emulsification - after which a stable drop diameter was achieved. The data at 400 rpm, 600 rpm and 800 rpm are plotted on Figure 6.7.

Figure 6.6 shows that at the catastrophic inversion point the size distribution of the O/W_m emulsion formed is very wide at each stirrer speed (at least 1000 drops were measured here because the distribution was so wide). At 400 rpm the inverted emulsion's drop size distribution is trimodal (peaks at 2, 7 and 25 μm). The distribution at 600 rpm was described above. The drop size distribution at 800 rpm is bimodal - peaks at 2 and 26 μm. It was noted that the surfactant was dispersed uniformly in the oil phase in the 800 rpm experiment, this had the result that much less gel phase was seen in the early stages of this run compared to the experiments at 600 rpm and 400 rpm.

If we compare the size distributions of the O/W_m emulsion after 1 hour of direct emulsification (figure 6.7) with figure 6.6, it can be seen that in the 400 rpm and 600 rpm experiments, the shape and position of the peaks in the direct emulsification case correspond with the first and second peak of the inverted emulsion's distribution. In the 800 rpm experiment, the further agitation peak corresponds to the first peak of the inverted emulsion's distribution.

Cumulative Distributions

In table 6.1 the drop size data of Table A5.2 for O/W_m emulsions produced at the catastrophic inversion point, is recalculated to give a cumulative distribution.

Table 6.1 - Cumulative Distribution Data

$(D_i+D_{i+1})/2$ (micron)	400rpm f_w=0.39 Cumalative Vol.>interval %	600rpm f_w=0.36 Cumulative Vol.>interval %	800rpm f_w=0.39 Cumulative Vol.>interval %
1.08	100.0	100.0	100.0
1.65	100.0	100.0	100.0
2.50	100.0	100.0	100.0
3.75	100.0	100.0	100.0
5.50	100.0	100.0	99.9
8.00	99.9	99.9	99.9
11.75	99.8	99.7	99.7
17.00	99.7	99.4	99.0
25.00	98.8	98.5	95.2
37.50	96.2	95.7	86.0
55.00	91.4	90.4	73.8
77.50	81.3	76.3	53.7
110.00	58.8	59.8	19.8
157.50	40.0	39.0	0.0
222.50	0.0	0.0	0.0

Although nearly 80% of the drops of the inverted emulsion are < 17 μm in size (see table A5.2), table 6.1 shows that these drops account for <1% of the dispersed phase volume. The D_{sm} of an inverted emulsion is therefore, dependent only on the large drops of the tail of the distribution. Hence, in the experimental results to follow, the obtaining of an overall size distribution for inverted emulsions was not attempted - only the large drops (>10 μm) of the distribution tail were measured.

Variation of Sauter Mean Diameter (D_{ow}) with Stirrer Speed - Direct Emulsification Comparison

Catastrophic inversions were performed at 400 rpm, 500 rpm, 600 rpm ,700 rpm and 800 rpm in the baffled glass vessel, with a rate of water addition of 20 ml/2 min. Full

drop size distribution data for the inverted emulsion at the inversion point and after 1 hour of direct emulsification is given in Table A5.3 of Appendix 5 and Table A5.4 of Appendix 5 respectively. D_{sm} for each condition was calculated from the distribution data.

Figure 6.8 is a plot of D_{ow} vs N (where, N = stirrer speed) for both sets of data. The slope of both of the lines on figure 6.8 is -1.2, hence, each set of data could be correlated by $D_{ow} \propto N^{-1.2}$.

6.5.3 Effect of Water Rate of Addition

Similar experiments to those described in part 6.5.1 of this section were also performed on the cyclohexane/NPE12 system, however, for these experiments the stirrer speed was kept constant (600 rpm) and the rate of water addition was varied. The drop size distribution results of the O/W_m emulsion formed at the inversion point at each addition rate are tabulated in Table 6.2 below:

Table 6.2 - Rate of Addition Results

$(D_i+D_{i+1})/2$ (microns)	FREQ % 20ml/1min f_w=0.39	FREQ % 20ml/2min f_w=0.36	FREQ % 20ml/5min f_w=0.31
14.0	23.6	29.1	28.3
18.5	17.3	15.7	20.3
24.5	16.2	18.1	18.9
33.0	14.4	11.0	13.3
44.5	8.1	6.2	10.4
60.0	7.4	8.6	4.0
81.0	7.4	7.1	1.6
110.0	4.8	3.6	2.1
149.5	0.7	0.3	0.8
202.5	0.0	0.3	0.3
274.0	0.0	0.0	0.0
D_{sm} (microns)	72	74	77

6.6 POLYISOBUTENE-CYCLOHEXANE/SML 2wt% HLB=14 SYSTEM

General Comments

In this section the results of catastrophic inversion studies on several polyisobutene - Cyclohexane/SML systems (differing in oil phase viscosity) are presented. The study of each system will be presented separately, however, there are some general observations which refer to the results of this section as a whole:

In chapter 2 catastrophic inversions were shown to occur at a specific point on a boundary (for set agitation conditions). However, it was found when using high volumes of emulsion, as in this part of the study, that (for each set of agitation conditions) catastrophic inversions could take place over a range of f_w, rather than at a specific value. Generally, it was found for the systems studied here, that catastrophic inversion point could vary by up to two aliquot additions between experiments which had the same agitation conditions. It was also found that the range was wider at lower stirrer speeds and that its width reduced as the oil phase viscosity increased.

The maximum oil phase viscosity that could be examined was set by the mixing tank performance. Upto an oil phase viscosity (the original continuous phase) of 2 poise, reasonably complete mixing throughout the tank was achieved at all stirrer speeds. However, at oil phase viscosities above this, a stagnant region of oil phase remained above the mixed zone. Therefore, systems of oil phase > 2 poise were not examined in detail. It was also found at high oil phase viscosities that the presence of baffles in the tank caused stagnant regions to form at the tank walls. Therefore, baffles were not fitted to the tank in most of the experiments to follow, so that comparisons between experiments could be made. NOTE: In chapter 4 it was shown that the vast majority of studies to be found in the literature, examined low viscosity systems in baffled vessels. In order to make direct comparisons with these studies, in the case of the Cyclohexane/SML (0.007 poise) system, baffles were fitted to the tank.

The effect of the oil phase viscosity on the value of f_w at the catastrophic inversion point is shown on figure 6.9 (agitation conditions: 800 rpm, rate of addition 20 ml/2 min) - the labels on figure 6.9 will be addressed in the discussion of this chapter. Note, similar graphs to figure 6.9 could be drawn for each set of experimental conditions.

Photomicrographs

Apart from altering the f_w at the catastrophic inversion point, rising oil phase viscosity also produced different drop types prior to inversion and also, differences in the catastrophic inversion mechanism were found.

Photomicrographic evidence of these differences is shown in figures 6.10, 6.11 and 6.12. Figure 6.10 shows the difference in the $O/W_m/O$ drop structure (before inversion) found in a low viscosity system (0.25 poise - figure 6.10(a)) and a high viscosity system (1.0 poise - figure 6.10(b)). Note at low oil phase viscosity the oil drops within the $O/W_m/O$ drops are small and each oil drop takes up only a small fraction of the volume of the $O/W_m/O$ drop. However, in the high viscosity system, the oil drops within the $O/W_m/O$ drops are larger and can take up virtually all of the $O/W_m/O$ drop volume with one single drop.

Figure 6.11 shows the state of a 0.25 poise oil viscosity system one aliquot addition away from a catastrophic inversion ie. the system is near to a "closest packed" condition. Figure 6.11 shows the system is reasonably close packed despite f_w=0.5 at the catastrophic inversion point.

It was found that in the case of the low viscosity systems, after catastrophic inversion had taken place, that the resulting emulsion consisted almost entirely of oil drops in water. However, in the case of high viscosity systems catastrophic inversion was slow; the emulsion gradually inverted with prolonged stirring. The start of catastrophic inversion in high oil phase viscosity systems was detected by violent fluctuations in electrical conductivity and by signs of foaming as the water phase became continuous. After catastrophic inversion had started to take place, large regions of the inverting emulsion remained oil continuous. Figure 6.12 shows the structure of an inverting emulsion for an oil phase viscosity of 2 poise. The light areas of figure 6.12 are oil phase and the dark areas are O/W_m emulsion. Note that the largest oil drop in figure 6.12 is approximately 3 mm in diameter and that the large oil drops contain $O/W_m/O$ drops. Hence, this emulsion structure could be written as $O/W_m/O/W_m$. After prolonged agitation (>1/2 hour), the inverted emulsion shown in figure 6.12 broke down into an O/W_m emulsion.

6.6.2 DROP SIZE STUDIES

(i) Cyclohexane/SML system - oil phase viscosity = 0.007 poise

In the experiments carried out on this system, the vessel (described in chapter 4), was fitted with 4 stainless steel baffles. The rate of addition of water phase was kept constant in each run (40ml/2min) and the effect of agitator speed on the drop sizes before and after catastrophic inversion was examined. Stirrer speeds of 400rpm, 500rpm, 700rpm and 800rpm were used and also, in one experiment agitation was supplied by an Ultra-Turrax (5000rpm) dispersing tool. Full drop size data is tabulated in Table A5.5 and A5.6 of Appendix 5. D_{sm} values were calculated from the size distribution data. For

conditions before catastrophic inversion $O/W_m/O$ D_{sm} values (D_{owo}) for each agitation condition are plotted against f_w on figure 6.13. D_{ow} (the D_{sm} of the oil drops of the inverted O/W_m emulsion) vs N data for the inverted O/W_m emulsion is plotted on figure 6.14.

Correlations - Turbine Agitator

The D_{owo} vs f_w data for the $O/W_m/O$ drops present before the catastrophic inversion fitted very well with the correlation below (the lines shown on figure 6.13 are the correlation's prediction):

$$D_{owo} = 0.1.N^{-1.2}.e^{(8/3.fw)} \quad \text{[6.1]}$$

From figure 6.14 it can be seen that the D_{ow} vs N data for the O/W_m emulsion formed at the catastrophic inversion point, conform to the following relationship:

$$D_{ow} \propto N^{-1.2}$$

Ultra-Turrax (HIGH INTENSITY AGITATOR - ROTOR-STATOR DEVICE)

When agitation was supplied by an Ultra-Turrax, a linear relationship was obtained between D_{owo} and f_w. Hence, for these conditions $D_{owo}=D^0_{owo}(1+11f_w)$. The D_{ow} calculated for the inverted O/W_m emulsion from the distribution data of Table A5.6.2 was 13 μm.

(ii) Polyisobutene - Cyclohexane/SML systems (higher oil phase viscosity systems)

In these experiments the unbaffled tank set up was used (note earlier comments). Catastrophic inversions were carried out on the system using oil phase viscosities of 0.25 poise, 0.5 poise, 1.0 poise and 2 poise. The rate of addition was kept constant in each experiment at 20 ml/2 min. Again the effect of agitation conditions on the drop sizes present before and after catastrophic inversion was examined. Stirrer speeds of 400 rpm, 500 rpm, 600 rpm and 800 rpm were used and in one experiment, agitation was supplied by an Ultra-Turrax (5000 rpm). Full drop size distribution data is given in Tables A5.7 to A5.15 of Appendix 5. Figures 6.15 to 6.18 are plots of D_{owo} vs f_w at each oil phase viscosity (see note [1] below). D_{ow} vs N data for the O/W_m emulsions formed at the inversion points, at each oil phase viscosity, are plotted on figure 6.14 (see note [2] below). For oil phase viscosity 0.25 poise, the change in the drop size distribution of the $O/W_m/O$ emulsions with f_w, at three different stirrer speeds is shown on figure 6.19. For conditions of constant stirrer speed (500 rpm), the change in the drop size distribution of $O/W_m/O$ emulsions with f_w, for three different oil phase viscosities is shown on figure 6.20.

NOTES

[1] Although the change in D_{owo} with f_w is used, it should be noted that for the systems in this part of the study, f_w is no way a true measurement of the actual dispersed phase fraction (f_{disp}) because a large amount of oil becomes "emulsified" within the $O/W_m/O$ drops. From the video studies, it becomes apparent that the amount of oil within the $O/W_m/O$ drops rises as the oil phase viscosity rises (see photomicrographs of figure 6.10). Hence, at oil phase viscosity 0.25 poise, where catastrophic inversion takes place at a fairly high f_w (0.55), f_w will be a reasonably accurate reflection of f_{disp}, however, for the 2 poise results this will not be so.

[2] It was shown in figure 6.12, that the oil drops formed at the catastrophic inversion point in the 2 poise system are very large (3 mm) compared to those formed in lower viscosity systems. In the case of the 2 poise system the drop size distribution of the inverted emulsion will be very wide and the D_{sm} value of the distribution will be very heavily influenced by the large drops. This makes fixing an accurate D_{sm} value for the inverted emulsion nearly impossible (also, the D_{sm} will be fairly meaningless in describing the sizes of the majority of the drops in the emulsion), hence, the values for the 2 poise system shown in table A5.14 and on figure 6.14 are imprecise and should not be used as "hard data" for use in calculations. The O/W_m drop sizing problem is not confined to the 2 poise system, it was found that as the oil phase viscosity increased and subsequently, the f_w at the catastrophic inversion point decreased, that the sizing problem became progressively worse. However, D_{ow} could be calculated with reasonable accuracy even for the 1 poise system.

Correlations - Turbine Agitator

For the catastrophic inversion experiments with oil phase viscosities of 0.5 poise, 1 poise and 2 poise it is impossible to present the results for the $O/W_m/O$ drops in terms of Weber Number correlations because f_{disp} is not known as discussed above. However, in the case of the 0.25 poise system, f_w may be reasonably close to the actual f_{disp} value. The experimental results were found to fit very well with the following correlation(the lines on figure 6.15 are the correlation results):

$$D_{owo} = 0.008.N^{-0.8}.e^{(5/2.fw)} \qquad [6.2]$$

O/W_m Drops at the Catastrophic Inversion Point

The value of D_{ow} increased with rise in the oil phase viscosity, for all N. The variation of D_{ow} with N determined from figure 6.14 for each viscosity examined is shown in Table 6.3 below:

Table 6.3 - $D_{ow} \propto N^y$ results

Oil Phase Viscosity (poise)	y
0.007	-1.2
0.25	-0.8
0.50	-0.8
1.00	-0.8
2.00	-0.8

N.B. Note the above comments on the accuracy of the 2 poise results and also, that in the case of high oil phase viscosity systems, that the inverted emulsion may not break down to a simple O/W_m emulsion.

Ultra-Turrax

In the case of the 0.25 poise system, a linear relationship between D_{owo} and f_w was obtained (similar to that found in the 0.007 poise system) when agitation was supplied by an Ultra-Turrax. Hence, for these conditions $D_{owo} = D^0_{owo}(1+6f_w)$. At higher oil phase viscosities, a linear relationship between D_{owo} and f_w was not obtained; this may be due to the fact that for these systems $f_w \neq f_{disp}$.

The D_{ow} values calculated for the inverted O/W_m emulsions also increased with rise in oil phase viscosity; the values are shown in table 6.4 below. For comparison the results of direct emulsifications (5 mins agitation time) on the systems ($f_w=f_{winv}$) under the same agitation conditions are also shown:

Table 6.4 - Ultra-Turrax D_{ow} Results - 5000 rpm, rate of addition 20ml/2min.

Oil Phase Viscosity (poise)	f_w at inversion point	Cat. Inversion Point D_{ow} (microns)	Direct Emul. (5 min) D_{ow} (microns)
0.007	0.75	13	2.6
0.50	0.52	60	3.0
1.00	0.39	64	3.8
2.00	0.18	99	4.2

6.6.3 The Relationship Between the $O/W_m/O$ Emulsion Drop Sizes Present Just Before The Catastrophic Inversion, With The O/W_m Emulsion Drop Sizes Formed at the Catastrophic Inversion Point.

Figure 6.13 and Figures 6.15 to 6.18 were used to determine the $O/W_m/O$ drop size D_{sm} (D_{owo}) at the catastrophic inversion point for each experiment in this section. These were then plotted against its corresponding D_{ow} result (determined from figure 6.14), for the O/W_m emulsion formed at the catastrophic inversion point, to obtain figure 6.21.

It can be seen from figure 6.21 that for all the systems studied (constant oil phase viscosity), a linear relationship between D_{owo} and D_{ow} was obtained. The relationship between agitation conditions, oil phase viscosity and drop sizes at the catastrophic inversion point, is very clearly shown by figure 6.21.

6.6.4 DIRECT EMULSIFICATION COMPARISON - Turbine Agitated Systems

A separate study was made using the Cyclohexane/SML 0.007 poise system, to find the time required to achieve a stable drop size using direct emulsification. To directly compare direct emulsification results with the catastrophic inversion results obtained for this system, a dispersed phase fraction of 0.3 (f_w=0.7) was used (catastrophic inversion occured at approximately f_w=0.7 in this system). Direct emulsifications were performed using a vessel fitted with baffles, at stirrer speeds of 400 rpm, 500 rpm, 600 rpm and 800 rpm. Samples were taken at regular time intervals and drop size distributions for the samples determined. All the drop size data is tabulated in table A5.16 of Appendix 5. A plot of D_{ow} vs N for the stable D_{sm} results is shown on figure 6.14.

Systems of Higher Oil Phase Viscosity

To investigate the effect of direct emulsification when the oil phase viscosity was 1 poise and 2 poise, at the end of each catastrophic inversion run, the resulting inverted

O/W_m emulsion was kept under agitation for a further 1.5 hours. It was found that it was impossible to determine an accurate size distribution for the system after this period of agitation because large differences were found between the drop sizes in different samples of the same emulsion. This indicates that mixing throughout the tank was not homogeneous. However, a large reduction was found in the drop sizes of the inverted emulsion after 1.5 hours agitation at all stirrer speeds. The drop sizes of the 1.5 hour samples were predominantly lower than 20 μm in size, but the size distributions were wide, with drops upto 300 μm present. The large drops boosted the D_{sm} of the samples; generally, D_{sm} values of 50 μm to 80 μm were found for the 1 poise samples and 60 μm to 100 μm for the 2 poise samples. No correlation of drop size with stirrer speed was attempted because of the sampling difficulties.

6.6.5 CATASTROPHIC INVERSIONS $O_m/W+W/O_m/W$ to W/O_m

A brief study was made of a catastrophic inversion O_m/W to W/O_m. To examine if there are any differences in mechanism and to investigate the effect of moving the viscosity ratio, $R_\mu=\mu_d/\mu_c$, for the initial emulsion condition, to >1.0 (oil phase viscosities of 0.007 poise and 1poise were used). Span 80 (HLB=8.6) was used as the stabilising surfactant. The oil phase was added to the water phase in 40 ml aliquots at 2 minute intervals. The sample withdrawal method was used to observe the $W/O_m/W$ drops, present before inversion.

In the experiments, the size of the oil drops increased as f_w decreased, $W/O_m/W$ drops were formed in the 0.007 poise case, however, in the 1 poise case, the amount of water incorporated into the $W/O_m/W$ drops was negligible. Catastrophic inversion took place at $f_w=0.5$ in the 0.007 poise system. In the 1 poise experiment, it was found that the water phase remained continuous until $f_w=0.18$. In the range $f_w=0.18$ to 0.12 it was impossible to distinguish which phase was continuous, this is illustrated by the photomicrographs in figure 6.22. In figure 6.22(a) the light lower area of the photomicrograph is inverted W/O_m emulsion, whereas, the top area is O_m/W emulsion. Note the difference in drop sizes of the two areas. On constant agitation of the semi-inverted emulsion at $f_w=0.12$, the system gradually broke down into a mixture of small water drops in oil and large $O_m/W/O_m$ drops - as shown in figure 6.22(b). With further agitation the $O_m/W/O_m$ drops released the oil drops and the system became a W/O_m emulsion.

In each experiment it was found that, the drop sizes of the W/O_m emulsion formed at the catastrophic point could be further broken up by further agitation.

6.7 DISCUSSION

The results in this chapter show which factors influence catastrophic phase inversions. The experiments carried out on the Cyclohexane/NPE system covered different aspects of catastrophic inversions from those carried out on Cyclohexane/SML systems, hence, the results of this section will be discussed individually.

6.7.1 CYCLOHEXANE/NPE SYSTEM RESULTS

The experiments on this system were concerned with determining the changes in the oil drop sizes within $O/W_m/O$ drops through a catastrophic inversion run and the effects of N and rate of addition, on the oil drop sizes of the inverted O/W_m emulsion.

Figure 6.4 is composed of photomicrographs taken at different stages of the inversion run, figure 6.5 shows how the drop size distribution of the O/W_m drops changes with rise in f_w upto and after a catastrophic inversion point, figure 6.6 shows the effect of stirrer speed on the size distribution of the inverted emulsion and figure 6.7 shows the drop size distribution of the inverted emulsion after 1 hour of direct emulsification.

To interpret the Cyclohexane/NPE results we shall first propose that the drops of the inverted O/W_m emulsion are produced by one of four different mechanisms:

(i) Surfactant Gel Phase Microemulsion Mechanism

It was noted that in the early stages of a run (low f_w) that a gel was present (see figure 6.4(a)) and that as the run progressed the gel disappeared, which coincided with the appearance of 1-2 μm size drops. In the 400 rpm and 600 rpm runs the surfactant was not pre-dissolved/dispersed (see section 6.5.1) in the oil phase, therefore, when agitation was started large "clumps" of surfactant will be dispersed in the oil. These "clumps" would constitute localised areas of high surfactant concentration. At high surfactant concentrations oil will dissolve in the surfactant (Shinoda 1986), hence, the gel maybe an oil in surfactant microemulsion (note water may also dissolve in the surfactant). The equilibrium phase behaviour of the system is such that the surfactant forms micelles in the water phase, hence, as equilibrium comes about the surfactant gel will dissolve into the water drops. As the gel dissolves, the oil in the microemulsion gel will be released into the water drop, forming very small oil drops.

(ii) Emulsification at the Drop Surface Mechanism

When the water drops are large and deformable the impact of turbulent eddies may cause part of the drop interface to become concave towards the continuous oil phase (the natural condition for type 1 systems). The desire of the surfactant to form concave interfaces with the oil phase, may then "pull" the water phase around oil caught in troughs in the water (or $O/W_m/O$) drop surface, thus encapsulating the oil as a drop within the water drop. Emulsification at the drop surface has been noted by Ohtake (1988).

As this mechanism is dependent on the turbulent eddy sizes (the same factor controlling drop sizes of stabilised emulsions in direct emulsification), it may be proposed that the drop sizes produced by this mechanism will be of a similar size to those produced in direct emulsification of stabilised emulsions.

(iii) Localised Catastrophe Mechanism

Oil drops may be formed from continuous oil phase trapped between coalescing water drops. It would seem that the likelihood of a number of drops coalescing together when the system is remote from a closest packing condition is very small, however, there are two possible cases when a number of drops may be close enough for a localised catastrophe condition to take place:

(a) Immediately after drop break up ie. re-coalescence of drops formed from a parent drop,

(b) at the injection point of adding more dispersed phase.

The drop sizes produced by this mechanism will be dependent on the $O/W_m/O$ drop sizes. It may be assumed that the size of the $O/W_m/O$ drops will increase as f_w rises, hence, the size of the oil drops (in the $O/W_m/O$ drops) produced by this mechanism will also rise with f_w.

(iv) Catastrophic Inversion Point Mechanism

This mechanism is similar to (iii), but concerns oil drops formed at the final catastrophic inversion point, from oil phase caught between $O/W_m/O$ drops. At the catastrophic inversion point the size of the $O/W_m/O$ drops will reach a maximum, therefore, it may be expected that the drops produced by this mechanism will be much larger than those formed by mechanisms (i) to (iii).

Note that when the $O/W_m/O$ drops coalesce at the catastrophic inversion point, the oil drops from within the water drops will be released to form part of the inverted O/W_m emulsion's size distribution.

Application of Drop Making Mechanisms to Results

Evidence for the existance and the proposed effects of the four drop making processes described above, can be found when studying figures 6.5 and 6.6. We will first consider the change in size distribution of the oil drops within the $O/W_m/O$ drops through the catastrophic inversion run shown in figure 6.5.

Figure 6.5

At low f_w (figure 6.5(a)), the distribution is relatively narrow and there is a pronounced peak at 1 to 2 μm. This is because in the early stages of the run, drop mechanism (i) will be active (before equilibrium is achieved) resulting in the 2 μm peak. The size distribution will be narrow because the $O/W_m/O$ drops will be relatively small and therefore, mechanism (iii) will not produce large drops. As f_w increases (figure 6.5(b) and (c)), a secondary peak appears and the size distribution width increases. The tail of the distribution stretches to higher drop diameters due to mechanism (iii) because the sizes of the $O/W_m/O$ drops are increasing with rise in dispersed phase fraction. The secondary peak is due to mechanism (ii); evidence for this can be found by noting that the value of the drop diameter of the peak, is the same as that of the further agitation peak in figure 6.5(e) (note earlier discussion). As will be shown when discussing figure 6.6, the shape and position of this secondary peak is also dependent on N. From the photomicrographs of figures 6.4(c) and 6.4(d) it is apparent that much larger oil drops are formed at the catastrophic inversion point, in line with mechanism (iv).

Figure 6.6

Figure 6.6 shows the drop size distributions of inverted O/W_m emulsions at three different stirrer speeds. Again the large peaks seen at 1-2 μm for stirrer speeds 400 rpm and 600 rpm can be accounted for by drop mechanism (i) (Note this peak represents $<<1\%$ of the dispersed phase volume, see Table 6.1 and hence, the "form" of the surfactant in the initial stages of emulsification will have a negligible effect on the D_{sm} of the final inverted emulsion). There is also a large peak at 1-2 μm in the 800 rpm case, however, these drops could not be produced by mechanism (i) because the surfactant was pre-dissolved/ dispersed in the oil phase in this experiment; this peak is due to mechanism (ii).

Further evidence that peak [2] in the 400 rpm and 600 rpm cases and peak [1] in the 800 rpm case are due to surface emulsification (mechanism (ii)) can be found, when comparing the shape and position of these peaks with those in figure 6.7 for the direct emulsification results. Note that as the stirrer speed increases a more pronounced peak

is obtained and at a lower drop diameter size; this is similar to results given by Nagata (1975) and Stamatoudis (1981), for the change in drop size distribution of dispersions with stirrer speed.

Although no peak was found in the drop size distribution due to mechanism (iii) in the case of the 600 rpm results, peaks attributed to this mechanism were obtained in the 400 rpm case (peak [3]) and 800 rpm case (peak [2]).

Hence, figures 6.5 and 6.6 show, that the drops of an O/W_m emulsion produced at a catastrophic inversion point, may be produced by 4 separate mechanisms. Each of the drop making mechanisms contributes drops in distinct size ranges to the overall emulsion's drop size distribution - this is shown schematically on figure 6.23.

NOTES:

(a) In $O/W_m/O$ drops, the oil drops within the water drops are stablised to coalescence due to the presence of surfactant. Some of the oil drops within the water drops are relatively large, this indicates that these oil drops may also be stable to drop break up ie. they are protected by the surrounding water drop.

(b) Studies of double emulsion drops (Ohtake 1987, 1988) have shown that entrainment of continuous phase into the dispersed phase can be depressed by increased volume fraction of the oil phase (as drops) within the $O/W_m/O$ drops and by decreasing surfactant concentration. These authors have also discussed some aspects of the problems of fitting Weber number correlations to double emulsion drop sizes: The volume of oil as drops within $O/W_m/O$ emulsion affects such factors as the dispersed phase viscosity, hence, the physical properties of an $O/W_m/O$ emulsion may be constantly changing through the course of a catastrophic inversion run.

6.7.2 CYCLOHEXANE/NPE CORRELATIONS - O/W_m EMULSIONS FORMED AT THE CATASTROPHIC INVERSION POINT

Weber number correlations for low viscosity systems agitated in a baffled stirred vessel often give the following relationship between D_{sm} and N : $D_{sm} \propto N^{-1.2}$, for isotropic turbulence conditions. The correlations found in the literature have only been applied to systems of low dispersed phase fraction, however, it may be argued that the same relationship will still apply at high dispersed phase fractions. If there is a direct relationship between the size of the drops present just before catastrophic inversion with those formed at the catastrophic inversion point, then it may be expected that $D_{sm} \propto N^{-1.2}$ will also apply to the oil drops of the O/W_m emulsion formed at the catastrophic inversion point. Note a linear relationship was found for cyclohexane/SML systems between the

size of the drops present before and those present after catastrophic inversion (for a constant oil phase viscosity), see figure 6.21) - this is in agreement with a closest packing model.

From figure 6.8 it can be seen that a $D_{sm} \propto N^{-1.2}$ relationship was obtained for the drops formed at the catastrophic inversion point in the cyclohexane/NPE system. However, this would seem quite remarkable because of the formation of $O/W_m/O$ drops in catastrophic inversions in this system, the oil drops present in the inverted O/W_m emulsion will have a range of ages ie. not all of the oil drops of the inverted O/W_m emulsion are formed at the inversion catastrophe. The fact that $D_{sm} \propto N^{-1.2}$ was still obtained may be explained by examining the cumulative distribution data of table 6.1. From table 6.1 it can be seen that the vast majority of the inverted O/W_m emulsion's drop volume is contained in drop sizes >25 μm. These drops are produced by catastrophic processes (mechanisms (iii) and (iv)); hence, D_{sm} is dependent mainly on drops made by catastrophic processes. If a direct relationship exists between the size of the $O/W_m/O$ drops and the oil drops (within the water drops), then the oil drops produced at any stage of the catastrophic inversion run, will show the same relationship with N as the $O/W_m/O$ drops. It will be argued in section 6.6.6 of this chapter, that the $O/W_m/O$ drops of the cyclohexane/NPE system will show the relationship $D_{sm} \propto N^{-1.2}$. Hence, at any stage of the catastrophic inversion run (including the catastrophic inversion point), the oil drops (within water drops) may be correlated by $D_{sm} \propto N^{-1.2}$, providing their rate of production is similar at each stirrer speed.

DIRECT EMULSIFICATION COMPARISON

After 1 hours further agitation the inverted O/W_m emulsion's drop size distribution became stable. A $D_{sm} \propto N^{-1.2}$ relationship was still found to hold (see figure 6.8). Direct emulsification produced a three-fold reduction in the drop sizes of the inverted O/W_m emulsion.

The stable D_{sm} value of the system agitated at 600 rpm was 23 μm (from figure 6.8) with a dispersed phase fraction of 0.64. In chapter 5 it was shown for a dispersed phase fraction of 0.2, that the stable drop diameter of the same system, under the same agitation conditions was 14 μm. Some authors (Walstra 1983) state " that the effect of volume fraction is unclear; it is probably small if the concentration of surfactant in the continuous phase after emulsification is kept constant". It is proposed here that the rise in D_{sm} with f_{disp} for systems containing a stabilising surfactant is most probably due to turbulence damping:

Turbulence Damping

It was shown in chapter 5 that coalescence was not a significant factor in determining the rate of drop breakage and final drop diameter size, in systems containing a stabilising surfactant, present in excess (ie. in O/W_m emulsions). Hence, the rise in D_{sm} seen here with increase in dispersed phase fraction is probably due to turbulence damping by the dispersed phase. Doulah (1975) showed theoretically that the effect of turbulence damping could be described by the following function:

$$D_{sm} = D^0_{sm}(1 + 3f_{disp}) \quad \text{[6.3]}$$

where, D^0_{sm} is the drop diameter at $f_{disp}=0$ (found by extrapolation).
From the value of D_{sm} at $f_{disp}=0.2$ obtained in this study, $D^0_{sm}=8.75$ μm, substitution of this value into equation [6.3] gives a prediction of $D_{sm}=25$ μm at $f_{disp}=0.64$, which is in good agreement with the experimental result. Hence, in systems containing a stabilising surfactant, the rise in D_{sm} with rise in f_{disp} can be reasonably accurately predicted by equation [6.3].

If the rate of drop breakage remains reasonably constant with rising f_w, then allowing for turbulence damping, figure 5.7 can be used to estimate the direct emulsification time to produce an O/W_m emulsion with a similar D_{sm} to that produced by catastrophic inversion. D_{sm} at 600 rpm produced by catastrophic inversion =74 μm for $f_{disp}=0.64$. From equation [6.3] it can be estimated that at $f_{disp}=0.2$ (allowing for a reduction in turbulence damping) $D_{sm}=40$ μ. From figure 5.7 the estimated direct emulsification time required to produce an O/W_m emulsion $D_{sm}=40$ μm is approximately 2 minutes, this compares with 30 minutes of processing time in the catastrophic inversion experiment. However, this is not strictly a true comparison as the overall catastrophic inversion time is controlled by the rate of addition of dispersed phase (discussed next), but it does indicate that catastrophic inversion is a far less energy efficient process than direct emulsification for producing small drop sizes.

6.7.3 EFFECT OF RATE OF ADDITION

Table 6.2 shows that as the time between additions increased, the value of f_w at the catastrophic inversion point decreased, the drop size distribution of the inverted O/W_m emulsion had more smaller drops, however, the width of the distribution increased, which led to an increase in D_{sm}. More small drops can form when the rate of addition is lower because there is more time for drops to be produced by mechanisms (ii) and (iii) at low f_w, when the size of the $O/W_m/O$ drops is relatively small. The size distribution widens as the addition rate lowers, in line with a lower f_w value at inversion. If the efficiency

of the catastrophic inversion process is measured by the smallness of the drops of the O/W_m emulsion produced, then from Table 6.1 it can be seen that the efficiency of the catastrophic inversion process increases as the rate of addition increases. Taking this argument to its extreme, then for systems similar to the cyclohexane/NPE system studied, the most efficient catastrophic inversion process would be one where all the dispersed phase is added in one addition to bring about inversion ie. a batch direct emulsification.

6.7.4 POLYISOBUTENE-CYCLOHEXANE/SML SYSTEMS

EFFECT OF THE OIL PHASE VISCOSITY ON THE CATASTROPHIC INVERSION POINT

The effect of the oil viscosity on the position of the catastrophic inversion point in the above system is shown on figure 6.9. In chapter 2, it was shown that the value of f_w at the catastrophic inversion point was dependent on the surfactant type. Figure 6.9, shows that f_{winv} is also dependent on the oil phase viscosity, for oil phase viscosities in the range 0.007 poise to 2.0 poise. Above 2 poise the value of f_{winv} remained constant (f_w=0.15) with rise in oil phase viscosity; this indicates that for oil phase viscosities above 2 poise the catastrophic inversion point is limited by a minimum volume of water which needs to be present.

6.7.5 LOW VISCOSITY SYSTEMS

DYNAMIC EFFECTS OF DROP COALESCENCE

The difference in the rates of $O/W_m/O$ drop production and hence, the difference in f_w at the catastrophic inversion point, in the cyclohexane/NPE and Cyclohexane/SML systems may be explained by considering the dynamic events that occur when drops coalesce.

A comprehensive review of the literature on drop breakage rates and drop coalescence rates is given by Tavlarides (1981). The coalescence of two drops is accomplished through the draining and rupture of the film of continuous phase.

The expressions describing drop coalescence rates are:

$$F(a,a')dada' = ce(a,a').z(a,a')\,dada' \quad \text{[6.4a]}$$

$$z(a,a')dada' = h(a,a').NA(a)NA(a')dada' \quad \text{[6.4b]}$$

where, F(a,a') is the number of coalescences per unit volume of dispersion per unit time, ce(a,a') is the collision efficiency of a collision between drops of sizes a and a', z(a,a') dada' is the number of binary collisions between drops of sizes a and a' per unit volume of dispersion per unit time, h(a,a') is the collision frequency between drops of sizes a and a' for a binary collision process based on number concentration, and NA(a) da is the number of drops of size a+da per unit volume of dispersion.

From figure 6.8 and figure 6.14 it can be seen that at all stirrer speeds the drops of the inverted O/W_m emulsion in the cyclohexane/NPE system are larger than those of the cyclohexane/SML system. Hence, using a closest packing model for catastrophic inversion, the $O/W_m/O$ drops of the cyclohexane/NPE system at the catastrophic inversion point will have been larger than those in the cyclohexane/SML system. Hence, z(a,a') will be larger in the Cyclohexane/SML system than in the cyclohexane/NPE system. However, coalescence rates are higher in the cyclohexane/NPE system than in the Cyclohexane/SML system, therefore, from equation [6.4a] it is apparent that this must be due to an increase in the collision efficiency.

The collision efficiency ce(a,a'), is defined as the fraction of collisions detween drops of diameter a and a' resulting in coalescence. The process by which two drops coalesce (film thinning and rupture) are determined by such factors as surfactant type, mass transfer, surface tension gradients, physical properties, Van der Waals forces, double layer forces and in turbulent flow, the contact time between drops (Tavlarides 1981). The collision efficiency accounts for these factors.

A qualitative assessment of collision efficiencies in cyclohexane/SML and cyclohexane/NPE systems can be made by considering the photomicrographs of the stages of drop coalescence in these systems - figures 6.24 and 6.25. The cyclohexane/SML system (figure 6.24) shows all the characteristic features of drop coalescence - film thinning, dimpling between drops. However, in the cyclohexane/NPE system (figure 6.25) the coalescence is quite different; the drops appear to "reach out" to meet each other suggesting there is a strong attraction between drops (film thinning occurring at a point instead of dimpling between drops resulting in film drainage along a length of interface). Hence, it may be argued that in the cyclohexane/NPE system, the collision efficiency is approximately 1, which would account for the large number of oil drops present in the $O/W_m/O$ drops and the low value of f_w at inversion.

6.7.6 HIGHER OIL PHASE VISCOSITY SYSTEMS

Figure 6.9 shows that as the oil phase viscosity rises the value of f_w at the catastrophic inversion point decreases, which is in agreement with Selker's (1965) observation that

"as the viscosity of the oil phase increased the more likely it was to become the dispersed phase". Reasons for this decrease can be found when examining the photomicrographs of figure 6.10, 6.11 and 6.12. The photomicrographs all show that as the oil phase viscosity increases the tendency of the water phase to emulsify larger and larger areas of oil phase increases. This effect is observed in, (i) $O/W_m/O$ drops - figure 6.10(b), where a drop can be almost entirely oil phase surrounded by a water surfactant film and (ii), at the catastrophic inversion point, where very large oil drops are present in the inverted O/W_m emulsion (figure 6.12).

The decrease in the value of f_w at inversion as the oil phase viscosity increases suggests there is an increase in the coalescence efficiency of the $O/W_m/O$ drops. An increase in the coalescence efficiency was found to be highly probable as the oil phase viscosity rises because:

(a) As the flow regime shifted more towards laminar, longer contact times between drops may be expected (note however, film drainage will be much slower in high viscosity systems),

(b) it was noted that as the oil phase viscosity increased the mechanism of coalescence became similar to that of the cyclohexane/NPE system, with attraction between drops observed.

However, an increase in the coalescence efficiency can only partly explain the decrease in f_w because different drop types and differences in the catastrophic inversion mechanism were also observed as the oil phase viscosity rises. These differences may be due to the changes in the mixing regimes, which will lead to different drop shapes:

Change in Reynold's Number With Oil Phase Viscosity

Equations [4.1] and [4.2] relate to calculating Reynold's Number for a stirred vessel. Equation [4.2] is used to calculate the emulsion's viscosity from the dispersed and continuous phase viscosities and fraction of dispersed phase. The dispersed phase fraction and dispersed phase viscosity are unknown in the systems studied here, due to the formation of $O/W_m/O$ drops. However, Reynold's numbers can be calculated for the initial conditions (low dispersed phase fraction) and these compared with the flow regimes given in table 4.1 - the initial flow type at each oil phase viscosity is given in table 6.5 below (note that in each case the Reynold's number will decrease as f_w increases during the catastrophic inversion run):

TABLE 6.5 - Flow Type at Each Oil Phase Viscosity (600rpm)

Oil Phase Viscosity	Flow Type
0.007 poise	Turbulent
0.25, 0.5, 1.0 poise	Transitional
2.0 poise	Laminar

Hence, in the case of the 0.007 poise system isotropic turbulence may be expected throughout the stirred vessel, in the case of the 0.25 poise, 0.5 poise and 1.0 poise systems turbulence exists in the region of the impeller and laminar shear flow in regions of the vessel remote from the impeller and in the case of the 2 poise system, laminar shear flow exists throughout the vessel before inversion.

From figure 6.10(b) (0.5 poise system), it is apparent that two different types of $O/W_m/O$ drops can form in transitional flow regimes. Drop [1] contains very small oil drops and is similar to $O/W_m/O$ drops formed in turbulent flow (see figure 6.3). However, drop [2] is unlike $O/W_m/O$ drops found in turbulent flow - containing large areas of oil; it may be that this type of $O/W_m/O$ drop is formed in the laminar regions of the vessel, remote from the stirrer.

With laminar shear flow many different drop shapes can form depending on the viscosity ratio ($R_v = \mu_d/\mu_c$) (Rumscheidt 1961) and on velocity gradients (Torza 1972). The dependence of drop shape and drop breakage on the viscosity ratio is shown in figure 6.26 (Torza 1972). At low R_v, (A), satellite drops may form from the tips of a drop as it is distorted in the shear field (although drop break up may not occur to a great extent), as R_v increases to intermediate values (B), the drops are stretched in the shear field into long cylinders (note, drop break up does not occur in B_2 systems) and at high R_v (C), drop distortion and drop break up become negligible. Note there are no sharp boundaries between the conditions A, B and C.

Figure 6.26 shows the equilibrium shape of drops in shear fields; Torza (1972) discussed the importance of velocity gradients on drop break up in shear fields, showing that under a high velocity gradient, a drop would be pulled into a cylinder and if the rate of distortion was greater than the relaxation time of the drop, the drop would break up due to the growth of instabilities.

When considering catastrophic inversion in high oil viscosity systems in a stirred vessel, it is apparent that all the shear flow features briefly summarised above, may be occuring throughout the run:

(i) There exists a wide range of velocity gradients throughout the vessel,

(ii) the fact that $O/W_m/O$ drops are formed means that R_v will vary from drop to drop and as a run progresses ie. a range of R_v will be present from the order of 0.001 to 1.0. Hence, type A and B drops will be present (type C drops could not be formed in the catastrophic inversions in the systems studied).

Cylindrical drops could not be observed in this study because the dynamic conditions in the observation cell are different from those of the stirred vessel. If long cylindrical drops do exist in laminar regions of the vessel, they may cause the formation of the type [2] drops seen in figure 6.10. The photomicrograph figure 6.10 shows the 1 poise system in a non-deformed state; on agitation the $O/W_m/O$ drops will be drawn into cylinders which may interconnect causing a localised catastrophic inversion. This explanation would also fit with the inverted emulsion structure found at 2 poise (figure 6.12), where large "areas" of oil are emulsified between "strands" of O/W_m emulsion.

Hence, drop shape is an important factor when considering catastrophic inversions in systems containing a high viscosity oil phase.

6.7.7 CYCLOHEXANE/SML SYSTEM - WEBER NUMBER CORRELATIONS

As discussed in the results section of this chapter, $O/W_m/O$ drops are not formed to a great extent in this system, hence, the dispersed phase fraction will be approximately known at each stage of the catastrophic inversion run. Therefore, Weber number type correlations can be applied to the drop size results of this system.

(i) $O/W_m/O$ Drops Present Before Catastrophic Inversion

The drop size results for these drops were found to correlate very well with:

$$D_{owo} = 0.1.e^{(8fw/3)}.N^{-1.2} \quad \text{[6.1]}$$

(see figure 6.13)

Note for this system $f_w \simeq f_{disp}$.

(a) N - Stirrer Speed

For this system a turbulent mixing regime with the agitation conditions used was expected from Reynold's number calculations (see Table 6.5). The exponent on N (-1.2) is in agrement with theory derived by Shinnar (1961), for drop breakage control in

isotropic turbulence. Many studies found in the literature have shown $D_{sm} \propto N^{-1.2}$, for low dispersed phase fractions (<0.2), this study has shown that the relation also holds at high dispersed phase fractions (upto 0.7).

(b) f_{disp} - Dispersed Phase fraction or Hold Up Fraction

Very little theoretical work exists in the literature concerning the effect of high hold fraction on drop sizes of dispersions. Most authors have been concerned only with fitting a function to their data to allow for the rise in drop sizes seen with rise in f_{disp}. Some of the functions to be found in the literature are summarised in table 6.6 below (all the functions apply to isotropic turbulence conditions in a stirred vessel):

Table 6.6 - Functions Used to Allow for the Effect of Rising Dispersed Phase Fraction.

Function $F(f_{disp})$	Range of f_{disp} Studied	Study
$(1+9.0f_{disp})$	0.0 to 0.2	Calderbank(1958)
$(1+5.4f_{disp})$	0.025 to 0.34	Mlynek(1972)
$(1+4.47f_{disp})$	0.025 to 0.15	Coulaloglou(1976)
$(1+3.0f_{disp})$	<0.002	Calabrese(1986)
$10^{a+bf_{disp}}$	0.079 to 0.583	Weinstein(1973)
$f_{disp}^{-0.66}$	0.0 to 0.08	Eckert(1985)
$f_{disp}^{0.27}$	0.0 to 0.1	Laso(1987)
$(\ln[c_3+c_4f_{disp}]/\ln c_3)^{-3/5}$	0.0 to 0.4	Delichatsios(1976)

The most typical Weber number correlations give a linear function to allow for the change in D_{sm} with f_{disp}, $F(f_{disp})=(1+af_{disp})$. Table 6.6 lists a few studies that have used this approach, (note there are many more to be found in the literature; see review by Tavlarides 1981). The constant a, in the function can vary from 2.5 to 9.0 (Mlynek1972), however, these studies refer almost exclusively to dispersions where $f_{disp}<0.2$ (note one study, Thornton (1967), gave a linear relationship for the range $f_{disp}= 0.2$ to 0.5, but this was based on a very limited amount of data). From figure 6.13 it can be seen that an approximately linear relationship between D_{owo} and f_w was obtained in the range $f_w = 0$ to 0.2, hence, the data in this range could be correlated by:

$$D_{owo}=0.1(1+3.5f_{disp}).N^{-1.2} \qquad [6.4]$$

This is in agreement with typical Weber number correlations to be found in the literature. However, figure 6.13 also shows that correlations of this type will become very inaccurate for $f_w>0.3$.

Studies that give functions for the effect of dispersed phase fraction of the type: $F(f_{disp})=f_{disp}^{\ b}$, were discussed by Eckert et al (1985); they showed that correlations have been given where b, varies from -0.53 to 1.0. Their results showed there to be an increase in D_{sm} with f_{disp} upto, $f_{disp}=0.02$, however, for $f_{disp}>0.02$, D_{sm} levelled off to a constant value with increasing f_{disp}. This would not seem to be in agreement with the results, at much higher f_{disp} values, shown on figure 6.13.

The most interesting $F(f_{disp})$ is by Delichatsios (1976) because this was derived from theoretical considerations. Delichatsios et al, showed that coalescence and not turbulence damping, is the only effect that could account for the large increase in D_{sm} with f_{disp}. The $F(f_{disp})$ function (equation 6.5 below) was derived by Delichatsios et al by equating expressions found for the coalescence frequency resulting from binary collisions, with an effective break up frequency, to yield a semi-empirical relation. The theory takes into account drops of different sizes (a Gaussian drop size distribution was assumed) and that drops will be moving at differing velocities in the turbulent regime.

$$F(f_{disp})= (\ln[c_3+c_4 f_{disp}]/\ln c_3)^{-3/5} \qquad [6.5]$$

where, $c_3=\exp(-4.5)$; a constant related to the cut off velocity in the probability function,

$c_4=3(A/B)$; where (A/B) is a constant proportional to the ratio of coalescence to break up coefficients. c_4 allows for differences in collision efficiencies in different systems . c_4 must be determined empirically and will differ from system to system, however, it should be of the order of 1.0. The data of figure 6.13 is replotted on figure 6.27 , the lines are the result of the correlation below, where $c_4=1.25$:

$$D_{owo}=0.09(\ln[c_3+1.25 f_{disp}]/\ln c_3)^{-3/5}.N^{-1.2} \qquad [6.6]$$

Figure 6.27 shows there to be exellent agreement between the experimental results and equation [6.6]. Hence, the function derived by Delichatsios was found to hold even at high dispersed phase fractions. The two correlations derived for this system both predict accurate results; equation [6.6] has greater theoretical justification, however, equation [6.1] is easier to use.

(ii) O/W_m Emulsion Formed at the Catastrophic Inversion Point

As was the case in the cyclohexane/NPE system, the inverted cyclohexane/SML emulsion results were found to correlate to $D_{ow} \propto N^{-1.2}$ (see figure 6.14). Figure 6.21 shows there to be a linear relationship (for constant oil phase viscosity) between the size of the $O/W_m/O$ drops at inversion and the size of the O/W_m drops formed at the inversion point (this agrees with closest packing theory). Therefore, as $D_{owo} \propto N^{-1.2}$, then $D_{ow} \propto N^{-1.2}$ is an expected result.

(iii) Direct Emulsification Comparison

Results similar to those found for the cyclohexane/NPE system were found for the cyclohexane/SML system; the exponent on N (-1.2) found from figure 6.14, again indicates that isotropic turbulence was the mechanism of drop break up and the drop sizes produced by direct emulsification were found to be much smaller than those that could be produced by catastrophic inversion (approximately 1/5 in the cyclohexane/SML case - see figure 6.14).

A brief study was made, to estimate the stirring time required in direct emulsification, to produce an O/W_m emulsion with the same D_{ow} as that of the emulsion formed at the catastrophic inversion point (for the same agitation conditions). This showed that <5 minutes would be required (this is similar to the cyclohexane/NPE results).

Having shown, in chapter 2, how the surfactant effects the drops present before and after a catastrophic inversion, it is now possible to explain the greater drop breaking efficiency of direct emulsification processes over catastrophic inversion processes, by considering the role of coalescence in each process:

(a) In the direct emulsification of nSOW systems, the surfactant present stabilises the droplets formed. It was shown in chapter 5 that coalescence rates are not significant in systems of this type, hence, energy input is not lost re-disrupting coalesced drops.

(b) In catastrophic inversions, the $O/W_m/O$ drops formed before inversion are unstable and therefore, a balance between drop disruption and drop coalescence dictates the drop sizes at any point. Hence, a much higher energy input is required to offset the rise in drop sizes caused by coalescence.

The correlations, equations [6.1] and [6.6], show that drop disruption is the dominant mechanism in the cyclohexane/SML system. They also show, that the relative rates of disruption and coalescence, are affected by f_{disp} (where coalescence rates increase with increase in f_{disp}), but may not be a strong function of N (the exponent on N remains constant at each f_{disp}).

The large rise in D_{owo} with increase in f_w shows that coalescence is an important factor in determining the size of the $O/W_m/O$ drops before inversion. Therefore, it may seem surprising that $D_{owo} \propto N^{-1.2}$ (a relationship initially derived for a non-coalescing system, where the drop diameter, D_{owo}, is the maximum drop diameter stable to break up in turbulent flow) was found to hold at high f_w. Other investigaters that have used coalescing systems, have found that $D_{sm} \propto N^{-1.2}$ fits their results and this has been explained in terms of a balance between break up and coalescence (Tavlarides 1981), but no theoretical treatment of this balance has been made. When coalescence has been considered to be the drop size controlling mechanism in models, a minimum drop diameter is specified, where drops smaller than D_{sm} are thought to be unstable to coalescence. In these models the relationship $D_{sm} \propto N^{-0.75}$ has been derived (Shinnar 1961, Sprow 1967). It is apparent from the results of this chapter, that drop coalescence occurs in systems having results agreeing with the predictions of drop disruption models. We shall return to this argument after discussing the results of the effect of changing oil phase viscosity on the drop sizes before and after inversion.

6.7.8 THE EFFECT OF THE OIL PHASE VISCOSITY ON DROP SIZES

Very little attention has been given to the effect of the continuous phase viscosity on drop sizes of dispersions, in work to be found in the literature. Apart from altering the systems Reynold's number, Stamatoudis and Tavlarides (1985) have shown how drop sizes and drop breakage rates can alter with changes in the continuous phase viscosity (μ_c):

(a) The time to reach a steady state drop diameter can rise dramatically with rise in μ_c; times upto 8 hours were reported (the systems studied had a range of viscosities from 3.5 cp to 223.1 cp).

(b) At certain stirrer speeds a rise in the drop diameter to a maximum and then a decrease was found with increasing μ_c, while at other stirrer speeds a minimum drop diameter occured with increase in μ_c, but there was very little overall change in D_{sm} with μ_c.

(c) The effect of the dispersed phase viscosity as μ_c rises, was also found to be of importance. The results (b) were obtained for low μ_d (1.4 to 1.9 cp), however, in a dispersion containing a dispersed phase of a much higher μ_d (26.4-26.7 cp), a very large decrease in D_{sm} (>50%) was found between a system of μ_c=10 cp and a system of μ_c=90 cp.

(d) A rise in D_{sm} with f_{disp} was found at all μ_c values studied.

The systems studied by Stamatoudis and Tavlarides had low dispersed phase fractions (0.025 to 0.15), much lower than those required for catastrophic inversion, however, their observations serve to highlight some added difficulties in interpreting data of systems with high μ_c. In catastrophic inversions the system dynamics become even more complex than those in simple dispersions because as previously discussed, μ_d is constantly changing as a result of the formation of $O/W_m/O$ drops. As a catastrophic inversion run progresses, coalescence efficiencies may alter, changes in drop shapes and drop types can occur and the flow regime which is initially transitional (at low f_{disp}), moves progressively towards laminar conditions as f_{disp} increases.

(a) 0.25 poise SYSTEM (figures 6.14 and 6.15)

Of the higher oil phase viscosity systems studied, the 0.25 poise system results are easiest to interpret as f_w will be reasonably close to f_{disp} (this is reflected in the high value of f_w at the catastrophic inversion point). The data for the $O/W_m/O$ drops present before inversion, are correlated by (see figure 6.15):

$$D_{owo}=0.008e^{(5fw/2)}.N^{-0.8} \quad \text{[6.2]}$$

The fact that a constant exponent on N was found to hold at each value of f_w indicates, that the change in the mixing conditions (transitional) due to rise in f_w (and therefore, a lowering in Reynold's number) was not significant and also again, that the relative rates of breakage and coalescence is not a strong function of N. In the 0.007 poise system the drop diameter D_{owo} was controlled by drop breakage ($D_{owo} \propto N^{-1.2}$), however, the exponent on N in the 0.25 poise system (-0.8), suggests that the drop sizes are coalescence controlled. The minimum stable drop diameter that could exist in turbulent flow, where coalescence is prevented by eddies, was shown to be dependent on $N^{-0.75}$ by Shinnar (1961). Sprow (1967) showed that when the force preventing coalescence was viscous shear that $D_{sm} \propto N^{-0.75}$ was also true. For the transition region Tavlarides (1981) derived exponents of -1 to -2.16 on N for drop breakage control and -0.75 to -1.04 for coalescence control (see chapter 4 for a complete review). Hence, the results for the $O/W_m/O$ drops of the 0.25poise system fit with drop coalescence control models. This may be related to the changes in the coalescence mechanism noted earlier in this discussion.

Note that baffles were not inserted into the tank for this experiment; some authors have shown drop sizes to be much larger in unbaffled vessels compared to baffled vessels (Leng 1982), however, others have shown there to be little difference (Weinstein 1973). The drop sizes of the 0.25 poise system are not significantly different in size to those

found in the baffled 0.007 poise system experiment. Hence, the presence of baffles did not cause large changes in drop sizes, however, baffles may have altered the exponent on N (see later discussion).

For constant oil phase viscosity conditions, a linear relationship between the $O/W_m/O$ drop sizes at the catastrophic inversion point and the drop sizes of the O/W_m emulsion formed, was again obtained (see figure 6.21). From figure 6.14 it can be seen that the drop sizes of the inverted O/W_m emulsion varied with stirrer speed as, $D_{ow} \propto N^{-0.8}$. This is to be expected as most of the drops of the O/W_m emulsion, were formed at the catastrophic inversion point and should therefore, have the same relationship with N as the $O/W_m/O$ drops before inversion.

The rise in D_{owo} with f_w (for the conditions before inversion), tends towards a linear relationship in the 0.25 poise case, compared to the 0.007 poise case and this trend was found to continue at higher oil phase viscosities.

(b) Oil Phase Viscosities 0.5 poise, 1 poise and 2 poise

The results of this part are shown on figures 6.14, 6.16, 6.17 and 6.18. For these systems $f_w \neq f_{disp}$, large changes in μ_d will occur between drops and the mixing regime will greatly alter through the run (being transitional at low f_w and becoming almost laminar near the catastrophic inversion point). In the case of the 2 poise system the mixing conditions will be laminar throughout the run. In view of of all these changing variables, it is quite remarkable that simple linear D_{owo} vs f_w relationships were obtained for each agitation condition, at each oil phase viscosity.

$O/W_m/O$ Drops Present Before Catastrophic Inversion

From figures 6.16, 6.17 and 6.18, which show the variation of D_{owo} with f_w for the 0.5 poise, 1.0 poise and 2.0 poise systems, it can be seen that the results at different stirrer speeds were parallel. The results suggest that for these oil phase viscosities, drop "growth" with rising f_w is independent of stirrer speed.

For the case of the first water aliquot addition (f_w=0.04) to the oil phase at each oil viscosity, the $O/W_m/O$ drops will be mainly water and therefore, $f_w = f_{disp}$. Hence, the data for the 0.5 poise, 1.0 poise and 2 poise systems at f_w=0.04 may be compared with the results of other workers. Figures 6.16, 6.17 and 6.18 show that the $O/W_m/O$ drop sizes decrease with rising N and decrease with increasing μ_c. The data can be correlated with reasonable accuracy by:

$$D_{owo} \propto \mu_c^{-0.33}.N^{-0.75} \quad [6.7]$$

The exponent on N is in agreement with coalescence control models derived by Shinnar (1961), Sprow (1967) and Tavalrides (1981). The coalescence control models derived by these workers also give a D_{sm} vs continuous phase viscosity relationship: $D_{sm} \propto \mu_c^{-0.5}$, where the exponent on μ_c is similar to equation [6.7]. The difference in the value of the exponent on μ_c may be due to the fact that the derived result is for steady state conditions, whilst the experimental result refers to drop sizes after 2 minutes agitation time. Stamatoudis (1985) showed that the time taken to achieve a steady state drop size, increases with increasing μ_c, hence, it may be expected that the exponent on μ_c will decrease with time.

O/W_m Emulsion Formed at the Catastrophic Inversion Point

From figure 6.14 it can be seen that the drop sizes of the O/W_m emulsions formed at the catastrophic inversion points, were found to correlate with $D_{ow} \propto N^{-0.8}$, for higher oil phase viscosity systems (note, the D_{ow} values for the 2 poise system could not be determined accurately because the drops had a very wide distribution). Figure 6.14 also shows, that the drop sizes of the inverted O/W_m emulsion increase with increasing oil phase viscosity. This may be due to changes in the O/W_m/O drop shape occurring in the vessel. A change from spherical to cylindrical at the closest packed condition is expected as the mixing regime becomes more laminar (note, this could not be observed with the experimental set up used in this study).

6.7.9 ULTRA-TURRAX HIGH INTENSITY AGITATOR RESULTS

The Ultra-Turrax device is a high energy agitator working on a rotor-stator principle. The device used in this study was designed to produce fine emulsions with drop sizes in the range (1 to 5 μm), after very short agitation times. Table 6.4 shows, that at each oil phase viscosity examined, when the surfactant can stabilise the emulsion (ie. in the production of O/W_m emulsions by direct emulsification), fine emulsions were produced (for D_{ow}<5 μm - a steady state drop size was produced in <2 minutes agitation time). The rise in the drop diameter with increase in oil phase viscosity shown in table 6.4, is due to the increase in the dispersed phase fraction (used for direct comparison with the catastrophic inversion results) with rising oil phase viscosity.

The size and variation of the $O/W_m/O$ drops present before inversion, at each oil phase viscosity, are shown on figures 6.13, 6.16, 6.17 and 6.18. These figures also show that in these experiments, the value of f_w at the inversion point does not vary significantly from that found when agitation was supplied by a turbine agitator. At each oil phase viscosity, the size of the $O/W_m/O$ drops at all f_w values, are smaller, but not greatly different in the Ultra-Turrax from those in the 800 rpm turbine agitator case. The decrease in the $O/W_m/O$ drop sizes is due to the increased drop breakage rates when agitation is supplied by an Ultra-Turrax.

The drop sizes of the O/W_m emulsion produced at the catastrophic inversion point, in the Ultra-Turrax experiments, also show the same trends seen in the turbine agitator experiments:

(a) The drop sizes increase with increase in the oil phase viscosity,

(b) the drop sizes produced by the catastrophic inversion are of a much greater size than those that could be produced by direct emulsification.

In the turbine agitator experiments, a sufficient length of time for the $O/W_m/O$ drops to obtain a steady state drop size at each f_w was not available because of the rate of additions used. However, in the Ultra-Turrax experiments, the time between additions (2 minutes) is sufficient for a steady state drop size to be produced at each f_w. Therefore, the size of the unstable $O/W_m/O$ drops present before catastrophic inversion, can now be compared with the stable O/W_m drop sizes.

Although there will be some differences in the drop breakage rates before and after inversion due to the differences in the physical properties of the continuous and dispersed phases, the results illustrated below are a striking example of how coalescence greatly increases the drop sizes of an unstable dispersion compared to the drop sizes of a stable dispersion, even for low dispersed phase dispersions in the presence of high shear fields: Consider the case of the Ultra-Turrax experiment on the 0.007 poise system. In this experiment, for conditions before inversion, $f_w=f_{disp}$. For this system, before inversion at $f_w=f_{disp}=0.25$, the steady state drop diameter of the unstable $O/W_m/O$ emulsion was, $D_{owo}=55\ \mu m$. After inversion, the steady state drop diameter of a stable O/W_m emulsion (ie. the direct emulsification result), with the same f_{disp} ($f_w=0.75$) was, $D_{ow}=2.6\ \mu m$. The difference in the two diameter values is mainly because coalescence can readily occur in $O/W_m/O$ emulsions, but coalescence is prevented in O/W_m emulsions.

NOTE: The illustration above assumes that in a nSOW system, the interfacial tension on a W_m/O interface is similar to the interfacial tension of a O/W_m interface. However, we have no experimental method for checking this.

6.7.10 DROP SIZE CONTROLLING MODELS

The deficiencies of drop breaking and drop coalescence models have been highlighted by the results of this chapter. Most of the deficiencies stem from the fact that in the models only drop breakage is supposed to be occuring in a system or only drop coalescence is supposed to be occuring in a system. However, both events must be occuring simultaneously during a dynamic inversion experiment.

The results of the studies of $O/W_m/O$ drops in this chapter show that when the oil phase viscosity was 0.007 poise, the drop size results could be correlated by drop breakage models. The drop size study (0.007 poise system) made when agitation was supplied by an Ultra-Turrax, high intensity agitator, showed that, the drop sizes of an unstable $O/W_m/O$ emulsion were >> the drop sizes of a stable O/W_m emulsion with the same dispersed phase fraction (and similar physical properties). Hence, coalescence must have been occuring before inversion in the unstable $O/W_m/O$ emulsion.

Sprow (1967) examined the effect of the sampling position on drop sizes in a stirred vessel. He found that drop sizes increased as the sampling position moved vertically towards the liquid surface and with increasing distance horizontally from the impellor tip. He showed that drop sizes near the impellor could be correlated by drop breakage models and drop sizes near the vessel walls by drop coalescence models. Sprow assumed isotropic turbulence was developed in the vessel, however, this could not be so if spatial variations in drop sizes occurs.

The variation of the turbulent velocity fluctuations within a stirred vessel have been investigated by a large number of studies. Generally, it has been found that a maximum velocity fluctuation occurs at the impellor tip. Holmes (1964) showed that, the radial velocity fluctuation x distance from the impellor = constant. Cutter (1966) calculated that 70% of the power input to the vessel was dissipated in the impellor stream and only 30% was dissipated in the tank bulk. On the other hand, Gunkel (1975) calculated that most of the energy dissipation takes place in the tank bulk.

It is tempting to explain the correlation of the $O/W_m/O$ drop sizes found in the 0.007 poise system in terms of there being drop breakage regions and drop coalescence regions in a stirred vessel (where, the exponent on N found experimentally depends on the sampling position). However, in the Ultra-Turrax agitation case, a very high level of energy is imparted to the emulsion. It may be assumed in this case that the turbulence in the vessel was isotropic (but, drop breakage and drop coalescence were still occuring at all stages). It is proposed below that there are two possible coalescence control types that can occur in agitated emulsion systems. The coalescence type depends on the energy relation in the tank at steady-state.

Turbulent Flow Energies

When a steady-state drop size distribution is reached, a number of different energy balances can be proposed. The form of the energy balance depends on the magnitude of the turbulent velocity fluctuations, the attractive force between drops and the rate controlling step in drop coalescence. The kinetic energy of the turbulent velocity fluctuations (E_k) can be dissipated as heat (E_h), creating surface area (E_s) and resisting attractive forces between drops (E_a).

Where (see chapter 4):

$E_k=k_1\rho_c u^2(d)d^3 = k_2\rho_c N^2 D^{4/3} d^{8/3}$

$E_h=k_3E_k$

$E_s=k_4\sigma d^2$

$E_a=Ad$

The following energy balances are possible when a steady-state drop size distribution is produced ($\Delta E_s=0$):

(a) $(E_k-E_h)=E_a$ ie. The drop sizes are such that the kinetic energy of the turbulent velocity fluctuations are just high enough to prevent coalescence. Here, coalescence is determined by film drainage rates. For this case the energy balance equations result in Shinnar's (1961) drop coalescence control model:

$d=k_5\rho_c^{-3/8}N^{-3/4}D^{-1/2}$

(b) $(E_k-E_h)=0$. In this case $E_a=0$. For $E_a=0$, the coalescence efficiency must be 0 or 1. The coalescence efficiency depends on the rate of film drainage between drops. The rate of film drainage between two colliding drops may be a function of their kinetic energy. Hence, if two drops of equal size d, collide with a sufficient relative velocity $u_r^2(d)$ then the coalescence efficiency=1. In this case the coalescence rate = collision rate. For conditions when the drop sizes are larger than the turbulent eddy sizes (the condition necessary for drop break up by turbulent pressure fluctuations), eddies impact on the drops at all directions causing the drops to move in a random fashion. This led researchers to assume that drop collisions were analogous to the collisions of molecules in gas kinetic theory. It has been shown that collision rate is dependent on the number of drops of an emulsion and the eddy mean square velocity fluctuations (see review by Tavlarides 1981). At steady-state the emulsion's drop sizes will be dependent on a balance (if $u^2(d) > u_r^2/2$) between the loss of surface area due to drops colliding and the gain in surface area due to drop break up. The gain in surface area of the dispersed phase drops (drop breakage) is dependent on the turbulent eddies' kinetic energy. For

conditions of constant dispersed phase fraction and drop size (steady-state) the loss in drop surface area due to drop collisions, is also dependent on the turbulent eddy kinetic energy. Hence for this case:

$d=k_6(\sigma/\rho_c)^{3/5}N^{-1.2}D^{-4/5}$

NOTES

If $E_a=0$ because there is no (or little) attractive force between drops, then we can consider two subcases of (b):

(i) $u^2(d) < u_r^2(d)/2$. For $\Delta E_s=0$, the drop sizes must be broken up to the smallest possible size in the turbulent flow ie. down to the smallest eddy sizes. All the turbulent kinetic energy will then be lost as heat.

(ii) $u^2(d) > u_r^2(d)/2$. For this case the collision efficiency need not be equal to 1. However, the collision efficiency must equal the breakage efficiency for $\Delta E_s=0$. Howarth (1964) developed an expression for collision efficiency by assuming an analogy to bimolecular gas reactions. He assumed that a critical relative velocity (u_r) exists along the lines of centres of two colliding drops, which must be exceeded for collision to result in a coalescence. He obtained the coalescence efficiency as the fraction of drops which have kinetic energy exceeding u_r:

coalescence efficiency = $\exp(-3u_r^2/4u^2)$

where, u^2 = mean square velocity.

Laminar and Transitional Flow

The treatment of laminar and transitional flows is much less well developed than turbulent flow. Tavlarides (1981) reviews models derived by Stamatoudis for laminar and transitional flows (see chapter 4). For each flow condition a drop breakage control and a drop coalescence control model was derived. In the derivation of the models, shear forces were assumed to be the drop size controlling mechanism. By comparison with the derivations for turbulent flow discussed above, it may be for laminar and transitional flows, that Stamatoudis's models for drop breakage control will apply when $E_a=0$ (ie. no attraction between drops or coalescence efficiency =1) and, drop coalescence control will apply when $(E_k-E_h)=E_a$.

Summary and Application to Results

The section above discussed the drop size controlling models in terms of an energy balance at steady-state. When attraction exists between drops, drop coalescence controls the drop sizes of an emulsion. The drop correlation depends on the relative magnitude

of the attractive force between drops and the turbulent velocity fluctuations. At steady-state the coalescence efficiency is either 0 or 1. When the coalescence efficiency=0, film drainage rate determines the coalescence rate and when the coalescence efficiency=1, collision rate determines the coalescence rate. The cases described above can be used to explain the drop size results of this chapter:

O/W_m Emulsions

The drops of O/W_m emulsions are stabilised by the surfactant. The net attraction and repulsion energies acting between drops with changing distance apart is shown in figure 6.24 (Tadros 1983). From figure 6.24 it can be seen that for two drops to coalesce an energy barrier G_{max} must be overcome. This can only be achieved if the two drops approach with sufficient kinetic energy (Tadros 1983) ie. drops of equal size have sufficient relative velocity $u_r^2(d)$. Then for an agitated emulsion there are two possible cases depending on the magnitude of the turbulent velocity fluctuations ($u^2(d)$):

$u^2(d) < u_r^2(d)/2$. In this case the approaching drops have insufficient relative velocity to overcome G_{max}. Hence $E_a=0$, as the adhesion force=0 (repulsion between drops). The drop sizes of the emulsion will be determined by the turbulent eddy sizes.

$u^2(d) > u_r^2(d)/2$. Here, the drops have sufficient kinetic energy to overcome G_{max} and coalescence will take place. $E_a=0$ (coalescence efficiency=1) and the drop sizes of the emulsion are determined by a balance of drop break up and drop coalescence. This relation may explain why the drop sizes of stabilised emulsions produced by high intensity agitators (Ultra-Turrax, homogenisers) are not signifcantly smaller than those that can be produced in an agitated vessel at a high stirrer speed.

In the results section of this chapter, it was shown that, the drop sizes of stable O/W_m emulsions produced by further agitation (or direct emulsification) in the cyclohexane/NPE12 and cyclohexane/SML (0.007 poise) systems could be correlated by $D_{ow} \propto N^{-1.2}$. This is in agreement with the $E_a=0$ cases described above.

$O/W_m/O$ Drops - Turbine agitator

For turbulent flow conditions (cyclohexane/SML 0.007 poise system) the sizes of these drops could be correlated by $D_{owo} \propto N^{-1.2}$ at all values of f_w. Hence, in this case $E_a=0$. The unstable $O/W_m/O$ drops are much larger than the stable O/W_m drops (when agitation was supplied by a turbine agitator or an Ultra-Turrax). Hence, for $E_a=0$, the drop sizes of the $O/W_m/O$ emulsion must be determined by the kinetic energy of the drops such that the coalescence efficiency=1. Since the coalescence efficiency=1, the drop sizes of the $O/W_m/O$ emulsion will be dependent on a balance of drop break up and drop coalescence, where coalescence rate is determined by collision rate. Collision rate is a strong function of f_{disp}. In section 6.6.7 of this chapter, the effect of f_{disp} on the drop sizes of unstable

emulsions was discussed. It was found with rise in f_{disp}, the exponent on N remained unchanged and the increase in the drop sizes could be correlated by a function derived by Delichatsios et al (1976). It is worth noting that Delichatsios et al's function was derived on the basis that, film drainage was not coalescence rate determining: Hence, coalescence rate = collision rate x a constant coalescence efficiency. Therefore, the basis for Delichatsios et al's function is in agreement with the theory discussed above.

It was impossible to measure the $O/W_m/O$ drop sizes (present before inversion) of the cyclohexane/NPE12 system with the sampling technique used here. However, photomicrographic evidence of the coalescence mechanism between $O/W_m/O$ drops of the cyclohexane/NPE system showed there was a strong attraction between drops (see figure 6.25). Hence, the coalescence efficiency in this system may be close to 1. The coalescence rate will therefore be determined by collision rate. From the above discussion we would expect the drop sizes to be correlated by $D_{owo} \propto N^{-1.2}$ (note discussion of the O/W_m emulsion drops formed at the inversion point which could be correlated by $D_{ow} \propto N^{-1.2}$).

Higher Oil Phase Viscosity Systems

The $O/W_m/O$ drop size results of the higher oil phase viscosity systems studied here could be correlated by drop coalecence control models. Hence, for these systems $E_s=0$ at steady-state and the kinetic or shearing energy input is balanced by the attraction energy between drops. A move towards coalescence control mechanisms is expected as the oil phase viscosity increases because:

(i) The velocity fluctuations will decrease at any stirrer speed,
(ii) photomicrographic evidence indicated that a greater attraction between drops was present.

Having discussed the correlation of $O/W_m/O$ drops before inversion and O/W_m drops after inversion we will now discuss the relation between the two drop types at the catastrophic inversion point.

6.7.11 Figure 6.21 - The relationship between the $O/W_m/O$ drop sizes at the catastrophic inversion point and the O/W_m drop sizes of the inverted emulsion

Figure 6.21 (PIB-Cyclohexane/SML systems) is a plot of the $O/W_m/O$ drop sizes (D_{owo}) at the catastrophic inversion point, against the D_{ow} size of the O/W_m emulsion formed at the catastrophic inversion point. The D_{ow} values are taken from figure 6.14 and the D_{owo} values from figures 6.13, 6.15, 6.16, 6.17 and 6.18. Lines of constant viscosity and constant stirrer speed are shown.

The 0.007 poise and 2 poise lines neatly divide the figure into turbulent, transitional and laminar mixing regions, as labelled on the figure. Many of the trends discussed in this chapter are summarised on figure 6.21:

(a) At each oil phase viscosity, the size of the $O/W_m/O$ drops at the inversion point will increase with decrease in N.

(b) At each oil phase viscosity, the size of the oil drops of the inverted O/W_m emulsion, increase with decrease in N.

(c) At each stirrer speed the size of the $O/W_m/O$ drops at the inversion point decrease with increase in the oil phase viscosity.

(d) At each stirrer speed the size of the inverted O/W_m emulsion drops increase with increasing oil phase viscosity.

(e) A direct relationship between the size of the drops present before inversion and the size of the drops after inversion, was obtained at each oil phase viscosity.

Apart from the changes in the oil phase viscosity, the other physical properties of the PIB-cyclohexane/SML systems studied (density, interfacial tension; see note in experimental section) may remain reasonably constant between systems. Also, each system was subjected to the same agitation conditions in the same vessel, hence, we may anticipate there to be a relationship between the inversion drop sizes in each system. Figure 6.21 shows that the lines at constant oil phase viscosity are linear and tend to converge as D_{ow} decreases.

ANALYSIS

In a closest packing arrangement a volume relation exists between, the oil drops produced at the catastrophic inversion point and the $O/W_m/O$ drops at the catastrophic inversion point. Consider the relationship between the phase volumes at the catastrophic inversion point:

$$V_{owo} - V_{ow} = Vf_{dinv} - V(1-f_{dinv}) = V(2f_{dinv}-1) \quad [6.8]$$

where, V_{owo} = volume of the $O/W_m/O$ drops,

V_{ow} = volume of the oil drops formed from continuous phase trapped between $O/W_m/O$ drops at the catastrophic inversion point,

V = total volume of emulsion,

f_{dinv} = dispersed phase fraction of $O/W_m/O$ drops at the catastrophic inversion point.

$$V_{owo} = D_{owo}.A_{owo}/6 \quad [6.9]$$

$$V_{ow} = D_{owo}.A_{ow}(1-\varphi)/6 \quad [6.10]$$

$$f_{dinv} = f_w + \varphi(1-f_w) \quad [6.11]$$

where, A_{owo} = surface area of the $O/W_m/O$ drops at the catastrophic inversion point,

A_{ow} = surface area of the oil drops of the O/W_m emulsion formed after catastrophic inversion,

φ = fraction of the total oil phase fraction, incorporated as oil drops within $O/W_m/O$ drops at the catastrophic inversion point.

hence:

$$D_{owo} = (1-\varphi)(A_{ow}/A_{owo})D_{ow} + 6V(2f_{dinv}-1)/A_{owo} \quad [6.12]$$

In a closest packing model $(1-\varphi)A_{ow} \propto A_{owo}$, hence, $(1-\varphi)(A_{ow}/A_{owo})$= constant. The dispersed phase fraction at closest packing is given by:

$$f_{dinv} = D_{owo}/[D_{owo} + (1-\varphi)(A_{ow}/A_{owo})D_{ow}] \quad [6.13]$$

0.007 poise Cyclohexane/SML System

For the 0.007 poise cyclohexane/SML system $f_{winv} = f_{dinv}$. Hence, using equation [6.13], values of $(1-\varphi)A_{ow}/A_{owo}$ (here φ=0) can be calculated for the system at each stirrer speed. These calculations show (see data in table 6.7) that $(1-\varphi)A_{ow}/A_{owo}$ = constant for this system (in line with closest packing theory). Comparison of the value for $(1-\varphi)A_{ow}/A_{owo}$ calculated from equation [6.13] with the gradient of a plot of D_{ow} vs D_{owo} for this system (see figure 6.21), reveals that:

$(1-\varphi)A_{ow}/A_{owo}$ = gradient of D_{ow} vs D_{owo}

Hence, from equation [6.12]:

$$6V(2f_{dinv}-1)/A_{owo} = D^0_{owo} \quad \text{[6.14]}$$

where, D_{0owo}=the value of the intercept at D_{ow}=0. Substitution of equation [6.9] in [6.14] gives:

$$f_{dinv} = D_{owo}/[2D_{owo} - D^0_{owo}] \quad \text{[6.15]}$$

From figure 6.21 it can be seen that a plot of D_{ow} vs D_{owo} is linear for each of the higher oil phase viscosity systems. Therefore, it is reasonable to suppose that equations [6.12] and [6.15] will apply to the higher oil phase viscosity systems. Hence, the gradient and intercept value of a plotof D_{ow} vs D_{owo} can be used with equations [6.9] to [6.15] to calculate values of f_{dinv}, $(1-\varphi)A_{ow}/A_{owo}$ and φ for each system at the catastrophic inversion point. The results calculated for each viscosity are tabulated in table 6.7.

Table 6.7 - Catastrophic inversion results calculated from the data of figure 6.21.

Oil phase viscosity	N rpm	D_{owo} μm	D_{ow} μm	f_{winv} experiment	f_{dinv} calculated	φ
0.007 poise	800	255	40	0.73	0.71	0.0
$(1-\varphi)A_{ow}/A_{owo}=2.83$	600	305	57	0.69	0.66	0.0
$D^0_{owo}=150\mu m$	500	345	70	0.65	0.64	0.0
	400	405	90	0.62	0.61	0.0
0.25 poise	800	170	55	0.56	0.71	0.34
$(1-\varphi)A_{ow}/A_{owo}=1.23$	600	180	67	0.53	0.69	0.34
$D^0_{owo}=100\mu m$	500	200	81	0.51	0.67	0.33
	400	220	99	0.50	0.65	0.30
0.5 poise	800	165	65	0.39	0.70	0.51
$(1-\varphi)A_{ow}/A_{owo}=1.00$	600	180	77	0.39	0.68	0.48
$D^0_{owo}=95\mu m$	500	190	95	0.39	0.67	0.46
	400	200	110	0.39	0.66	0.44
1.0 poise	800	156	90	0.36	0.69	0.52
$(1-\varphi)A_{ow}/A_{owo}=0.68$	600	162	113	0.36	0.68	0.50
$D^0_{owo}=85\mu m$	500	167	134	0.36	0.67	0.48
	400	174	156	0.36	0.66	0.47
2.0 poise	800	152	181	0.18	0.66	0.59
$(1-\varphi)A_{ow}/A_{owo}=0.37$	600	156	221	0.18	0.66	0.59
$D^0_{owo}=75\mu m$	500	162	257	0.18	0.65	0.57
	400	166	314	0.18	0.65	0.57

NOTES: Equation [6.12] and the Results of Table 6.7

(i) In the case of the cyclohexane/SML (0.007 poise) system it was noted that $f_{winv}=f_{dinv}$. From table 6.7 it can be seen that the experimental f_{winv} value and the f_{dinv} value calculated from equation [6.15] (using $D^0_{owo}=150\mu m$) are in good agreement. The difference in the values at each stirrer speed, is less than the change in f_w that results from one aliquot addition.

(ii) In the case of the higher oil phase viscosity systems, the dispersed phase fraction at the catastrophic inversion point is in the range 0.65 to 0.71. This is in agreement with closest packing theory.

(iii) The tendency of the water drops to emulsify an increasing volume of oil phase (as oil drops in $O/W_m/O$ drops) as the oil phase viscosity rises, is shown by the value of φ for each oil phase viscosity.

(iv) Table 6.7 shows that the increase in f_{dinv} with increase in stirrer speed seen in the 0.007 poise system, also occurs in the higher oil phase viscosity systems. It is now possible to discuss an upper and lower limit on the value of f_{dinv}:

Upper limit

Although the upper limit on f_{dinv} set by equation [6.15] is 1.0, the maximum dispersed phase fraction that is physically possible in an unstable emulsion is unlikely to be >0.85. Using this limit it is possible to calculate a minimum set of D_{owo}, D_{ow} values at inversion (from equations [6.15] and [6.12]) for each oil phase viscosity (see table 6.8):

Table 6.8 - Minimum drop diameter sizes at maximum f_{dinv}.

Oil Phase Viscosity (poise)	D_{ow} μm	D_{ow} μm
0.007	182*	11
0.25	121	17
0.50	115	20
1.00	103	26
2.00	91	43

* An estimate of the stirrer speed required to produce an $O/W_m/O$ emulsion (0.007 poise system, f_{dinv}=0.85) can be obtained using equation [6.1]. Estimated stirrer speed = 1300 rpm.

Lower limit

A lower limit of f_{dinv} can be obtained from equation [6.14]. Examination of equation [6.14] reveals that f_{dinv} must be >0.5 (providing $D^0_{owo}>0$) because A_{owo} cannot physically be negative. This limit is reached when $D_{owo}\rightarrow\infty$.

(v) Also, from equation [6.12], a physical limit on the slope of a plot of D_{owo} vs D_{ow} is apparent. The gradient must be >0 because $(1-\varphi)A_{ow}/A_{owo}$ cannot be negative. From figure 6.21 it can be seen that this limit is controlled by the viscosity ratio R_v.

(vi) Figure 6.21 shows that the catastrophic inversion point D_{owo} vs D_{ow} lines at constant oil phase viscosity, tend to converge as D_{owo} decreases. At the intercept $D^0_{owo} = 6V/A^0_{owo}$ and $f_{dinv}=1$, hence, equation [6.] reduces to:

$$V=D^0_{woo}A^0_{owo}/6$$

Therefore, the intercept value at $D_{ow}=0$ is dependent on factors that affect the drop sizes of emulsions ie. the dynamic conditions and physical properties of the system. It was noted above that as we move down a line of constant oil phase viscosity towards $D_{ow}=0$, the value of D_{owo} decreases and f_{dinv} increases, hence, the stirrer speed required would have to increase. With increasing stirrer speed the effect of the continuous phase viscosity on the drop sizes of emulsions diminishes. When a turbulent flow condition is reached at each oil phase viscosity (the continuous phase), the changing oil phase viscosity will have no effect on the D_{owo} size (if drop break up is by turbulent eddies). Hence, the lines of constant oil phase viscosity are expected to converge as D_{owo} decreases.

However, at $D_{ow}=0$ the flow regime in the case of each oil phase viscosity is expected to be turbulent (note the position of the Ultra-Turrax points on figure 6.21). The fact that the lines of constant oil phase viscosity have not converged when $D_{ow}>0$ is because of the differences in the value of f_{winv} with change in oil phase viscosity.

It can be seen from figure 6.21 that the (D_{ow},D_{owo}) points for agitation supplied by an Ultra-Turrax are in reasonably good agreement with the turbine agitator results. The Ultra-Turrax points are not expected to lay exactly on the lines of constant oil phase viscosity because of the change in the vessel geometry.

6.7.12 CATASTROPHIC INVERSIONS OF THE TYPE $O_m/W+W/O_m/W$ to W/O_m

From the observations made on the catastrophic inversion when a low viscosity oil phase was used, it is apparent that there is no difference in the mechanism of catastrophic inversion between inversions, $O_m/W+W/O_m/W$ to W/O_m and inversions $W_m/O+O/W_m/O$ to O/W_m. The same phenomena were seen through the catastrophic inversion run ie. as the dispersed phase fraction increased the drop sizes increased and $W/O_m/W$ drops were formed, large water drops were present in the inverted W/O_m emulsion and these could be further broken up by prolonged agitation. Hence, it may be expected for low oil phase viscosity systems, that similar results to those found for W_m/O to O/W_m inversions will apply to O_m/W to W/O_m inversions.

Differences in the catastrophic inversion mechanism were found in the 1 poise oil viscosity experiment. In this experiment the stable emulsion form has the higher viscosity phase as the continuous phase. The differences in mechanism observed can all be anticipated in respect of Selker et al's (1965) observation, that the high viscosity phase will tend to become the dispersed phase. Hence, we may expect:

(a) Few $W/O_m/W$ drops to formed in high oil phase viscosity systems because the initially dispersed oil phase drops will resist the entrainment of continuous phase.

(b) A high dispersed phase fraction at inversion (this fits with the trend seen on figure 6.9, where as the viscosity ratio ($R=\mu_d/\mu_c$) for the inital dispersion conditions increases, a higher dispersed phase fraction was required at inversion).

(c) That mechanical energy will be required to break down the $O_m/W/O_m$ drops of the inverted emulsion that form as an initial stage after a closest packed condition is reached.

Therefore, in high oil phase viscosity catastrophic inversions of the type O_m/W to W/O_m, there are two competing factors:

(i) The tendency of the phase of highest viscosity to "want" to become dispersed, and,

(b) the tendency of the surfactant we have chosen here, to "want" to make the high viscosity phase continuous.

This completes this chapter on drop sizes in catastrophic inversions. In the last chapter, the findings discussed in chapters 2, 3, 5 and 6, will be drawn together in a concluding discussion.

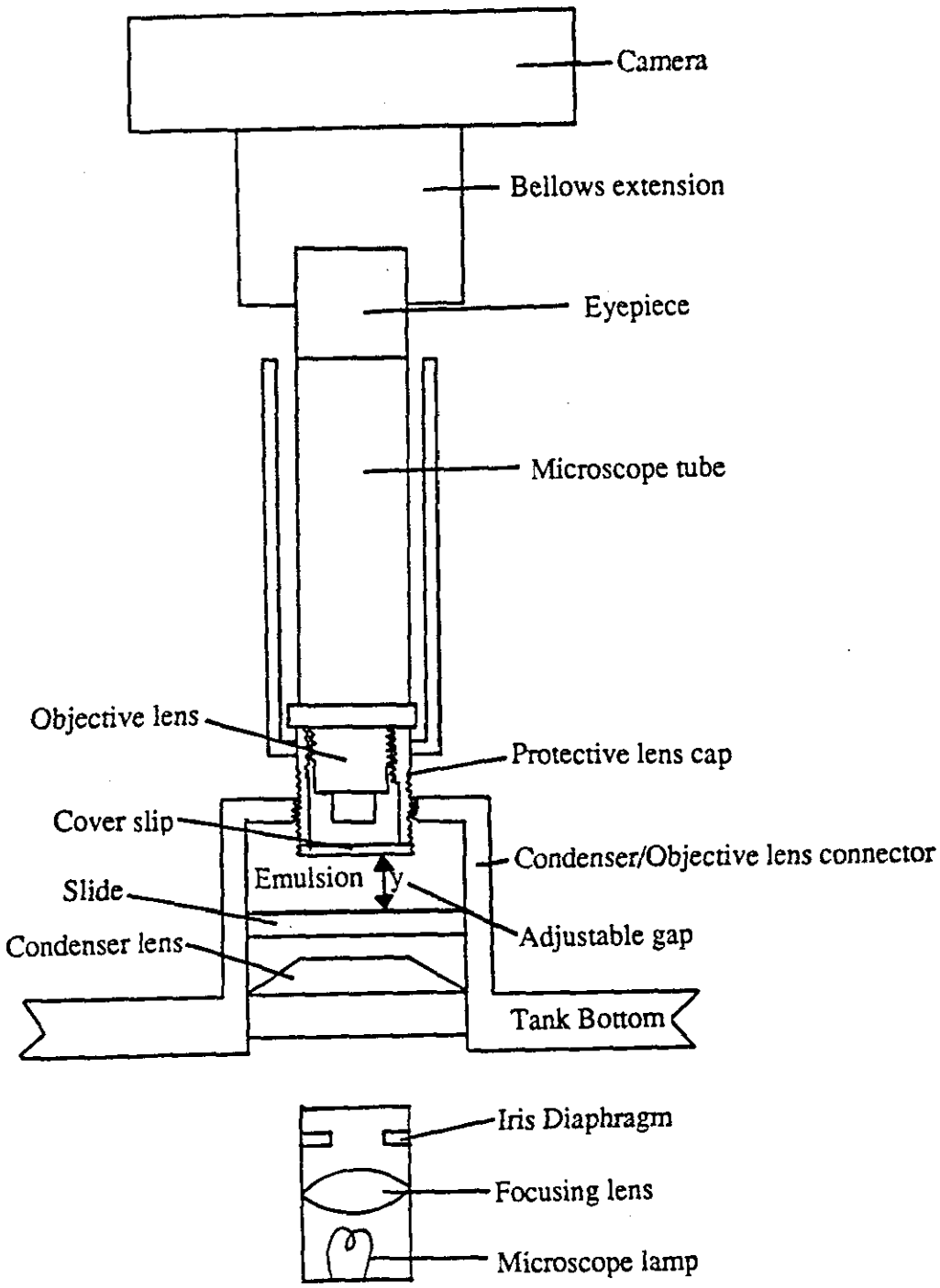

FIGURE 6.1 - Microscope probe designed to size unstable drops from within a stirred vessel.

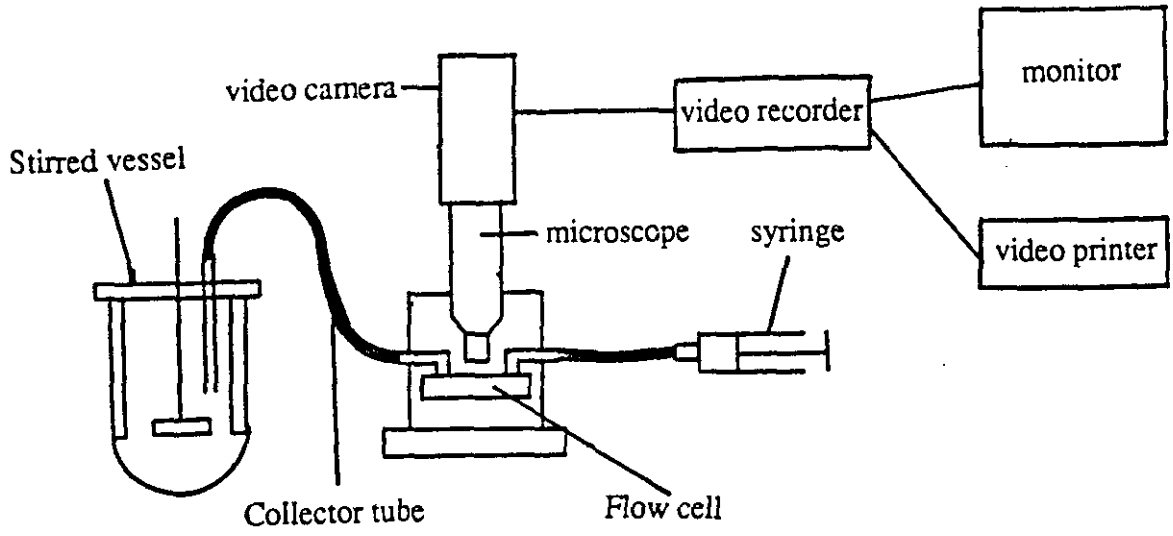

FIGURE 6.2(a) - Flow cell arrangement.

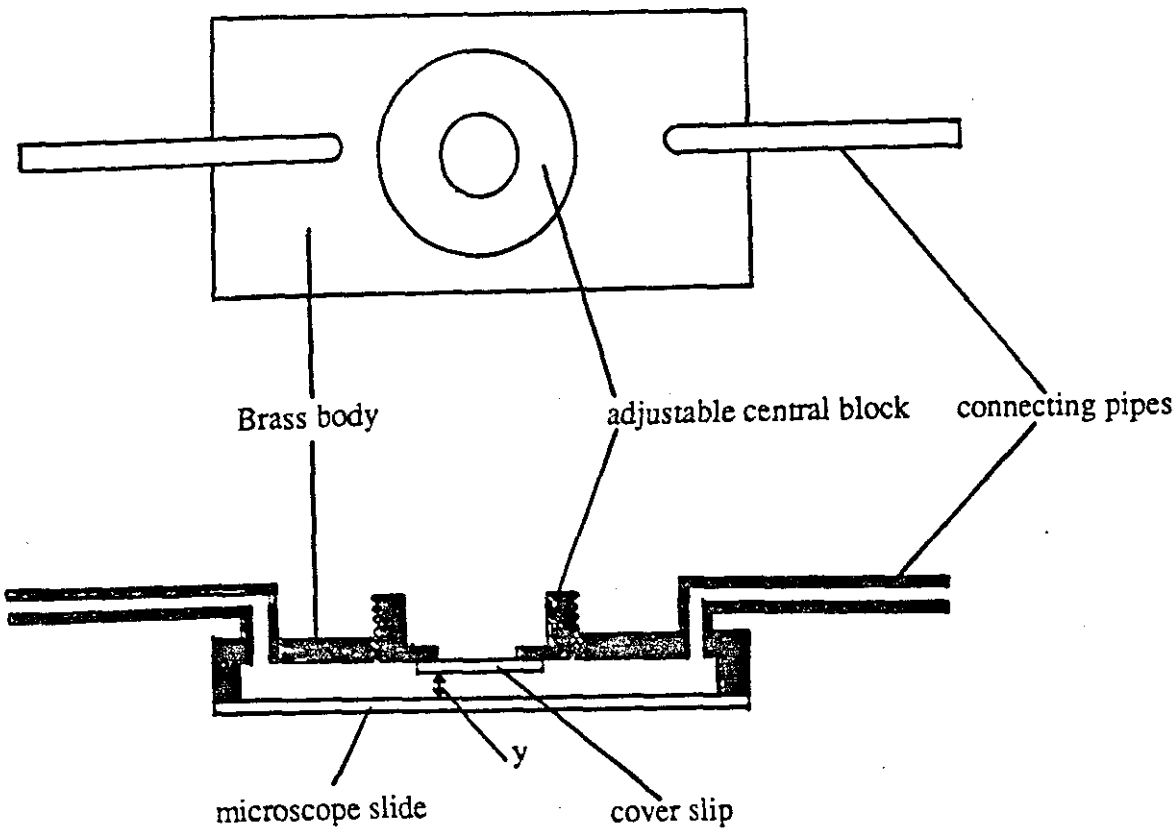

FIGURE 6.2(b) - Flow cell.

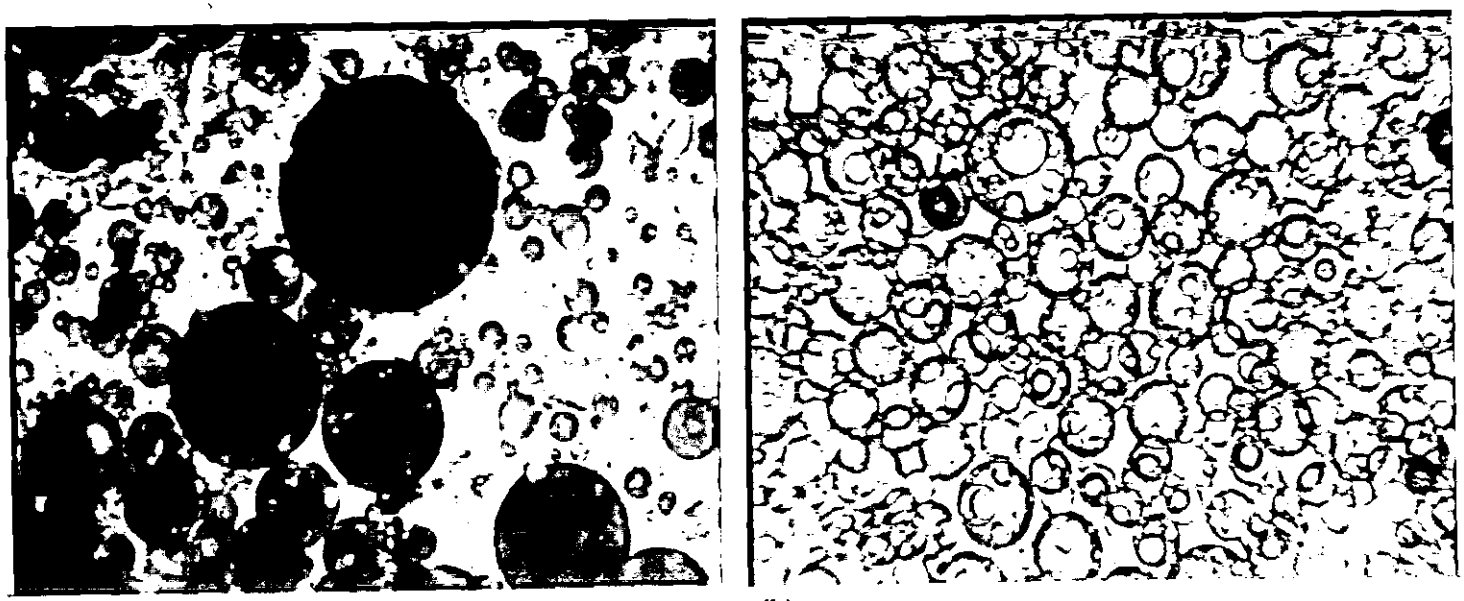

FIGURE 6.3 - O/W_m/O drop types in cyclohexane/NPE, (a), and cyclohexane/SML, (b), systems.

(All Cyclohexane/NPE12 system)

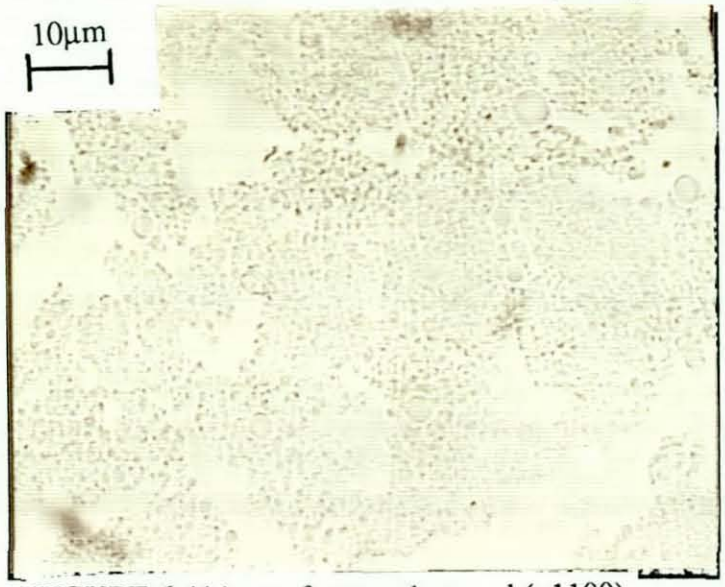

FIGURE 6.4(a) - surfactant phase gel (x1100).

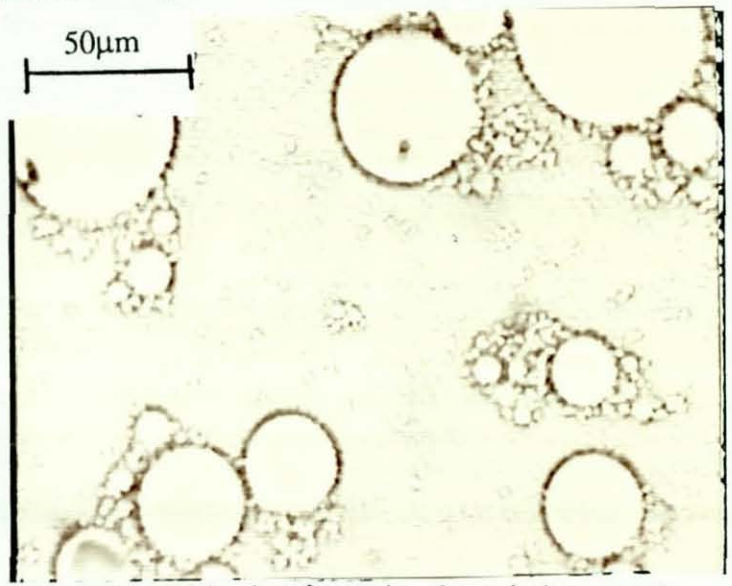

FIGURE 6.4(b) - 1 to 2μm size drops in between large drops (x440).

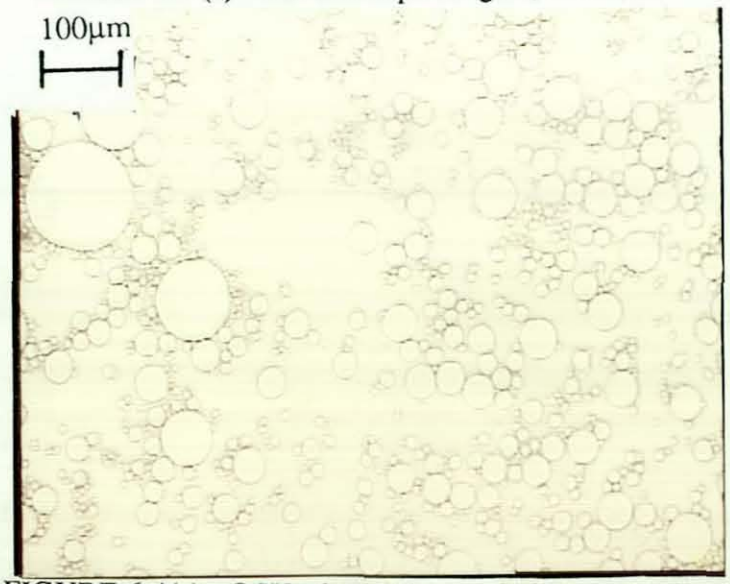

FIGURE 6.4(c) - O/W_m drops (from within a water drop) just prior to catastrophic inversion (x110)

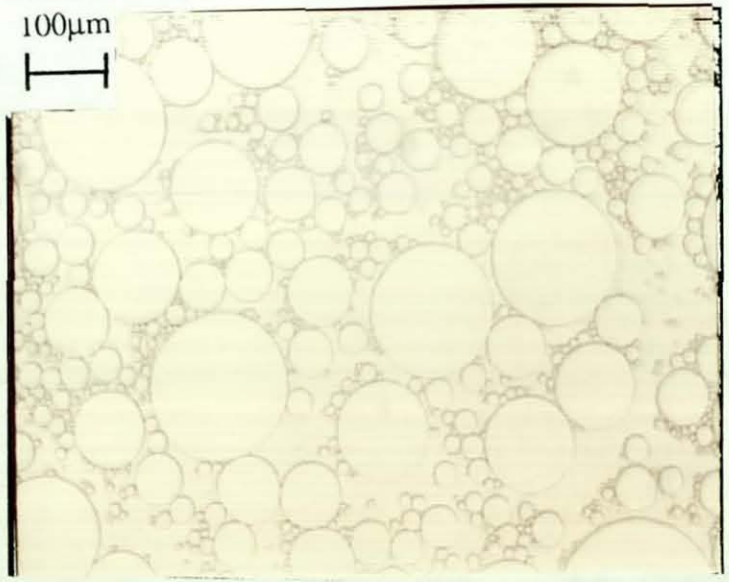

FIGURE 6.4(d) - O/W_m emulsion drops at the catastrophic inversion point (x110)

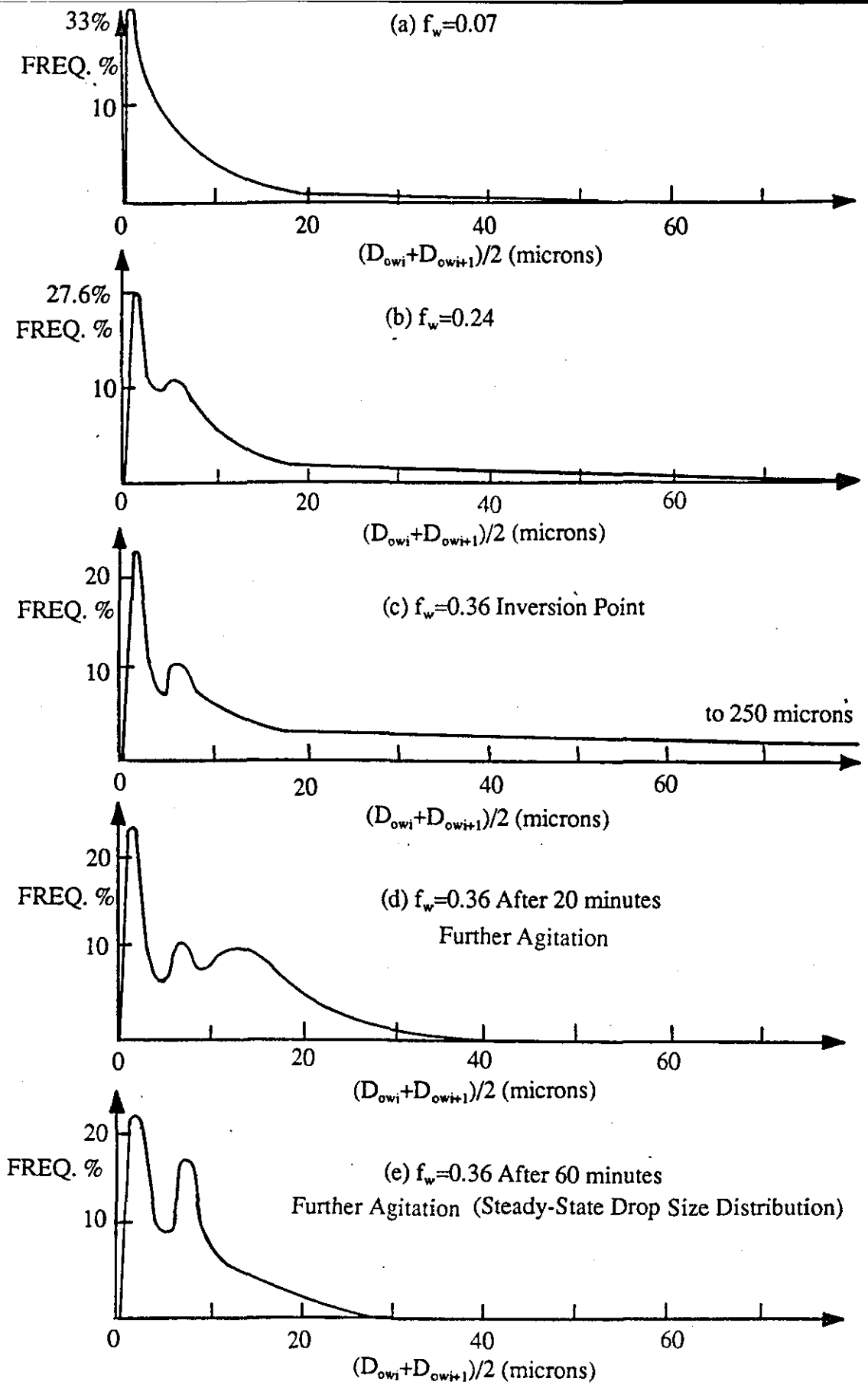

FIGURE 6.5 - The change in the oil drop size distribution of oil drops in $O/W_m/O$ and O/W_m emulsions with f_w (N=600 rpm, rate of addition = 20ml/2min).

Where, D_{owi} = drop diameter of size interval i (average value of D_{owi} and D_{owi+1} is used to obtain a continuous curve from histogram data).

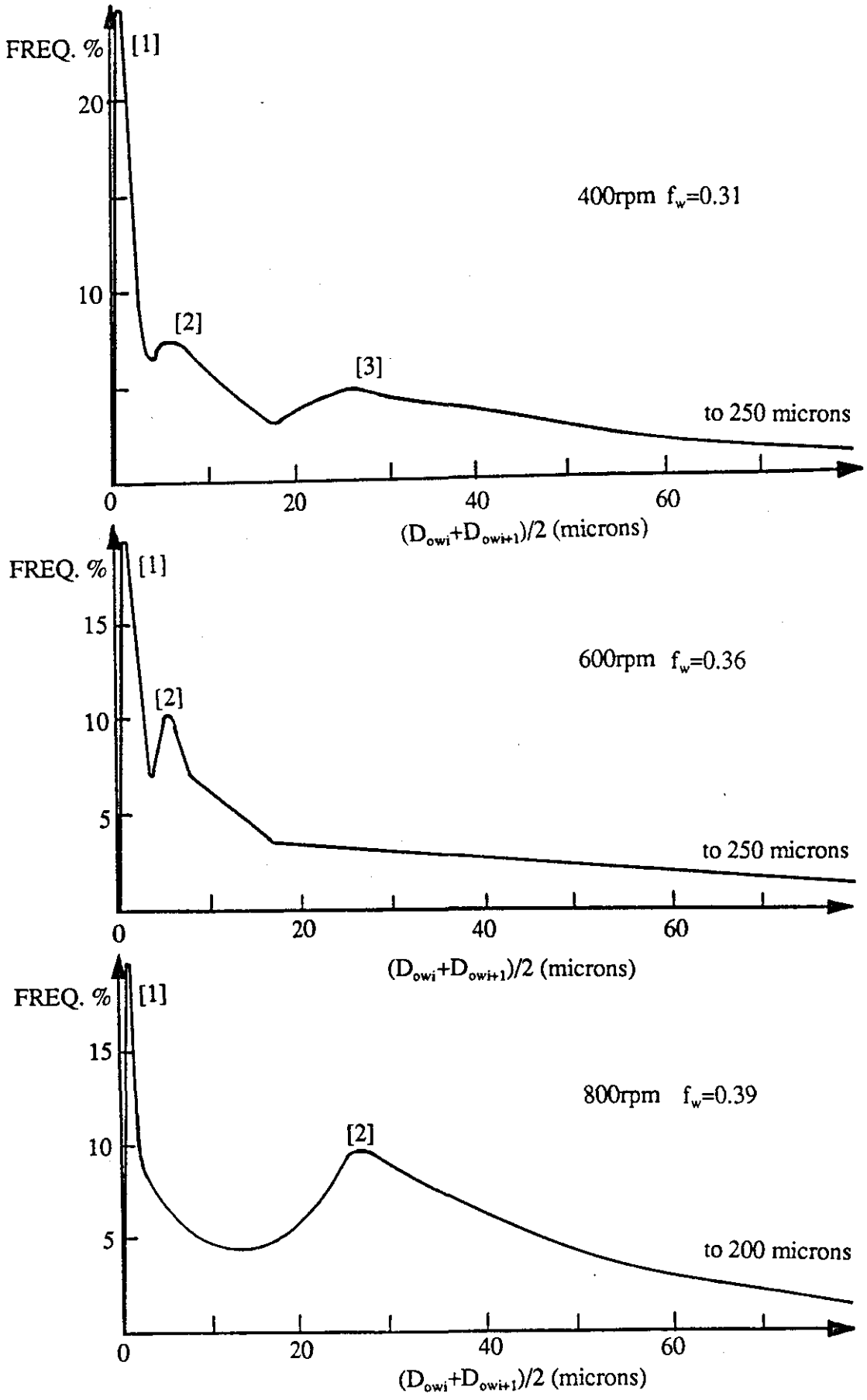

FIGURE 6.6 - Change in the inverted O/W_m emulsion's drop size distribution with stirrer speed (N) (cyclohexane/NPE systems). (water addition rate = 20ml/2min)

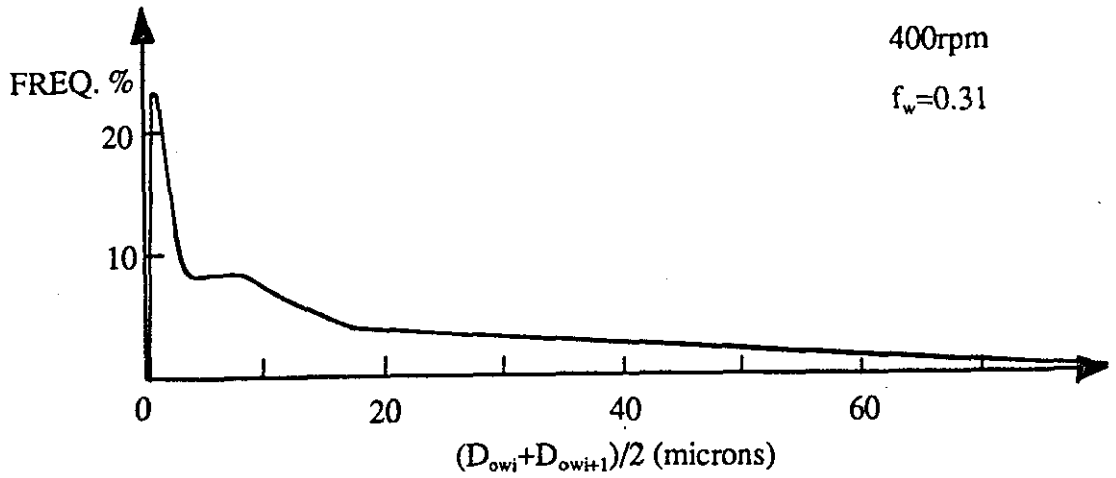

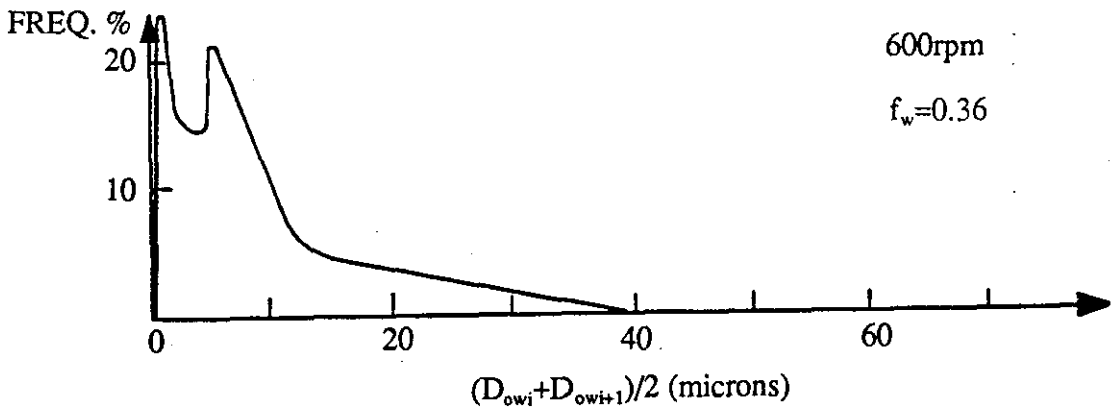

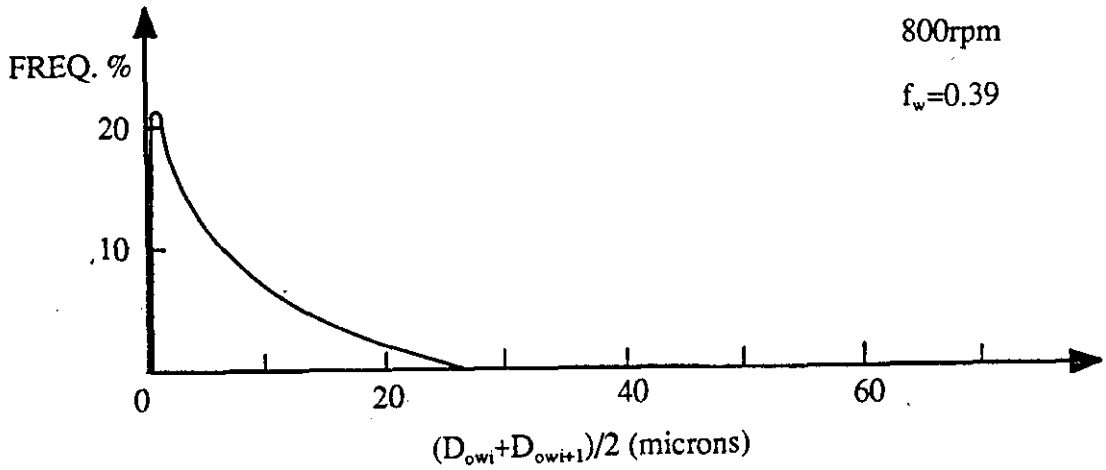

FIGURE 6.7 - Cyclohexane/NPE systems, variation of steady-state O/W_m emulsion size distribution with stirrer speed N (ie after 1 hours direct emulsification).

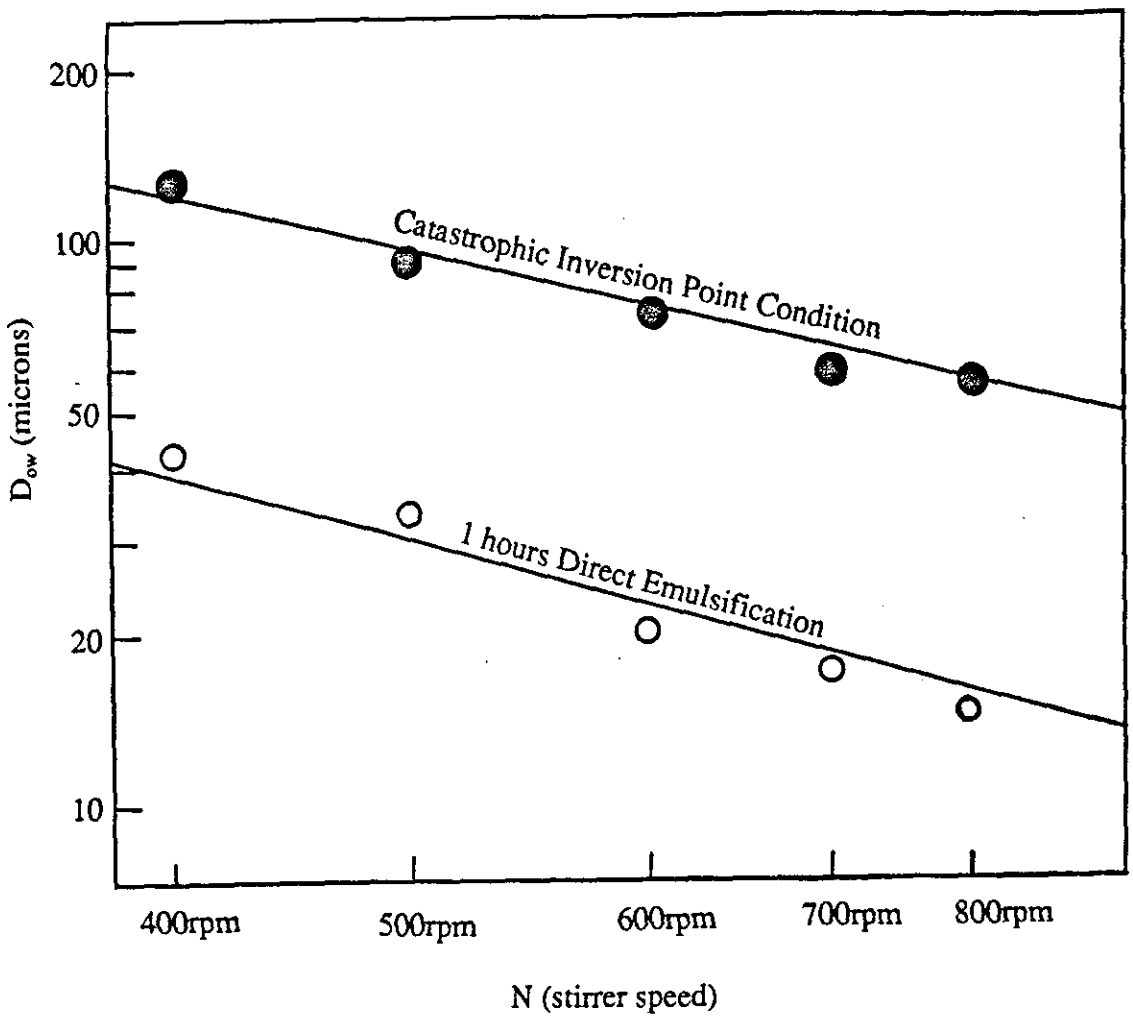

FIGURE 6.8 - Cyclohexane/NPE12 system - D_{ow} vs N (Stirrer speed).

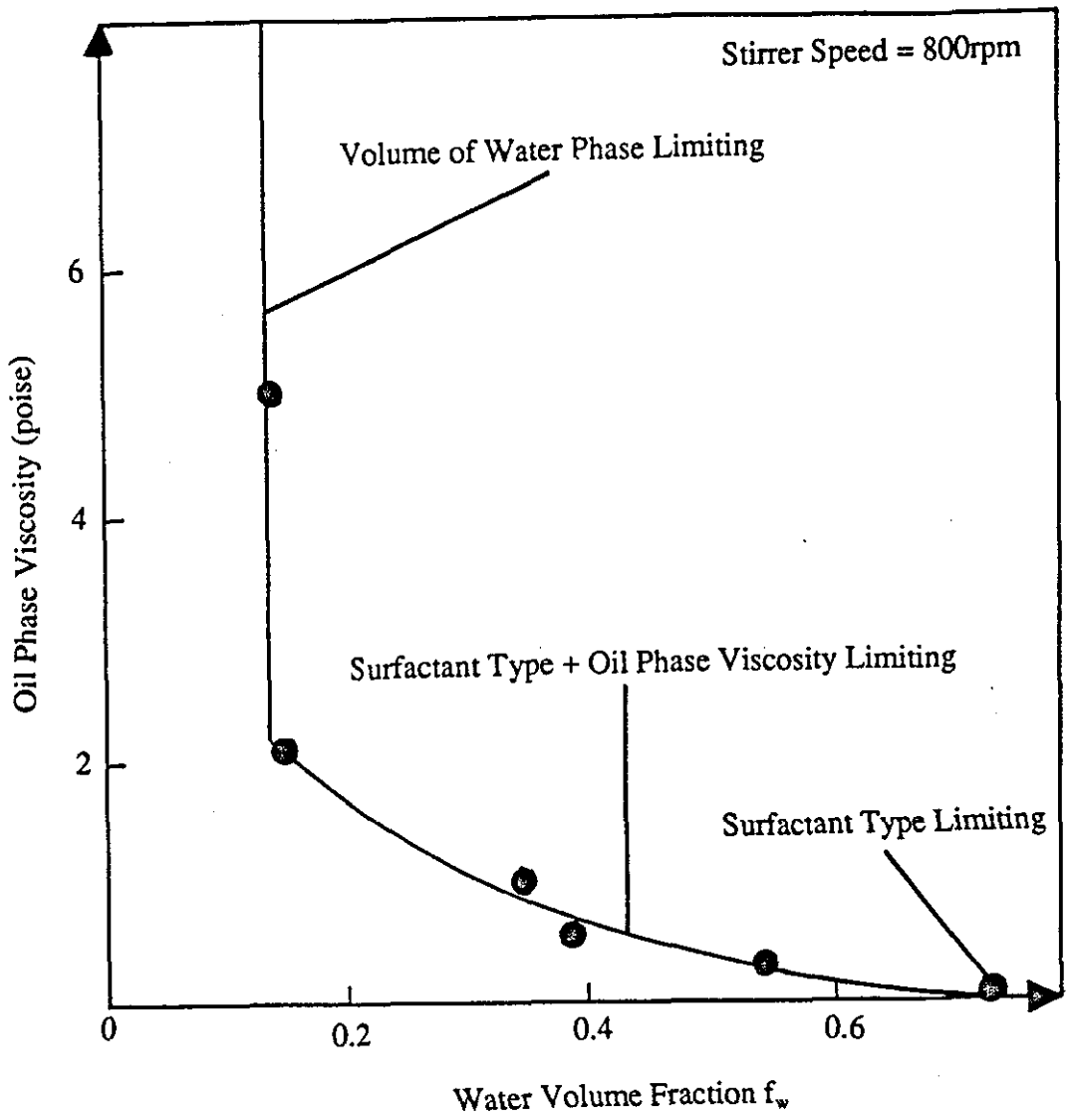

FIGURE 6.9 - The effect of the Oil Phase Viscosity on the value of f_w at the Catastrophic Inversion Point.

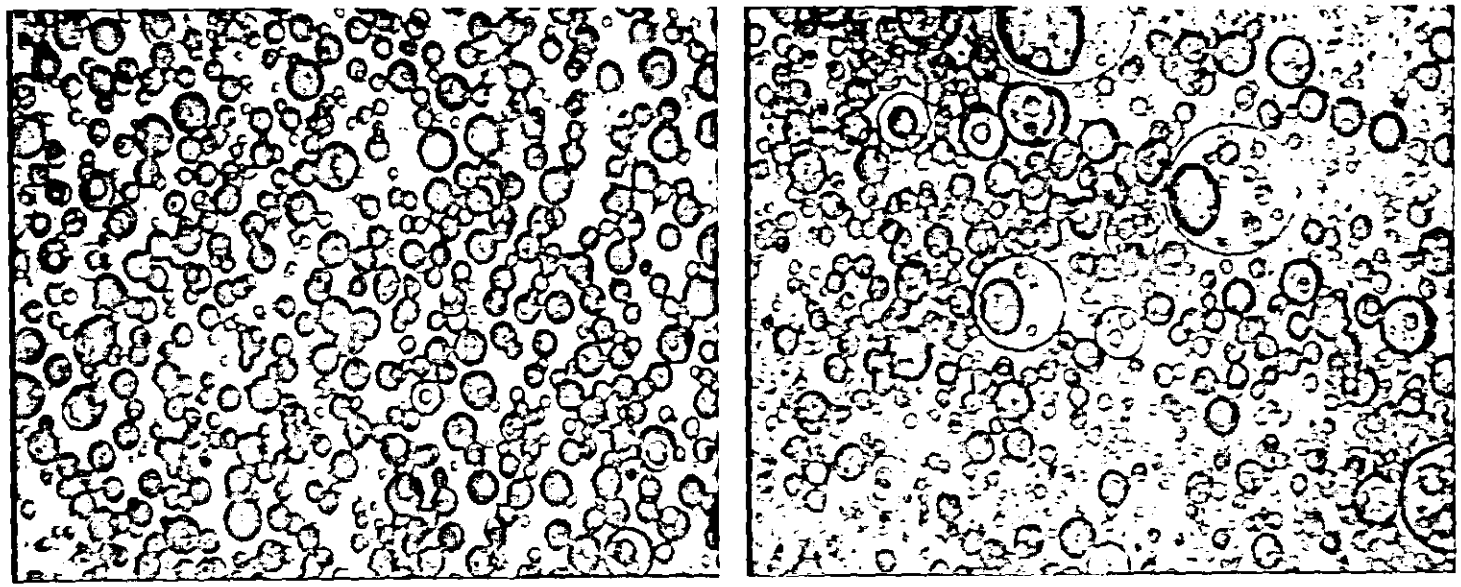

FIGURE 6.10 - PIB-Cyclohexane/SML: O/W_m/O drop types present in (a) low oil phase viscosity systems, (b) high oil phase viscosity systems. (N=600rpm, rate of addition=20ml/2min)

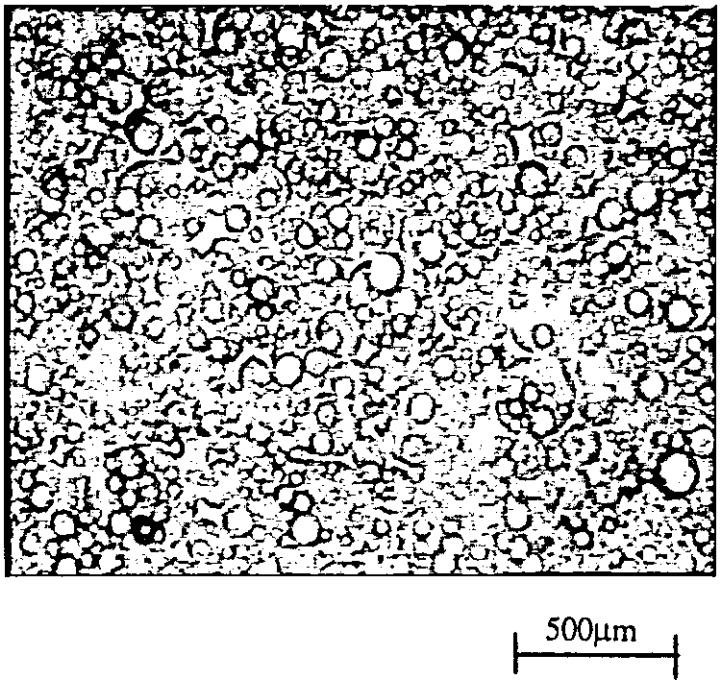

FIGURE 6.11 - PIB-Cyclohexane/SML system (0.25 poise) one aliquot addition from catastrophic inversion.

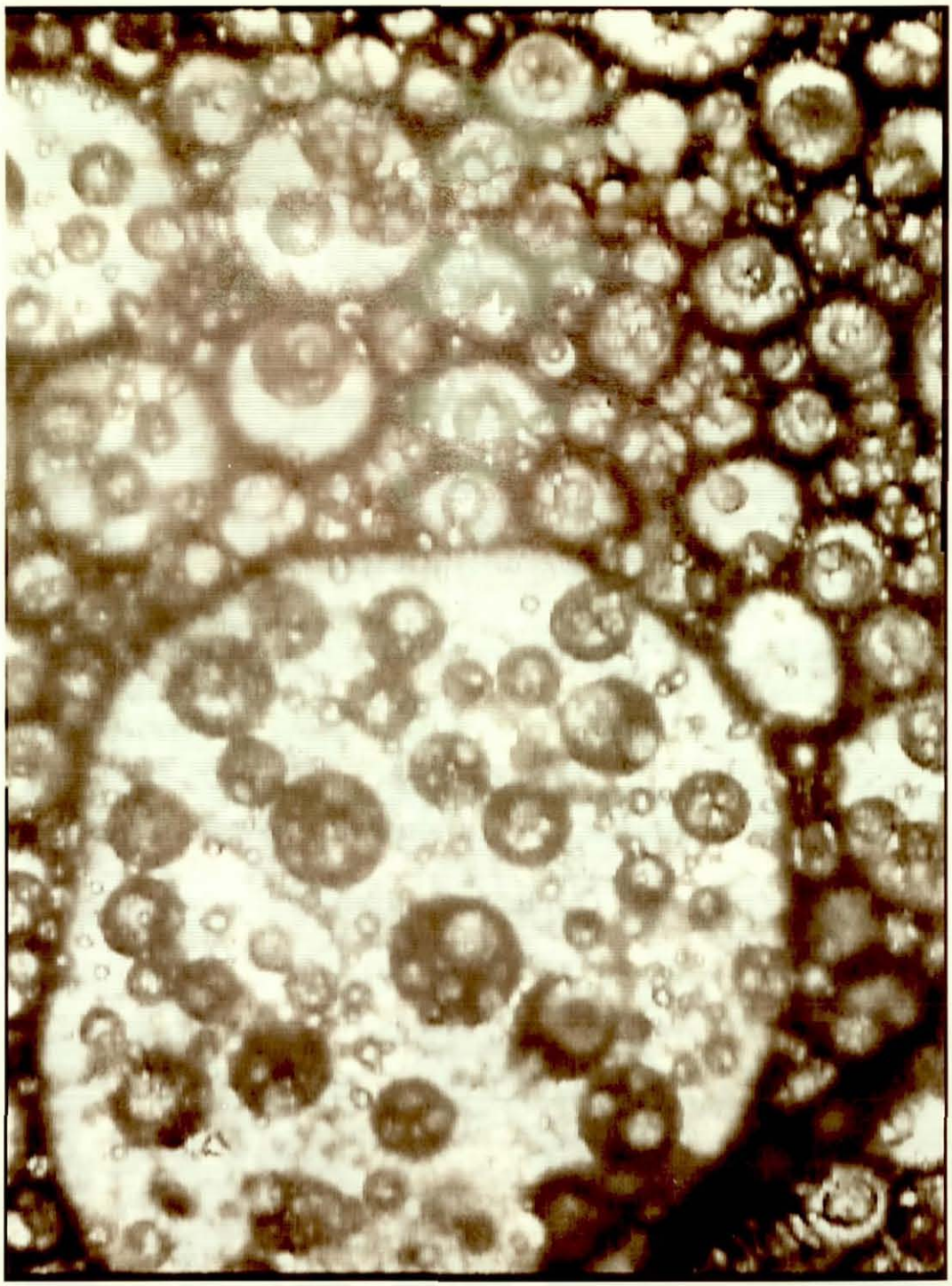

FIGURE 6.12 - PIB-Cyclohexane/SML system: Structure of the 2.0 poise system at the catastrophic inversion point (x88) - N=400 rpm.

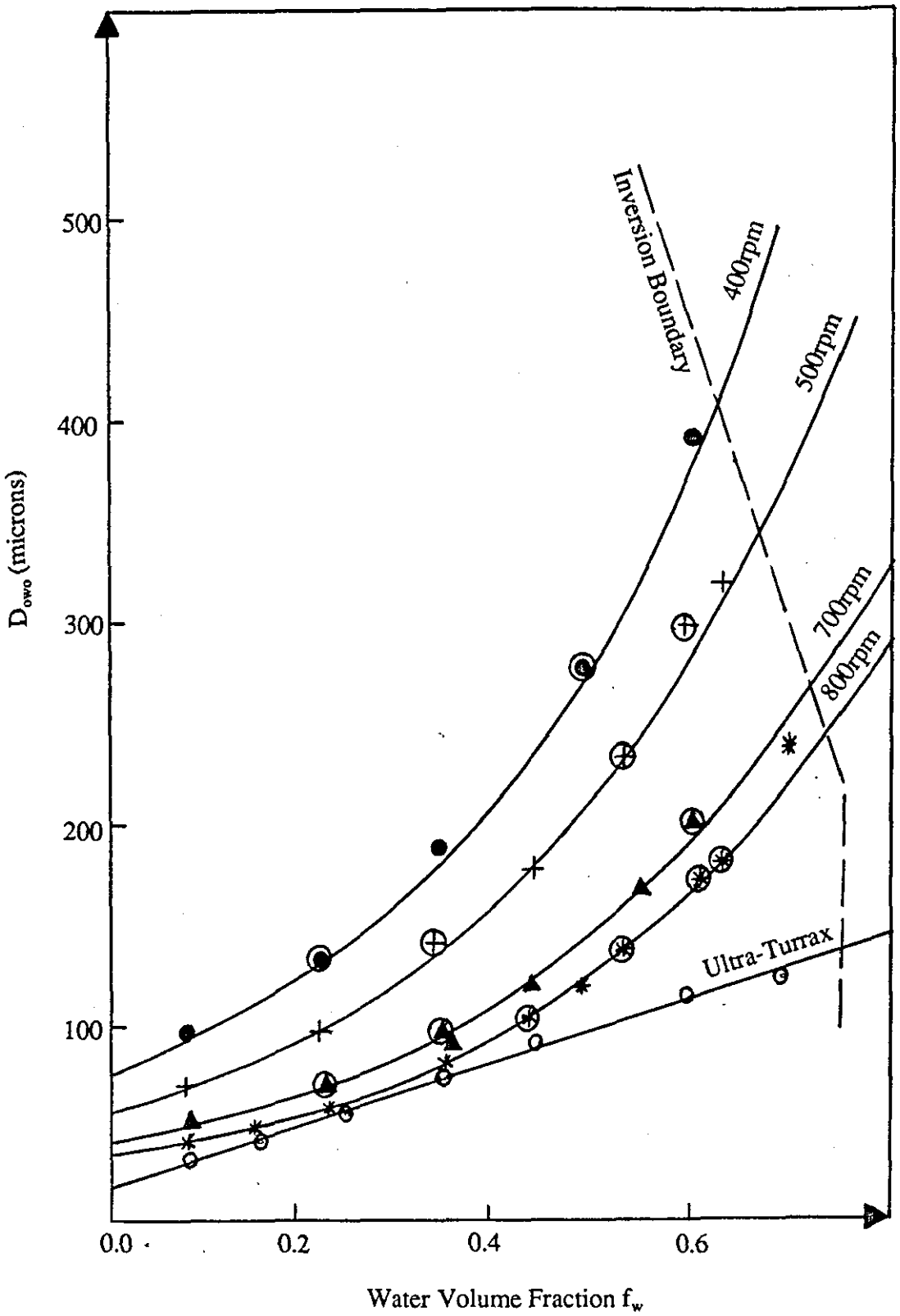

FIGURE 6.13 - D_{owo} vs f_w cyclohexane/SML (0.007 poise) system (rate of addition = 40ml/2min). The lines are the prediction of equation [6.1]. The points circled are calculated from the results at other stirrer speeds assuming $D_{owo} \propto N^{-1.2}$ (plotted to show the "goodness" of fit of equation [6.1]).

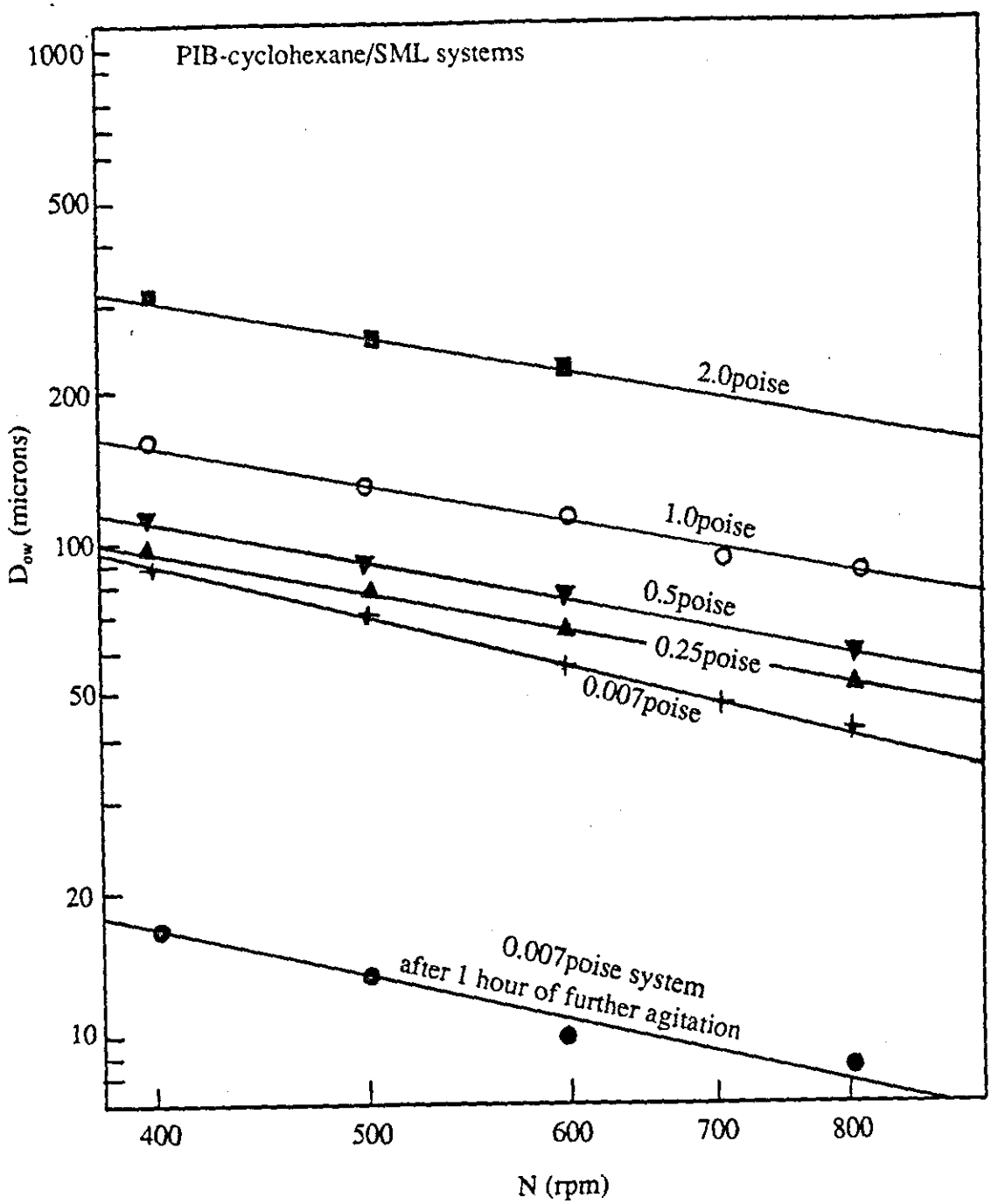

FIGURE 6.14 - D_{ow} vs N (Stirrer speed) for the O/W_m emulsions formed at the catastrophic inversion point. 0.007 poise results refer to a baffled vessel and the higher oil phase viscosity results to an unbaffled vessel.

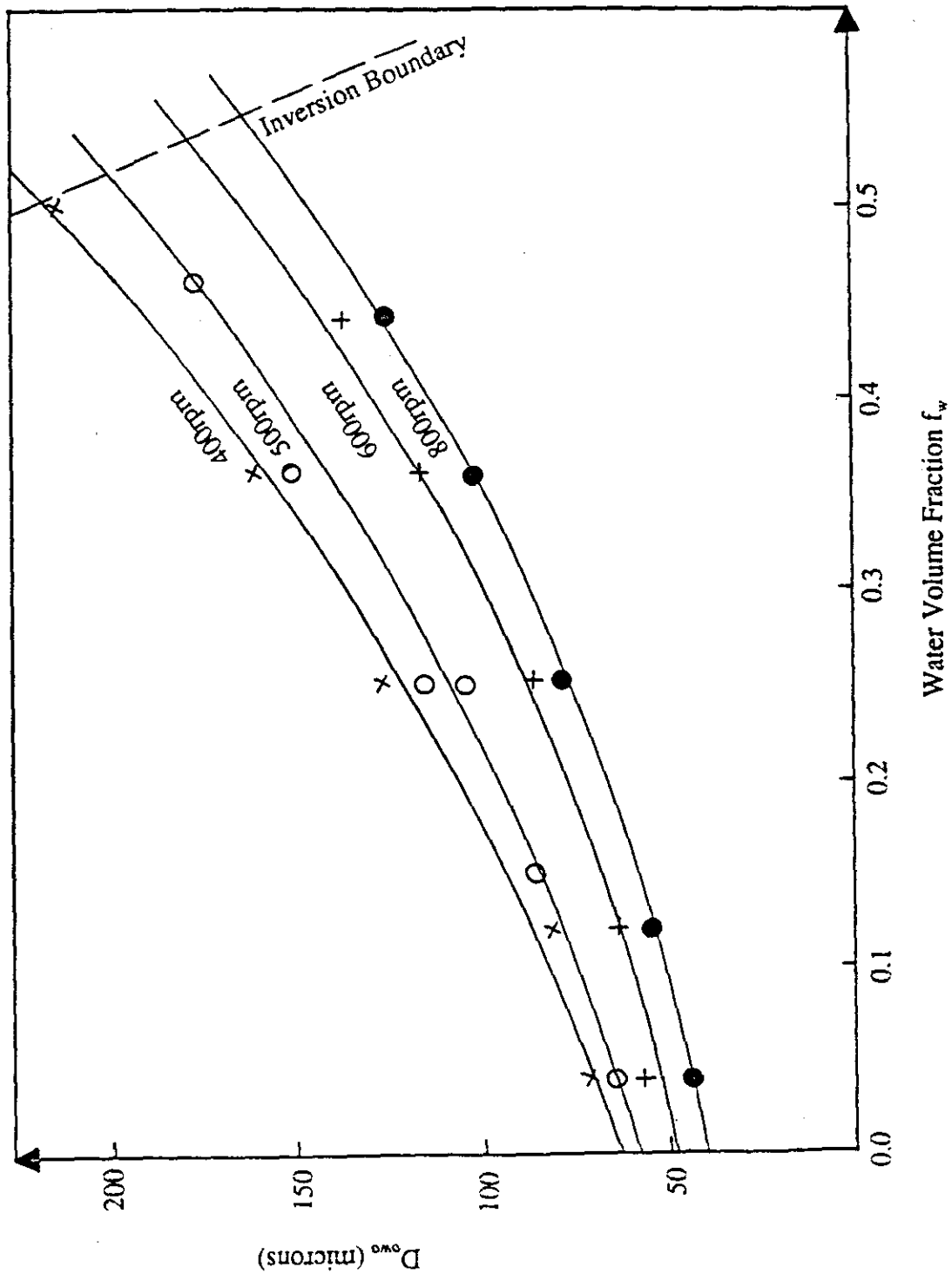

FIGURE 6.15 - D_{owo} vs f_w PIB-cyclohexane/SML (0.25 poise) system (rate of addition = 20ml/2min). The lines are the prediction of equation [6.2].

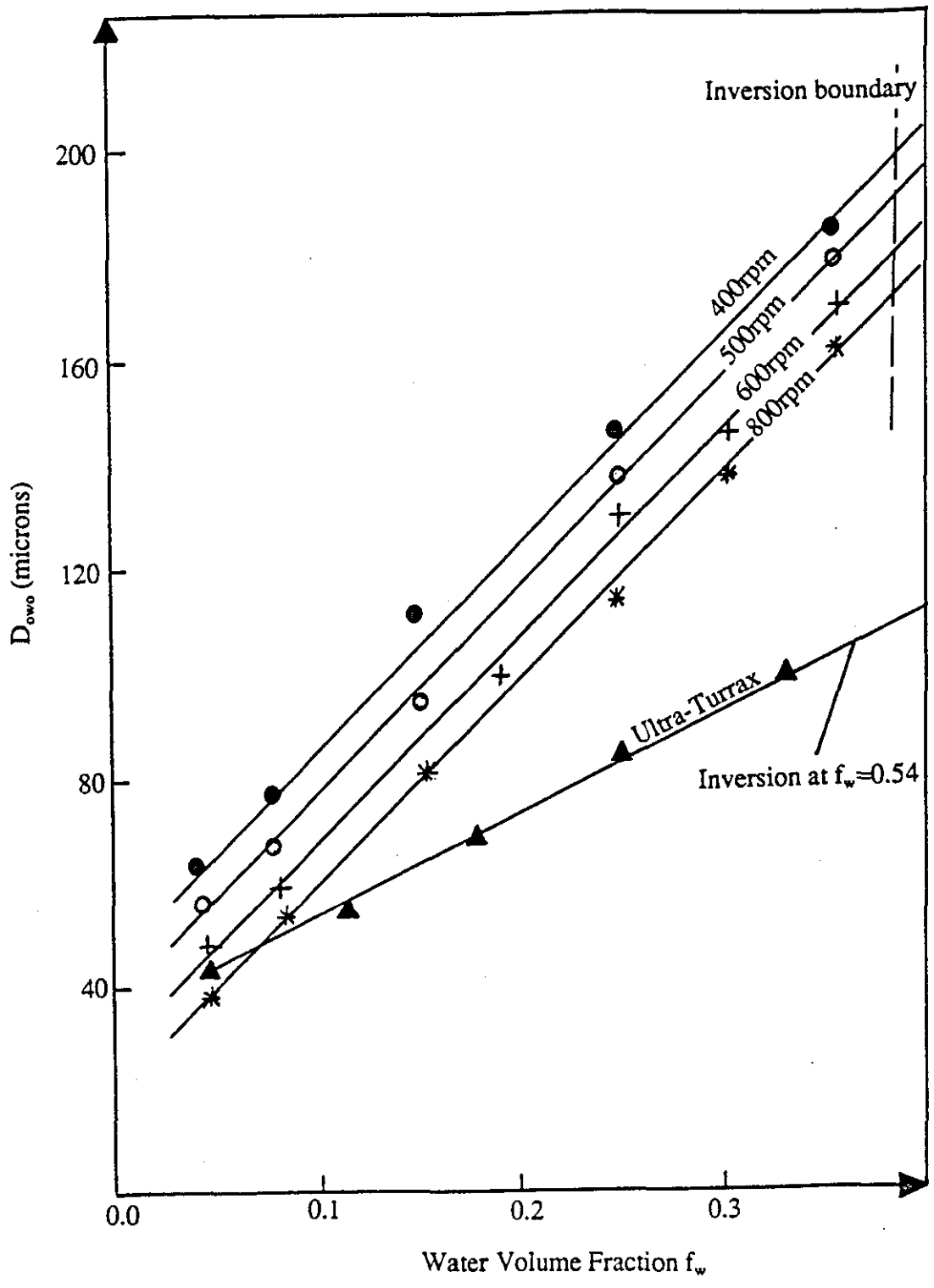

FIGURE 6.16 - D_{owo} vs f_w PIB-cyclohexane/SML (0.5 poise) system (rate of addition = 20ml/2min).

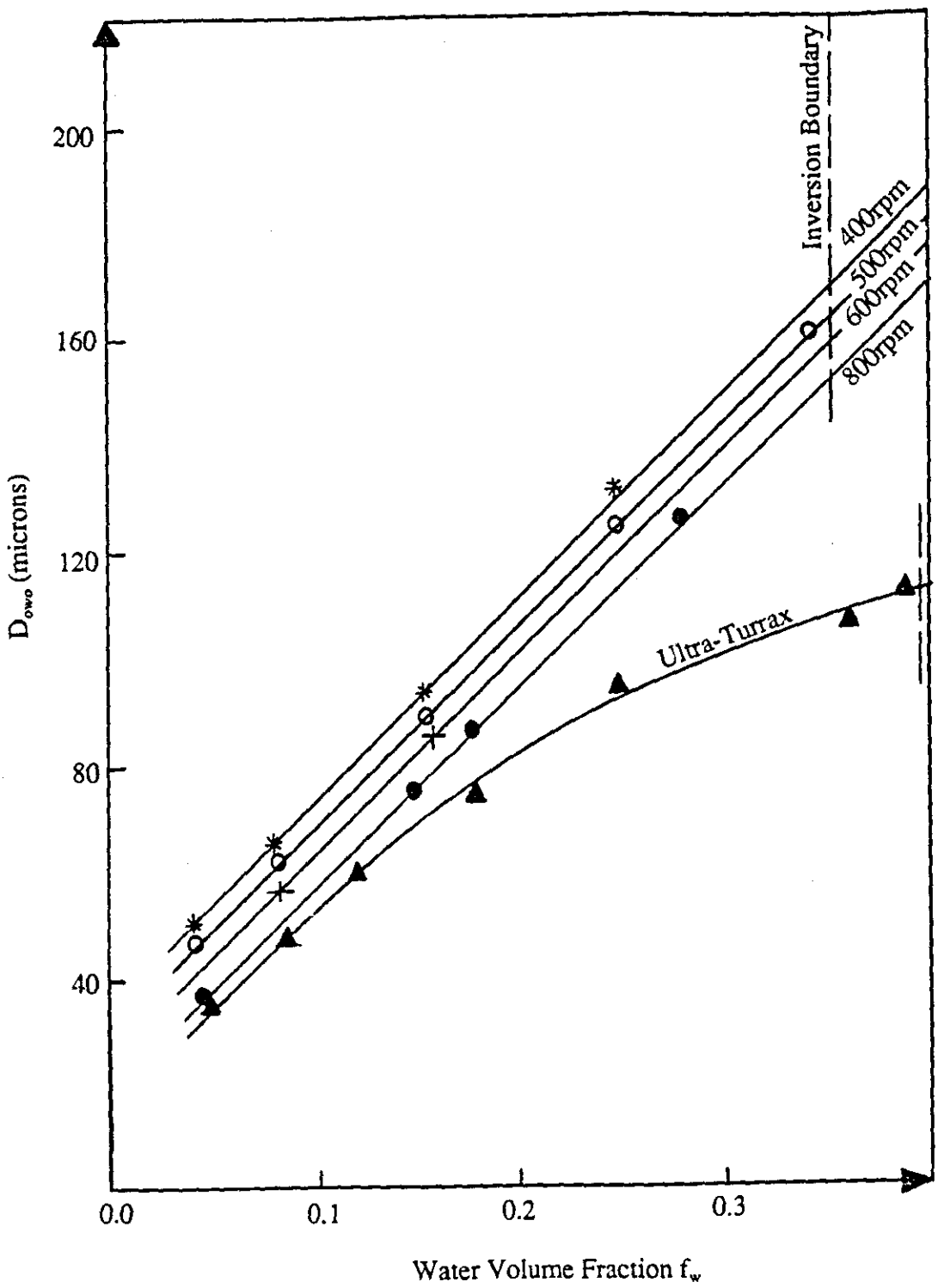

FIGURE 6.17 - D_{owo} vs f_w PIB-cyclohexane/SML (1.0 poise) system (rate of addition = 20ml/2min).

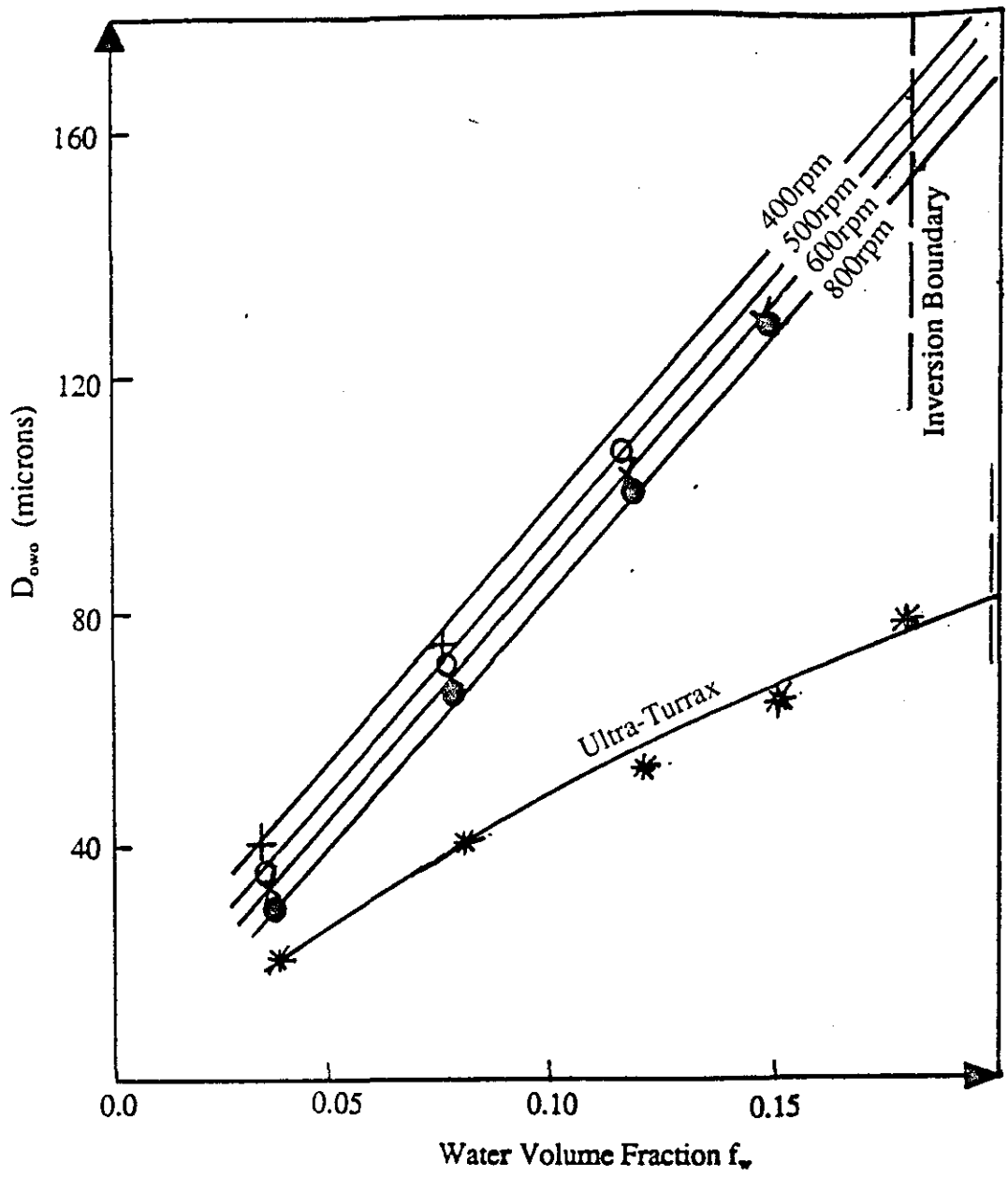

FIGURE 6.18 - D_{owo} vs f_w PIB-cyclohexane/SML (2.0 poise) system (rate of addition = 20ml/2min).

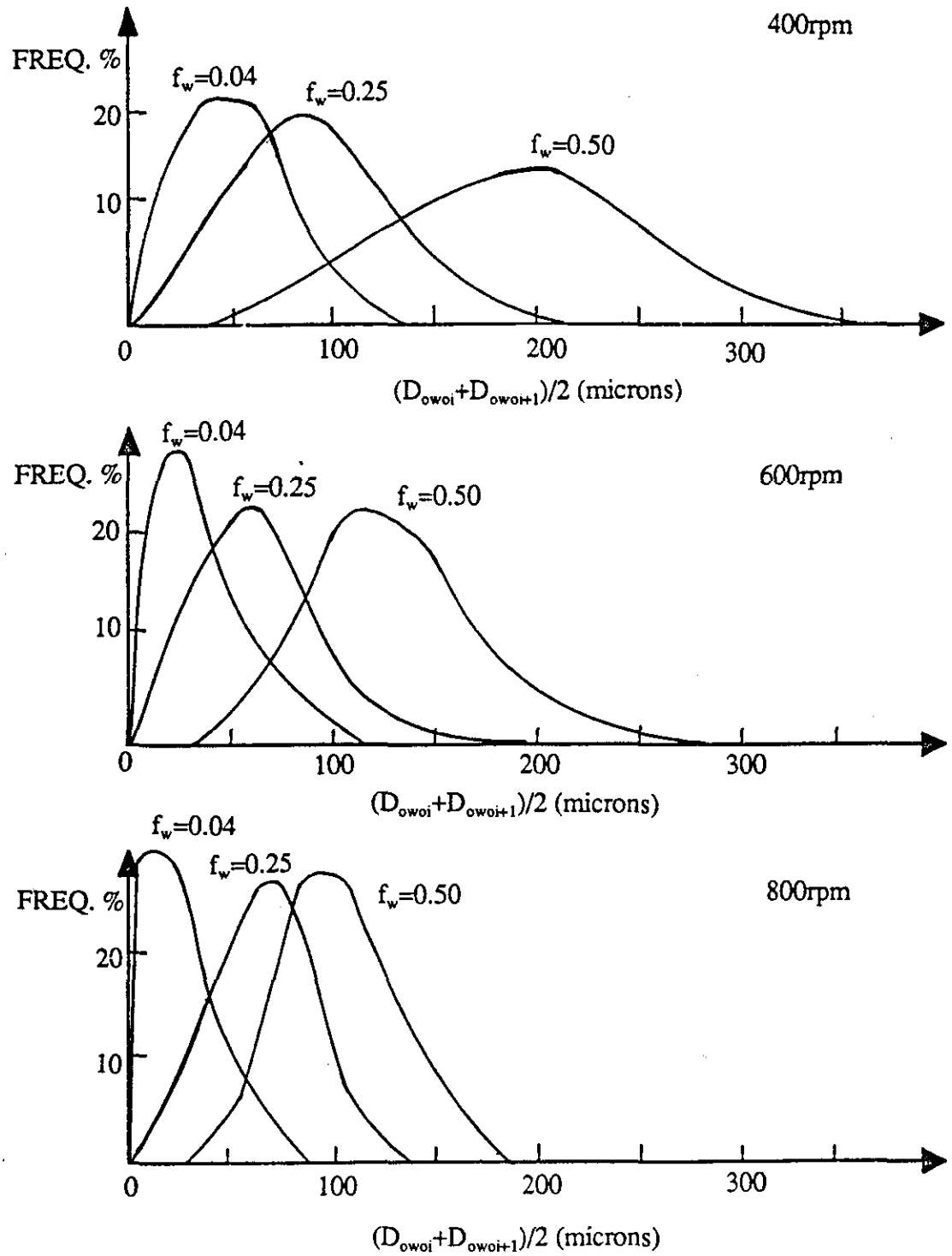

FIGURE 6.19 - PIB-Cyclohexane/SML 0.25 poise system: Change in the $O/W_m/O$ drop size distribution with f_w at three different stirrer speeds.

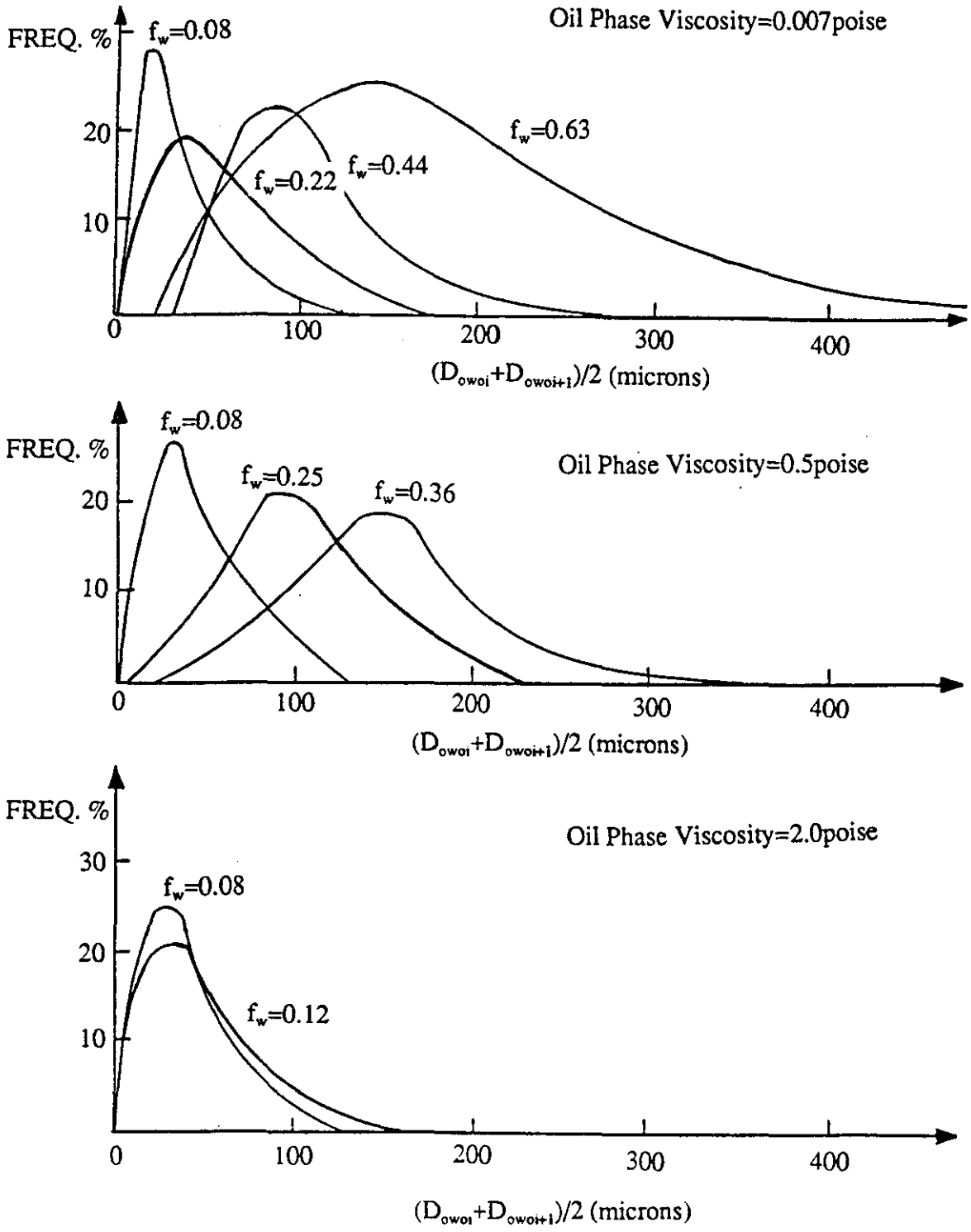

FIGURE 6.20 - PIB-Cyclohexane/SML system: Change in the $O/W_m/O$ drop size distribution with f_w at three different oil phase viscosities (500 rpm).

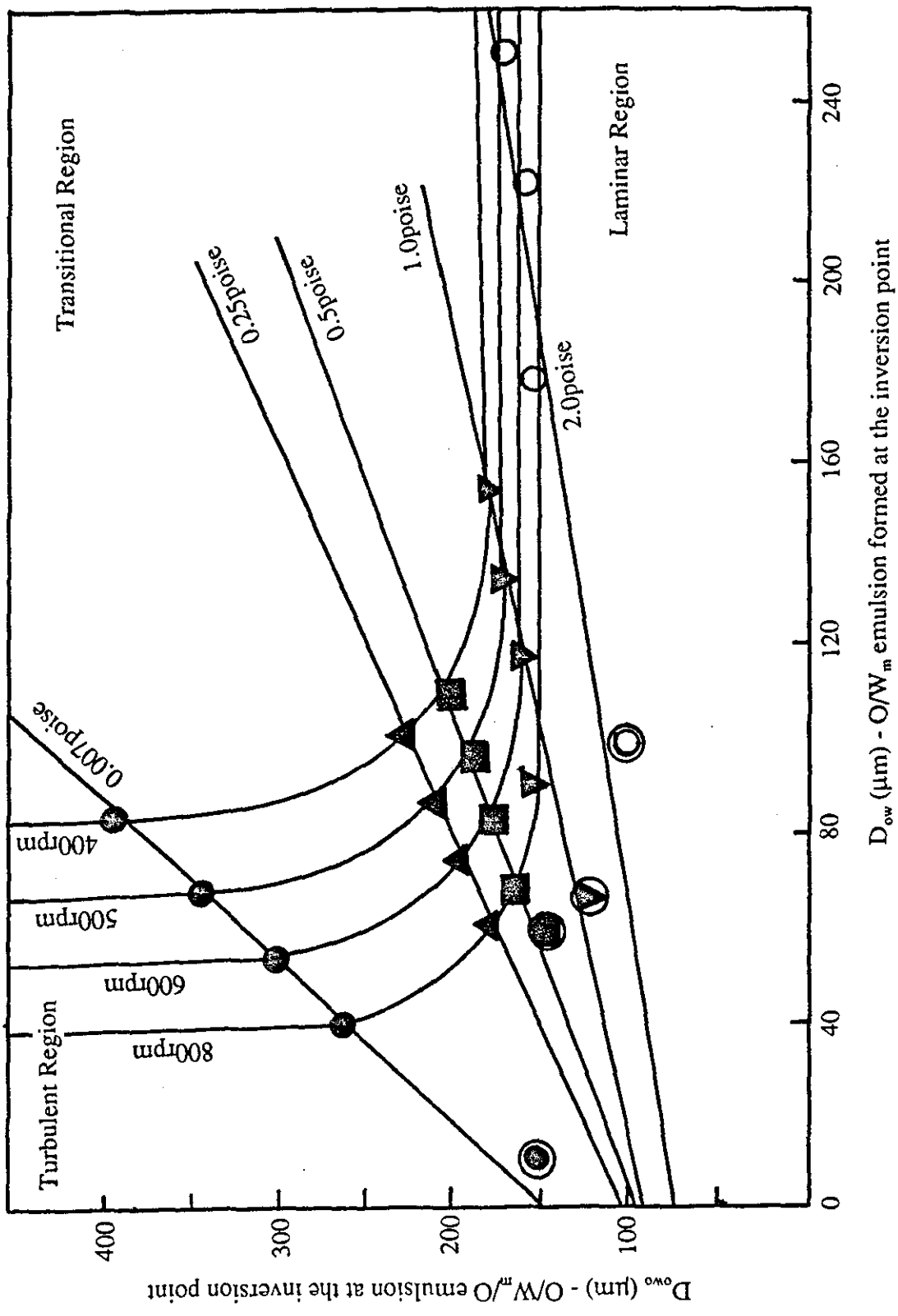

FIGURE 6.21 - PIB-Cyclohexane/SML system: Plot of D_{owo} at the catastrophic inversion point, against D_{ow} of the O/W$_m$ emulsion formed at the catastrophic inversion point (the circled points refer to results obtained when agitation was supplied by an Ultra-Turrax).

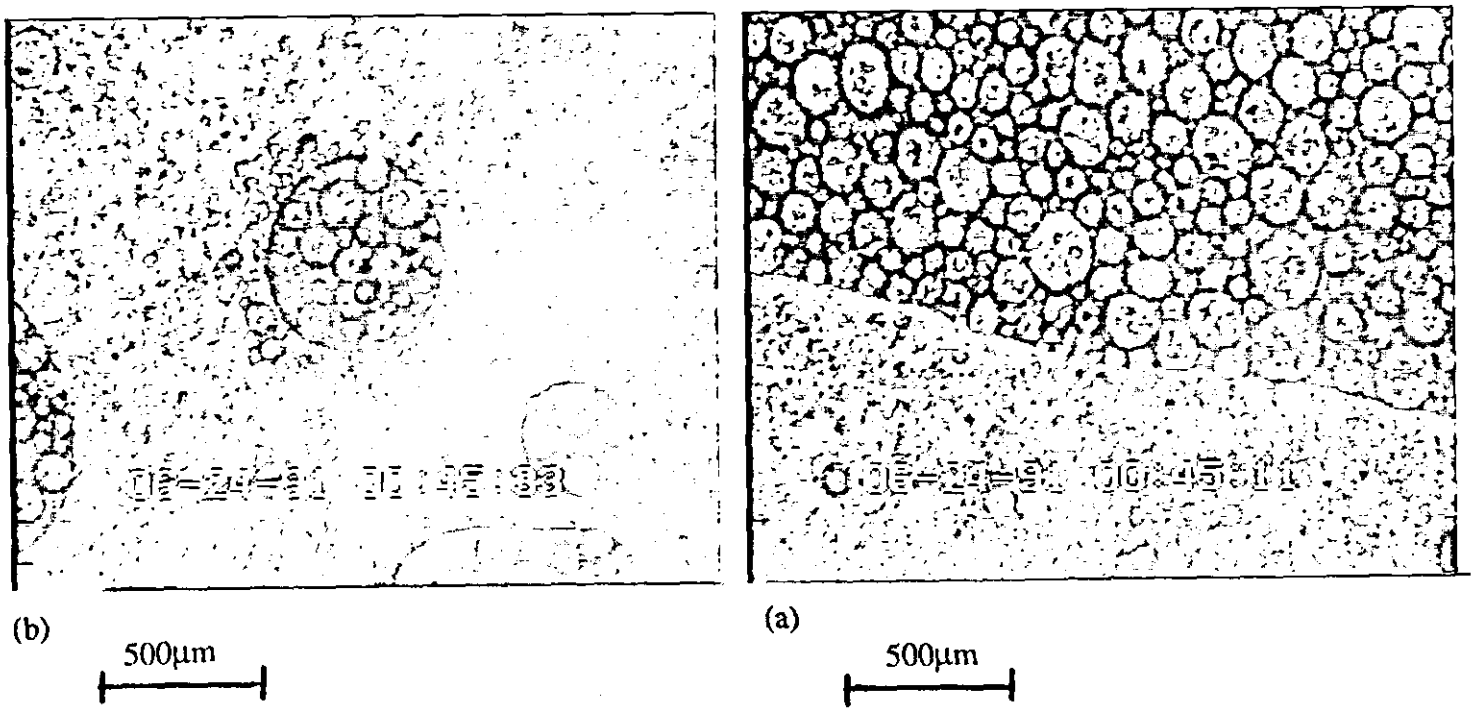

FIGURE 6.22 - Catastrophic Inversion $O_m/W+W/O_m/W$ to W/O_m, in a system of high oil phase viscosity. PIB-Cyclohexane/SML (HLB=8.6)

(a) Inverted and uninverted regions near the catastrophic inversion point (x44).

(b) $O_m/W/O_m$ drops formed after catastrophic inversion. These drops were gradually broken up by agitation and the emulsion will become W/O_m (x44).

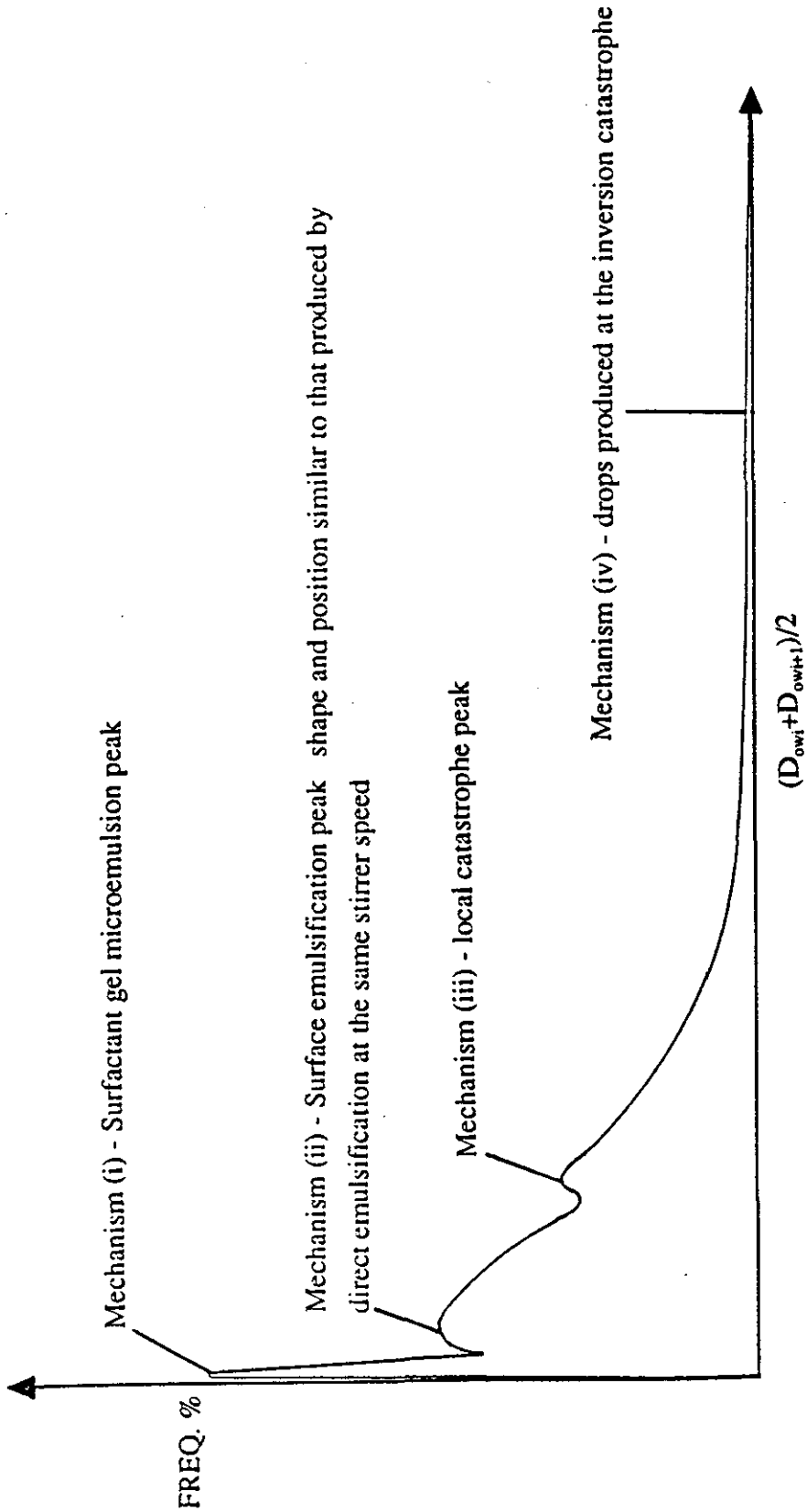

FIGURE 6.23 - A schematic representation of an O/W_m emulsion's drop size distribution, produced by catastrophic inversion.

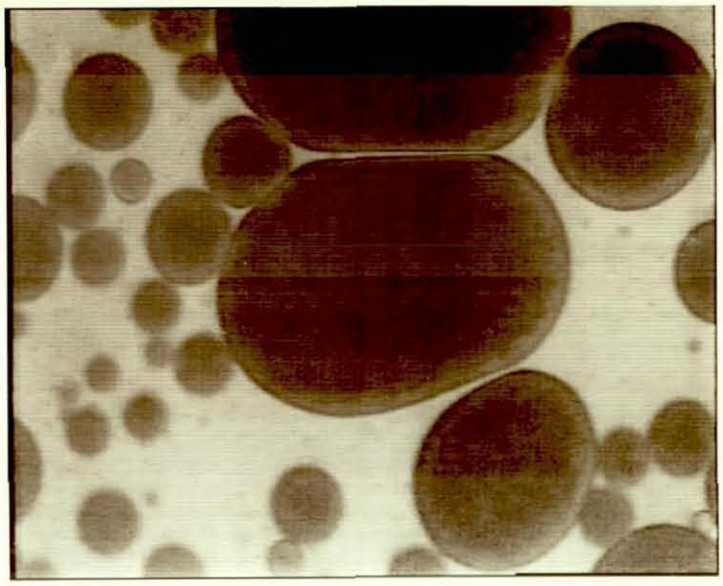

FIGURE 6.24 - Coalescence mechanism of $O/W_m/O$ drops in the cyclohexane/SML system (x110).

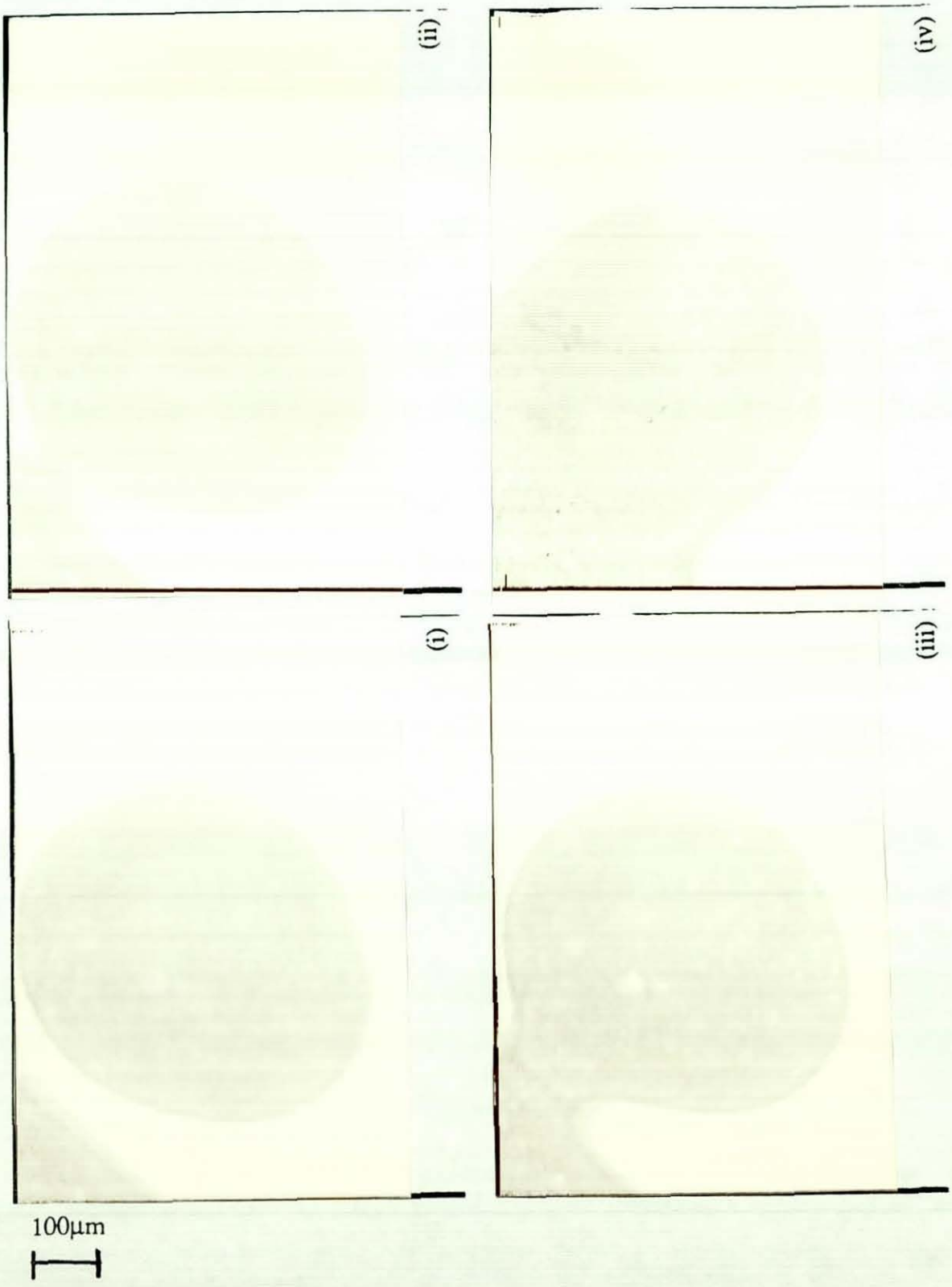

FIGURE 6.25 - Coalescence mechanism of $O/W_m/O$ drops in the cyclohexane/NPE

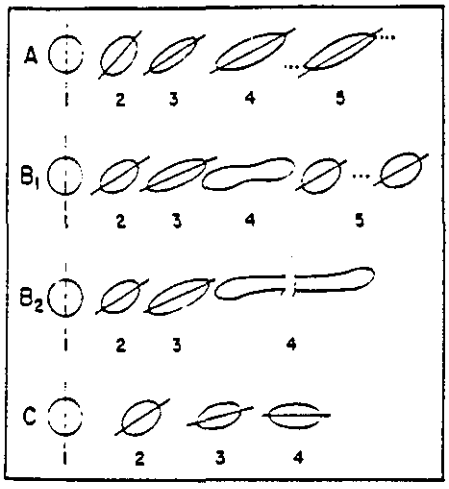

Tracings from photographs of drops in shear fields described by Rumscheidt (1961), illustrating the behaviour of drops in shear flow up to burst. Shown are: Class A ($R \leq 0.2$); class B_1 and B_2 ($0.03 < R \leq 2.2$); class C ($R > 3.8$). It was reported that the three classes were related to R_v but that there were no sharp boundaries between them.

FIGURE 6.26 - Drop shapes in laminar shear field (Torza 1972).

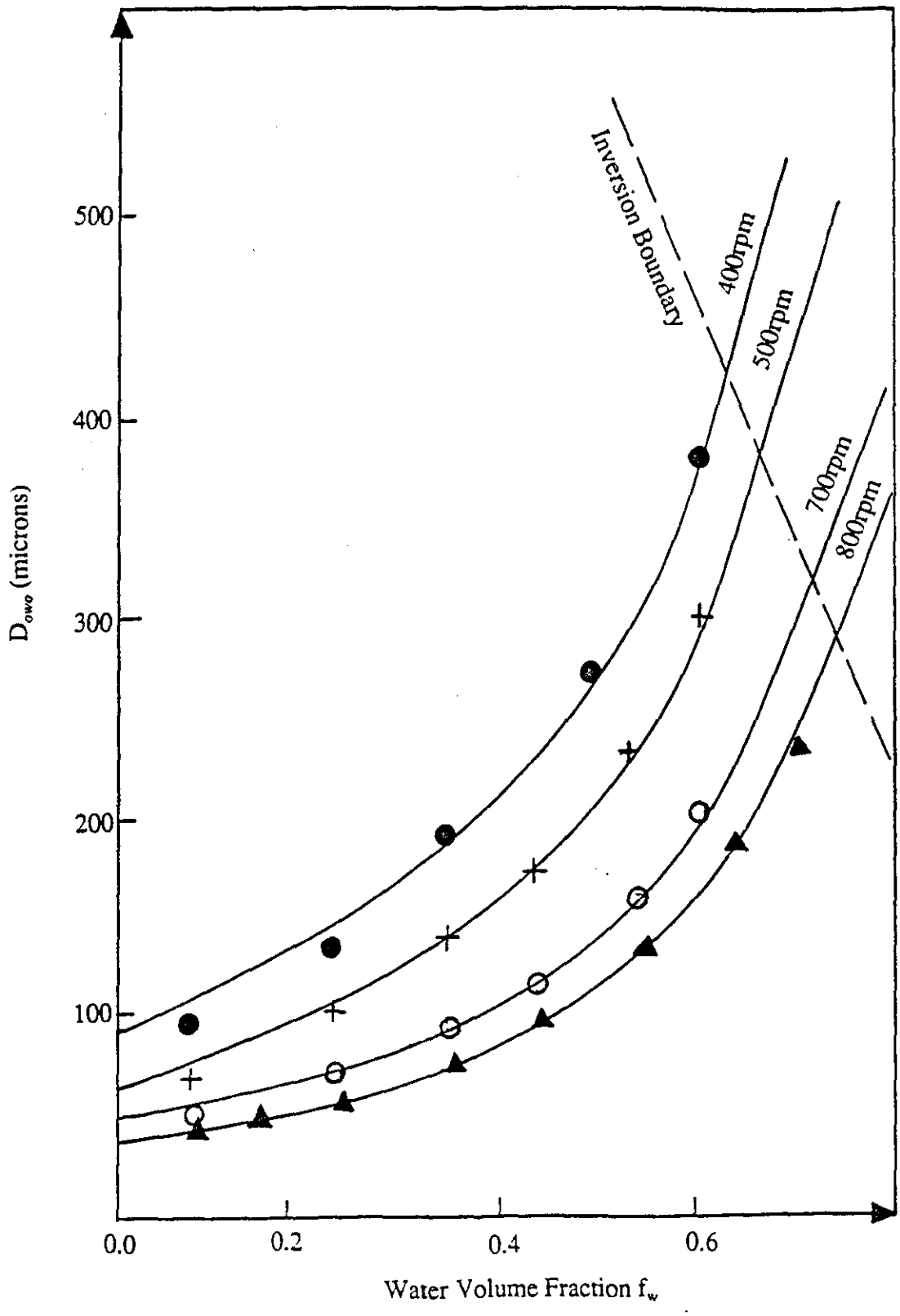

FIGURE 6.27 - D_{owo} vs f_w Cyclohexane/SML (0.007 poise) system, lines given by correlation equation [6.6]. Rate of addition = 40ml/2min.

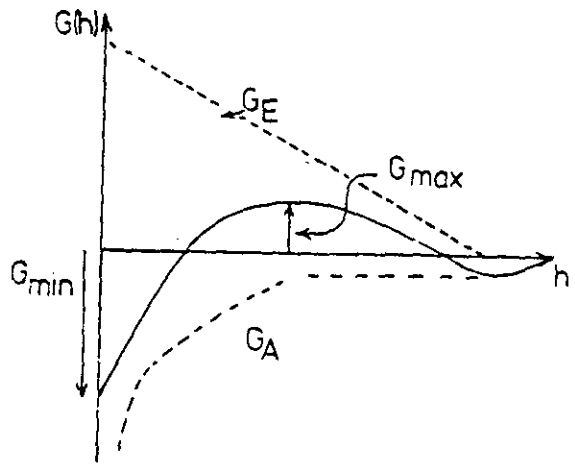

FIGURE 6.28 - Change in the attraction (G_A) and repulsion energies (G_E) with distance (h) between drops, for a stabilised emulsion (Tadros 1983).

CHAPTER 7 - CONCLUDING DISCUSSION

7.1 INTRODUCTION

Phase inversion in nSOW systems is closely related to nSOW phase behaviour. There are two types of phase inversion that can occur in nSOW systems: Transitional inversions induced by altering the surfactant's affinity for the oil and water phases and, catastrophic inversions induced by changes in the emulsion's WOR. Previous studies of dynamic inversions include, PIT studies (transitional inversions) and EIP studies (catastrophic inversions). However, these have only examined the shift of inversion boundaries with changes in the nSOW composition. No studies of the effect of agitation conditions were made. Drop size measurements were made in only a few cases. Those dynamic inversion studies which have looked at the effect of agitation conditions have only been concerned with oil-water systems with no surfactant present (hence, these were catastrophic inversions). Again in oil-water system studies, no attempt has been made to investigate the changes in drop sizes during a dynamic inversion.

In this study, an experimental mapping procedure and drop sizing techniques have been developed to examine dynamic inversions. The different inversion mechanisms have been characterised and it has been shown which drop types are present at each stage of a dynamic inversion. The factors affecting the drop sizes before and after inversion have been examined and a theoretical treatment of the drop size controlling mechanisms has been developed. The dynamic inversion map developed in this study provides an excellent framework for examining dynamic inversions in nSOW systems:

7.2 DYNAMIC INVERSION MAPS - the relationship between dynamic inversion and nSOW phase behaviour

In the first half of this study (chapters 1, 2 and 3), an understanding of inversion mechanisms was developed. The factors affecting each inversion type were examined. The result was a dynamic inversion map, the essential features of which remained similar in each nSOW system studied. The exact form of the map depended on the nature of the oil and surfactants which were present.

The basis for the dynamic inversion map (SAD vs f_w) was first used by Salager et al, for equilibrium phase behaviour. The framework was extended here to study dynamic inversions and it was shown that the results of other workers (ie. PIT and EIP studies) could be represented within the map. Note, triangular diagrams which are normally used to show the phase behaviour of 3 phase systems, could not be used to show nSOW phase behaviour because the surfactant was not a single species. The link between phase inversion and nSOW phase behaviour is clearly shown on the map:

(i) Transitional inversions occur when the nSOW phase behaviour is Type 3. An inversion SAD+ to SAD- follows a progression from a stable W/O_m emulsion to a stable O/W_m emulsion. The transitional inversion mechanism is discussed along with the drop size studies in section 7.4 of this chapter.

(ii) Catastrophic inversions occur when the nSOW phase behaviour is Type 1 or Type 2. True catastrophic inversions can only take place when the initial dispersed phase is unstable. In nSOW systems, true catastrophic inversions can take place when moving the WOR in one direction only, hence, the term "inversion hysterisis" used by some authors is misleading. Catastrophic inversion mechanisms are discussed with the drop size studies in section 7.5 of this chapter.

The importance of being able to determine the phase behaviour that a surfactant will induce on an oil-water system is highlighted by the above section ie. in order to predict the effect a dynamic composition change will have on a system, the nSOW phase behaviour changes must be known (to determine the inversion type). Note, in some nSOW systems, a composition change resulting in a phase behaviour change SAD- to SAD+ across SAD=0, may not result in a transitional inversion (eg. SML systems where the initial emulsion's dispersed phase fraction <0.7). However, the composition change will result in a stable O/W_m emulsion becoming an unstable O_m/W emulsion; this effect can only be predicted with a dynamic inversion map.

The nSOW phase behaviour depends on the surfactant's affinity for the oil and water phases. Some success was achieved in this study relating surfactant affinity to thermodynamic parameters.

7.3 THE PARTITIONING OF SURFACTANT BETWEEN OIL, WATER AND A SURFACTANT INTERFACIAL PHASE - A BASIS FOR SURFACTANT CLASSIFICATION

In Type 3 systems the surfactant's affinity for the oil and water phases is balanced (SAD=0). The surfactant's affinity has been shown by Salager et al (1988) to be dependent on, surfactant concentration, temperature, oil type (EACN), ethyleneoxide chain length of the surfactant (EON), salt concentration and the presence of alcohols. Correlations between SAD and the above factors have been developed for nonionic surfactants (eg. Bourrel 1980). In this study a thermodynamic relationship for surfactant affinity was derived, based on the partitioning of surfactant between oil, water and a surfactant interfacial phase.

A model was derived in chapter 3 which can be used to calculate mixed CMC_o values of lipophilic surfactants from transitional inversion data. It was shown how the effect of surfactant concentration on SAD is no-longer apparent if only interfacial surfactant was considered. The transitional inversion line then becomes a horizontal line on the inversion map (the same for all surfactant concentrations). The calculated CMC results were used to estimate the partition coefficient ($K_{o/w}$) at the transitional inversion point. From the $K_{o/w}$ data it was shown that for a particular nonionic surfactant type, ΔH and ΔS, the enthalpy and entropy of phase transfer respectively, were constant at the transitional inversion point in all the oil-water systems studied. At each temperature, the value of ΔG_{inv} (free energy of phase transfer) can be calculated from the values of ΔH_{inv} and ΔS_{inv} ($\Delta G=\Delta H-T\Delta S$). The nSOW system phase behaviour can then be determined by referencing its ΔG ($=-RTlnK_{o/w}$) with ΔG_{inv}, where:

$\Delta G < \Delta G_{inv}$ Type 2 phase behaviour
$\Delta G = \Delta G_{inv}$ Type 3 phase behaviour
$\Delta G > \Delta G_{inv}$ Type 1 phase behaviour

Using the above basis, it was also shown in chapter 3 that the ethyleneoxide chain length of a surfactant at SAD=0, has a linear relationship with 1/PIT.

Having established the nSOW phase behaviour, it is now possible to consider the two inversion types:

7.4 TRANSITIONAL INVERSIONS

A transitional inversion is brought about by changing the surfactant's affinity and crossing SAD=0. PIT studies are examples of transitional inversions and PITs have been shown to be linear with change in f_w (Shinoda 1986) for a large number of systems. The transitional inversion line slopes down from left to right across a SAD map. The slope of the line depends on the surfactant concentration, however, as discussed above, the transitional inversion line becomes horizontal if the affinity of the interfacial surfactant only is considered.

Mechanisms

The transitional inversion mechanism for inversion SAD+ to SAD- has been shown by Salager (1983b) when considering equilibrium phase behaviour, to involve a transition from a W/O_m emulsion, through a 3 phase system M_sOW, to a O/W_m emulsion. However, it has been shown here, that dynamic transitional inversions depend on the surfactant type. From the results of chapter 2, it is apparent that transitional inversions in systems containing NPE surfactants are reversible and can occur over a wide range of f_w. It was postulated that the dynamic inversion mechanism for NPE systems was:

$W/O_m \rightarrow W/M_o \rightarrow (O+W)/M_s \rightarrow O/M_w \rightarrow O/W_m$

This mechanism was confirmed by the photomicrographic evidence in chapter 5 and by the subsequent drop size analysis. Note, the 3-phase system continuous phase (M_s) may only contain surfactant when the system is agitated. Dynamic transitional inversions in systems containing SML surfactants were not found to be reversible and only occurred if the initial dispersed phase fraction was >0.7. When an inversion SAD+ to SAD- could be induced, the photomicrographic evidence of chapter 5 showed that in SML systems, the dynamic transitional inversion mechanism followed:

$W/O_m \rightarrow W/M_o \rightarrow (O+W)/M_s/W \rightarrow O/M_w \rightarrow O/W_m$

Drop Sizes

In the three phase region (SAD=0), ultra-low interfacial tension exists between phases (Cayais 1974) and this phenomenon can be used to produce fine emulsions with low energy input (Shinoda 1986 - note the effect of agitation conditions was not examined by Shinoda et al). In this study, the effect of agitation conditions, surfactant concentration and increasing oil phase viscosity, on the drop sizes of emulsions produced by transitional inversion was examined. The drop size controlling mechanism was established.

The start point of a transitional inversion is either a O/W_m emulsion (Type 1 systems), or a W/O_m emulsion (Type 2 systems). In a transitional inversion, the start emulsion is taken to a SAD=0 (Type 3) condition and then can either be shifted back to its original state, or the inversion can be completed. The drop sizes of Type 1 and Type 2 emulsions were found to be controlled by different mechanisms to Type 3 emulsions:

Type 1 and Type 2 Systems

The results of chapter 5 and 6 showed that for W/O_m emulsions in Type 2 systems and O/W_m emulsions in Type 1 systems the following results apply (note, these results refer to the direct emulsification of stabilised systems):

(i) The time required to produce a steady-state drop size distribution and the steady-state drop size, reduced as SAD moved towards SAD=0. This was due to the changes in interfacial tension across the phase transition.

(ii) The drop sizes of these stabilised emulsions (under turbulent conditions) could be correlated by drop breakage control models, where $D_{sm} \propto N^{-1.2}$.

(iii) Drop coalescence was negligible. However, an increase in drop size was found with increase in dispersed phase fraction (note, this was not a dynamic increase in dispersed phase fraction). This increase could be attributed to the effects of turbulence damping. A function describing the increase in drop sizes due to turbulence damping,

$F(f_{disp})$, derived by Doulah (1975), was found to fit the experimental results of this study. Hence, the final drop correlation derived for stable emulsions in turbulent flow, has the form:

$$D_{sm} = k(1+3f_{disp})We^{-0.6} \quad [7.1]$$

Type 3 Systems

The measurements of drop sizes of emulsions produced at the transitional inversion point made in this study, showed that extremely fine emulsions could be produced after a very short agitation time. Equation [7.1] was not found to apply to Type 3 emulsions. Hence, the drop sizes of O/M_w, $(O+W)/M_s$ and W/M_o emulsions were controlled by a different mechanism. In chapter 5, it was shown that for NPE systems, the level of turbulence had little or no effect on the drop sizes of Type 3 emulsions (simple shaking was as effective as a high intensity agitator).

The drop sizes of Type 3 emulsions were found to be dependent on the surfactant concentration. By considering the concentration of interfacial surfactant, analysis showed that the surface area of the drops of Type 3 emulsions could be equated to the maximum area of coverage of the interfacial surfactant. Hence, the interfacial surfactant concentration and the area of coverage per surfactant molecule, are the drop size controlling factors in Type 3 emulsions.

Unlike in Type 2 and Type 1 emulsions, where the drop breakage mechanism was by turbulence or viscous shear, in Type 3 emulsions the drops are produced by the "desire" of the surfactant to become the continuous phase - spontaneous emulsification was observed. The exact process by which the surfactant becomes continuous is unclear, however, it was speculated that this was achieved through the production of $(O+W)/M_s/O$ drops (photomicrographs of such drops were shown in chapter 5).

To be able to measure the drop sizes of Type 3 emulsions, the emulsion was shifted from SAD=0 to SAD- to aid stability and, so that the final emulsion was 2 phase. In common with the results of Shinoda et al (1986), it was found that when the initial emulsion was produced close to the inversion point, the shifted emulsion had smaller drop sizes than when the initial emulsion was produced at the inversion point. This was explained here in terms of the surfactant area of coverage theory - where, the dispersed phase volume of a O/M_w emulsion >> $(O+W)/M_s$ emulsion.

When systems of higher oil phase viscosity were examined, it was found that fine emulsions with low energy input could still be produced by the transitional inversion method. However, the time required to produce a steady-state drop size distribution was dependent on the way of adding the system's components before SAD=0 was reached. It was suggested that good practice for producing fine emulsions would be to approach SAD=0 with the low viscosity phase continuous, to aid pre-mixing of the system's components.

7.5 CATASTROPHIC INVERSIONS

Catastrophic inversions occur due to the complete coalescence of the dispersed phase at a closest packing condition. Using a uniform hard sphere model, Ostwald (1910) showed that a catastrophic inversion would occur when f_{disp}=0.74. Other studies have shown that catastrophic inversions can occur when $f_w << 0.74$ and, it is suggested that in these cases $O/W_m/O$ drops are formed, which boost the actual dispersed phase volume (Becher 1966). Catastrophic inversion points have been found to depend on the oil phase viscosity and on agitation conditions. However, no drop size studies of catastrophic inversions are present in the literature.

Mechanisms

It has been shown in this study that true catastrophic inversions can only occur when moving the WOR in one direction. For SAD- conditions, when water phase is added to a continuous oil phase, $O/W_m/O$ drops may be produced depending on the surfactant type and the oil phase viscosity. A true catastrophic inversion will occur at a closest packed condition and the final emulsion will be O/W_m. However, if oil phase is added to a continuous water phase, a catastrophic inversion will not occur. As further oil phase is added the O/W_m emulsion's dispersed phase fraction will increase and a point will be reached when all the excess surfactant (ie. surfactant not dissolved as monomers in the oil and water phases) is used up forming an interface. Any further addition of oil phase will result in the emulsion transforming into an $O/W_m/O$ emulsion. For normal surfactant concentrations, this transition occurs at very high dispersed phase fractions. Hence, inversion hysterisis does not occur in nSOW systems.

The dynamic inversion maps of chapter 2, show that for a wide range of nSOW compositions, the emulsion type will depend on its processing history. True catastrophic inversion boundaries are shown on the maps and the location of these was found to be dependent on stirrer speed and rate of dispersed phase addition. In chapter 6, the location of catastrophic inversion boundaries was also shown to be dependent on the initial

emulsion's viscosity ratio. As was the case in transitional inversions, catastrophic inversions, can be induced over a wide range of f_w. An emulsion whose initial dispersed phase fraction was 0.1, can be made to invert using an agitation-settling cycle.

The drops of an emulsion produced by catastrophic inversion may be produced by one of four mechanisms (as discussed in chapter 5): (i) surfactant gel microemulsion mechanism, (ii) emulsification at the drop surface mechanism, (iii) localised catastrophe mechanism and, (iv) catastrophic inversion point mechanism. Mechanisms (i) to (iii) cause the formation of oil drops within $O/W_m/O$ drops before inversion and mechanism (iv) concerns drops produced at the inversion point catastrophe. Each of the above mechanisms produces drops in distinct and different size ranges. It was shown in chapter 6, that the drop size distribution of an emulsion produced by catastrophic inversion can be very wide. The distribution can be trimodal, with peaks due to each of mechanisms (i) to (iii). The largest drop sizes of the inverted emulsion's distribution are produced by mechanism (iv).

Drop Sizes

Studies of drop breakage and drop coalescence in turbulent flow found in the literature have been concerned mainly with dispersions having low dispersed phase fractions. Drop breakage control and drop coalescence control models have been derived by (Shinnar 1961) and (Stamatoudis, see Tavlarides 1981) for turbulent and laminar/transitional flows respectively. In this study unstable emulsions and stable emulsions have been examined in each flow type. The effect of high dispersed phase fractions on the drop sizes of unstable and stable emulsions has been shown and coalescence mechanisms have been proposed. The relationship between the drop sizes of $O/W_m/O$ emulsions at the catastrophic inversion point and the oil drop sizes of the O/W_m emulsion formed after catastrophic inversion, has been established. As a catastrophic inversion progresses, the changes in drop sizes and drop controlling mechanisms were as follows:

Unstable $O/W_m/O$ drops (present before inversion)

Catastrophic inversions occur at high dispersed phase fractions. In chapter 6, functions $F(f_{disp})$ used by other authors for the increase in drop sizes with f_{disp} in turbulent flows were reviewed. It was found that a linear function was valid for low f_{disp} (<0.2), however, for f_{disp}>0.2, functions of this type lead to large errors. For turbulent flow conditions, an exponential function best fitted the experimental data in this study. Also, a theoretical function derived by Delichatsios (1976) was found to be in good agreement.

For turbulent flow conditions the drop sizes of $O/W_m/O$ emulsions were correlated by $D_{owo} \propto N^{-1.2}$, at all values of f_{disp}. This relation has been derived by Shinnar (1961) for drop breakage control ie. for conditions where coalescence does not take place. However, in the dynamic catastrophic inversions of this study, coalescence must have been occurring because: (i) the drop sizes of the unstable $O/W_m/O$ emulsion increased as f_w was increased (by aliquot additions), (ii) the drop sizes of an unstable $O/W_m/O$ emulsion >> the drop sizes of a stable O/W_m emulsion which has similar phase properties. It has been often quoted that an emulsion's steady-state drop size distribution is the result of a balance between drop break up and coalescence. A theoretical treatment of this "balance" was discussed in chapter 6. The final drop correlation found for unstable $O/W_m/O$ drops in turbulent flow was:

$$D_{owo}=k[\ln(c_3+c_4 f_{disp})/\ln c_3]^{-3/5} We^{-0.6} \quad [7.2]$$

In the case of the higher oil phase viscosity systems studied here, the flow was sometimes transitional and sometimes laminar. For these systems $f_w \neq f_{disp}$ (due to the formation of $O/W_m/O$ drops). The rate of entrainment of oil phase into $O/W_m/O$ drops increased as the oil phase viscosity increased. For the case of the initial water aliquot addition to the oil phase (here $f_w=f_{disp}$), the emulsion drop sizes could be correlated by drop coalescence control models - where the drop coalescence prevention mechanism was viscous shear. As the oil phase viscosity increased a plot of D_{owo} against f_w became linear. For oil phase viscosities >0.5 poise, the rate of drop growth with increase in f_w was independent of stirrer speed.

The size of the $O/W_m/O$ drops at the catastrophic inversion point depended on the oil phase viscosity and stirrer speed. The lower the stirrer speed and also, the lower the oil phase viscosity, the larger were the $O/W_m/O$ drop sizes at the catastrophic inversion point. The results of chapter 6 show that the more deformable the drops of the $O/W_m/O$ emulsion, the lower the value of f_{dinv} will be. Larger $O/W_m/O$ drops are more deformable than smaller $O/W_m/O$ drops, hence, f_{dinv} decreased with decrease in N. As the oil phase viscosity increases, the flow regime moved progressively towards laminar shear flow and the $O/W_m/O$ drops will become more deformable (for $O/W_m/O$ drops, $R_v<1$). This explains why the comparatively small $O/W_m/O$ drops of high oil phase viscosity systems at the catastrophic inversion point, could form a close packed arrangement when $f_{dinv}<0.74$.

The relationship between the $O/W_m/O$ drop sizes present at the catastrophic inversion point, with the drop sizes of the O/W_m emulsion formed after catastrophic inversion

A direct relationship between the size of the $O/W_m/O$ drops present before catastrophic inversion and the size of the O/W_m drops after catastrophic inversion, was obtained at each oil phase viscosity examined. In chapter 6, it was shown that the gradient of a plot of D_{ow} vs D_{owo} corresponded to the ratio of the areas of the oil drops formed at the inversion point, to the area of the $O/W_m/O$ drops at the inversion point. The value of f_{dinv} could be calculated from D_{owo} and D^0_{owo}, where:

$$f_{dinv}=D_{owo}/(2D_{owo}-D^0_{owo}) \quad [7.3]$$

D^0_{owo} is dependent on the agitation type ie. stirrer and tank dimensions. The value of D^0_{owo} cannot be negative, hence, from equation [7.3], f_{dinv} must be >0.5. The value of f_{dinv} obtained from equation [7.3] can be used to calculate the fraction of the oil phase volume emulsified as drops within $O/W_m/O$ drops at the catastrophic inversion point.

Stable (to coalescence) O/W_m emulsion formed after catastrophic inversion

The drop sizes of the O/W_m emulsion produced at the catastrophic inversion point, showed the same correlation with N as the $O/W_m/O$ drops before inversion. This was an expected result as D_{owo} has a linear relationship with D_{ow} (for catastrophic inversion point conditions). The drops sizes of the inverted O/W_m emulsion were found to increase with increasing oil phase viscosity and with decreasing stirrer speed. In all cases the drop sizes of the inverted O/W_m emulsion could be reduced by further agitation (a 5-fold reduction in the drop sizes was a typical result). Note, for the higher oil phase viscosity systems, where the dispersed phase fraction was very high after catastrophic inversion, a very long agitation time was required to achieve a steady-state drop size distribution.

It was found that when the rate of addition was increased in the catastrophic inversion, the drop sizes of the inverted O/W_m emulsion decreased. It was argued that the most effective catastrophic inversion (for producing small drop sizes) would be one where, the dispersed phase required to cause the inversion was added in one addition ie. a direct emulsification.

This completes the review of the main conclusions (discussed in detail in chapter 1 to 6) of this study.

7.6 FUTURE WORK

Considerable success has been achieved in realising the aims set down in the introduction of this study. Techniques have been developed for studying the dynamics of phase inversion. For nSOW systems, the link between phase inversion types and nSOW phase behaviour has been established and inversion mechanisms have been characterised. Qualitative and quantitative analysis of the factors controlling the drop sizes of emulsions through an inversion run have been developed. Future work should address the following:

(i) Examining phase inversion in systems containing other surfactant types. Can an inversion map, similar to the nSOW map developed here, be produced for an ionic surfactant - co-surfactant system? Do the same inversion types occur and are the drop sizes produced similar to nSOW systems? Inversions have also been induced by the addition of finely divided solids to an emulsion - what is the inversion mechanism here and what drop sizes are produced?

(ii) In chapter 3, a surfactant classification system based on thermodynamic parameters was derived. There is much scope for study of surfactant partitioning in multi-phase systems. In particular more effective experimental analysis is required to measure the CMCs of each chain length of a distributed surfactant in an oil-water system. Accurate CMC measurements are difficult to obtain and this analysis may require considerable expertise. It has been shown here that EON_{inv} is linear with 1/T; future work could derive similar relationships between SAD and EACN and between SAD and salt concentration and allow for the effect of alcohols.

(iii) The complete understanding of catastrophic inversions requires further work on the relative rates of drop breakage and coalescence in turbulent, transitional and laminar flows, the effect of high dispersed phase fractions and the development of coalescence mechanisms.

(iv) The drop size controlling mechanism of transitional inversions in systems containing NPE surfactants has been established in this study. However, in systems containing SML surfactants, the inversion mechanism was different and a reduction in drop sizes was not apparent. Future studies of transitional inversion could examine the effect of surfactant type on: (i) the inversion mechanism and, (ii) the drop sizes produced.

APPENDIX 1
LIST OF SYMBOLS

$A(h)$ = constant dependent on the adehesion force between drops

A_{ow} = surface area of the inverted $O/W_m/O$ emulsion formed at the catastrophic inversion point

A_{owo} = surface area of the $O/W_m/O$ drops at the catastrophic inversion point

A_s = area of coverage per surfactant molecule at the oil-water interface

B = baffle width

C_h = concentration of hydrophilic surfactant in the system

C_l = concentration of lipophilic surfactant in the system

C_m = concentration of interfacial surfactant in the system

C_o = Total concentration of surfactant in the oil phase

C_t = Total concentration of surfactant in the system

C_w = Total concentration of surfactant in the water phase

CMC_o = Critical micelle concentration of surfactant in the oil phase

CMC_w = Critical micelle concentration of surfactant in the water phase

d = drop diameter

d_{max} = maximum drop diameter that is stable to breakage in isotropic turbulence

d_{min} = minimum drop diameter that is stable to coalescence in isotropic turbulence

D = Stirrer diameter

D_i, D_{i+1} = Drop size intervals

D_{ow} = Sauter mean diameter of O/W_m emulsion drops

D_{owo} = Sauter mean diameter of $O/W_m/O$ emulsion drops

D^0_{owo} = Sauter mean diameter of $O/W_m/O$ emulsion drops at $f_{disp}=1$

D_{sm} = Sauter mean diameter

D^0_{sm} = Sauter mean diameter at $f_{disp}=0$

$D_{sm\infty}$ = Steady-state drop size distribution Sauter mean diameter

D_t = tank diameter

E_{ad} = drop adhesion energy

E_h = Energy lost as heat loss

E_k = Kinetic energy of the turbulent velocity fluctuations

E_s = Surface energy

EON = Ethyleneoxide number of a surfactant chain

EON_{inv} = Ethyleneoxide number of the surfactant chain at the transitional inversion point

F = Adhesion force

f_{dinv} = dispersed phase volume fraction at the catastrophic inversion point

f_{disp} = dispersed phase volume fraction

f_w = water volume fraction

f_{winv} = water volume fraction at the inversion point

ΔG = Free Energy of phase transfer

ΔG_{inv} = Free Energy of phase transfer for the transitional inversion point condition

H = tank height

ΔH = Enthalpy of phase transfer

ΔH_{inv} = Enthalpy of phase transfer for the transitional inversion point condition

HLB_{act} = The HLB of the pseudo surfactant phase

HLB_h = hydrophile-lipophile-balance number of a hydrophilic surfactant

HLB_i = hydrophile-lipophile-balance number of surfactant i

HLB_l = hydrophile-lipophile-balance number of a lipophilic surfactant

$HLB_{mol.av}$ = mole average hydrophile-lipophile-balance number of a surfactant mixture

$HLB_{wt.av}$ = weight average hydrophile-lipophile-balance number of a surfactant mixture

k = rate constant

$K_{o/w}$ = partition coefficient of surfactant between oil and water

M_o = Winsor Type 3 oleic microemulsion

M_s = Winsor Type 3 surfactant phase microemulsion

M_w = Winsor Type 3 aqueous microemulsion

N	=	Stirrer Speed
N_A	=	Avogadro's Number
O	=	Oil phase containing surfactant monomers at a concentration $<CMC_o$
O_m	=	Oil phase containing surfactant micelles
p_i	=	fraction of the total number in interval i
R	=	Gas Constant
R_v	=	Viscosity ratio (μ_d/μ_c)
Re	=	Reynold's Number
ΔS	=	Entropy of phase transfer
ΔS_{inv}	=	Entropy of phase transfer for the transitional inversion point condition
t	=	time
T	=	Temperature
u^2	=	mean square turbulent velocity fluctuation
$u^2(d)$	=	mean square of relative velocity fluctuations between two points a distance d apart
u_r	=	critical relative velocity along the lines of centres of two colliding drops for coalescence to occur
∇u	=	local velocity gradient
V	=	total volume of the system
V_i	=	tank viscosity group
V_o	=	total volume of the oil phase
V_{ow}	=	volume of the inverted O/W_m emulsion formed at the catastrophic inversion point
V_{owo}	=	volume of the $O/W_m/O$ drops at the catastrophic inversion point
V_w	=	Total volume of the water phase
W	=	Water phase containing surfactant monomers at a concentration $<CMC_w$
W_m	=	Water phase containing surfactant micelles
We	=	Weber Number
We_{crit}	=	critical Weber Number

x_h = mole fraction of hydrophilic surfactant in the pseudo surfactant phase

x_i = mole fraction of surfactant i in the pseudo surfactant phase

x_l = mole fraction of lipophilic surfactant in the pseudo surfactant phase

Z = number of drops / unit volume

Greek

Γ = surface excess surfactant

ε = Energy dissipation

λ = eddy size

λ_k = Kolmorgoroff length

μ_c = continuous phase viscosity

μ_d = dispersed phase viscosity

μ_{eff} = effective emulsion viscosity

μ_{oi}, μ_{wi} = chemical potentials of surfactant i in the oil and water phases

μ^*_{ci}, μ^*_{wi} = standard chemical potential of surfactant i in the oil and water phases

μ_{mi} = chemical potential of surfactant i in mixed micelles

μ_{moi} = chemical potential of surfactant i in pure micelles

π = surface pressure

ρ_c = continuous phase density

ρ_d = dispersed phase density

ρ_{eff} = effective emulsion density

υ = kinematic viscosity

φ = fraction of the total oil phase fraction, incorporated as oil drops within $O/W_w/O$ drops at the catastrophic inversion point

APPENDIX 1 - REFERENCES

Allan, G.C., Aston, J.R., Grieser, F. and Healy, T.W., *J.Coll.Interf.Sci.* **128**(1), 258, (1989).

Anton, R.E., Castillo, P. and Salager, J.L., *J.Disp.Sci.Tech.* **7**(3),319,(1986).

Arai, K., Konno, M., Matunaga, Y. and Saito, S., *J.Chem.Eng.Jpn.* **10**(4),325,(1977).

Arashmid M. and Jeffreys, G.V., *A.I.Ch.E.J.* **26**(1),51,(1980).

Baker, R.C. and Tadros, Th.F., in "*Microemulsion Systems*", Ed. Rosaro, H.L. and Clausse, M., *Surf.Sci.Ser.* **24**,345,(1987), Dekker, New York.

Bancroft, W.D., *J.Phys.Chem* **17**,501,(1913).

Bates, R.L., Fondy, P.L. and Corpsten, R.R., *Ind.Eng.Chem.Proc.Des.Dev.* **2**,(310,(1963).

Becher, P., "*Emulsion: Theory and Practice*", 2nd Ed., Reinhold, New York (1966).

Becher, P. and Schick, M.J., in "*Nonionic Surfactants: Physical Chemistry*", Ed. Schick, M.J., Dekker, New York (1987).

Bourrel, M., Graciaa, A., Schecter, R.S. and Wade, W.H., *J.Coll.Interf.Sci.* **72**(1),161,(1979).

Bourrel, M. and Salager, J.L., *J.Coll.Interf.Sci.* **75**, 451, (1980).

Calabrese, R.V., Chang, T.P.K. and Dang, P.T., *A.I.Ch.E.J.* **32**(4),657,(1986a).

Calabrese, R.V., Wang, C.Y. and Bryner, N.P., *A.I.Ch.E.J.* **32**(4),677,(1986b).

Calderbank, P.H., *Trans.Inst.Chem.Eng.* **36**,443,(1958).

Cash, I., Cayais, J.L., Fournier, G., Macallister, D., Schares, T., Schecter, R.S. and Wade, W.H., *J.Coll.Interf.Sci.* **59**,39,(1977).

Cayais, J.L., Schecter, R.S. and Wade, W.H., "*Adsorption at Interfaces*",Ed. Mittal, K.L., *A.C.S. Symp.Ser.* 8,234,(1974).

Chand, T., *Coll.Polym.Sci.* **258**,1204,(1980).

Chen, H.T. and Middleman, S., *A.I.Ch.E.J.* **13**,989,(1967).

Clarke, S.I. and Sawistowski, H., *Trans.I.Chem.E.* **56**,50,(1978).

Collins, S.B. and Knudsen J.G., *A.I.Ch.E.J.* **16**,1072,(1970).

Coulaloglou, C.A. and Tavlarides, L.L., *A.I.Ch.E.J.* **22**,289,(1976).

Crook, E.H., Fordyce, D.B. and Trebbi, G.F., *J.Phys.Chem.* **67**, 1987, (1963).

Crook, E.H., Fordyce, D.B. and Trebbi, G.F., *J.Coll.Sci.* **20**,191,(1965).

Cutter, L.A., *A.I.Ch.E.J.* **12**,35,(1966).

Das, P.K., Kumar, R. and Ramkrishna, D., *Chem.Eng.Sci.* **42**(2),213,(1987).

Davies, J.T. and Rideal, E., *"Interfacial Phenomena"*, Acad.Press 2nd Ed., New York, (1963).

Davies, J.T., *Chem.Eng.Sci.* **40**(5),839,(1985).

Davies, R., Graham, D.E. and Vincent, B., *J.Coll.Interf.Sci.* **126**(2),616,(1988).

Delichatsios, M.A. and Probstein, R.F., *Ind.Eng.Chem.Fund.* **15**(2),135,(1976).

Dickinson, E., *J.Coll.Interf.Sci.* **87**(2),416,(1982).

Doulah, M.S., *Ind.Eng.Chem.Fund.* **14**(2),137,(1975).

Eckert, R.E., McLaughlin, C.M. and Rushton, J.H., *A.I.Ch.E.J.* **31**(11),1811,(1985).

Gilchrist, A., Dyster, K.N., Moore, I.P.T. and Nienow, A.W., *Chem.Eng.Sci.* **44**,23381,(1989).

Gopal, E.S.R., in *"Emulsion Science"*,Ed. Sherman, P., Academic Press, London (1968).

Graciaa, A., Barakat, Y., Schecter, R.S., Wade, W.H. and Yiv, S., *J.Coll.Interf.Sci.* **89**(1),217,(1982).

Graciaa, A., Lachaise, J., Sayous, J.G., Grenier, P., Yiv, S., Schecter, R.S. and Wade, W.H., *J.Coll.Interf.Sci.* **93**(2), 474, (1983).

Graciaa, A., Lachaise, J., Marion G., *Langmuir* **5**,1315,(1989).

Griffin, W.C., *J.Soc.Cosmet.Chem.* **1**,311,(1949).

Guilinger, T.R., Grislingas, A.K. and Erga, O., *Ind.Eng.Chem.Res.* **27**,298,(1988).

Gunkel, A.A. and Weber, M.E., *A.I.Ch.E.J.* **21**,931,(1975).

Harusawa, F., Saito, T., Nakajima, H. and Fukushima, S., *J.Coll.Interf.Sci.* **74**(2),435,(1980).

Harusawa, F. and Tanaka, M., *J.Phys.Chem.* **85**, 882, (1981).

Hinze, J.O., *A.I.Ch.E.J.* **1**,289,(1955).

Holmes, D.B., Vancken, R.M. and Dekker, J.A., *Chem.Eng.Sci.* **19**,201,(1964).

Hong, P.O. and Lee, J.M., *Ind.Eng.Chem.Pro.Des.Dev.* **22**,130,(1983).

Howarth, W.J., *Chem.Eng.Sci.* **19**,33,(1964).

Hsiao, L., Dunning, H.N. and Lorenz, P.B., *J.Phys.Chem.* **60**,657,(1956).

Kato, S., Nakayama, E. and Kawasaki, J., *Can.J.Chem.Eng.* **69**,222,(1991).

Keey, W.J. and Glen, J.B., *A.I.Ch.E.J.* **15**,942,(1969).

Kolmogoroff, A.N., *C.R.Acad.Sci.USSR* **30**,301,(1941); **32**,16,(1941).

Kolmogoroff, A.N., *Dokl.Acad.Nauk.USSR* **66**,825,(1949).

Kunieda, H. and Shinoda, K., *Bull.Chem.Sov.Jpn.* **55**,1777,(1982).

Lange, H., in "*Nonionic Surfactants*", Vol 1, Ed. Schick, M.J., Dekker, New York (1967).

Laso, M., Steiner, L. and Hartland, S., *Chem.Eng.Sci.* **42**(10),2437,(1987).

Lee, J.C., Tasakorn, P. and Belghazi, A., *Chem.Eng.Aspects-Formation of Liq.-Liq. Disp.*, 22ndFeb.(1984).

Leng, D.E. and Quarderer, G.J., *Chem.Eng.Commun.* **14**,177,(1982).

Marszall, L., *Cosmet.Perfum.* **90**(2),37,(1975).

Marszall, L., *J.Coll.Interf.Sci.* **59**(2),376,(1977a).

Marszall, L., *J.Coll.Interf.Sci.* **60**(3),570,(1977b).

Marszall, L., *J.Coll.Interf.Sci.* **107**(2),572,(1985).

Marszall, L., in "*Nonionic Surfactants: Physical Chemistry*", Ed. Schick, M.J., Dekker, New York (1987).

Meguro, K, Ueno, M. and Esumi, K, In "*Nonionic Surfactants: Physical Chemistry*", Surfactant Science Series Vol.23, Ed. Schick, M.J., Dekker, New York, (1984).

Mersmann, A. and Grossman, H., *Int.Chem.Eng.* **22**(4),581,(1982).

Metzner, A.B., Feehs, R.H., Ramos, H.L., Otto, R.E. and Tuthill, J.D., *A.I.Ch.E.J.* **7**,3,(1961).

Milos, F.S. and Wasan, D.T., *Coll.Surf.* **4**,91,(1982).

Minana-Perez, M., Jarr, P., Perez-Sanchez, M., Ramirez-Gouveia, M. and Salager, J.L., *J.Disp.Sci.Tech.* **7**(3),331,(1986).

Mitsui, T., Machida, Y. and Harusawa, F., *Bull.Chem.Soc.Jpn.* **43**,3044,(1970).

Mlynek, Y. and Resnick, W., *A.I.Ch.E.J.* **18**,122,(1972).

Nagata, S., "*Mixing Principles and Applications*", Wiley, New York (1975).

Ohtake, T., Hano, T., Takagi, K. and Nakashio, F., *J.Chem.Eng.Jpn.* **20**(5),443,(1987).

Ohtake, T., Hano, T., Takagi, K. and Nakashio, F., *J.Chem.Eng.Jpn.* **21**(3),272,(1988).

Oldshue, J.Y., "*Fluid Mixing Technology*", McGraw-Hill, New York, (1983).

Ostwald, W., *Kolloid Z.* 7,64,(1910); *Kolloid Z.* **7**,103,(1910).

Park, J.Y. and Blair, L.M., *Chem.Eng.Sci.* **30**,1057,(1975).

Parkinson, C. and Sherman, P., *J.Coll.Interf.Sci.* **41**,328,(1972).

Perry, R.H. and Chilton, C.H., "*Chemical Engineers' Handbook*",5thEd.,McGraw-Hill (1974).

Quinn, J.A. and Sigloh, D.B., *Can.J.Chem.Eng.* **41**,15,(1963).

Rodger, W.A., Trice, V.G. and Rushton, J.H., *Chem.Eng.Prog.* **52**,515,(1956).

Rosen, M.J., "*Surfactants and Interfacial Phenomena*", 2nd Ed., John Wiley & Sons, New York, (1989).

Rumscheidt, F.D. and Mason, S.G., *J.Coll.Interf.Sci.* **16**,238,(1961).

Rushton J.H., Costich, E.W. and Everett, H.J., *Chem.Eng.Prog.* **46**,375,467,(1950).

Saito, H. and Shinoda, K., *J.Coll.Interf.Sci.* **32**,647,(1970).

Salager, J.L., Quintero, L., Ramos, E. and Andrez, J.M., *J.Coll.Interf.Sci.* **77**(1),288,(1980).

Salager, J.L., Loaiza-Maldonado, I., Minana-Perez, M. and Silva, F., *J.Disp.Sci.Tech.* **3**(3),279,(1982).

Salager, J.L., Minana-Perez, M., Anderez, J.M., Grossa, J.L., Rojas, C.I. and Layrisse, I., *J.Disp.Sci.Tech.* **4**(2),161,(1983a).

Salager, J.L., Minana-Perez, M., Perez-Sanchez, M., Ramirez-Gouveia, M. and Rojas, C.I., *J.Disp.Sci.Tech.* **4**(3), 313, (1983b).

Salager, J.L., In "*Encyclopedia of Emulsion Technology Vol.3*", Edit. Becher, P, New York, (1988).

Salager, J.L., Lopez-Castellanos, G., Minana-Perez, M., Parra, C., Cucuphat, C., Graciaa, A. and Lachaise, J., *J.Disp.Sci.Tech.* (1991).

Schindler, H.D. and Treybal, R.E., *A.I.Ch.E.J.* **14**,790,(1968).

Selker, A.H. and Sleicher, C.A., *Can.J.Chem.Eng.* **43**,298,(1965).

Shinnar, R., *J.Fluid.Mech.* **10**,259,(1961).

Shinoda, K. and Friberg, S. "*Emulsions and Solubilisation*", Wiley, New York, (1986).

Smith, D.H. and Fleming, P.D., *J.Coll.Interf.Sci.* **105**,80,(1985).

Smith, D.H. and Kyung-Hee, L., *J.Phys.Chem.* **94**,3746,(1990).

Sprow, F.B., *A.I.Ch.E.J.* **13**,995,(1967).

Stamatoudis, M. and Tavlarides, L.L., *Chem.Eng.J.* **21**,77,(1981).

Stamatoudis, M. and Tavlarides, L.L., *Ind.Eng.Chem.Pro.Des.Dev.* **24**,1175,(1985).

Stephenson, R., *I.Chem.E. Symp.Ser.* 38,paper C4,(1974).

Tadros, Th.F. and Vincent, B., in "*Encyclopedia of Emulsion Technology Vol.1*", Ed. Becher, P., Dekker, New York (1983).

Tavlarides, L.L. and Stamatoudis, M., *Adv.Chem.Eng.* **11**,200,(1981).

Taylor, G.I., *Proc.R.Soc.* **A138**,41,(1932).

Thornton, J.D. and Bonyotiotes, I., *I.Chem.E.Symp.Series* **26**,43,(1967).

Torza, S., Cox, R.G. and Mason, S.G., *J.Coll.Interf.Sci.* **38**,395,(1972).

van Boekel, M.A.J.S. and Walstra, P., *Coll.Surf.* **3**,99,(1981).

Van Heuvan, J.W. and Hoevenaar, J.C., *Proc.Eur.Symp.Chem.React.Eng.* 4th, Brussels, (1968).

van Voorst Vader, F., *Trans.Faraday.Soc.* **56**,1078,(1960).

Walstra, P., in "*Encyclopedia of Emulsion Technology Vol.1*",Ed. Becher, P.,Dekker, New York (1983).

Wang, C.Y. and Calabrese, R.V., *A.I.Ch.E.J.* **32**(4),667,(1986).

Weast, R.C. and Astle M.J., "*CRC Handbook of Chemistry and Physics*", CRC press, Florida (1982).

Weinstein, B. and Treybal, R.E., *A.I.Ch.E.J.* **19**(2),304,(1973).

Winsor, P.A., *Trans.Faraday.Soc.* **44**,376,(1948).

Winsor, P.A., "*Solvent Properties of Amphillic Compounds*", Butterworth Sci. Pub., London (1954).

APPENDIX 2 - Dynamic Inversion Map Data

TABLE A2.1 - Cyclohexane/NPE 2wt% system 20°C, Phase Inversion Data

Surfactants: Hydrophilic Igepal co720
Lipophilic Igepal co520
Igepal co210

Table A2.1.1 - Setting SAD=0 (Transitional Inversion Data)

f_w	$HLB_{mol.av}$
0.84	10.9
0.76	10.8
0.66	10.6
0.56	10.5
0.33	10.2
0.10	9.9*

* Igepal co210 added ($O/W_m/O$ emulsion produced at HLB=10)

Table A2.1.2 - Phase changes at constant SAD (HLB)

SAD+ (adding water to oil)

HLB	f_{winv}
10.0	0.96
7.6	0.95

SAD- (adding oil to water)

HLB	f_{winv}
11.0	0.04
14.2	0.04

Table A2.1.3 - Catastrophic Inversion Points (500rpm, 5ml/30sec)

SAD+ (Adding oil to water)

HLB	f_{winv}
6.0	0.20
7.3	0.56
8.7	0.59
10.0	0.53

SAD- (adding water to oil)

HLB	f_{winv}
11.05	0.76
12.10	0.68
13.15	0.47
14.20	0.43

Table A2.1.4 - Variation of catastrophic inversion boundary with stirrer speed.

Stirrer Speed (rpm)	$HLB_{wt.av}$ / f_{winv} 14.2	12.1	11.0
200	0.38	0.52	0.70
400	0.44	0.57	0.72
600	0.50	0.61	0.72
800	0.52	0.62	0.72

Table A2.1.5 - Variation of cataastrophic inversion boundary with rate of addition (stirrer speed = 400 rpm).

Time Between Additions/sec	$HLB_{wt.av}$ / f_{winv} 14.2	12.1	11.0
15	0.47	0.57	0.70
30	0.44	0.57	0.72
120	0.38	0.50	0.63

TABLE A2.2 - n-heptane/NPE 2wt% system 20°C, Phase Inversion Data

Surfactants: Hydrophilic Igepal co720
Lipophilic Igepal co210

Table A2.2.1 - Setting SAD=0 (Transitional Inversion Data)

f_w	$HLB_{mol.av}$
0.20	5.91
0.36	6.52
0.57	7.34
0.74	7.97

Table A2.2.2 - Phase changes at constant SAD (HLB)

SAD+ (adding water to oil)

HLB	f_{winv}
7.0	0.96

SAD- (adding oil to water)

HLB	f_{winv}
9.0	0.04
14.2	0.04

Table A2.2.3 - Catastrophic Inversion Points (500rpm, 5ml/30sec)

SAD+ (Adding oil to water)

HLB	f_{winv}
4.6	0.20
6.0	0.32

SAD- (adding water to oil)

HLB	f_{winv}
9.00	0.23
11.05	0.38
14.20	0.60

TABLE A2.3 - toluene/NPE 0.01135 moles/l system 22°C, Phase Inversion Data

Surfactants: Hydrophilic Igepal co720
Lipophilic Igepal co520

Table A2.3.1 - Setting SAD=0 (Transitional Inversion Data)

f_w	$HLB_{mol.av}$
0.72	10.34
0.77	11.06
0.88	12.10
0.90	12.20

Table A2.3.2 - Phase changes at constant SAD (HLB)

SAD+ (adding water to oil)

HLB	f_{winv}
10.0	0.96
12.0	0.96

SAD- (adding oil to water)

HLB	f_{winv}
10.0	0.10
11.0	0.09
14.2	0.04

Table A2.3.3 - Catastrophic Inversion Points (500rpm, 5ml/30sec)

SAD- (adding water to oil)

HLB	f_{winv}
11.0	0.60
12.1	0.44
14.2	0.41

TABLE A2.4 - Cyclohexane/SML 2wt% system 20°C, Phase Inversion Data

Surfactants: Hydrophilic Tween20
Lipophilic Span20

Table A2.4.1 - Setting SAD=0 (Transitional Inversion Data)

f_w	$HLB_{mol.av}$
0.90	13.3
0.80	13.1
0.15	10.9
0.05	10.6

Table A2.4.2 - Phase changes at constant SAD (HLB)

SAD+ (adding water to oil)

HLB	f_{winv}
8.6	0.96
10.0	0.96

SAD- (adding oil to water)

HLB	f_{winv}
16.7	0.04
14.0	0.04

Table A2.4.3 - Catastrophic Inversion Points (500rpm, 5ml/30sec)

SAD+ (Adding oil to water)

HLB	f_{winv}
8.6	0.63
10.0	0.20

SAD- (adding water to oil)

HLB	f_{winv}
16.7	0.80
14.0	0.80

TABLE A2.5 - n-heptane/SML 2wt% system 20°C, Phase Inversion Data

Surfactants: Hydrophilic Tween20
Lipophilic Span20

Table A2.5.1 - Setting SAD=0 (Transitional Inversion Data)

f_w	$HLB_{mol.av}$
0.90	13.2
0.80	13.1
0.20	11.4
0.05	11.05

Table A2.5.2 - Phase changes at constant SAD (HLB)

SAD+ (adding water to oil)

HLB	f_{winv}
8.6	0.96
10.0	0.96

SAD- (adding oil to water)

HLB	f_{winv}
16.7	0.04
14.0	0.04

Table A2.4.3 - Catastrophic Inversion Points (500rpm, 5ml/30sec)

SAD+ (Adding oil to water)

HLB	f_{winv}
8.6	0.28
10.0	0.20

SAD- (adding water to oil)

HLB	f_{winv}
16.7	0.83
14.0	0.83

TABLE A2.6 - toluene/SML 2wt% system 20°C, Phase Inversion Data

Surfactants: Hydrophilic Tween20
Lipophilic Span20

Table A2.6.1 - Setting SAD=0 (Transitional Inversion Data)

f_w	$HLB_{mol.av}$
0.90	12.3
0.80	12.1
0.70	12.0
0.20	11.4
0.10	11.3

Table A2.6.2 - Phase changes at constant SAD (HLB)

SAD+ (adding water to oil)

HLB	f_{winv}
8.6	0.96
12.1	0.96

SAD- (adding oil to water)

HLB	f_{winv}
16.7	0.04
13.3	0.04

Table A2.4.3 - Catastrophic Inversion Points (500rpm, 5ml/30sec)

SAD+ (Adding oil to water)

HLB	f_{winv}
8.6	0.56
9.8	0.24
11.0	0.17

SAD- (adding water to oil)

HLB	f_{winv}
16.7	0.83
15.0	0.83
12.7	0.72

APPENDIX 3 - Chapter 3: Inversion Data

TABLE A3.1 - CYCLOHEXANE/NPE5-NPE12 at 20°C

LINE	OVERALL SURFACTANT CONC. (Moles/l)	f_w	MOLE AV. HLB
1	2.27×10^{-2}	0.61	10.04
		0.72	10.24
		0.82	10.40
2	4.54×10^{-2}	0.32	10.12
		0.44	10.22
		0.64	10.39
		0.73	10.48
		0.83	10.58
3	6.81×10^{-2}	0.24	10.24
		0.45	10.38
		0.64	10.48
		0.83	10.62
4	11.35×10^{-2}	0.15	10.40
		0.38	10.47
		0.66	10.58
		0.83	10.67

TABLE A3.2 - CYCLOHEXANE/NPE2-NPE12 at 20°C

LINE	OVERALL SURFACTANT CONC. (Moles/l)	f_w	MOLE AV. HLB
1	11.34×10^{-2}	0.57	6.52
		0.70	7.48
		0.79	8.44
		0.92	9.40
2	22.70×10^{-2}	0.21	6.52
		0.42	7.48
		0.67	8.44
		0.85	9.40

TABLE A3.3 - TOLUENE/NPE5-NPE12 at 22°C

LINE	OVERALL SURFACTANT CONC. (moles/l)	f_w	MOLE AV. HLB
1	11.35×10^{-2}	0.70	10.42
		0.77	11.06
		0.90	12.10
2	22.70×10^{-2}	0.56	11.0
		0.70	11.7
		0.87	12.3

TABLE A3.4 - n-HEPTANE/NPE2-NPE12 at 20°C

OVERALL SURFACTANT CONC. (g/l)	f_w	WT. AV. HLB
20	0.20	5.91
	0.36	6.52
	0.57	7.34
	0.74	7.97

TABLE A3.5 - SML SYSTEMS at 20°C

OVERALL SURFACTANT CONCENTRATION = 20g/l

OIL	f_w	WT. AV. HLB
CYCLOHEXANE	0.90	13.3
	0.80	13.1
	0.15	10.9
	0.05	10.6
N-HEPTANE	0.90	13.2
	0.80	13.1
	0.20	11.4
	0.05	11.05
TOLUENE	0.90	12.3
	0.80	12.1
	0.70	12.0
	0.20	11.4
	0.10	11.3

TABLE A3.6 - TEMPERATURE EFFECT CYCLOHEXANE/NPE5-NPE12

OVERALL SURFACTANT CONCENTRATION = 4.54×10^{-2} moles/l

LINE	TEMPERATURE/°C	f_w	MOLE AV. HLB
1	20	0.32	10.12
		0.44	10.22
		0.64	10.39
		0.73	10.48
		0.83	10.58
2	40	0.38	10.45
		0.61	10.89
		0.83	11.26
		0.90	11.47
3	60	0.28	10.45
		0.72	11.84
		0.94	12.49

TABLE A3.7 - TEMPERATURE EFFECT nHEPTANE/NPE

LINE	TEMPERATURE/°C	f_w	MOLE AV. HLB
1	30	0.20	6.0
	(NPE2 -NPE12)	0.30	6.7
		0.34	6.5
		0.47	6.9
		0.52	7.6
		0.67	7.9
		0.70	8.3
		0.82	8.3
		0.83	8.7
2	50	0.15	6.0
	(NPE2 - NPE12)	0.32	6.9
		0.43	7.3
		0.57	8.7
		0.75	9.5
		0.85	10.0
3	50	0.25	10.25
	(NPE5 - NPE12	0.35	10.30
		0.55	10.45
		0.74	10.60
		0.83	10.70

TABLE A3.8 - ISO-OCTANE/EOP DATA (GRACIAA 1989)

(surfactant concentration = 0.034 moles/l, 25°C)

SURFACTANT PAIR	x_{hinv}	fw	HLB_{inv}
EOP3-EOP9	0.125	0.2	8.4
	0.190	0.5	8.8
	0.340	0.8	9.6
EOP3-EOP7	0.205	0.2	8.66
	0.305	0.5	9.08
	0.485	0.8	9.80
EOP1.5-EOP9	0.100	0.5	5.7
	0.355	0.8	7.8
EOP1.5-EOP7	0.280	0.5	6.8
	0.570	0.8	8.9

EOP1.5 - HLB=4.85

EOP3 - HLB=7.81

EOP7 - HLB=11.98

EOP9 - HLB=13.12

APPENDIX 4 - Chapter 5: Drop Size Distribution Data

Table A4.1 - Oil Phase Viscosity Calibration (20°C).

Concentration of Polymer in Cyclohexane (g/l)	Oil Phase Viscosity (poise)
75	8.50
64	4.50
53	2.56
42	1.40
31	0.86
20	0.47
10	0.25
0	0.007*

* from Weast (1983).

Table A4.2 - Interfacial surfactant concentration calculations.

The interfacial surfactant concentration C_m was kept conatant at 0.03 moles/l. For a set HLB_{act}, x_l, x_h, C_t, C_h and C_l, were calculated using the equations and data below:

$$C_t = C_m + (1-f_w)(x_l CMC_{ol}+x_h CMC_{oh}) + f_w(x_l CMC_{wl}+x_h CMC_{wh})$$

$$x_h = [HLB_{act}-HLB_l]/[HLB_h-HLB_l]$$

$$x_l = 1 - x_h$$

$$C_h = x_h[C_m + f_w CMC_{wh} +(1-f_w CMC_{oh})]$$

$$C_l = C_t - C_h$$

Surfactant	Mol.Wt.	CMC_o	CMC_w
NPE2	308	0.448	10^{-5}
NPE5	440	0.069	10^{-5}
NPE12	750	10^{-4}	10^{-4}

Table A4.3 - Variation of D_{sm} with time at various HLB_{act} values (600rpm).

Table A4.3.1 - HLB_{act}=14.2

$(D_i+D_{i+1})/2$*	FREQ. % - Time (minutes)					$(D_i+D_{i+1})/2$	FREQ.%	
(μm)	1	5	10	20	40	(μm)	60	90
4.5	4.5	15.6	18.6	39.4	35.5	1	10.4	11.0
9.0	12.3	22.3	23.3	30.3	29.0	2	15.6	13.2
14.0	14.8	19.0	18.6	14.3	20.0	3	15.6	15.8
18.0	18.9	14.7	16.3	8.7	10.5	5	14.9	17.6
25.0	23.5	14.2	14.0	5.2	4.0	6	13.2	13.6
34.0	16.0	10.0	7.0	0.9	1.0	9	11.5	12.5
43.0	4.5	1.9	1.4	0.9		11	6.6	6.3
52.0	2.1	1.4	0.5	0.4		13	4.5	5.9
61.0	1.6	0.9	0.5			15	3.8	1.5
70.0	0.8					18	1.0	0.7
80.0	0.4					20	0.7	0.7
89.0	0.4					22	0.7	0.3
						24	0.7	0.0
						27	0.3	0.3
						29	0.3	0.3
D_{sm} (μm)	40.5	32	28	24	17		14	13

*Note: In the tables of drop size distribution data of Appendix 4 and Appendix 5, the average value of each size distribution interval is given. Having the data in this form is more convenient for calculating D_{sm} values and for plotting the "smooth curve" size distributions presented in this thesis. However, it should be noted that the drop size distribution data was initially compiled in a histogram format. In the majority of the drop size distribution tables of Appendix 4 and Appendix 5, the spread of the data is not too wide and arithmetic progression was used to set the interval class boundaries (interval diameter range D_i to D_{i+1}). When the drop size distribution was very wide (eg. O/W_m catastrophic inversion point data tables of Appendix 5), the class boundaries were chosen so that the class interval divided by the average class diameter was approximately constant.

Table A4.3.2 - HLB_{act}=12.1

$(D_i+D_{i+1})/2$	FREQ %	$(D_i+D_{i+1})/2$	FREQ.%-Time (min)		
(μm)	1min	(μm)	10	20	60
4.5	37.2	1	22.6	28.6	19.7
9.0	25.6	2	22.6	28.6	18.4
14.0	16.3	3	15.8	11.1	15.0
18.0	11.6	5	9.9	7.9	14.5
25.0	4.2	6	9.7	6.1	14.5
34.0	3.3	9	7.2	4.5	9.3
43.0	0.9	11	3.7	3.7	3.2
52.0	0.5	13	1.6	3.4	1.5
61.0	0.5	15	1.6	2.9	2.7
70.0		18	1.6	2.1	0.2
80.0		20	0.6	0.5	0.7
89.0		22	0.6	0.5	0.0
		24	0.4		0.2
		27	0.4		
		29	0.4		
		31	0.4		
D_{sm} (μm)	28		20	13	11

Table A4.3.3 - HLB_{act}=11.5

$(D_i+D_{i+1})/2$	FREQ.%-Time (min)		
(μm)	5	20	60
1	20.0	20.0	20.5
2	20.0	20.0	20.0
3	15.0	14.9	19.1
5	12.9	14.3	18.4
6	12.4	17.1	12.8
9	6.4	10.4	5.1
11	4.3	4.8	1.5
13	2.6	2.2	1.0
15	2.1	1.7	0.8
18	1.7	0.3	0.5
20	0.9		
22	0.9		
24	0.4		
27	0.4		
D_{sm} (μm)	14	9	8

Table A4.3.4 - HLB_{act}=10.5

$(D_i+D_{i+1})/2$	FREQ.%-Time (min)				
(μm)	2	5	20	40	60
0.5	25.0	28.0	25.4	28.2	27.0
0.9	46.0	45.4	47.2	46.0	44.2
1.4	21.0	19.3	18.7	17.5	20.6
1.8	6.0	5.2	6.3	6.4	6.2
2.5	1.0	1.1	1.0	1.0	1.1
3.4	1.0	1.0	0.9	0.9	0.9
D_{sm} (μm)	1.0	1.0	1.0	1.0	1.0

Table A4.4 - Cyclohexane/NPE 2wt% 20°C, f_w=0.8, 800rpm. Drop sizes of Type 3 emulsions, shifted to SAD- and SAD+ (all diameters are in μm).

Start $HLB_{wt.av}$	O/W_m Shift				W/O_m Shift			
	Average interval diameter	Freq %	D_{sm}	PCS	Average interval diameter	Freq %	D_{sm}	PCS
10.00	0.5 0.9 1.4 1.8 2.5 3.4 4.3	26.1 41.4 26.8 3.8 0.6 0.6 0.6	1.2	3.5	0.5 0.9 1.4 1.8 2.5	31.0 50.0 15.0 3.0 1.0	1.2	1.99
10.25	0.5 0.9 1.4 1.8 2.5 3.4	25.0 46.0 21.0 6.0 1.0 1.0	1.4	0.93	0.5 0.9 1.4 1.8 2.5 3.4	22.3 44.8 26.1 5.2 0.7 0.7	1.3	2.0
10.50	0.5 0.9 1.4 1.8	58.1 28.4 12.5 1.0	1.0	1.6	0.5 0.9 1.4 1.8	60.0 28.0 11.0 1.0	1.0	1.8
11.00	0.5 0.9 1.4 1.8 2.5	35.2 49.2 13.5 1.1 1.0	1.1	2.0	0.5 0.9 1.4 1.8 2.5	32.4 46.2 14.8 3.0 0.6	1.1	2.0

Table A4.5 - Cyclohexane/NPE 2wt% 20°C, f_w=0.2. Drop sizes of Type 3 emulsions, shifted to SAD- and SAD+ (all diameters are in μm).

Start $HLB_{wt.av}$	O/W_m Shift			W/O_mShift		
	Average interval diameter	Freq %	D_{sm}	Average interval diameter	Freq %	D_{sm}
10.00	0.5 0.9 1.4 1.8 2.5	33.2 49.8 13.0 3.1 1.0	1.2	0.5 0.9 1.4 1.8 2.5	No Drops were seen	<0.5
10.25	0.5 0.9 1.4 1.8 2.5	36.0 42.1 18.0 3.0 0.9	1.0	0.5 0.9 1.4 1.8 2.5	31.8 49.2 15.0 3.0 1.0	1.0
10.50	0.5 0.9 1.4 1.8 2.5	31.2 47.4 17.5 3.0 0.9	1.0	0.5 0.9 1.4 1.8 2.5	33.7 45.2 17.2 3.0 0.9	1.0
11.00	0.5 0.9 1.4 1.8 2.5	35.6 44.1 16.4 3.0 0.9	1.0	0.5 0.9 1.4 1.8 2.5	37.8 39.8 18.5 3.0 0.9	1.0

Table A4.6 - Cyclohexane/NPE. Steady-state drop diameters at HLB_{act}=6 and HLB_{act}=8 (600rpm).

$(D_i+D_{i+1})/2$	FREQ.% - HLB_{act}	
(μm)	6.0	8.0
1.0	29.2	
1.8	26.4	11.5
2.5		35.9
3.4	22.7	27.0
4.3	15.5	20.0
5.2		11.5
6.1	6.2	7.0
7.0		0.0
8.0		1.5
8.9		0.0
9.8		0.8
D_{sm} (μm)	4.2	4.4

Table A4.7 - Cyclohexane/NPE. Effect of agitation conditions

$(D_i+D_{i+1})/2$	FREQ.% - Agitator		
(μm)	200rpm	Ultra-Turrax	Simple Shaking
0.5	20.1	36.0	34.0
0.9	29.9	40.5	34.5
1.4	33.6	18.0	23.5
1.8	10.4	4.5	5.8
2.5	3.7	0.9	1.0
3.4	2.2		1.0
D_{sm} (μm)	1.6	1.2	1.4

(for 800rpm results see Table A4.4)

Table A4.8 - Cyclohexane/NPE. Effect of surfactant concentration.

Surfactant Conc. (g/l)	Av. Int. Diameter (μm)	Freq. %	Drop Diameter (μm) *denotes PCS result
10	0.5 0.9 1.4 1.8 2.3 2.7 3.2 3.6 4.1 4.5 5.0 5.5 5.9	12.0 19.1 21.5 11.0 9.1 8.6 7.2 5.3 2.9 1.0 1.0 1.0 0.5	3.3
20			1.0 (see table A4.4)
50			0.24*
80			0.15*
120			0.073*

Table A4.9 - PIB-Cyclohexane/NPE (800rpm). Effect of oil phase viscosity on inversions SAD+ to SAD-.

Table A4.9.1 - oil phase viscosity = 1.0 poise.

$(D_i+D_{i+1})/2$	FREQ.%-Time (min)		
(μm)	1	3	10
1.1	33.1	44.0	33.1
2.3	19.1	19.2	29.1
3.4	16.6	17.6	23.3
4.5	9.6	12.6	4.7
5.7	7.6	3.3	4.1
6.8	7.6	1.6	3.5
8.0	4.5	1.6	2.3
9.1	1.3		
10.2	0.6		
D_{sm} (μm)	6.0	4.5	1.9

Table A4.9.2 - oil phase viscosity = 2.0 poise.

$(D_i+D_{i+1})/2$	FREQ.% - Time (min)			
(μm)	1	5	10	20
1.1	57.3	57.9	19.2	36.3
2.3	16.1	17.8	41.7	34.5
3.4	9.9	10.0	14.7	23.6
4.5	4.5	4.8	10.9	4.5
5.7	1.8	4.1	5.8	0.9
6.8	1.4	1.9	1.9	
8.0	1.3	1.2	1.9	
9.1	1.3	0.8	1.3	
10.2	1.3	0.4	0.6	
11.4	1.3	0.2	0.6	
12.5	1.3	0.2	0.6	
13.6	1.1	0.2	0.6	
14.7	1.1	0.2		
15.9	0.4	0.2		
17.0	0.2	0.2		
D_{sm} (μm)	10.0	7.0	2.7	1.3

Table A4.9.3 - oil phase viscosity = 5.0 poise.

$(D_i+D_{i+1})/2$	FREQ.% - Time (min)		
(μm)	3	10	20
1.1	29.2	33.9	33.9
2.3	19.5	26.0	24.0
3.4	14.8	23.4	24.0
4.5	11.4	7.0	8.0
5.7	9.5	4.2	3.9
6.8	5.3	1.3	1.3
8.0	3.3	1.0	1.3
9.1	1.7	1.0	1.2
10.2	1.7	1.0	0.9
11.4	0.8	0.3	0.6
12.5	0.8		0.3
13.6	0.6	0.3	0.3
14.7	0.3		0.3
15.9	0.3	0.3	
17.0	0.3	0.3	
18.2	0.3		
19.1	0.3		
20.3	0.3		
D_{sm} (μm)	10.0	2.9	3.0

Table A4.10 - PIB-Cyclohexane/NPE (800rpm). Effect of oil phase viscosity on transitions SAD- to SAD=0 to SAD-.

$(D_i+D_{i+1})/2$	FREQ.%-Oil phase viscosity (poise)					
(μm)	0.007	1	2	5	10	30
0.5	25.0	25.0	31.7	28.2	22.3	27.1
0.9	46.0	48.8	31.7	38.5	32.6	31.8
1.4	21.0	19.1	21.2	16.9	25.5	19.4
1.8	6.0	6.0	7.9	7.2	10.9	8.5
2.3	1.0	1.1	5.8	4.1	2.7	8.5
2.7	1.0	1.0		2.1	1.6	2.3
3.2			0.5	1.0	1.6	2.3
3.6			0.5	0.5	1.1	
4.1				0.5	1.1	
4.5			0.5	0.5		
5.0				0.5		
D_{sm} (μm)	1.0	1.0	1.9	2.3	2.2	1.9

Table A4.11 - PIB-cyclohexane/NPE: Direct emulsification (higher oil phase viscosity systems - 800rpm)

$(D_i+D_{i+1})/2$	FREQ.%		$(D_i+D_{i+1})/2$	FREQ. % - Oil phase viscosity (poise) Time (minutes)						
(μm)	2 1	5 1	(μm)	5 20	5 40	2 10	2 40	2 60	10 20	30 20
4.5	24.9	16.8	1.1	37.0	30.2	31.8	29.3	26.8	31.1	31.8
9.1	26.5	21.3	2.3	24.1	28.8	27.5	23.1	25.7	29.3	28.4
13.6	17.4	11.0	3.4	15.4	15.0	14.4	14.5	19.3	15.5	18.2
18.2	12.8	11.0	4.5	10.8	12.0	9.2	10.5	12.9	10.4	9.1
22.7	8.4	11.0	5.7	4.3	5.0	4.0	8.6	5.9	4.6	6.8
27.2	2.5	7.0	6.8	2.8	4.3	4.0	6.2	4.4	3.7	2.0
31.8	1.6	6.7	8.0	2.5	2.0	2.8	4.6	1.3	2.7	1.5
36.3	1.2	1.8	9.1	1.2	0.8	1.2	1.5	1.3	1.1	0.5
40.9	0.9	1.8	10.2	0.3	0.5	0.9	0.9	0.9	0.4	0.5
45.5	0.9	1.8	11.4	0.3	0.3	0.6	0.3	0.9	0.2	0.5
50.0		1.8	12.5	0.3	0.3	0.6	0.3	0.6	0.2	0.5
54.5	0.6	2.4	13.6	0.3	0.3	0.6	0.3	0.3	0.2	0.5
59.1		1.5	14.8		0.3	0.3			0.2	0.3
63.6	0.6	0.9	15.9	0.3	0.3	0.3			0.2	
68.2	0.3	0.6	17.0		0.3	0.3			0.2	0.3
72.7		0.3	18.2			0.3			0.2	0.3
77.3	0.3	0.9	19.3			0.3				
81.2	0.3	0.3	20.5	0.3		0.3				
86.4	0.3	0.6	21.6			0.3				
90.9	0.3	0.3	22.3			0.3				
D_{sm} (μm)	43	49	D_{sm} (μm)	8	8	12	7	7	8	8

Table A4.12 - cyclohexane/NPE. Rate of emulsification 800rpm.

HL_{Bact}	time (min)	D_{sm} (μm)	ln $[D_{sm}-D_{sm\infty}/D_{sm}]$
14.2	1	40.0	-0.393
$D_{sm\infty}$=	10	28.5	-0.61
13μm	20	23.0	-0.83
	30	19.0	-1.2
	40	16.0	-1.67
	60	14.0	-2.64
	70	13.5	-3.29
12.1	1	28.0	-0.47
$D_{sm\infty}$=	10	19.0	-0.80
10.5μm	20	13.0	-1.65
	30	11.0	-3.09
	40	10.7	-4.00
11.5	1	16.0	-0.69
$D_{sm\infty}$=	10	11.0	-1.30
8.0μm	20	9.0	-2.19
	30	8.2	-3.71

APPENDIX 5 - Chapter 5: Drop Size Distribution Data

Table A5.1 - Cyclohexane/NPE 2wt% 600rpm, 20ml/2min. Catastrophic Inversion: Oil drops within $O/W_m/O$ drop study.

$(D_i+D_{i+1})/2$	FREQ.% f_w (catastrophic inversion point, f_w=0.356)						
(μm)	0.066	0.127	0.237	0.334	0.356 5sec	0.356 20min	0.356 60min
1.08	32.9	28.9	27.6	24.6	23.2	23.4	22.5
1.65	27.9	26.7	24.6	21.6	20.6	19.8	18.8
2.50	12.2	13.8	10.9	12.8	11.2	10.9	9.8
3.75	8.3	8.3	9.9	8.2	7.2	6.6	9.4
5.50	7.9	8.4	10.8	11.0	10.4	10.7	17.9
8.00	5.2	4.6	5.9	6.5	7.0	7.9	10.3
11.75	3.0	3.3	4.2	4.6	5.7	10.3	6.0
17.00	1.6	2.7	2.5	3.3	3.6	8.6	4.
25.00	0.5	1.8	1.9	3.1	3.4	2.4	1.2
37.50	0.3	1.0	0.8	2.5	3.0	0.2	
55.00	0.1	0.6	0.7	1.2	1.8		
77.50			0.2	0.4	1.7		
110.00				0.15	0.7		
157.50				0.05	0.3		
222.50					0.2		

Table A5.2 - Cyclohexane/NPE 2wt% 20ml/2min. Catastrophic Inversion: Effect of stirrer speed on the drop sizes of the inverted O/W_m emulsion.

$(D_i+D_{i+1})/2$	FREQ.% f_{winv} / Stirrer speed N		
(μm)	0.31/400	0.36/600	0.39/800
1.08	24.3	23.2	15.2
1.65	23.1	20.6	20.0
2.50	9.5	11.2	11.2
3.75	6.4	7.2	8.3
5.50	7.0	10.4	7.5
8.00	6.7	7.0	5.6
11.75	4.8	5.7	4.8
17.00	3.1	3.6	5.3
25.00	4.8	3.4	9.5
37.50	4.0	3.0	6.9
55.00	2.4	1.8	2.9
77.50	1.8	1.7	1.7
110.00	1.4	0.7	1.0
157.50	0.4	0.3	0.2
222.50	0.3	0.2	

Table A5.3 - Cyclohexane/NPE 2wt% - O/W_m emulsion drop size distribution after 1 hour direct emulsification.

$(D_i+D_{i+1})/2$	FREQ.% f_{winv} / Stirrer speed N (rpm)				
(μm)	0.31/400	0.33/500	0.36/600	0.39/700	0.39/800
1.08	24.0		20.4		15.1
1.65	21.2		17.1	24.9	21.9
2.50	11.6	18.5	11.6	24.0	20.8
3.75	8.3	20.4	10.6	24.9	12.7
5.50	8.3	19.8	17.4	9.8	10.1
8.00	7.8	12.5	8.1	6.8	7.8
11.75	6.0	9.7	6.4	5.5	6.1
17.00	4.5	7.0	4.5	3.7	3.6
25.00	4.0	5.5	2.6	0.3	1.9
37.50	2.2	3.6	1.2		
55.00	1.6	1.2			
77.50	0.4	0.3			
D_{sm} (μm)	42	35	21	17	15

Table A5.4 - Cyclohexane/NPE 2wt% (20ml/2min)- O/W_m emulsion drop size distribution at the catastrophic inversion point.

$(D_i+D_{i+1})/2$	FREQ.% f_{winv} / Stirrer speed N (rpm)				
(μm)	0.31/400	0.33/500	0.36/600	0.39/700	0.39/800
14.0	16.9	20.1	29.1	25.4	21.6
18.5	17.2	18.2	15.7	20.1	16.6
24.5	18.6	21.1	18.1	21.1	24.7
33.0	16.9	21.1	11.0	12.4	11.7
44.5	10.3	7.3	6.2	6.9	11.7
60.0	9.6	7.7	8.6	9.3	9.0
81.0	4.4	2.7	7.1	2.4	4.0
110.0	3.4	1.0	3.6	2.0	0.6
149.5	1.2	0.5	0.3	0.2	
202.5	1.0	0.2	0.3	0.2	
274.0	0.5	0.2			
D_{sm} (μm)	124	90	74	58	54

Table A5.5.1 - (0.007 poise system) Cyclohexane/SML 2wt% (400 rpm, 40ml/2min) - Change in $O/W_m/O$ drop sizes with f_w, before catastrophic inversion.

$(D_i+D_{i+1})/2$	FREQ.% - f_w		$(D_i+D_{i+1})/2$	FREQ.%- f_w
(μm)	0.08	0.34	(μm)	0.60
11.25	0.7		28.5	2.1
22.25	6.6		85.0	16.0
34.25	16.0	1.5	142.0	16.4
45.50	19.7	5.4	199.0	15.3
62.50	25.7	12.6	255.5	12.9
85.25	17.0	15.1	312.5	11.0
108.00	8.6	15.1	369.5	8.2
130.75	3.3	13.3	426.0	7.1
153.50	0.7	11.2	483.0	5.7
176.25	0.4	9.3	540.0	3.6
198.75		7.2	596.5	1.8
221.50		2.9		
244.25		1.8		
267.00		1.5		
289.75		1.5		
312.50		1.1		
335.35		0.7		
D_{owo} (μm)	96	189	D_{owo} (μm)	391

Table A5.5.2 - (0.007 poise system) Cyclohexane/SML 2wt% (500 rpm, 40ml/2min) - Change in $O/W_m/O$ drop sizes with f_w, before catastrophic inversion.

$(D_i+D_{i+1})/2$	FREQ.% - f_w			$(D_i+D_{i+1})/2$	FREQ.%- f_w
(μm)	0.08	0.22	0.44	(μm)	0.62
11.25	22.2	10.7		28.5	5.6
22.25	29.5	16.3		85.0	20.8
34.25	18.6	18.6	2.3	142.0	24.9
45.50	14.6	18.1	9.4	199.0	19.5
62.50	8.2	15.3	18.5	255.5	12.0
85.25	4.0	10.5	22.6	312.5	7.8
108.00	1.8	5.8	19.0	369.5	4.0
130.75	0.9	2.9	10.3	426.0	2.3
153.50		1.3	6.1	483.0	1.5
176.25		0.5	3.3	540.0	1.0
198.75			2.8	596.5	0.7
221.50			1.5		
244.25			0.9		
267.00			0.9		
289.75			0.9		
312.50			0.9		
335.35			0.6		
D_{owo} (μm)	68	94	177	D_{owo} (μm)	318

Table A5.5.3 - (0.007 poise system) Cyclohexane/SML 2wt% (700 rpm, 40ml/2min) - Change in $O/W_m/O$ drop sizes with f_w, before catastrophic inversion.

$(D_i+D_{i+1})/2$	FREQ.% - f_w				$(D_i+D_{i+1})/2$	FREQ.% f_w
(μm)	0.08	0.22	0.34	0.53	(μm)	0.65
11.25	19.9	18.8	12.7		28.5	6.8
22.25	28.5	20.1	18.0		85.0	27.8
34.25	26.2	20.0	21.1		142.0	31.5
45.50	15.4	17.8	18.0	4.0	199.0	20.3
62.50	9.0	13.5	13.0	11.4	255.5	6.8
85.25	1.0	6.3	9.1	27.0	312.5	3.4
108.00		2.4	4.7	19.1	369.5	1.0
130.75		0.4	2.2	15.7	426.0	1.0
153.50			1.1	9.2	483.0	1.0
176.25				6.1	540.0	0.3
198.75				3.3	596.5	
221.50				1.7		
244.25				1.0		
267.00				0.7		
289.75				0.4		
312.50				0.4		
335.35						
D_{owo} (μm)	48	67	86	155	D_{owo} (μm)	253

Table A5.5.4 - (0.007 poise system) Cyclohexane/SML 2wt% (800 rpm, 40ml/2min) - Change in $O/W_m/O$ drop sizes with f_w, before catastrophic inversion.

$(D_i+D_{i+1})/2$	FREQ.% - f_w					$(D_i+D_{i+1})/2$	FREQ% f_w
(μm)	0.08	0.15	0.22	0.34	0.49	(μm)	0.69
11.25	33.7	17.2	11.6	1.7		28.5	10.1
22.25	26.3	22.7	17.8	3.4	1.3	85.0	19.2
34.25	17.7	27.6	22.8	13.9	4.4	142.0	28.7
45.50	13.3	17.9	22.1	19.3	9.1	199.0	21.5
62.50	8.3	13.0	18.2	31.5	21.5	255.5	11.5
85.25	0.7	1.6	7.6	20.3	31.2	312.5	6.2
108.00				7.5	18.1	369.5	2.0
130.75				2.0	7.5	426.0	0.6
153.50				0.3	3.7	483.0	0.2
176.25					1.7	540.0	
198.75					1.0	596.5	
221.50					0.3		
244.25					0.3		
267.00					0.3		
289.75							
312.50							
335.35							
D_{owo}(μm)	45	50	59	82	121	D_{owo} (μm)	240

Table A5.5.5 - (0.007 poise system) Cyclohexane/SML 2wt% (Ultra-Turrax 5000 rpm, 40ml/2min) - Change in $O/W_m/O$ drop sizes with f_w, before catastrophic inversion.

$(D_i+D_{i+1})/2$	FREQ.% - f_w						
(μm)	0.08	0.15	0.22	0.34	0.44	0.60	0.69
11.25	41.1	8.5	7.5	0.6	0.5	0.4	
22.25	48.1	29.8	17.5	7.3	7.9	1.5	
34.25	7.8	34.0	24.6	12.3	14.9	2.6	
45.50	3.0	17.6	23.8	20.7	19.8	4.5	4.0
62.50		8.5	20.6	34.6	24.8	17.5	17.8
85.25		1.6	8.5	17.3	17.3	32.3	38.5
108.00				5.0	4.0	20.8	17.2
130.75				1.7	1.5	13.0	9.8
153.50				0.6	0.5	3.7	6.9
176.25					0.5	3.3	2.9
198.75					0.5	0.4	1.1
221.50							0.6
244.25							0.6
267.00							0.6
289.75							
312.50							
335.35							
D_{owo}(μm)	35	47	60	80	89	116	124

Table A5.6.1 - Cyclohexane/SML 2wt% (40ml/2min)- O/W_m emulsion drop size distribution at the catastrophic inversion point.

$(D_i+D_{i+1})/2$	FREQ.% f_{winv} / Stirrer speed N (rpm)				
(μm)	0.61/400	0.63/500	0.66/600	0.69/700	0.72/800
14.0	17.0	23.5	31.0	29.5	30.9
18.5	16.8	19.2	19.2	24.4	25.7
24.5	16.8	18.7	16.0	18.8	20.7
33.0	15.8	15.0	11.2	12.6	10.5
44.5	12.8	11.3	8.6	7.1	7.1
60.0	11.0	7.4	8.6	5.8	4.7
81.0	5.5	3.0	3.2	1.3	0.8
110.0	2.5	1.3	2.2	0.4	0.2
149.5	1.0	0.5			
202.5	0.8	0.2			
274.0					
D_{sm} (μm)	93	72	58	48	42

Table A5.6.2 - PIB-Cyclohexane/SML 2wt% (Ultra-Turrax 5000 rpm, 20ml/2min - 40ml/2min 0.007 poise case) - inverted O/W_m emulsion drop size distributions.

$(D_i+D_{i+1})/2$	FREQ.% - oil phase visc. (poise)			$(D_i+D_{i+1})/2$	FREQ.%
(μm)	0.5	1.0	2.0	(μm)	0.007
14.0	26.7	21.8	6.3	4.5	53.6
18.5	24.5	25.3	13.4	9.1	38.3
24.5	23.0	19.7	28.4	13.6	4.0
33.0	11.0	15.3	20.6	18.2	1.7
44.5	7.1	7.9	12.5	25.0	1.7
60.0	5.2	5.2	10.3	34.0	0.4
81.0	1.5	2.6	4.1	43.0	0.2
110.0	0.6	1.7	2.8	52.0	0.1
149.5	0.3	0.4	0.9	61.0	
202.5			0.3	70.0	
274.0			0.3	80.0	
				89.0	
f_{winv}	0.52	0.39	0.18	f_{winv}	0.75
D_{owo} (μm)	60	64	99	D_{owo} (μm)	13

Table A5.6.3 - PIB-Cyclohexane/SML 2wt% (Ultra-Turrax 5000rpm)- O/W_m emulsion drop size distribution after 5 minutes direct emulsification.

$(D_i+D_{i+1})/2$	FREQ.% f_{winv} / oil phase viscosity (poise)			
(μm)	0.75/0.007	0.52/0.5	0.39/1.0	0.18/2.0
1.1	51.7	58.9	57.3	41.2
2.3	41.4	29.5	28.9	41.2
3.4	11.8	7.9	8.6	6.3
4.5	1.0	2.6	3.4	6.3
5.7	0.2	0.8	0.6	3.1
6.8		0.4	0.6	1.6
8.0			0.6	0.6
9.1			0.3	0.3
D_{sm} (μm)	2.6	3.0	3.8	4.2

Table A5.7.1 - (0.25 poise system) PIB-Cyclohexane/SML 2wt% (400 rpm, 20ml/2min) - Change in $O/W_m/O$ drop sizes with f_w, before catastrophic inversion.

$(D_i+D_{i+1})/2$	FREQ.% - f_w				
(μm)	0.04	0.12	0.25	0.36	0.50
11.25	10.0	6.6	2.8		
22.25	15.9	11.9	5.1		
34.25	20.4	19.3	9.3	0.4	
45.50	20.9	21.3	12.1	0.4	
62.50	20.3	20.3	16.4	3.2	2.0
85.25	9.3	13.3	19.6	12.6	4.1
108.00	2.3	5.8	15.3	20.0	7.3
130.75	0.9	0.9	10.2	22.5	9.6
153.50		0.4	5.1	19.4	12.1
176.25			2.3	11.9	13.4
198.75			0.7	5.8	14.5
221.50			0.7	1.8	13.5
244.25			0.4	1.4	9.6
267.00				0.4	6.8
289.75				0.4	3.3
312.50					1.3
335.35					1.3
358.00					1.3
D_{owo}(μm)	70	79	125	160	214

Table A5.7.2 - (0.25 poise system) PIB-Cyclohexane/SML 2wt% (500 rpm, 20ml/2min) - Change in $O/W_m/O$ drop sizes with f_w, before catastrophic inversion.

$(D_i+D_{i+1})/2$	FREQ.% - f_w				
(μm)	0.04	0.15	0.25	0.36	0.46
11.25	10.7	4.1	0.5		
22.25	20.3	10.0	1.5		
34.25	25.7	17.1	4.4	0.9	
45.50	24.1	22.3	6.4	1.4	0.5
62.50	11.8	24.9	20.1	6.8	1.5
85.25	4.8	13.4	29.4	20.5	5.0
108.00	2.1	4.8	24.5	22.6	13.0
130.75	0.5	2.6	6.9	18.2	24.0
153.50		0.4	3.4	15.9	24.5
176.25		0.4	1.5	7.0	15.5
198.75			1.0	3.6	8.5
221.50			0.5	1.8	3.5
244.25				0.9	1.5
267.00				0.5	1.0
289.75					1.0
312.50					0.5
D_{owo}(μm)	64	85	115	150	175

Table A5.7.3 - (0.25 poise system) PIB-Cyclohexane/SML 2wt% (600 rpm, 20ml/2min) - Change in $O/W_m/O$ drop sizes with f_w, before catastrophic inversion.

$(D_i+D_{i+1})/2$	FREQ.% - f_w				
(μm)	0.04	0.12	0.25	0.36	0.48
11.25	17.9	10.1	4.7	0.7	
22.25	28.5	19.4	11.0	3.4	
34.25	22.4	26.4	17.1	5.1	0.4
45.50	16.5	23.5	21.0	10.3	1.5
62.50	9.7	14.0	22.7	23.0	6.0
85.25	3.9	5.2	15.5	24.5	13.5
108.00	1.1	0.7	4.6	19.8	22.6
130.75		0.3	2.1	7.7	21.2
153.50		0.3	0.8	3.4	15.4
176.25				1.0	9.0
198.75				0.3	4.9
221.50				0.3	3.0
244.25					1.5
267.00					0.7
289.75					0.4
D_{owo}(μm)	58	63	85	116	161

Table A5.7.4 - (0.25 poise system) PIB-Cyclohexane/SML 2wt% (800 rpm, 20ml/2min) - Change in $O/W_m/O$ drop sizes with f_w, before catastrophic inversion.

$(D_i+D_{i+1})/2$	FREQ.% - f_w				
(μm)	0.04	0.12	0.25	0.36	0.44
11.25	30.3	10.5	2.3		
22.25	28.8	23.6	8.9	0.4	
34.25	22.7	25.3	14.1	2.8	1.6
45.50	11.6	21.5	19.1	7.3	2.7
62.50	5.6	15.6	26.3	29.0	13.0
85.25	1.0	3.4	23.0	33.1	27.6
108.00			4.6	15.7	27.6
130.75			1.3	8.1	16.2
153.50			0.3	2.8	7.0
176.25				0.8	2.6
198.75					1.1
221.50					0.5
D_{owo}(μm)	44	54	78	103	124

Table A5.8 - 0.25 poise system. PIB-Cyclohexane/SML 2wt% (20ml/2min)- O/W_m emulsion drop size distribution at the catastrophic inversion point.

$(D_i+D_{i+1})/2$	FREQ.% f_{winv} / Stirrer speed N (rpm)			
(μm)	0.52/400	0.54/500	0.54/600	0.56/800
14.0	15.0	22.3	20.3	31.5
18.5	14.8	19.1	18.7	21.7
24.5	14.7	15.5	18.1	18.6
33.0	14.7	13.3	13.2	13.2
44.5	14.7	12.4	12.5	9.2
60.0	14.5	10.7	9.6	4.6
81.0	6.8	3.8	5.1	0.9
110.0	2.5	2.9	2.0	0.6
149.5	1.0	0.9	0.5	0.3
202.5	0.8	0.3		
274.0	0.4			
D_{sm} (μm)	103	83	66	51

Table A5.9.1 - (0.50 poise system) PIB-Cyclohexane/SML 2wt% (400 rpm, 20ml/2min) - Change in $O/W_w/O$ drop sizes with f_w, before catastrophic inversion.

$(D_i+D_{i+1})/2$	FREQ.% - f_w				
(μm)	0.04	0.08	0.15	0.25	0.36
11.25	11.0	9.3	2.0	1.7	
22.25	21.3	15.2	7.4	4.8	
34.25	23.0	18.5	10.2	7.6	1.1
45.50	23.2	20.4	14.8	10.5	3.2
62.50	14.8	18.4	22.4	15.9	7.8
85.25	4.8	13.1	21.0	19.4	12.0
108.00	1.4	3.8	12.5	17.1	14.7
130.75	0.5	1.1	4.7	11.3	14.7
153.50		0.2	2.8	5.3	13.8
176.25		0.2	1.1	2.9	12.0
198.75			0.5	1.2	9.3
221.50			0.2	0.7	5.4
244.25			0.2	0.5	2.8
267.00			0.2	0.5	1.3
289.75				0.3	0.8
312.50				0.3	0.8
335.35					0.3
D_{owo}(μm)	63	78	113	143	185

Table A5.9.2 - (0.50 poise system) PIB-Cyclohexane/SML 2wt% (500 rpm, 20ml/2min) - Change in $O/W_m/O$ drop sizes with f_w, before catastrophic inversion.

$(D_i+D_{i+1})/2$	FREQ.% - f_w				
(μm)	0.04	0.08	0.15	0.25	0.36
11.25	15.1	12.3	8.3	0.8	
22.25	23.6	22.5	14.4	2.8	
34.25	26.1	26.6	18.6	5.2	1.4
45.50	18.6	16.4	19.5	8.4	2.2
62.50	13.6	13.5	16.0	14.0	4.3
85.25	2.5	6.1	11.4	19.6	8.4
108.00	0.5	2.5	6.8	18.8	13.1
130.75			3.4	12.4	17.3
153.50			1.1	8.0	18.3
176.25			0.4	6.8	15.9
198.75				2.4	9.6
221.50				0.8	4.8
244.25					2.2
267.00					1.3
289.75					0.6
312.50					0.3
335.35					0.3
D_{owo}(μm)	54	65	93	138	180

Table A5.9.3 - (0.50 poise system) PIB-Cyclohexane/SML 2wt% (600 rpm, 20ml/2min) - Change in $O/W_m/O$ drop sizes with f_w, before catastrophic inversion.

$(D_i+D_{i+1})/2$	FREQ.% - f_w					
(μm)	0.04	0.08	0.18	0.25	0.31	0.36
11.25	17.8	12.6	4.7	3.9	1.0	
22.25	24.2	24.1	9.4	7.5	3.3	
34.25	30.0	24.4	15.2	10.4	5.1	0.6
45.50	17.4	21.0	17.8	12.5	8.4	2.3
62.50	9.6	14.2	24.0	15.8	13.0	6.9
85.25	1.0	2.5	16.8	17.9	20.0	13.0
108.00		0.9	6.9	12.5	21.0	18.0
130.75		0.3	2.1	9.2	13.4	20.5
153.50			1.9	5.0	6.5	18.0
176.25			1.2	2.5	4.5	8.9
198.75				1.7	1.6	4.3
221.50				0.8	0.7	3.0
244.25				0.3	0.7	2.3
267.00					0.4	1.3
289.75					0.2	0.3
312.50					0.2	0.3
335.35					0.2	0.3
D_{owo}(μm)	45	58	96	129	146	170

Table A5.9.4 - (0.50 poise system) PIB-Cyclohexane/SML 2wt% (800 rpm, 20ml/2min) - Change in O/W_m/O drop sizes with f_w, before catastrophic inversion.

$(D_i+D_{i+1})/2$	FREQ.% - f_w					
(μm)	0.04	0.08	0.15	0.25	0.31	0.36
11.25	20.2	11.6	3.8	1.4		
22.25	36.5	20.6	8.5	4.8	1.0	0.3
34.25	28.8	32.2	14.2	7.6	2.4	0.8
45.50	11.1	19.7	18.9	11.0	4.9	2.0
62.50	3.4	14.1	30.1	18.1	13.4	6.3
85.25		1.6	15.6	26.9	23.0	13.0
108.00		0.3	6.3	16.1	22.0	19.5
130.75			1.3	9.0	15.6	20.5
153.50			0.7	3.3	9.2	17.4
176.25				1.2	3.2	9.3
198.75				0.4	2.5	5.5
221.50				0.2	2.5	2.3
244.25					0.3	2.0
267.00						0.8
289.75						0.3
D_{owo}(μm)	39	53	82	114	140	163

Table A5.10 - 0.50 poise system. PIB-Cyclohexane/SML 2wt% (20ml/2min)- O/W_m emulsion drop size distribution at the catastrophic inversion point.

$(D_i+D_{i+1})/2$	FREQ.% Stirrer speed N (rpm) f_{winv}=0.39			
(μm)	400	500	600	800
14.0	15.6	15.9	30.0	30.7
18.5	15.6	15.9	26.9	26.6
24.5	15.0	15.4	13.9	23.7
33.0	14.7	15.4	8.1	7.3
44.5	13.8	14.0	6.7	3.5
60.0	11.0	11.2	5.2	3.3
81.0	6.9	7.0	4.7	2.7
110.0	4.2	3.2	2.5	1.6
149.5	2.1	1.4	1.6	0.3
202.5	0.9	0.6	0.5	0.3
274.0	0.3			
D_{sm} (μm)	113	91	83	63

Table A5.11.1 - (1.0 poise system) PIB-Cyclohexane/SML 2wt% (400 rpm, 20ml/2min) - Change in $O/W_m/O$ drop sizes with f_w, before catastrophic inversion.

$(D_i+D_{i+1})/2$	FREQ.% - f_w			
(μm)	0.04	0.08	0.15	0.25
11.25	20.2	15.1	7.4	1.2
22.25	26.4	23.8	15.7	3.9
34.25	25.0	24.4	17.3	7.7
45.50	20.0	19.2	18.9	11.3
62.50	6.0	12.1	18.0	19.0
85.25	2.0	3.7	12.3	19.5
108.00	0.4	1.1	6.6	14.5
130.75		0.5	2.2	9.7
153.50		0.3	0.9	7.0
176.25			0.3	3.9
198.75			0.3	1.0
221.50				0.7
244.25				0.5
267.00				0.3
D_{owo}(μm)	49	65	92	134

Table A5.11.2 - (1.0 poise system) PIB-Cyclohexane/SML 2wt% (500 rpm, 20ml/2min) - Change in $O/W_m/O$ drop sizes with f_w, before catastrophic inversion.

$(D_i+D_{i+1})/2$	FREQ.% - f_w				
(μm)	0.04	0.08	0.15	0.25	0.35
11.25	11.2	11.6	6.3	1.7	
22.25	27.6	24.9	12.0	3.8	
34.25	34.7	26.6	17.3	9.0	1.0
45.50	19.4	19.6	20.7	15.2	4.1
62.50	5.1	12.3	23.3	18.2	11.8
85.25	2.0	3.3	13.3	18.6	19.8
108.00		1.0	3.3	15.2	20.8
130.75		0.3	2.0	8.7	18.4
153.50		0.3	1.0	6.2	10.8
176.25			0.3	1.7	5.8
198.75			0.3	0.7	3.0
221.50				0.3	1.5
244.25				0.3	1.0
267.00				0.3	0.7
289.75					0.7
312.50					0.3
335.25					0.3
D_{owo}(μm)	46	62	88	125	161

Table A5.11.3 - (1.0 poise system) PIB-Cyclohexane/SML 2wt% (600 rpm, 20ml/2min) - Change in $O/W_m/O$ drop sizes with f_w, before catastrophic inversion.

$(D_i+D_{i+1})/2$	FREQ.% - f_w	
(μm)	0.08	0.15
11.25	14.0	6.0
22.25	22.8	13.4
34.25	26.3	18.5
45.50	20.1	20.1
62.50	13.3	20.7
85.25	1.8	12.9
108.00	0.6	4.8
130.75	0.3	2.8
153.50		0.4
176.25		0.4
D_{owo}(μm)	55	85

Table A5.11.4 - (1.0 poise system) PIB-Cyclohexane/SML 2wt% (800 rpm, 20ml/2min) - Change in $O/W_m/O$ drop sizes with f_w, before catastrophic inversion.

$(D_i+D_{i+1})/2$	FREQ.% - f_w			
(μm)	0.04	0.15	0.18	0.28
11.25	26.5	4.2	2.6	
22.25	30.5	7.7	7.7	
34.25	21.7	19.4	17.9	3.1
45.50	12.9	27.1	21.3	7.6
62.50	7.2	26.7	26.2	17.6
85.25	1.2	9.7	13.2	22.4
108.00		3.1	6.1	20.0
130.75		1.1	3.8	15.9
153.50		0.7	0.9	7.6
176.25		0.3	0.3	3.5
198.75				2.3
D_{owo}(μm)	46	75	89	128

Table A5.12 - 1.0 poise system. PIB-Cyclohexane/SML 2wt% (20ml/2min)- O/W_m emulsion drop size distribution at the catastrophic inversion point.

$(D_i+D_{i+1})/2$	FREQ.% Stirrer speed N (rpm) f_{winv}=0.36				
(μm)	400	500	600	700	800
14.0	14.8	16.8	15.8	18.0	18.6
18.5	13.9	15.9	14.9	17.1	17.0
24.5	13.5	14.8	14.4	16.2	16.1
33.0	13.1	13.9	13.0	14.4	14.7
44.5	11.3	11.2	12.6	11.7	11.6
60.0	10.0	8.9	10.2	9.0	9.4
81.0	8.3	7.6	8.4	7.2	7.1
110.0	6.1	5.1	6.1	4.1	3.8
149.5	4.4	3.3	3.3	1.8	1.3
202.5	3.1	1.7	0.9	0.5	0.4
274.0	1.5	0.6	0.3		
D_{sm} (μm)	158	135	116	95	89

Table A5.13.1 - (2.0 poise system) PIB-Cyclohexane/SML 2wt% (400 rpm, 20ml/2min) - Change in $O/W_m/O$ drop sizes with f_w, before catastrophic inversion.

$(D_i+D_{i+1})/2$	FREQ.%-f_w	
(μm)	0.04	0.08
11.25	31.3	14.8
22.25	43.7	23.8
34.25	15.1	25.0
45.50	7.6	16.3
62.50	1.7	13.0
85.25	0.6	4.6
108.00		1.2
130.75		1.9
153.50		0.7
176.25		0.4
D_{owo}(μm)	39	70

Table A5.13.2 - (2.0 poise system) PIB-Cyclohexane/SML 2wt% (500 rpm, 20ml/2min) - Change in $O/W_m/O$ drop sizes with f_w, before catastrophic inversion.

$(D_i+D_{i+1})/2$	FREQ.% - f_w		
(μm)	0.04	0.08	0.12
11.25	26.5	4.7	12.1
22.25	35.2	23.4	15.3
34.25	29.1	24.5	17.3
45.50	7.5	17.2	17.3
62.50	1.7	13.0	17.3
85.25		4.7	12.1
108.00		2.0	4.5
130.75		0.5	1.4
153.50			1.0
176.25			0.7
198.75			0.7
221.50			0.3
D_{owo}(μm)	35	64	105

Table A5.13.3 - (2.0 poise system) PIB-Cyclohexane/SML 2wt% (600 rpm, 20ml/2min) - Change in $O/W_m/O$ drop sizes with f_w, before catastrophic inversion.

$(D_i+D_{i+1})/2$	FREQ.% - f_w			
(μm)	0.04	0.08	0.12	0.15
11.25	29.2	12.0	4.7	4.4
22.25	35.1	21.8	12.5	7.2
34.25	26.3	24.3	24.1	13.6
45.50	8.8	19.4	19.5	15.3
62.50	0.6	15.0	14.8	17.3
85.25		6.3	11.3	16.3
108.00		1.0	5.1	11.2
130.75			3.1	6.1
153.50			2.0	5.1
176.25			1.6	1.4
198.75			1.0	1.7
221.50			0.3	0.6
D_{owo}(μm)	34	64	102	128

Table A5.13.4 - (2.0 poise system) PIB-Cyclohexane/SML 2wt% (800 rpm, 20ml/2min) - Change in $O/W_m/O$ drop sizes with f_w, before catastrophic inversion.

$(D_i+D_{i+1})/2$	FREQ.% - f_w			
(μm)	0.04	0.08	0.12	0.15
11.25	53.0	15.0	2.5	
22.25	32.0	19.1	5.9	
34.25	9.0	21.4	11.3	3.2
45.50	6.0	19.7	16.7	9.6
62.50		17.3	20.8	20.9
85.25		6.4	20.4	24.1
108.00		1.2	13.6	14.5
130.75			5.4	11.6
153.50			2.1	8.4
176.25			0.9	3.9
198.75			0.5	2.0
221.50				0.3
D_{owo}(μm)	30	62	100	128

Table A5.14 - 2.0 poise system. PIB-Cyclohexane/SML 2wt% (20ml/2min)- O/W_m emulsion drop size distribution at the catastrophic inversion point (f_{winv}=0.18).

$(D_i+D_{i+1})/2$	FREQ.% Stirrer speed N(rpm)		
(μm)	400	500	600
28.5	29.5	35.9	45.6
85.0	28.3	33.5	36.5
142.0	26.4	19.3	15.2
199.0	8.0	6.2	0.9
255.5	2.6	2.6	0.6
312.5	1.9	1.2	0.3
369.5	0.7	0.2	0.3
426.0	0.7	0.2	0.3
483.0	0.5	0.2	0.3
540.0	0.5	0.2	
596.5	0.5	0.2	
653.5	0.2	0.2	
710.0	0.2		
D_{sm} (μm)	315	253	227

Table A5.15.1 - (0.5 poise system) PIB-Cyclohexane/SML 2wt% (Ultra-Turrax 5000 rpm, 20ml/2min) - Change in $O/W_m/O$ drop sizes with f_w, before catastrophic inversion.

$(D_i+D_{i+1})/2$	FREQ.% - f_w							
(μm)	0.04	0.12	0.18	0.25	0.34	0.41	0.48	0.51
11.25	30.6	13.3	11.4	2.8	4.0	1.1		
22.25	35.7	16.8	15.1	8.8	9.0	5.3		0.5
34.25	15.3	24.5	16.3	12.2	12.5	8.0	2.7	1.5
45.50	11.7	23.1	18.1	16.6	13.0	10.6	15.5	6.4
62.50	6.1	18.9	24.1	29.3	18.5	22.9	35.4	10.8
85.25	0.5	3.5	12.0	16.6	22.0	23.4	22.1	35.3
108.00			3.0	9.9	10.0	13.8	15.9	24.5
130.75				2.8	8.5	9.0	6.2	8.3
153.50					2.5	4.8	1.3	7.4
176.25						1.1	0.9	2.9
198.75								1.5
221.50								1.0
D_{owo}(μm)	42	54	69	84	101	109	117	126

Table A5.15.2 - (1.0 poise system) PIB-Cyclohexane/SML 2wt% (Ultra-Turrax 5000 rpm, 20ml/2min) - Change in $O/W_m/O$ drop sizes with f_w, before catastrophic inversion.

$(D_i+D_{i+1})/2$	FREQ.% - f_w					
(μm)	0.04	0.12	0.18	0.25	0.36	0.39
11.25	30.2	11.8	10.1	11.4		
22.25	41.5	17.8	15.0	13.6	1.7	1.1
34.25	22.6	20.7	15.5	15.9	3.4	2.2
45.50	5.7	24.9	15.5	15.9	4.5	5.5
62.50		18.3	24.6	15.9	28.2	24.5
85.25		5.9	14.5	15.9	29.9	41.4
108.00		0.6	4.3	5.5	19.8	12.5
130.75			0.5	4.1	9.6	8.4
153.50				1.4	1.1	1.8
176.25				0.5	0.6	0.7
198.75					0.6	0.7
221.50					0.6	0.7
244.25						0.4
D_{owo}(μm)	31	59	74	95	106	113

Table A5.15.3 - (2.0 poise system) PIB-Cyclohexane/SML 2wt% (Ultra-Turrax 5000 rpm, 20ml/2min) - Change in $O/W_m/O$ drop sizes with f_w, before catastrophic inversion.

$(D_i+D_{i+1})/2$	FREQ.% - f_w				
(μm)	0.04	0.08	0.12	0.15	0.18
11.25	45.6	12.5	14.6	5.3	2.3
22.25	31.9	21.9	21.2	21.3	4.4
34.25	16.4	37.5	26.3	27.1	9.2
45.50	6.1	22.5	21.9	21.3	19.2
62.50		5.6	12.4	16.5	32.4
85.25			2.9	5.3	27.6
108.00			0.7	3.2	4.4
130.75				0.3	0.5
153.50					
176.25					
198.75					
221.50					
244.25					
D_{owo}(μm)	30	42	53	68	75

Table A5.16 - 0.007 poise system. Cyclohexane/SML 2wt% - O/W_m emulsion drop size distribution after 1 hour direct emulsification (f_{winv}=0.70).

$(D_i+D_{i+1})/2$	FREQ.% Stirrer speed N (rpm)			
(μm)	400	500	600	800
1.7	36.1	38.6	36.9	36.7
4.0	23.2	25.9	31.4	34.8
6.3	14.6	13.4	13.7	14.8
8.5	9.0	9.8	15.5	7.6
10.8	4.6	5.4	4.7	4.0
13.1	3.5	2.8	1.2	2.9
15.3	3.1	1.9	0.8	1.4
17.6	2.1	1.0	1.6	0.2
19.9	1.5	0.4		
22.2	0.8	0.2	0.4	
24.4	0.4	0.2		
26.7	0.2	0.2		
29.0	0.2	0.2		
31.2	0.2	0.2		
33.5	0.2			
35.8				
38.1	0.2			
D_{sm} (μm)	17.0	13.5	10.0	9.0

ACRONYMS - PHASE INVERSION IN NONIONIC SURFACTANT-OIL-WATER SYSTEMS

SYSTEM ACRONYMS

CMC = critical micelle concentration
EACN = equivalent alkane carbon number
EIP = emulsion inversion point
nSOW = nonionic surfactant-oil-water
PIB = polyisobutene
PIT = phase inversion temperature
SAD = surfactant affinity difference
WOR = water-to-oil ratio

SURFACTANT ACRONYMS

EON = Ethylene oxide number
EOP = polyoxyethylene octylphenylether
HLB = hydrophile-lipophile-balance
HLB_{act} = hydrophile-lipophile-balance of the interfacial surfactant
NPE = polyoxyethylene nonylphenylether
SML = polyoxyethylene sorbitonmonolaurate

PHASE BEHAVIOUR

M_o = Type 3 oleic microemulsion
M_s = Type 3 surfactant phase microemulsion
M_w = Type 3 aqueous microemulsion
O = oil phase containing surfactant at a concentration $<CMC_o$
O_m = Type 2 oil phase containing surfactant micelles
W = water phase containing surfactant at a concentration $<CMC_w$
W_m = Type 1 water phase containing surfactant micelles

SYSTEM CLASSIFICATION	POSSIBLE PHASES (depending on composition)
SAD+ or TYPE 2	O, O_m, W
SAD=0 or TYPE 3	O, W, M_s, M_o, M_w
SAD- or TYPE 1	W, W_m, O

APPENDIX 6 - ACRONYMS